UNIVERSITY OF BIRMINGHAM

A MYCOBACTERIAL GLYCOSIDE HYDROLASE 76 ENZYME ENABLES ARABINOMANNAN RELEASE TO SIGNAL EXIT FROM LAG PHASE

by

AARON FRANKLIN

A thesis submitted to the University of Birmingham for the degree of

DOCTOR OF PHILOSOPHY

School of Biosciences

College of Life and Environmental Sciences

University of Birmingham

October 2023

Abstract

A key component of the mycobacterial cell envelope are the glycolipids. These molecules play important roles in both structural support and modulation of the host immune system. One of the major phospholipids produced by mycobacteria is phosphatidylinositol. This molecule can be glycosylated to produce phosphatidylinositol mannosides, as well as lipomannan and lipoarabinomannan. These mannosylated glycolipids make up the majority of the lipids in the cytoplasmic membrane. However, within the capsule of mycobacteria are lipid-free glycans thought to be derived from lipomannan and lipoarabinomannan. Currently, there is no explanation as to how arabinomannan and mannan are released from their lipid anchors. In this thesis, a glycoside hydrolase family 76 enzyme is identified which cleaves lipomannan and lipoarabinomannan and drives export of the carbohydrate domains to the capsule. In addition, this thesis demonstrates that the loss of this enzymes activity results in a loss of capsular arabinomannan. Furthermore, the loss of arabinomannan leads to an increase in lag phase and significantly slower exponential growth. This thesis provides evidence that arabinomannan acts as a signalling molecule which triggers the transition from lag phase to exponential growth. The findings presented in this thesis will serve as a basis for a better understanding of the digestion of mycobacterial glycolipids and the trafficking of these molecules to the outer most layer of the cell. This may lead to a more detailed appreciation of the role lipoarabinomannan and its derivatives play in host-pathogen interactions and bacterial physiology.

Acknowledgements

I would like to take this opportunity to thank everyone who has supported me during my PhD. First and foremost, I would like to thank my supervisor, Dr Patrick Moynihan, for giving me the opportunity to join the Moynihan lab. This thesis would not be possible without the guidance and expertise Patrick has shared with me, and the confidence he has given me. Additionally, I would like to thank all the members of the Moynihan lab and the larger tuberculosis research group, past and present, for making it such a welcoming and supportive environment to work in. I give special thanks to our awesome lab tech, Abi, for her help and support during my PhD, and my fellow PhD students Sam, Greg, Clare, and Rudi.

I would also like to thank Dr Elisabeth Lowe, Dr Todd Mize, and Dr Nichollas Scott. Without their collaboration, many of the experiments in this thesis would not have been possible.

Finally, I would like to thank my family. Who without their love, encouragement, and support I would not be able to submit this thesis.

The work carried out in this thesis will contribute towards my upcoming publication. This publication has similarities to Chapters 3, 4, 5, and 6. This thesis is my own work with no significant contribution from the co-authors of my publication.

Table of Contents

Figure List

Table List

Abbreviation List

ADC	Albumin, Dextrose, Catalase
AM	Arabinomannan
APS	Ammonium Peroxydisulfate
BCG	Bacillus Calmette-Guerin
CPM	Counts per Minute
DMSO	Dimethyl sulfoxide
DNA	Deoxyribonucleic acid
GH	Glycoside Hydrolase
HIV	Human Immunodeficiency Virus
IPTG	Isopropyl β-D-1-thiogalactopyranoside
kb	Kilo Base
kDa	Kilo Dalton
L	Litre
LAM	Lipoarabinomannan
LB	Luria-Bertani
LM	Lipomannan
M	Molar
mA	Milli Amp
ManLAM	Mannose-capped Lipoarabinomannan
Man*p*	Mannopyranose
mg	Milli Gram

mL	Milli Litre
mM	Milli Molar
mol	Moles
MPA	Phosphomolybdic Acid
MPI	Mannosyl Phosphate Inositol
NEB	New England Biolabs
ng	Nano Gram
nm	Nano Meter
OADC	Oleic acid, Albumin, Dextrose, Catalase
OD_{600}	Optical Density at 600nm
PBS	Phosphate Buffered Saline
PCR	Polymerase Chain Reaction
pH	Power of Hydrogen
PI	Phosphatidyl-*myo*-inositol
PIM	Phosphatidyl-*myo*inositol Mannoside
pmol	Pico Mole
rpm	Rotations per Minute
SDS	Sodium Dodecyl Sulfate
SDS-PAGE	Sodium Dodecyl Sulfate-Polyacrylamide Gel Electrophoresis
TAE	Tris, Acetic Acid, EDTA
TB	Tuberculosis
TBST	Tris Buffered Saline with 0.05% Tween20
TEMED	Tetremethylethylenediamine

TLC	Thin Layer Chromatography
UV	Ultra Violet
v/v	Volume per Volume
V	Voltage
w/v	Weight per Volume
WHO	World Health Organisation
YPD	Yeast, Peptone, Dextrose
µL	Micro Litre
µM	Micro Molar

Chapter 1

Introduction

1. Introduction

1.1 The Mycobacterium genus

The *Mycobacterium* genus was named in 1896 by Lehmann and Neumann after they identified specific characteristics of the human pathogen *Mycobacterium tuberculosis,* the causative agent of tuberculosis (Lehmann and Neumann, 1896). However, the first discovery of mycobacteria came in 1874 when Hansen identified the bacillus-shaped bacteria, *Mycobacterium leprae,* in patients suffering with the disease leprosy (Kobro, 1925). Mycobacteria belong to the order of Actinomycetales which was codified in 1916. This is a group of mould-like bacteria (Williams *et al.,* 1993). To date, the *Mycobacterium* genus consists of over 190 species which includes *M. tuberculosis* and other human pathogens such as *M. leprae,* as well as non-tuberculosis mycobacteria such as *Mycobacterium avium* and *Mycobacterium abscessus* (Meehan *et al.,* 2021).

Mycobacterium species are aerobic bacteria in the Actinomycetota phylum (Ghosh and Chaudhuri, 2015; Cook *et al.,* 2009). They are guanine and cytosine (G+C) rich organisms with unique cell walls that have both Gram-positive and Gram-negative features (Cook *et al.,* 2009). They are identified as acid-fast bacilli. This is a physical property of the bacilli that enables the bacterium to resist decolourisation by acids during staining procedures (Marlon, Mirza and Sandeep, 2022). All mycobacteria share a complex cell wall structure with the defining mycolic acids feature that contributes to making the cells hydrophobic and resistant to treatment (Asselineau and Lederler, 1950).

One clear difference amongst mycobacteria, which was identified very early, was the variability in growth rates of the bacteria (Tsukamura, 1967). This means the genus can be subdivided into two categories; slow-growing bacteria where more than seven days are required for colonies to form, and fast-growing bacteria where colonies form in less than seven days (Nataraj *et al.*, 2015). These two groups can then be further divided into specific complexes. For example, the *M. tuberculosis* complex is a group of slow-growing mycobacteria that cause tuberculosis in humans or other animals. It includes the organisms: *M. tuberculosis, Mycobacterium bovis, Mycobacterium canetti, Mycobacterium orygis, Mycobacterium microti, Mycobacterium caprae, Mycobacterium pinnipedi, Mycobacterium suricattae, Mycobacterium mungi,* and *Mycobacterium africanum* (Fedrizzi *et al.,* 2017).

In 2018, Gupta, Lo and Son proposed to further divide the *Mycobacterium* into five genera based on their genome sequences. These were: *Mycobacterium* based on the slow-growing tuberculosis-simiae clade, *Mycobacteroides* based fast-growing abscessus-chelonae clade, *Mycolicibacillus* based on the slow-growing triviale clade, *Mycolicibacter* based on the slow-growing terrae clade, and *Mycolicibacterium* based on the fast-growing fortuitum-vaccae clade (Gupta, Lo and Son, 2018). However, due to the complicated nature of diagnosing and treating these organisms, a return to the original convention of *Mycobacterium* has been widely supported (Gupta, Lo and Son, 2018; Meehan *et al.,* 2021).

1.2 The history of tuberculosis

Tuberculosis (TB) is an ancient disease. It is estimated that *M. tuberculosis* is roughly 70,000 years old (Hayman, 1984). However, it is believed that the *Mycobacterium* genus originated over 150 million years ago, during the Jurassic period, with the *Mycobacterium ulcerans* species (Hayman, 1984). As recent as 3 million years ago, there were *M. tuberculosis* ancestors which were infecting the early hominids in East Africa (Gutierrez *et al.,* 2005), and there have been Egyptian mummies from 2400 BC which show skeletal deformities consistent with tuberculosis infection (Morse, Brothwell and Ucko, 1964).

The earliest written documents describing tuberculosis are from around 2000 to 3000 years ago, and these were found in China and India (Barberis *et al.,* 2017). Tuberculosis is also mentioned in the Old Testament of the bible where the ancient Hebrew word *schachepheth* is used to describe the disease (Daniel and Daniel, 1999). Furthermore, the ancient Greeks referred to the disease as *Phtisis* where the symptoms were accurately identified by Hippocrates (Barberis *et al.,* 2017). During this time, some of the earliest tuberculosis researchers proposed that the disease was infectious and could therefore be transmitted from person to person (Daniel, 2006).

During the 1700's, tuberculosis was known as the 'white plague' due to the paleness of those suffering with the disease. The term 'tuberculosis' was not used until 1834 when Johann Lukas Schonlein used the word to describe diseases that were characterised by the presence of tubercules (Barberis *et al.,* 2017).

It was not until the late 1800's that tubercule bacilli were first successfully isolated and proven to be infectious. Robert Koch identified the presence of the bacterium in animal serum, isolated them, and then inoculated laboratory animals with the bacilli to reproduce the disease. Koch then presented these findings to the Society of Physiology on the 24th March 1882 where he announced his discovery of the bacterium responsible for causing tuberculosis. This was during a period where the disease was responsible for the deaths of one in every seven people living in the United States and Europe (Gradmann, 2001). One hundred years to the day later, The 24th of March became World TB Day. This is a day dedicated to educating the public about the global impact tuberculosis still has (CDC, 2016).

1.3 Tuberculosis

Today, tuberculosis is the second biggest infectious killer worldwide behind COVID-19, and the thirteenth leading cause of death globally (WHO, 2022). During the year 2021, it is estimated that 10.6 million people became ill with tuberculosis including 1.2 million children (WHO, 2022). Tuberculosis is predominantly a disease of the poor, with 87% of new cases in 2021 coming from 30 of the high burden countries. These include countries such as India, China, and Indonesia (Xue *et al.,* 2022). India was responsible for over a quarter of new tuberculosis cases during 2021. This is predominately due to the lack of available diagnostics. Typically, tuberculosis in India is diagnosed through sputum smears taken throughout the day. There is a high margin of error involved in this test, and positive tuberculosis cases will often be diagnosed after an individual has become sick (Xue *et al.,* 2022).

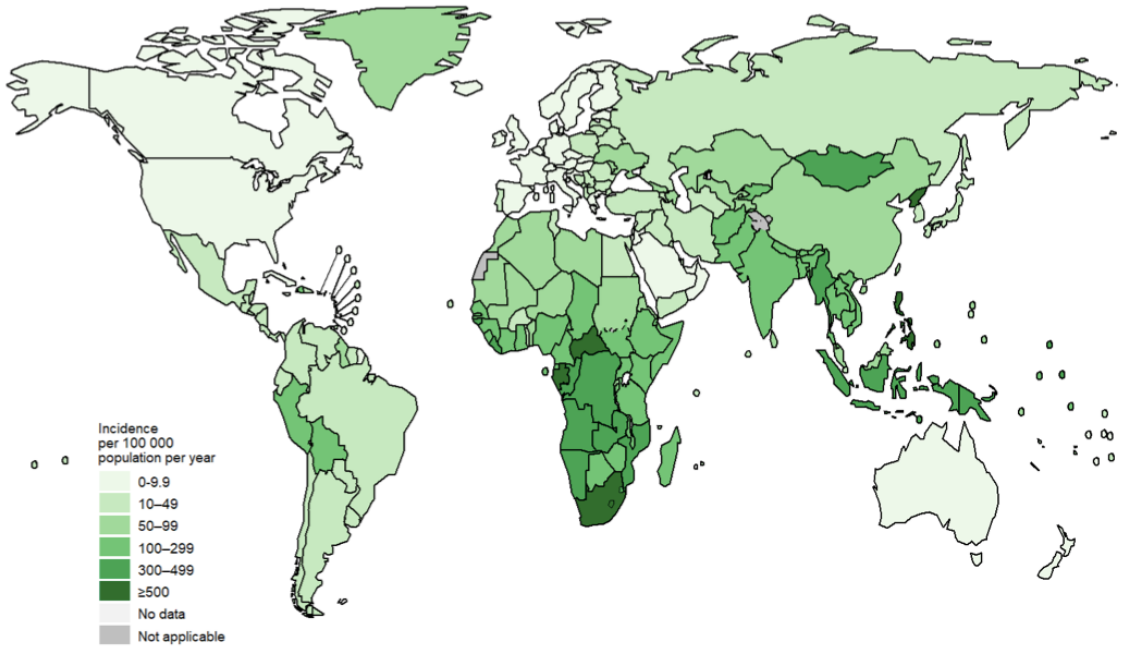

Figure 1: Estimated tuberculosis incidence rate during 2021. Darker green indicates higher incidence rate. Incidence is defined as proportion of people with a new episode of TB. Highest incidence rates during 2021 were mostly seen in African countries. Figure taken from World Health Organisation, (2022). Global Tuberculosis Report.

As shown in Figure 1, tuberculosis is present all over the world. According to the Office for National Statistics, there are around 4000 people infected with the disease each year in the UK (GOV.UK, 2022). The infected demographic is largely found in the London area, and this consists mostly of individuals born outside of the UK (GOV.UK, 2022). The UK remains a low incidence country however, with an infection rate of 7.3 per 100,000 people in 2020. This is below the 10 per 100,000 which the World Health Organisation defines as a low incidence country. In contrast, high incidence is defined as more than 100 infections per 100,000 people (WHO, 2021).

Tuberculosis will primarily affect the lungs, but it is capable of infecting other parts of the body such as the brain and spine. Pulmonary tuberculosis is the most common clinical presentation of the disease, and symptoms of this infection will include a chronic cough, chest pain, weakness, fatigue, weight loss, fever, and night sweats (Zaman, 2010). Around 95% of people infected with the pathogen will never go on to develop active tuberculosis, with just 5% of infected individuals going on to develop the disease (Haddad *et al.,* 2018). Tuberculosis will predominantly affect adults, but no age group is immune to infection. Those individuals most at risk of developing active tuberculosis are people living in low to middle income countries, and people infected with human immunodeficiency virus (HIV). Those infected with HIV are 16 times more likely to develop active tuberculosis. Malnutrition can also be a contributing factor to an increased risk of active tuberculosis, as during 2021 2.2 million cases of reported tuberculosis could be attributed to undernutrition (WHO, 2022).

Tuberculosis will primarily be transmitted through the inhalation of aerosolized droplets from an infected individual. These droplets, containing the tubercule bacilli, will be deposited into the lungs where there are several possible outcomes (Churchyard *et al.,* 2016). First, and the most common outcome, is that the host will immediately clear the pathogen from the body and prevent infection. Second, the body is unable to deal with the invading bacilli and this leads to active tuberculosis. Third, the host will contain the bacteria, but will not clear them from the body. This leads to a latent infection which can last a person's lifetime. This occurs in around 40% of people exposed to tuberculosis (Young, Gideon and Wilkinson, 2009). Weakening of this person's immune system, or a general reduction in health, can lead to reactivation of the latent infection and this can become active tuberculosis (Delogu, Sali and Fadda, 2013). The general life cycle of *M. tuberculosis* is shown in Figure 2.

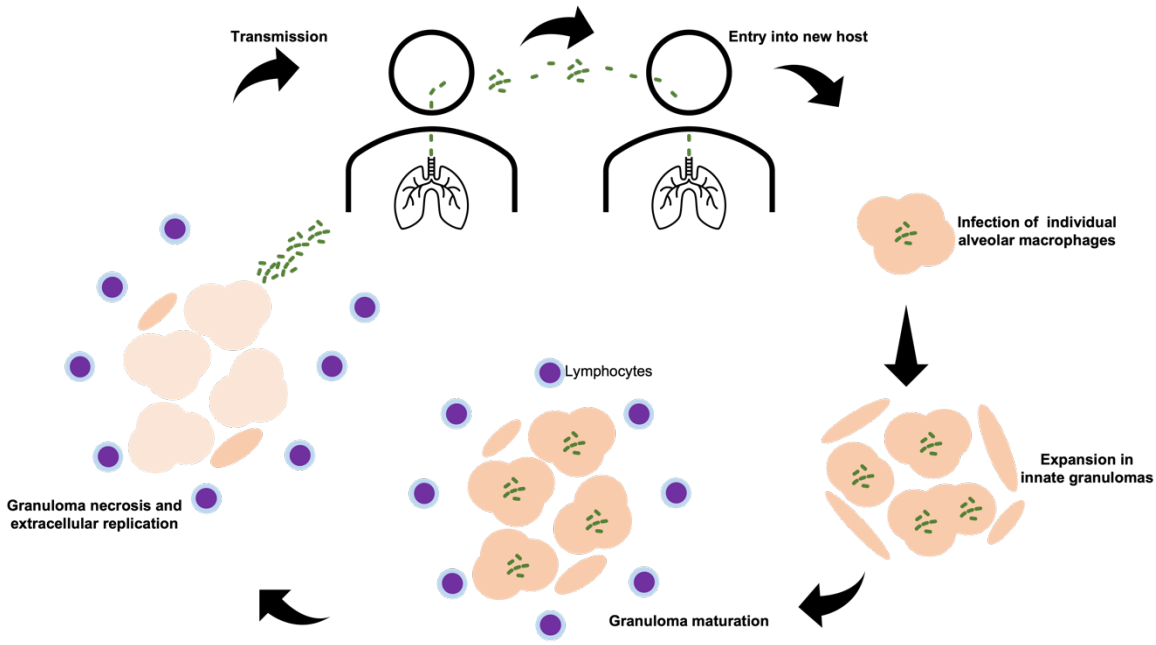

Figure 2: Life cycle of *M. tuberculosis.* Infection begins with inhalation of *M. tuberculosis* bacilli which has been released by a person with active tuberculosis. The bacilli will enter the lungs of a new host and adhere to the surface of alveolar macrophages. The macrophage engulf the bacteria and provide both protection and a mode of transport across the lung epithelium. Additional macrophages and other immune cells are recruited to deal with the growing infection, forming the granuloma. The bacteria continue to grow inside the granuloma, until necrosis occurs and the bacteria are released. At this point, they can be transmitted to a new host. Figure adapted from Cambier, Falkow and Ramakrishnan, (2014).

Upon inhalation of tubercule bacilli, and transport to the lungs, the bacteria will be engulfed by alveolar macrophages if the innate immune system has not cleared the infection (Urdahl, Shafiani and Ernst, 2011). *M. tuberculosis* produces many virulence factors, including the presence of arabinomannan within the capsule, that will inhibit the maturation of the macrophage into a phagolysosome. This enables the bacilli to establish a niche inside the immune cell where they will begin to proliferate (Chowdhury *et al.,* 2018). Infected macrophages will produce chemokines and cytokines that will attract other immune cells such as neutrophils and monocytes. This leads to the formation of a granulomas structure referred to as a tubercle. Within this structure, the bacilli can keep proliferating until an effective immune response can develop (Githinji, Gray and Zar, 2018). If the host is unable to effectively control the proliferating bacilli, it can lead to extensive damage. This is because the release of tumour necrosis-factor alpha, reactive oxygen species, and cytotoxic cells can all contribute to host damage if they are unsuccessful in eliminating the tubercule bacilli (Githinji, Gray and Zar, 2018). If the bacilli are allowed to grow without host intervention, it can lead to dissemination of the pathogen which will result in multi organ infection. Without treatment, the mortality rate in this case will be above 80% (Chowdhury *et al.,* 2018). The primary site of tuberculosis infection will be the lungs and will be referred to as the Ghon focus (Innes, Schaaf & Cotton, 2009). The Ghon focus will typically enter a state of dormancy in most people as a latent infection (MacPherson *et al.,* 2020). For most people who become ill with tuberculosis, they do so after reactivation of the Ghon focus. This can also be referred to as secondary tuberculosis and will occur in around 5% of latent tuberculosis infections (Githinji, Gray and Zar, 2018).

To diagnose active tuberculosis, several tests are used including a chest x-ray, sputum evaluation, and lipoarabinomannan urine assays. This will include an acid-fast bacilli smear, and mycobacterial culture to confirm the presence of *M. tuberculosis* (Fachri *et al.,* 2018). Sputum samples will be taken at multiple points during a day, where the Acid-Fast Bacilli test will confirm the presence of mycobacteria. It will not however diagnose the infecting species. Mycobacterial culture can be used to diagnose active tuberculosis and will be performed on both solid and liquid media. It can also be used to test for drug susceptibility to help direct the treatment approach (Pfyffer and Wittwer, 2012). Within the past few years, a lateral flow test based on the presence of mycobacterial lipoarabinomannan in urine has emerged. Although the test is not suitable for use in all situations, it has been shown to be particularly effective at diagnosing tuberculosis in individuals infected with HIV as the lower CD4 cell count improves the sensitivity of the test (Bulterys *et al.,* 2019). CD4 cells participate in protection against tuberculosis, and so the lower cell count in HIV-infected individuals allows for greater proliferation of tubercule bacilli (Lu *et al.,* 2021). For those who do not have active tuberculosis, it is possible to test for a latent infection using the Mantoux test or Interferon Gamma Release assays (Nayak and Acharjya, 2012). The Mantoux test involves injecting a purified protein derivative into the arm of a patient and observing the skin for a period of time. If a person has mycobacteria present, the purified protein derivative will cause a small, red bump to form within two days of the injection (Nayak and Acharjya, 2012). An increasingly more common test for latent tuberculosis is the Interferon Gamma Release assay. This is a much simpler test that quantifies the level of TB-specific

inflammatory cytokines in the blood. However, this is a much more expensive test, and requires technical training to perform (Pai *et al.,* 2014).

Treatment of active tuberculosis involves taking multiple drugs over a course of 6 months. This will include isoniazid, rifampin, ethambutol, and pyrazinamide. For multi-drug resistant infections, fluoroquinolones are used, and these will be required for over two years (Peloquin and Davies, 2021). Tuberculosis medication can be highly toxic to the liver and can cause other side effects such as: loss of appetite, blurred vision, nausea, vomiting, yellow coloured skin, and easy bruising and bleeding (Bansal, Sharma and Singh, 2018). Due to this, patient compliance can be poor, and this has contributed to the rise of multi-drug resistant and extensively-drug resistant strains of *M. tuberculosis* (Seung, Keshavjee and Rich, 2015).

1.4 The mycobacterial cell wall complex

The unique and complex cell wall of all mycobacteria is an important feature that enables the bacteria to evade host immune systems, survive within the alveolar macrophages and resist antibiotic treatments (Abrahams and Besra, 2018). It has been well-studied over the past 15 years, and this has led to a detailed understanding of the biosynthetic pathways involved in producing the cell wall complex (Dulberger, Rubin and Boutte, 2020).

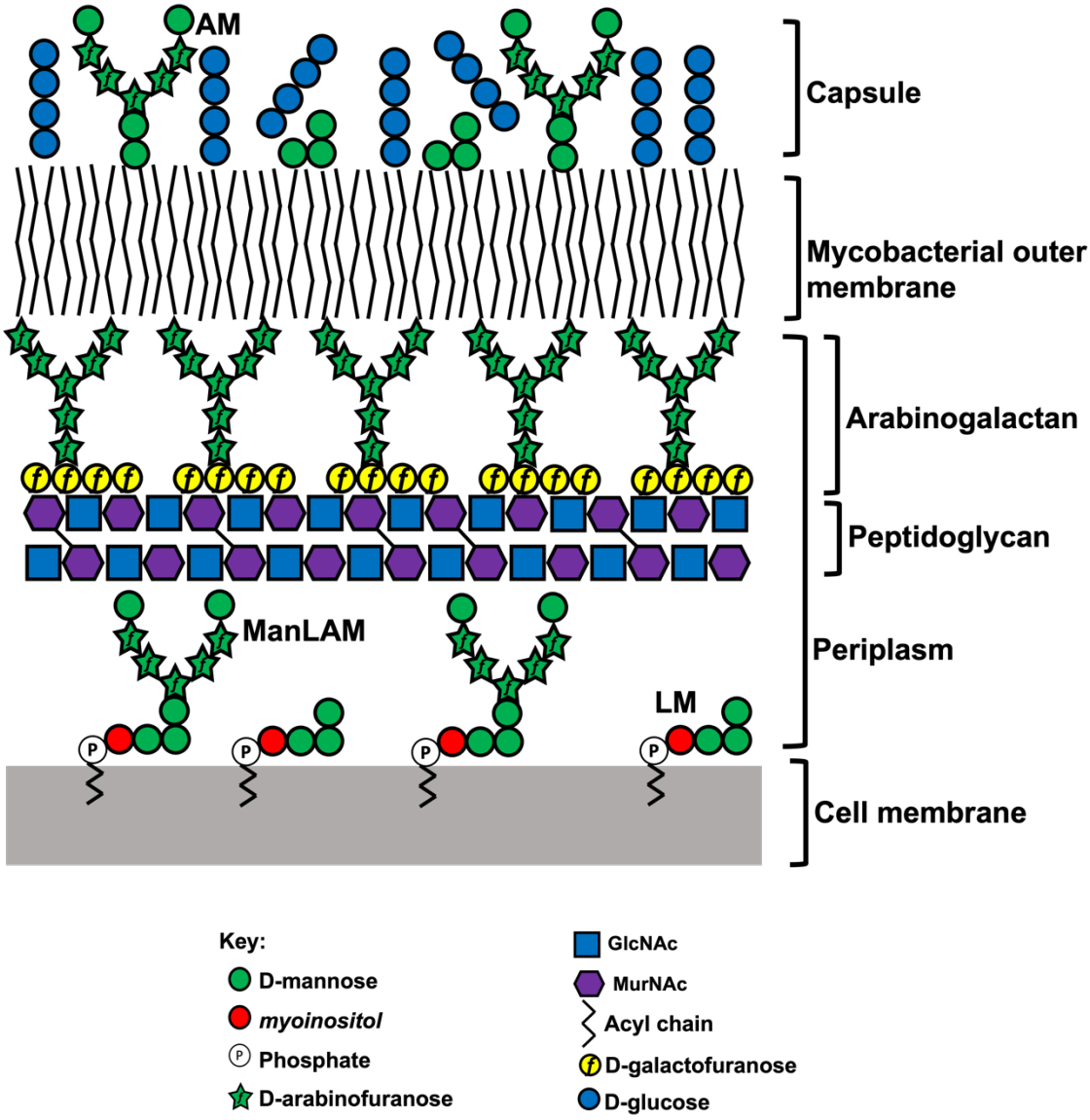

Figure 3: The mycobacterial cell wall. A cross-section schematic depiction of the mycobacterial cell wall. Prominent positions of glycolipids are shown anchored to the cell membrane. The glycan-rich capsule consists of AM and α-glucan. LM, lipomannan; ManLAM, mannose-capped lipoarabinomannan; AM, arabinomannan.

As shown in Figure 3, the mycobacterial cell envelope is a massive molecular structure that consists of three main essential components: the peptidoglycan, arabinogalactan, and mycolic acids. This was primarily studied from 1950 to 1975 and was defined by groups from Japan and France (Adam *et al.,* 1969; Lederer *et al.,* 1975; Wietzerbin-Falszpan *et al.,* 1970; Petit *et al.,* 1969). The outermost layer is the capsule, which contains a mixture of polysaccharides and secreted proteins, and has important roles in both interacting with the host immune system and in virulence (Daffe and Etienne, 1999). Biosynthesis of the mycobacterial cell envelope requires many enzymes to build and regulate the complex. There will be cell wall precursor enzymes, transport proteins, cell wall assembly proteins, and cell wall synthesis regulators involved in the process (Shetty and Dick, 2018). The whole envelope structure is rich in both lipids and carbohydrates making it an effective permeability barrier and ensuring that the pathogen is capable of surviving and thriving inside host immune systems during the infection process (Jarlier and Nikaido, 1994).

1.4.1 Peptidoglycan

Peptidoglycan is the first major component of the mycobacterial envelope. It is found in the cell wall of both Gram-positive and Gram-negative bacteria, and its primary function is to maintain the cell shape and resist osmotic pressure from the cytoplasm (Vollmer, Blanot and de Pedro, 2008). It is comprised of alternating *N*-acetylglucosamine and *N*-acetylmuramic acid residues which are then crosslinked by peptide stems. The *N*-acetylglucosamine and *N*-acetylmuramic acid residues are bonded together through β-1,4 linkages. This forms a very rigid structure which is essential in most bacteria for

growth and survival (Petit *et al.,* 1969). However, as peptidoglycan is only found in prokaryotes and some plants this has made it an ideal target for antibiotics – as reviewed by Wright, (1999).

1.4.2 Arabinogalactan

Covalently bound to the peptidoglycan layer is another polysaccharide called arabinogalactan. This is comprised of D-galactose and D-arabinose sugars in the 5-carbon furanose ring form (McNeil *et al.,* 1987). The arabinogalactan polymers are connected to the peptidoglycan layer through a rhamnose-*N*-acetylglucosamine linker unit (Besra *et al.,* 1995). As shown in Figure 4, the galactan is a linear chain of β-D-galactofuranose residues which consists of β-1,5 and β-1,6 linkages, and then highly branched arabinan chains which extend from the galactan. This consists of α-1,2, α-1,3, and α-1,5 as well as β-1,2 linkages. The non-reducing ends of the arabinan chains will serve as attachment points for mycolic acids (Liu *et al.,* 1996). Arabinogalactan has only been described in the cell wall of mycobacteria, but it is highly prevalent in many plant species (Abrahams and Besra, 2018).

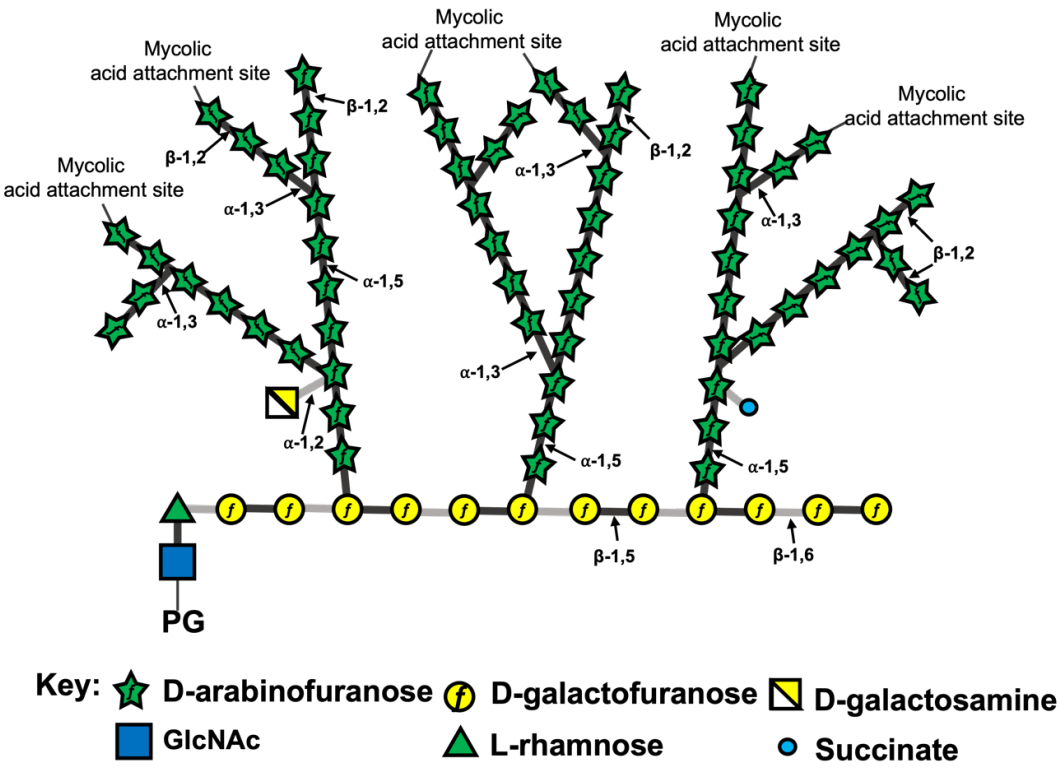

Figure 4: Schematic structure of mycobacterial arabinogalactan. Arabinan chains branch out from linear galactan. Which is connected to the peptidoglycan layer. Termini of arabinan chains serve as attachment points for mycolic acids. Key bonds are indicated by arrows.

1.4.3 Mycolic acids

The mycobacterial outer membrane is the final major component of the cell wall complex. It is composed of mycolic acids which are attached to the arabinogalactan layer. These are long chain fatty acids which consist of a long beta-hydroxy chain and a short alpha-alkyl side chain (Nataraj *et al.,* 2015). There are three classes of mycolic acids: alpha-mycolates, methoxy-mycolates, and keto-mycolates. The structure of these are shown in Figure 5. The mycolic acids are essential for cell viability and virulence, and have roles in cell wall permeability (Liu *et al.,* 1996).

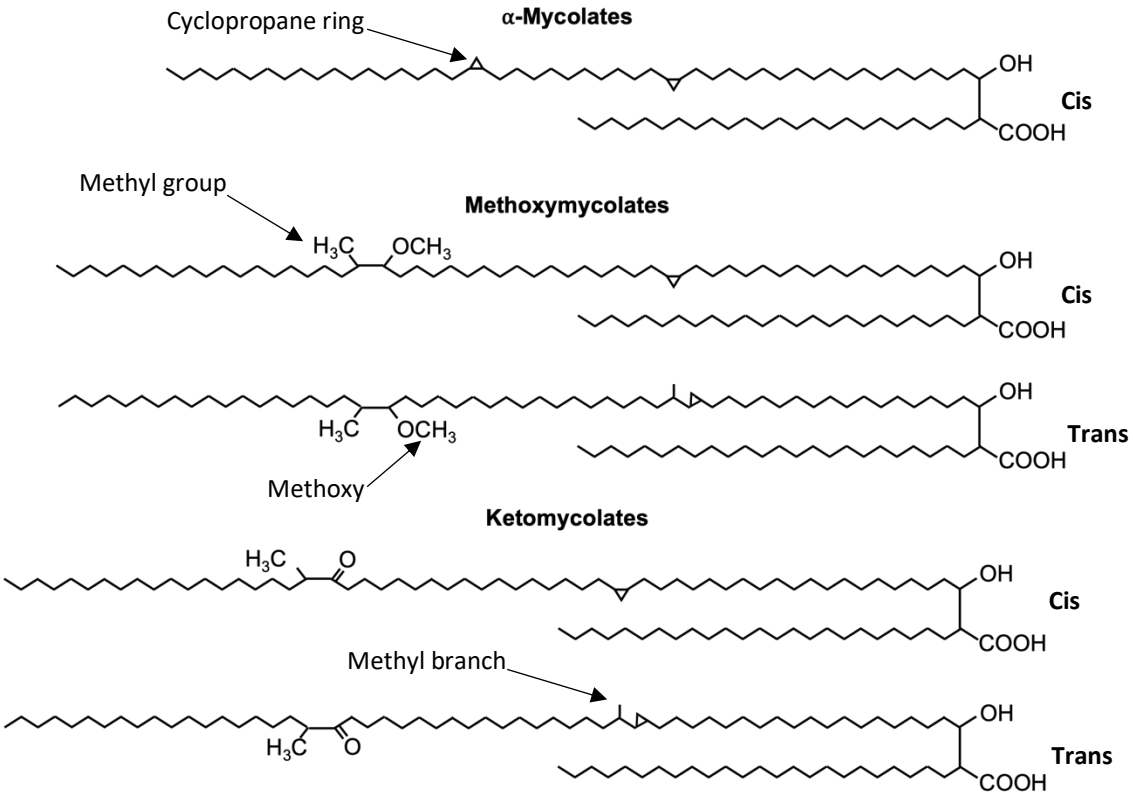

Figure 5: Mycolic acids present in *M. tuberculosis.* Structures of alpha-mycolates, methoxymycolates, and keto-mycolates are shown. Alpha-mycolates account for more than 70% of all mycolic acids whilst methoxy- and keto- mycolic acids combined account for the remaining 30%. Alpha-mycolates are cis-dicyclopropyl fatty acids whilst metho- and keto- can be either cis- or trans-cyclopropane rings. Figure adapted from Basso *et al.,* (2005).

1.5 The mycobacterial glycolipids

Within the cytoplasm and periplasm of mycobacteria there are glycolipids non-covalently anchored to the cell membrane (Dao, *et al.,* 2004). These are the phosphatidyl-*myo*-inositol mannosides (PIMs), lipomannan (LM), and lipoarabinomannan (LAM). These structures share a common biosynthetic pathway and have important roles in maintaining cell wall integrity and host immune system interactions (Guerardel *et al.,* 2002). It has been suggested by Bansal-Mutalik and Nikaido (2014), that PIMs are likely to be involved in reducing the permeability of the mycobacterial cell envelope and that this contributes to increased resistance to chemotherapeutic agents (Bansal-Mutalik and Nikaido, 2014).

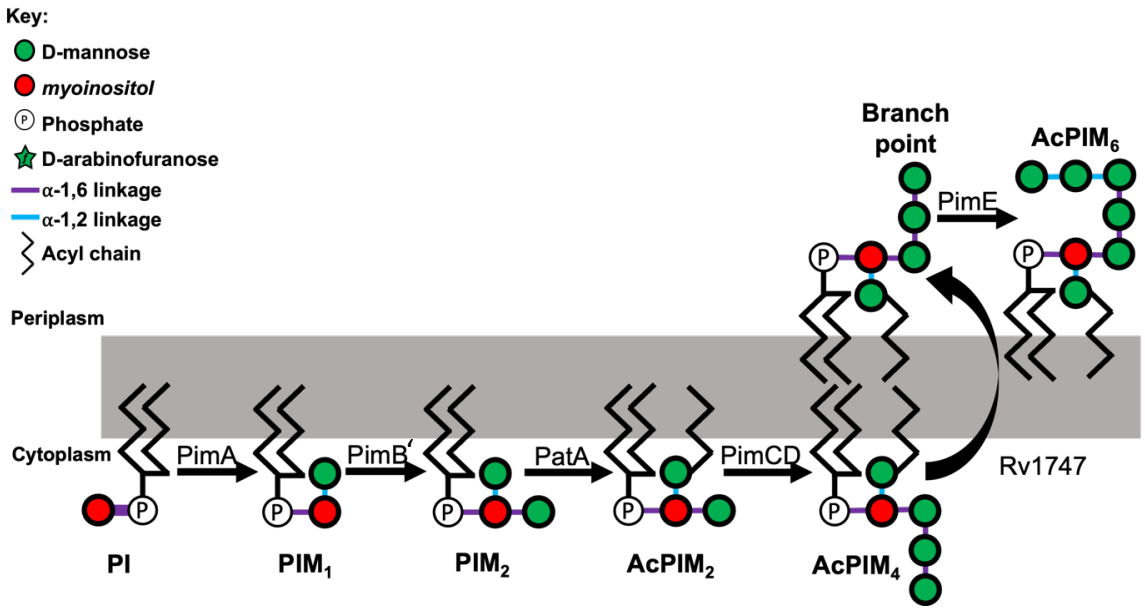

Figure 6: PIMs biosynthesis pathway. A schematic representation of the current understanding of the pathway required to synthesise PIMs. Initial biosynthesis takes place in the cytoplasm until the branch point molecule is produced. This is then translocated across the membrane into the periplasm where higher-order PIMs can be synthesised.

PIMs consist of a core phosphatidyl inositol (PI) anchor unit which can then be glycosylated with mannopyranose (Man*p*) units (Ballou, Vilkas and Lederer, 1963). Mannosylation at the O-2 and O-6 positions of the PI unit results in the formation of the mannosyl phosphate inositol (MPI) anchor (Guerin *et al.,* 2009). The MPI anchor can then be further mannosylated and acylated to form the PIM species: PIM_1, PIM_2, $AcPIM_2$, Ac_2PIM_2, $AcPIM_3$, $AcPIM_4$, Ac_2PIM_4, $AcPIM_5$, $AcPIM_6$, and Ac_2PIM_6 (Ac_xPIM_y where x is the number of acyl chains and y is the number of Man*p* units) (Guerin *et al.,* 2009). The most abundant forms of PIMs in the mycobacterial cell wall are $AcPIM_2$, Ac_2PIM_2, $AcPIM_6$, and Ac_2PIM_6 (Court *et al.,* 2011). These are predominantly found in the cytoplasm and periplasm anchored to the cell membrane (Bansal-Mutalik and Nikaido, 2014). It is predicted that the PIMs contribute to around 56% of all phospholipids in the cell envelope of mycobacteria (Court *et al.,* 2011). In addition to their roles in structural support, cell wall integrity, and permeability, it has also been suggested that PIMs have an essential role in septation and cell division (Fukuda *et al.,* 2013). This was demonstrated when Patterson *et al.,* (2003) knocked out the enzyme phosphomannose isomerase which is required for mannose metabolism in *M. smegmatis.* The result was that of a phenotype unable to grow in media unless supplemented with a source of mannose and which grew with a hyperseptation phenotype (Patterson *et al.,* 2003). More recently, Sparks *et al.,* (2023), demonstrated that septation in *M. smegmatis* is regulated by LAM. Through the use of *M. smegmatis* mutants with LAM deficiencies, they show that LAM is required for the cells to maintain cell wall integrity in media specific conditions. For example, when grown on LB agar plates, the mutant cultures formed significantly smaller colonies. However, when grown on 7H10 agar the colonies

were much more comparable to wild type. Additionally, LAM deficiencies are also shown to be associated with increased envelope deformations as well as the formation of abnormal septa and new poles (Sparks *et al.,* 2023). On the other hand, in *M. smegmatis* mutants producing abnormally large LAM, they highlight that cells form multiple septa (Sparks *et al.,* 2023). This study highlighted that LAM plays an important role in the division of mycobacteria.

The biosynthesis of PIMs begins with the phosphatidyl inositol anchor unit in the cytoplasm. The initial step involves the transfer of one Man*p* residue from a GDP-Man*p* donor to the O-2 position of the PI anchor ring to form PIM_1 by the enzyme PimA (Korduláková *et al.,* 2002). Next, a second Man*p* residue will be transferred to the O-6 position of the inositol ring by a second mannosyltransferase, PimB', to produce PIM_2 (Guerin *et al.,* 2009). Following this, the acyltransferase, PatA, will acylate the first Man*p* residue, in the O-2 position on the inositol ring, to form $AcPIM_2$ (Boldrin *et al.,* 2021). Further acylation on the inositol can be performed by an unknown enzyme to form Ac_2PIM_2 (Angala *et al*., 2014). The enzyme PimC will further mannosylate $AcPIM_2$ to form $AcPIM_3$, however currently a homologue of this enzyme has not been identified in *M. tuberculosis* (Kremer *et al.,* 2002). The hypothesised enzyme, PimD, will transfer the fourth Man*p* unit to produce $AcPIM_4$ and then subsequent acylation can be performed by an unknown enzyme to form Ac_2PIM_4 (Angala *et al*., 2014). This is discussed further below. Formation of $AcPIM_4$ is regarded as the transition point towards synthesis of the higher order PIMs, and so it is termed the 'branch point' molecule. It is hypothesised that at this point in the pathway, $AcPIM_4$ is flipped from the cytoplasm to the periplasm

by the ATP-binding cassette transporter, Rv1747, and the remaining steps in the pathway will subsequently take place in the periplasm (Glass *et al.,* 2017). However, the role of Rv1747 as a PIM transporter has yet to be proven. Glass *et al.,* (2017) argued the role of the enzyme as a transporter. This was because a *M. tuberculosis* Rv1747 mutant had an atypical PIM profile. Currently, there is no data to prove that this is the case though and the exact transporter remains unknown. Additionally, the exact point at which PIMs are flipped across the membrane has also yet to be proven. Once transported into the periplasm, biosynthesis can continue in two different pathways. $AcPIM_4$ can either be further mannosylated to produce higher order PIMs, or it can be hyper-mannosylated to form lipomannan. Within the periplasm, the mannosyltransferases can no longer rely on nucleotide-based sugars as mannose donors, and so use polyprenyl-phosphate-based mannose donors (Berg *et al.,* 2007). Up to this point, the Man*p* residues have been linked through α-1,6 linkages (Berg *et al.,* 2007). In the biosynthesis of higher order PIMs, $AcPIM_4$ is further mannosylated by PimE to produce $AcPIM_5$ and then $AcPIM_6$. The two additional Man*p* residues are added via an α-1,2 linkage (Morita *et al.,* 2006). This pathway is shown in Figure 6. Alternatively, $AcPIM_4$ can be hyper-mannosylated by the mannosyltransferases MptA and MptB to produce lipomannan (Mishra *et al.,* 2008). It has been suggested by Crellin *et al.,* (2008) that the lipoprotein LpqW will direct $AcPIM_4$ towards either higher order PIMs synthesis or lipomannan biosynthesis (Crellin *et al.,* 2008). The α-1,6 linked mannan backbone of LM is then decorated with α-1,2 linked Man*p* residues via the enzymes MptC and MptD. This results in the formation of mature LM (Mishra *et al.,* 2011). This pathway is summarised in Figure 7.

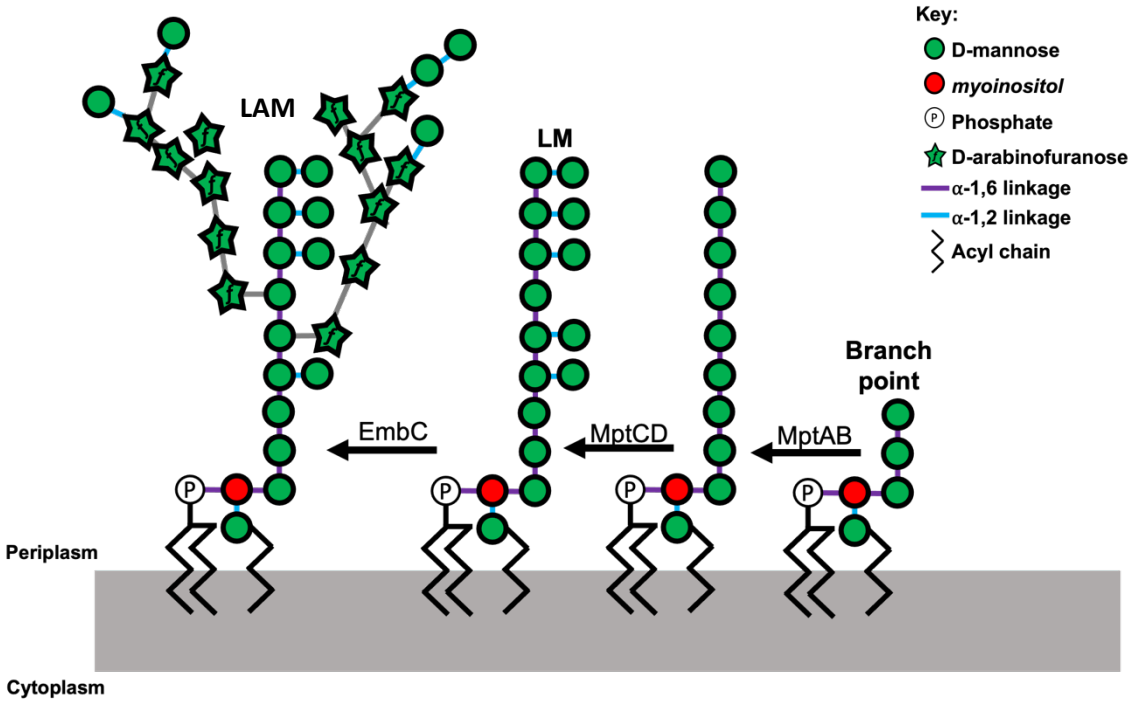

Figure 7: LM and LAM biosynthesis pathway. A schematic representation of the current understanding of the pathway required to synthesise LM and LAM starting from $AcPIM_4$. The branch point molecule is translocated across the membrane into the periplasm. Production of LM requires hyper-mannosylation of the mannan backbone. This can then be further elaborated with an arabinan domain to produce LAM.

Mature LM can be further modified to produce LAM. To do this, around 80 arabinofuranose residues are added in a similar structure to that of the arabinogalactan domain. This is initiated by an unknown D-arabinofuranose transferase. Following this, EmbC will elongate the arabinan domain adding D-arabinofuranose residues with α-1,5 linkages (Shi *et al.,* 2006). An enzyme named AftC, also required for arabinogalactan synthesis, will integrate α-1,3 linked branch point arabinofuranose residues (Birch *et al.,* 2008). The arabinan domain will then be terminated with β-1,2 linked arabinofuranose residues. This is catalysed by AftB (Jankute *et al.,* 2017; Seidel *et al.,* 2007). Finally, the LAM molecule can be capped. In many slow-growing pathogenic species such as *M. tuberculosis* LAM is capped with α-1,2 linked Man*p* residues to produce ManLAM. This is catalysed by the enzyme CapA (Rv2181) which will add the first Man*p* residue (Dinadayala *et al.,* 2006). MptC will then add additional Man*p* residues (Kaur *et al.,* 2008). This is done using polyprenyl-phosphate-based mannose donors (Stoop *et al.,* 2013). In some fast-growing, non-pathogenic mycobacteria, the LAM is capped with phosphatidylinositol. This modification can, however, be move diverse. In some species, such as *M. chelonae,* their LAM is uncapped and termed AraLAM (Brown and Taffet, 1995). The function of CapA was characterised by Dinadayala *et al.,* (2006) who disrupted the gene, *Rv1635c*, by transposition in *M. tuberculosis* CDC1551. They found that when comparing the LAM to that of the wild-type strain, the mutant LAM migrated more rapidly and it did not react with concanavalin A, a carbohydrate-binding protein, which the wild-type LAM did. Furthermore, since there is no orthologue of *Rv1635c* in *M. smegmatis,* a recombinant strain was constructed and CapA was expressed. The result of this was the LAM from this recombinant strain had a higher molecular weight

than that of the wild-type, and was reactive with concanavalin A. In addition, structural analysis revealed the presence of a single mannose residue capping the terminal arabinan. These results suggested that CapA is a mannosyltransferase responsible for synthesising the first mannose residue in mannose-capped LAM (Dinadayala *et al.,* 2006).

As described previously, the mono-acylated PIM_2 and PIM_6 can be further acylated on the inositol, by an unknown enzyme, to produce Ac_2PIM_2 and Ac_2PIM_6. However, the mono-acylated forms are the dominant PIMs in standard culture conditions, with the di-acylated forms being relatively low in abundance (Larrouy-Maumus *et al.,* 2016). This may suggest that acylation of $AcPIM_2$ and $AcPIM_6$ is a response to stress, as Larrouy-Maumus *et al.,* (2016), report that the abundance of Ac_2PIM_2 and Ac_2PIM_6 increases in response to increasing levels of salt (Larrouy-Maumus *et al.,* 2016). This suggestion has been further supported by Nguyen *et al.,* (2022), who report that acylation is induced by increased concentrations of benzyl alcohol, and that this is a rapid response to stress. Additionally, they show that this is an enzymatic response as acylation occurs when translation has been inhibited (Nguyen *et al.,* 2022). These findings support the hypothesis that inositol-acylation is a response to severe membrane stress in mycobacteria. Nguyen *et al.,* (2022) hypothesise that inositol-acylation helps to maintain cell wall integrity and low permeability of the membrane. This could be utilised by the bacteria during antibiotic treatment for example. It is therefore a last resort to ensure continued survival of the bacteria, and is not quickly reversible (Nguyen *et al.,* 2022).

It is predicted that PIM biosynthesis predominately occurs during logarithmic growth in mycobacteria, but it is downregulated during stationary phase (Morita *et al.,* 2004). This prediction is based on the fact that the universal stress protein (USP), which inhibits PIM transport, is downregulated during log phase (Pang *et al.,* 2007), but upregulated in stationary phase by the activator proteins DosR and PknG (Rustard *et al.,* 2008). Currently, there is no PIM abundance data to support this. Activated USP will bind to the putative PIM transporter Rv1747 to inhibit transport of $AcPIM_4$ to the periplasmic face of the membrane (Glass *et al.,* 2017). Therefore, it is hypothesised that when USP is active, in stationary phase, the relative abundance of PIMs in the periplasm will be reduced (Dulberger, Rubin and Boutte, 2020). This hypothesis has been further supported by Zhang *et al,* (2013) who reported that *pimE* is less important for cell survival in chronic stage mouse infections compared to active phase infections. This suggests that the biosynthesis of higher order PIMs is not as important during stationary phase as it is during log phase (Zhang *et al,* 2013). During the early stages of infection, when the cells are undergoing logarithmic growth, PIMs are required to induce cytokines to form the granuloma. Therefore, it is logical that there should be a higher abundance of PIMs during this stage compared to stationary phase (Dulberger, Rubin and Boutte, 2020).

LM and LAM are predicted to have an alternative expression pattern to PIMs. In this case, expression of LM and LAM is relatively low during logarithmic growth, but they are highly expressed during stationary phase (Dulberger, Rubin and Boutte, 2020). It has also been show by Bacon *et al.,* (2014) that during nutrient-depletion in stationary

phase, mycobacteria will modify the LAM to have increased arabinan chains in response to the stress (Bacon, *et al.,* 2014). Furthermore, Betts *et al.,* (2002) describe how the gene *lpqW* is upregulated during periods of starvation (Betts *et al.,* 2002), but the genes *embC* and *mptA* are downregulated during log phase (Peterson *et al.,* 2019). It would therefore appear that there is upregulation of genes involved in LM and LAM synthesis during stationary phase, but a downregulation of these genes during logarithmic growth.

There have been several studies that have investigated how knock out of genes involved in the PIMs/LM/LAM biosynthesis pathway will affect cell viability. Previous studies have shown that the genes *pimA* and *pimB* are essential in *M. smegmatis* and knock-out of the *patA* gene will result in severe growth defects. However, knock-out of *pimE*, the protein product of which is responsible for committing the branch point PIM to synthesis of higher order PIMs, results in much more mild growth defects. When grown on solid media, a mutant *pimE* colony appears small and lumpy compared to the larger wrinkled phenotype of the wild-type cells (Eagen *et al.,* 2018). These studies have demonstrated that genes involved in the earlier stages of the PIMs pathway are essential to mycobacteria, but mycobacteria can survive when genes involved in the production of higher-order PIMs are lost.

1.5.1 Structure and function of lipoarabinomannan

It is estimated that LAM contributes to around 15% of the total mass of mycobacterial cells (Lowary and Achkar, 2022). Combined with its role as an immunomodulator, this

has made it a good target for tuberculosis diagnosis. Anti-LAM antibodies have long been used to detect LAM or LAM fragments in urine samples of immunocompromised individuals, such as HIV positive patients, due to the high *M. tuberculosis* load and increased quantity of LAM in the urine (Flores, Cancino and Chavez-Galan, 2021). However, recent improvements in antibody generation have resulted in more sensitive anti-LAM antibodies with higher affinity for the antigen. This has resulted in more effective LAM based diagnostic testing in HIV negative individuals (Sigal *et al.,* 2018).

As eluded to above, lipoarabinomannan has a tripartite structure that begins with a phosphatidylinositol lipid anchor, followed by a mannan core, and finally a capped-arabinan domain (Lowary and Achkar, 2022). This is shown in figure 8.

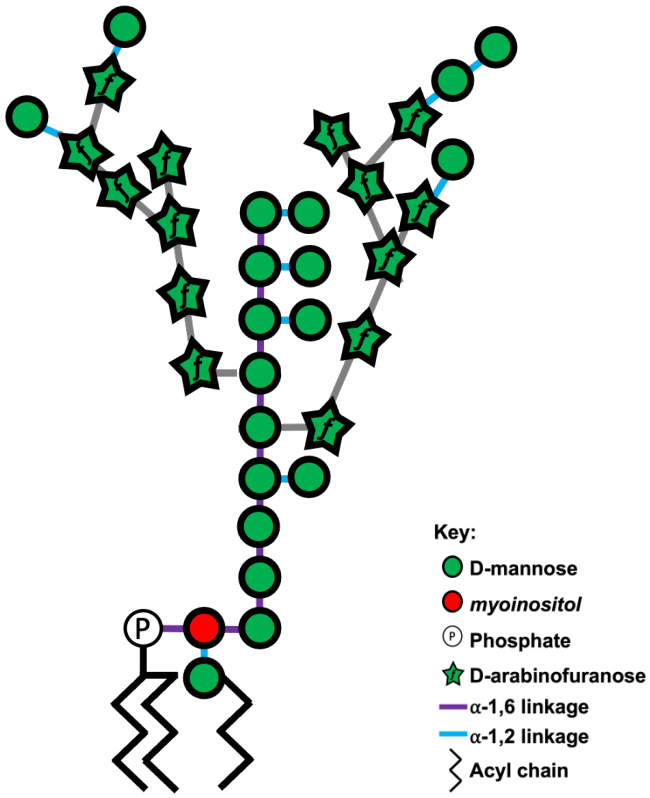

Figure 8: Structural schematic of lipoarabinomannan. Three structural domains characterise LAM. First, a phosphatidylinositol lipid anchor; secondly, an α-1,6 linked mannan backbone with α-1,2 linked mannose side chains; and thirdly, a mannose-capped arabinan domain. The precise number of Man*p* residues in the mannan backbone is not currently known.

The immunomodulatory properties of LAM have previously been well studied. The host immune system can have a number of responses to the lipoglycan and these will vary in severity (Correia-Neves *et al.,* 2019). However, little is currently known about which parts of the molecule are required to trigger an immune response. Previously, it was believed that the mannose caps of ManLAM were vital to the pathogenesis of *M. tuberculosis* infection (Maeda *et al.,* 2003). This was performed with purified ManLAM. This was until Afonso-Barroso *et al.,* (2013) showed that the mutations in the mannose caps of *M. tuberculosis* had no effect on the virulence of the pathogen as well as having very little impact on triggering inflammatory responses in mouse macrophages (Afonso-Barroso *et al.,* 2013). There are several host cell receptors which will interact with mycobacteria during the initial infection process, for example Toll-like receptors and C-type lectins (Correia-Neves *et al.,* 2019). These pathogen recognition receptors will recognise and bind to ManLAM through carbohydrate recognition domains which are present on the surface of innate immune cells such as macrophages (Schnaar, 2015). These receptors include the mannose receptor, DC-SIGN, DC-SIGNR, Dectin-2, and langerin. They have been shown to interact with the mannose caps of purified LAM (Yonekawa *et al.,* 2014). The recognition and binding of ManLAM by receptors on innate immune cells will induce endocytosis and internalisation of the tuberculosis bacilli. Furthermore, it has been shown that purified ManLAM can trigger antimicrobial signalling pathways via the C-type lectin Dectin-2 in immune cells which will result in the secretion of pro-inflammatory cytokines (Decout *et al.,* 2018).

Once engulfed by alveolar macrophages, the role of ManLAM is not over. Mycobacteria will prevent maturation of the phagosome and fusion with lysosomes to ensure the bacilli can survive (Fratti *et al.,* 2003). This is facilitated by LAM which acts as a mimic to do so. The host cell lipid, phosphatidylinositol 3-phosphate, is required by macrophages to drive phagosome maturation and lysozyme fusion. However, its formation and accumulation has been shown to be inhibited by the presence of isolated ManLAM meaning that phagosome maturation cannot occur (Torrelles and Schlesinger, 2010; Sweet *et al.,* 2010).

1.5.2 Capsular arabinomannan

As shown in Figure 3, LAM is not thought to be present on the outermost surface of mycobacterial cells (Alsteens *et al.,* 2008; Kalscheuer *et al.,* 2019). Consequently, one mechanism for LAM to interact with host cell receptors is via processing and transport to the capsule. The capsule has been studied in mycobacteria for more than 60 years (Barksdale and Kim, 1977). These early studies were focussed on the capsules of *M. leprae* and *M. lepraemurium* and they concluded that the capsules were accumulations of released glycopeptidolipids (Barksdale and Kim, 1977). However, later studies have shown that mycobacterial capsules are diverse in their make-up, consisting of polysaccharides, proteins, and small amounts of lipids (Ortalo-Magne *et al.,* 1995; Ortalo-Magne, Andersen and Daffe, 1996). It has been shown that in slow-growing mycobacteria, polysaccharides will be the main constituent of the capsule, whereas proteins will dominate in fast-growing mycobacteria (Ortalo-Magne *et al.,* 1996). In the *M. tuberculosis* capsule there are three major polysaccharides: α-D-glucan; D-arabino- D-

mannan (AM); and D-mannan (Kalscheuer *et al.,* 2019). As shown in Figure 9, the structure of the arabinomannan found in the capsule looks to be identical to the carbohydrate moieties found in LAM in the periplasm.

If the capsular AM is a derivative of periplasmic LAM, then a currently unknown enzymatic step is required to remove the PI anchor from the molecule (Pitarque *et al.,* 2008). It has been reported that LAM is restricted to the periplasm, so the mechanism by which AM is able to travel to the capsule is also unknown (Hoffmann *et al.,* 2008). Two different studies have suggested that a lipoprotein, LprG, could be involved in transferring LAM from the periplasm to the capsule (Shukla *et al.,* 2014; Gaur *et al.,* 2014). In either case, it could be possible that the missing enzymatic step required to cleave the PI anchor from LAM could take place either at the periplasm prior to AM transport to the capsule, or in the mycomembrane during transport of LAM to the capsule (Kalscheuer *et al.,* 2019). In support of these hypotheses, mycobacteria produce extracellular vesicles, and it has been shown that these extracellular vesicles in pathogenic mycobacteria are enriched in lipoproteins. Furthermore, lipidomic analysis revealed that the vesicles originate at the cytoplasmic membrane and travel to the capsule during phagosome infection (Kalscheuer *et al.,* 2019). Additionally, the extracellular vesicles are abundant with LAM. It is therefore possible that the missing enzymatic step could be happening inside the vesicle (Kalscheuer *et al.,* 2019). It has been shown that under standard growth conditions, the major capsular polysaccharide is α-D-glucan (Glatman-Freedman *et al.,* 2004). However, it is possible that this is not the case in different growth conditions. It is therefore likely that α-D-glucan and AM have

different secretion pathways. Synthesis of AM could start in the cytoplasm where $AcPIM_4$ is flipped across the cell membrane into the periplasm, allowing for biosynthesis of LAM to take place. Following this, LAM is processed by an unknown enzyme to produce AM, which is then trafficked to the capsule where it is able to interact with the host immune system as described previously. This pathway is summarised in Figure 10.

As shown in Figure 10, for LAM to be processed into AM, an unidentified enzyme is required to cleave the PI anchor from the molecule. The structure of LAM includes an α-1,6 linked mannan backbone that is covalently attached to the PI anchor. Therefore, it is possible that the missing enzyme is cleaving the mannan backbone close to the PI anchor allowing the resulting AM product to be trafficked to the capsule. Enzymes involved in cleaving glycosidic bonds, such as those found in the mannan backbone, are called glycoside hydrolases and polysaccharide lyases.

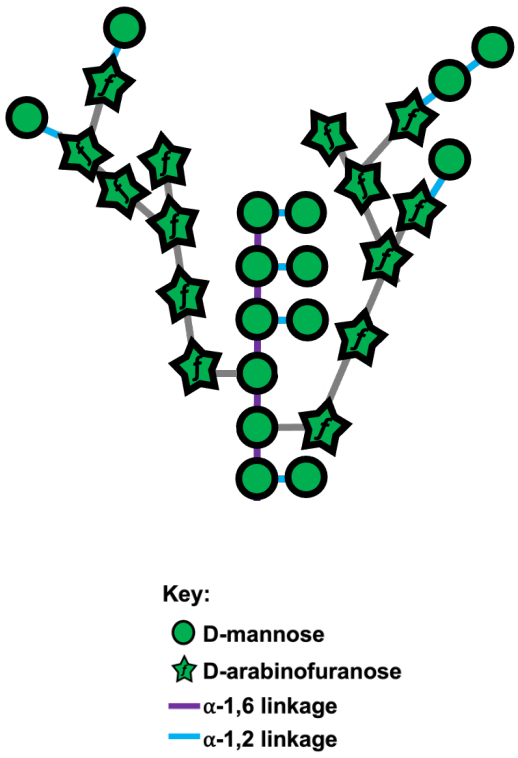

Figure 9: Structure of capsular arabinomannan. The α-1,6 mannan core is decorated with α-1,2 linked mannopyranose residues, and arabinan side chains. Terminal arabinan residues are capped with α-1,2 linked mannopyranose (Ortalo-Magne, Andersen and Daffe, 1996). The structure of capsular AM is identical to that of the carbohydrate domain of lipoarabinomannan.

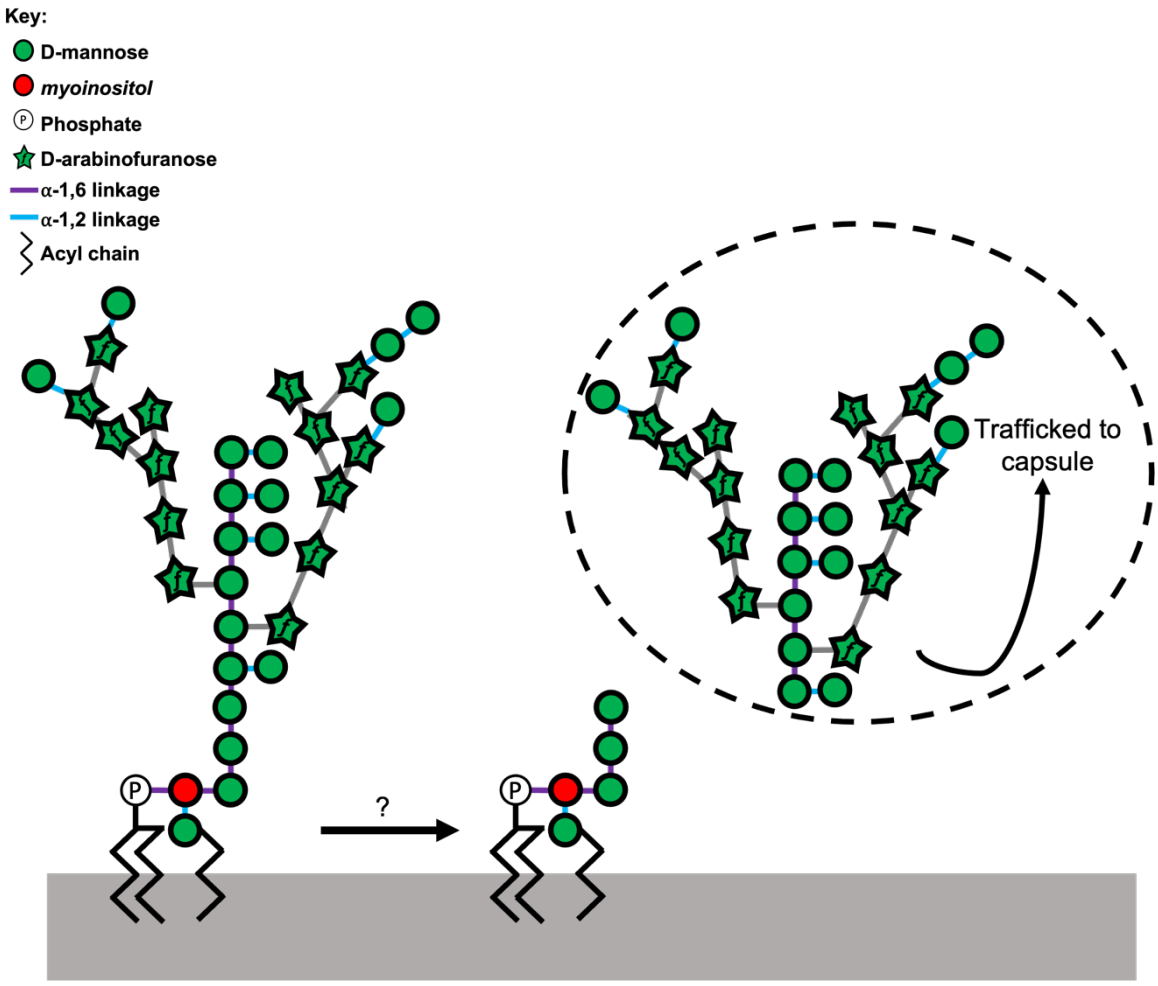

Figure 10: Pathway of LAM being processed into AM. An unidentified enzymatic step is represented by a question mark. Cleavage of the lipid carrier would result in a carbohydrate moiety similar to that found in capsular AM.

1.6 Glycoside Hydrolases

Carbohydrates play a variety roles in life. They act as structural components of cell walls, are involved in cell-cell signalling, and can be used as energy sources (Ardèvol and Rovira, 2015). They are the most abundant biomolecules in nature and exist in diverse structures. This means there needs to be a diverse group of enzymes that are responsible for synthesising, degrading, and modifying these glycans (Davies and Henrissat, 1995). This group of proteins are called carbohydrate-active enzymes, or CAZymes, and they include glycoside hydrolases (GHs), glycosyltransferases (GTs), polysaccharide lyases (PLs), and carbohydrate esterases (Davies, Gloster and Henrissat, 2005). Carbohydrates are held together by glycosidic bonds, and the synthesis and cleavage of these bonds is the responsibility of GTs and GHs/PLs respectively (Ardèvol and Rovira, 2015).

Glycoside hydrolases are found in most, if not all living organisms and will be involved in metabolism, pathogenesis, virulence, and defence against antimicrobials (Naumoff, 2011). Due to the considerable diversity of characterised GHs, and the variety of roles they play, the enzymes are grouped into families. To date, there are over 180 GH families listed on the CAZy database (www.cazy.org) (Henrissat and Romeu, 1995). These families are based on shared similarities in amino acid sequences and substrate specificities. GH families can also be grouped into clans. A clan is a group of GH families which share significant similarities in tertiary structures, catalytic residues, and their mechanism. These clans are assigned a letter, and currently GH clans A-R exist (Voung and Wilson, 2010). It is believed that clans consist of GHs that have a common

evolutionary ancestry (Amin *et al.,* 2021). Alternatively, GHs can be classified based on whether they cut carbohydrates at the end of the glycan chain to produce monomers (exo-acting), or if they cut in the middle of a glycan chain (endo-acting) (Davies and Henrissat, 1995). This is shown in Figure 11.

Glycoside hydrolases can also be classified based on their mechanism of action. GHs can either be inverting or retaining enzymes. This is regarding whether hydrolysis involves retention or inversion of the anomeric carbon – shown in Figure 12 (Davies and Henrissat, 1995). Typically, there are two catalytic residues required which are usually aspartic or glutamic acids and they will be closely located to each other. In retaining enzymes there is an average distance between the two catalytic residues of around 5.5 Å. In inverting enzymes, this distance is greater with an average of around 10 Å between the two residues (Davies and Henrissat, 1995). These residues will act as either a general acid/proton donor, or as a base/nucleophile to cleave a glycosidic bond (McCarter and Withers, 1994).

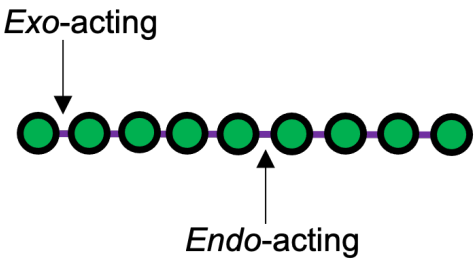

Figure 11: Classification of GHs based on location of action. Exo-acting GHs cut at the end, typically the non-reducing end, of a glycan chain. Endo-acting GHs cleave in the middle of a glycan chain.

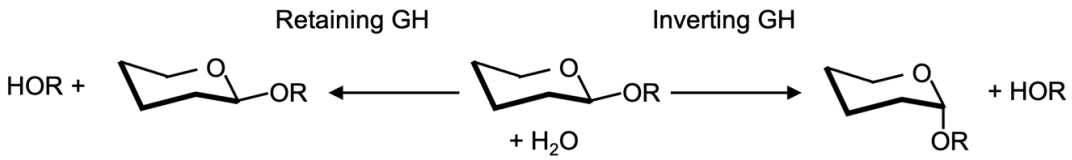

Figure 12: Classification of GHs based on mechanism of action. Retaining and inverting mechanism is shown, based on configuration of anomeric carbon after hydrolysis (Davies and Henrissat, 1995).

1.6.1 Glycoside hydrolases of *M. tuberculosis*

According to the CAZy database, *M. tuberculosis* H37Rv encodes 32 known glycoside hydrolase from 17 different GH families. Of these 32 genes, 15 belong to the GH13 and GH23 families (van Wyk *et al.,* 2017). To date, only a proportion of these genes have been biochemically characterised. Therefore, it is only possible for their function to be hypothesised based on the GH family they are a member of. As shown in Table 1, the 32 GHs of *M. tuberculosis* are grouped into 5 main categories: α-glucan targeting enzymes, β-glucan targeting enzymes, peptidoglycan remodelling enzymes, α-mannan degrading enzymes, and arabinofuranose degrading enzymes.

Table 1: Glycoside hydrolases of *M. tuberculosis* H37Rv

Name	Gene Name	Glycoside Hydrolase Family	3D Structure Determined?
α-glucan targeting enzymes			
Rv1327c	*glgE*	GH13	PDB: 4U33
Rv1326c	*glgB*	GH13	PDB: 3K1D
Rv1562c	*treZ*	GH13	No
Rv1564c	*treX*	GH13	No
Rv0126	*treS*	GH13	PDB: 4LXF
Rv1563c	*treY*	GH13	No
Rv2741	*aglA*	GH13	No
Rv2402	*Rv2402*	GH15	No
Rv3031	*Rv3031*	GH57	No
Rv2006	*otsB1*	GH65	No

Rv3401	*Rv3401*	GH65	No
Rv1781	*malQ*	GH77	No
β-glucan targeting enzymes			
Rv0186	*bglS*	GH3	No
Rv3096	*Rv3096*	GH5	No
Rv0062	*celA1*	GH6	PDB: 1UP0
Rv1089	*celA2b*	GH12	No
Rv0315	*Rv0315*	GH16	No
Peptidoglycan remodelling enzymes			
Rv0237	*lpqI*	GH3	PDB: 5G3R
Rv2450c	*rpfE*	GH23	PDB: 4OW1
Rv1009	*rpfB*	GH23	PDB: 4EMN
Rv1022	*lpqU*	GH23	No
Rv1230c	*Rv1230c*	GH23	No
Rv0867c	*rpfA*	GH23	No
Rv1884c	*rpfC*	GH23	No
Rv2389c	*rpfD*	GH23	No
Rv3896c	*Rv3896c*	GH23	No
Rv2525c	*Rv2525*	GH25*	PDB: 4PMR
α-mannan degrading enzymes			
Rv0648	*Rv0648*	GH38	No
Rv0365c	*Rv0365c*	GH76	No

Rv0584	*Rv0584*	GH92	No
Arabinofuranose degrading enzymes			
Rv1754c	*Rv1754c*	GH183	No
Rv3707c	*Rv3707c*	GH183	PDB: 8AN0

* Not yet classified as a GH25 as no biochemical data to support it.

1.6.2 Alpha-glucan targeting enzymes

Alpha-glucan is a polysaccharide consisting of D-glucose monomers. It is commonly found in bacteria, yeast, plants, and insects. In mycobacteria, α-glucan is used to synthesise carbohydrates such as trehalose and glycogen (Rashid *et al.,* 2016). As shown in Table 1, a large proportion of *M. tuberculosis* GH encoding genes are predicted to be involved in targeting α-glucan. Furthermore, of these α-glucan targeting enzymes, over half belong to the family GH13. This family is one of the largest families in the CAZy database with over 20 different enzymatic activities associated with these proteins. Due to this reason, the GH13 family was one of the first to be divided into subfamilies, where each subfamily is only associated with one enzymatic activity (Stam *et al.,* 2006).

1.6.3 Beta-glucan targeting enzymes

Beta-glucans are polysaccharides that are composed of β-glucose monomers. For example, cellulose is comprised of β-glucan. As shown in Table 1, *M. tuberculosis* possess 5 genes that are predicted to be involved in targeting β-glucan. The genes Rv0062 and Rv1089 for example have been shown to be capable of hydrolysing acid swollen cellulose and other β-glucan substrates (Varrot *et al.,* 2005; Mba Media *et al.,* 2011). However, despite *M. tuberculosis* having the ability to hydrolyse cellulose-like substrates, the pathogen is not considered to be cellulolytic as it has yet to be proven that the organism can utilise the crystalline form of cellulose (Koeck *et al.,* 2014). Furthermore, as *M. tuberculosis* and many other mycobacteria are present in an intracellular environment, it is unlikely that they would utilise cellulose as an energy source. This is with the exception of *M. bovis* which may require secreted β-glucan

targeting enzymes to hydrolyse the substrate when infecting cows for example (Varrot *et al.,* 2005). It has been reported that *M. tuberculosis* is capable of synthesising cellulose in order to form biofilms (Trivedi *et al.,* 2016). However, currently the enzymes involved in the synthesis or degradation of mycobacterial cellulose have not been identified.

1.6.4 Peptidoglycan remodelling enzymes

As shown in Table 1, a large proportion of enzymes involved in peptidoglycan remodelling belong to the family GH23. This family of enzymes have peptidoglycan lytic transglycosylase activity and show structural similarities to lysozymes found in eukaryotic organisms (Cohen-Gonsaud *et al.,* 2004). These enzymes are therefore lyases, but have been grouped into the GH23 family. One noteworthy enzyme that has been grouped into the peptidoglycan remodelling enzymes is Rv2525c. This was identified by Saint-Joanis *et al.,* (2006) as having a possible role in peptidoglycan remodelling when a genetic knockout of *rv2525c* showed increased sensitivity to β-lactams (Saint-Joanis *et al.,*2006). However, the enzyme has not yet been assigned to a specific GH family. Despite this, the structure of the protein has been solved to a resolution of 1.5 Å by Bellinzoni *et al.,* (2014). Rv2525c has an alpha/beta barrel fold consisting of 8 beta strands and 5 alpha helices. Conventionally, alpha/beta barrel proteins will have 8 beta strands and 8 alpha helices. This unusual structure of Rv2525c with just 5 alpha helices is a structure that has only been found previously in the GH25 family (Vollmer *et al.,* 2008). There is evidence therefore that Rv2525c belongs to the GH25 family, but the lack of biochemical data means that it cannot be truly classified.

1.6.5 Alpha-mannan degrading enzymes

There are three enzymes in *M. tuberculosis* that are predicted to be involved in degradation of α-mannan. These are Rv0648, Rv0365c, and Rv0584. They each belong to a different GH family, implying they each have a different role in α-mannan hydrolysis. In *M. tuberculosis,* and other species, mannosylation is the process of adding activated mannose sugar units onto lipids and proteins. This is seen in the biosynthesis of PIMs, LM, LAM, and mannoproteins. As discussed previously, there are a large, but incomplete, number of mannosyltransferases involved in the biosynthesis of these glycolipids and so our understanding of these pathways is detailed. However, current understanding of the hydrolysis of these substrates, and how this affects virulence of *M. tuberculosis* is very limited. This is due to the lack of characterisation of the three α-mannanases. To date, only Rv0648 has been shown to have α-mannanase activity, as Rivera-Marrero *et al.,* (2001) detected activity when assaying the protein on synthetic α-mannan substrates (Rivera-Marrero *et al.,* 2001). The true substrate for this enzyme therefore remains unknown.

1.7 Alpha 1,6 mannan degrading enzymes

As shown in Table 1, *M. tuberculosis* encode just one predicted GH76 enzyme – Rv0365c. Glycoside hydrolase family 76 enzymes are endo-acting α-mannanases which have previously been studied in fungi and bacteria. They will specifically recognise and cleave α-1,6 linked mannan which is found in mannoproteins in fungi as well as in the mycobacterial glycolipids as previously discussed. The GH76 family began with the characterisation of the founding member Aman6 from *Bacillus circulans* – an

opportunistic, environmental human pathogen (Nakajima, Maitra and Ballou, 1976). It was shown that this enzyme was able to cleave α-1,6 linked mannan to produce mannobiose and mannotriose. Further study revealed that mannotriose was the shortest length polysaccharide that Aman6 was capable of hydrolysing (Maruyama and Nakajima, 2000). To date, only 11 GH76 enzymes have been characterised, and these have predominantly been in non-pathogenic species.

Glycoside hydrolase family 76 enzymes have been primarily studied in *Bacteroides thetaiotaomicron* as this organism encodes several GH76 proteins (Cuskin & Lowe *et al.,* 2015). In *B. thetaiotaomicron,* the carbohydrate degradation enzymes are often organised into polysaccharide utilization loci (PULs). These are regions of the genome which will be up-regulated in the presence of glycans, for example when fungal α-1,6 linked mannan is present. This was shown to be consistent in *Salegentibacter,* a marine bacterium, which also encode a GH76 located within a PUL used for degrading fungal mannan (Solanki *et al.,* 2022). Studies have shown that these GH76 enzymes are active on undecorated α-1,6 mannan, but are not active on wild-type α-1,6 mannan which is highly branched with α-1,2 mannose residues (Cuskin & Lowe *et al.,* 2015). In *B. thetaiotaomicron,* several of the GH76 enzymes are located on the cell surface where they degrade partially digested yeast mannan which has the α-1,6 backbone exposed (Cuskin & Lowe *et al.,* 2015). GH76s located within the periplasm however, have only shown to be active on short α-1,6 mannan polysaccharides (Cuskin & Lowe *et al.,* 2015). This demonstrates that the GH76s are involved in a pathway of enzymes, and they require the substrate to be partially digested before they can act on the α-1,6. It has

been speculated that some fungal GH76s can act as transglycosylases. As there is evidence to suggest the enzymes are involved in cross-linking glycosylphosphatidylinositol-anchored proteins into the cell wall of *Saccharomyces cerevisiae* (Kitagaki *et al.,* 2002). This was proven by Vogt *et al.,* (2020), who demonstrated that GH76 enzymes are responsible for transferring glycosylphosphatidylinositol- anchored proteins to the nonreducing ends of acceptor glycans in the fungal cell wall.

Glycoside hydrolase family 76 enzymes have been shown to be endo-acting, retaining enzymes. This was first proven by Cuskin & Lowe *et al.,* (2015) using a *B. thetaiotaomicron* GH76 and Nuclear Magnetic Resonance analysis when the enzyme was used to hydrolyse the substrate 4-nitrophenyl α-mannosyl-1,6-α-mannopyranose (Cuskin & Lowe *et al.,* 2015). To date, 8 GH76 proteins have had their three-dimensional structures solved, such as Aman6 and the *B. thetaiotaomicron* enzymes BT2949 and BT3792. As shown in Figure 13, it has been revealed that these enzymes have an alpha/alpha 6 helix fold (Thompson *et al.,* 2015). The structure of BT3792, shown in Figure 14, revealed the catalytic residues to be a pair of consecutive aspartic acids, D258 and D259 (Cuskin & Lowe *et al.,* 2015). The catalytic residues of Aman6 were then also confirmed to be a pair of aspartic acid residues, D124 and D125, and identified as the catalytic nucleophile and the general acid/base respectively using X-ray analysis of the protein in complex with its substrate (Thompson *et al.,* 2015). The Williams and Davies group reported the first inhibitor of a GH76 when they identified that Aman6 could be inhibited by α-mannosyl-1,6-isofagomine (Thompson *et al.,* 2015). By performing highly

detailed mechanistic, structural, and conformational analysis of the catalytic domain of Aman6 the group identified that when Aman6 was in complex with a substrate the protein distorted to a skew-boat conformation. However, when the protein is in complex with its inhibitor, α-mannosyl-1,6-isofagomine, it adopts a high-energy $B_{2,5}$ conformation (Thompson *et al.,* 2015). Additionally, the Williams and Davies group report that Aman6 is unlike other mannosidase families, such as the GH38 and GH92 families, as Aman6 does not require metal ions to distort the geometry of its substrate. The addition of EDTA had no effect on the activity of the enzyme, and there was no evidence to suggest metal ions were required in any of the structures they determined (Thompson *et al.,* 2015).

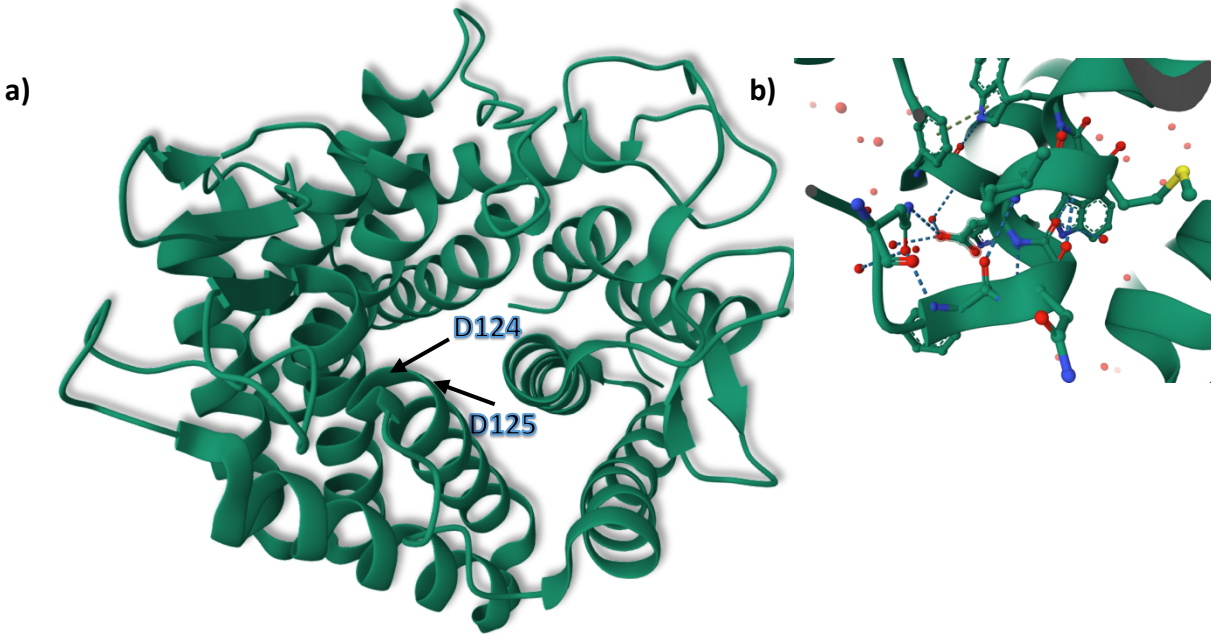

Figure 13: Crystal structure of Aman 6. a) Structure was determined by X-ray diffraction to a resolution of 1.38 angstroms (Striebeck *et al.,* 2013). Arrows indicate the catalytic residues D124 and D125. **b)** Catalytic site of Aman 6.

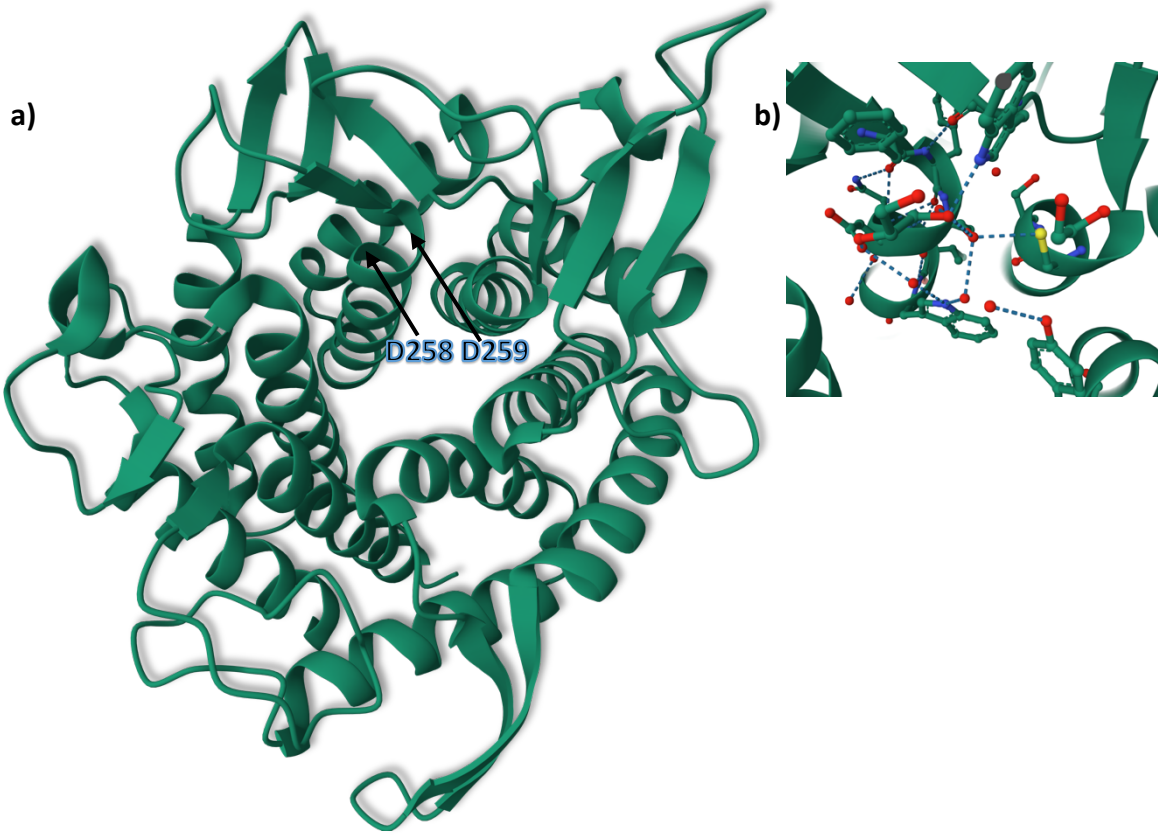

Figure 14: Crystal structure of BT3792. a) Structure was determined by X-ray diffraction to a resolution of 2.10 angstroms (Cuskin & Lowe *et al.,* 2015). Arrows indicate the catalytic residues D258 and D259. **b)** Catalytic site of BT3792.

1.7.1 Rv0365c

The gene *rv0365c* is predicted to encode the only GH76 present in the *M. tuberculosis* genome. This is a 1131bp gene with a protein product of 41.5 kDa in size and 376 amino acids in length. A BLAST search (https://blast.ncbi.nlm.nih.gov/Blast.cgi) reveals that it has homologues in *M. bovis, M. smegmatis, Mycobacterium marinum, M. canetti,* and *M. abscessus* as shown in Table 2.

Table 2: BLAST analysis of mycobacterial homologues of *rv0365c*

Organism	Gene / Sequence ID	E Value
Mycobacterium canetti	ID: WP_230872063	0.0
Mycobacterium marinum	MMAR_0667	0.0
Mycobacterium bovis	Mb0372c, BCGDan_0378	0.0
Mycobacterium smegmatis	MSMEG_0740	9e-163
Mycobacterium abscessus	MAB_4257c	8e-121

There are many genetic screens conducted in mycobacteria which provides a rich source of functional information for individual genes. For example, Rv0365c was highlighted in a screen by Miller and Shinnick (2001) where they were looking for genes involved in macrophage survival. To do this, a library of *M. smegmatis* which contained an individual integrated cosmid containing *M. tuberculosis* DNA was used to infect the human macrophage THP-1 (Miller and Shinnick, 2001). The study focussed on looking for *M. smegmatis* clones that exhibited a significant increase in survival rate compared to the wild-type, non-pathogenic cells. The result of this was the identification of two genes, which they named sur2 and sur3, that increased *M. smegmatis* ability to survive inside

the macrophages. The genes were identified as *rv0365c* and *rv2235* respectively. The study demonstrated that when *M. smegmatis* cells carrying the *rv0365c* gene were used to infect the macrophage, there was an increase in ratio of *rv0365c* to wild-type colonies from 1:1 at 0 hours post infection to 20:1 at 24 hours post infection. As shown in Figure 15, these results demonstrated the increased survival rate *rv0365c* provided *M. smegmatis* (Miller and Shinnick, 2001).

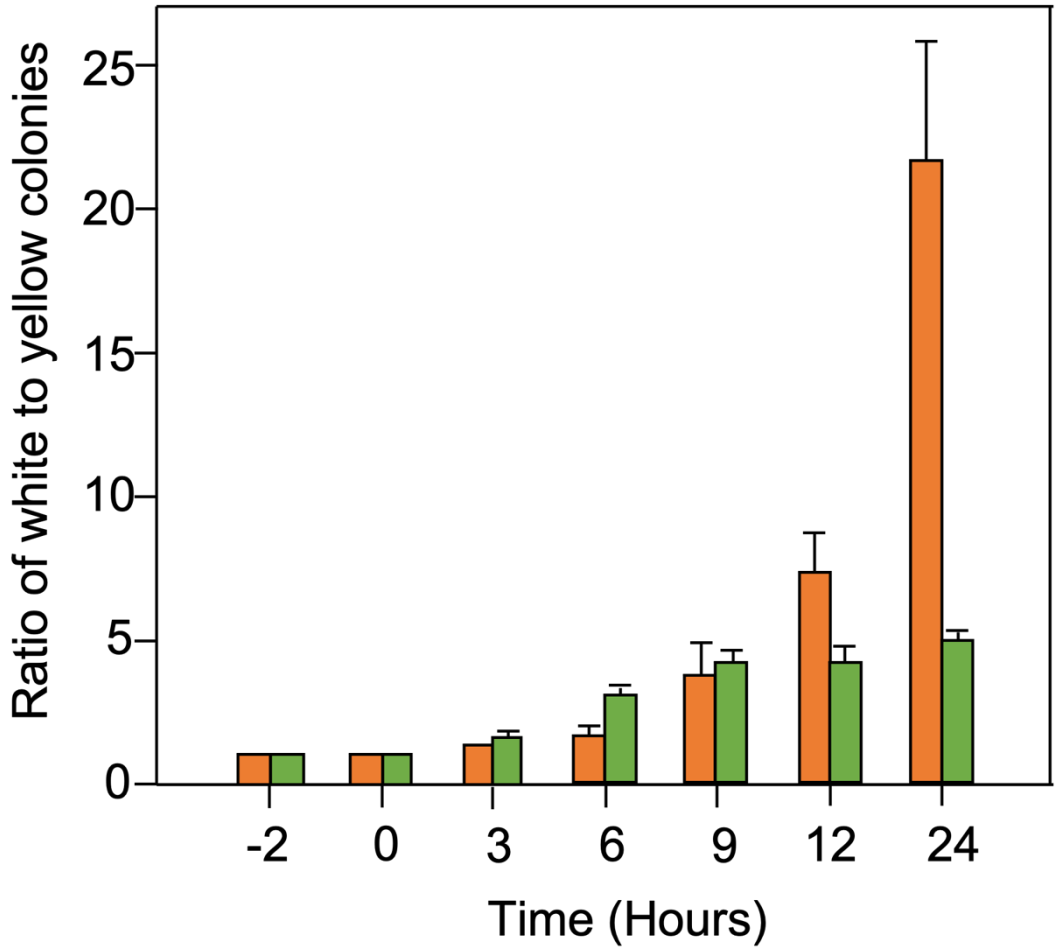

Figure 15: Survival rate of *M. smegmatis* expressing *rv0365c* (orange) and *rv2235* (green) compared to wild-type cells. The wild-type cells express the *xylE* gene product, catechol 2,3-dioxygenase, and so will remain white when sprayed with catechol. The recombinant cells however, do not express this gene and so will turn yellow. This allows direct comparisons to be made. Figure adapted from Miller and Shinnick, (2001).

It has also been reported that the gene *rv0365c* is non-essential in *M. tuberculosis* H37Rv (Griffin *et al.,* 2011). In this study, Griffin *et al.,* (2011) generated a transposon insertion library in *M. tuberculosis* H37Rv. Loss of gene function was dependent upon where the transposon was inserted within a gene. For instance, when the transposon is inserted close to the start of the gene, then there would be a greater loss of function compared to when the transposon is inserted close to the end of the gene. The result of this study was that *rv0365c* was identified as a gene which loss of function was not essential for *in vitro* growth of *M. tuberculosis* H37Rv (Griffin *et al.,* 2011). This study built on previous work by Sassetti, Boyd and Rubin, (2003) who also found Rv0365c to be non-essential. Since then, there have been further projects that have also confirmed the non-essentiality of Rv0365c (DeJesus *et al.,* 2017; Minato *et al.,* 2019).

Using two-dimensional liquid chromatography-mass spectrometry, it has been shown that Rv0365c is present in the membrane fraction of *M. tuberculosis* H37Rv (de Souza *et al.,* 2011). In this study, the authors defined the proteomic content of either culture filtrate, membrane fraction, or whole cell lysate from *M. tuberculosis* H37Rv. Mass spectrometry was then used to identify the proteins found in each fraction. From this study, it was reported that Rv0365c is located within the membrane fraction (de Souza *et al.,* 2011). This result supported earlier studies that also reported the presence of Rv0365c in the membrane fraction of *M. tuberculosis* (Mawuenyega *et al.,* 2005; Xiong *et al.,* 2005). The current understanding of Rv0365c is therefore that it is a non-essential membrane-localised protein that promotes intracellular survival of *M. smegmatis* inside macrophages when overexpressed.

1.8 Alpha 1,2 mannan degrading enzymes

M. tuberculosis, as shown in Table 1, also encode two other putative α-mannan degrading enzymes which are predicted to be active on α-1,2 linked mannan. These enzymes, Rv0648 and Rv0584, belong to the GH families GH38 and GH92 respectively.

1.8.1 Glycoside hydrolase family 38

Glycoside hydrolase family 38 enzymes are exo-acting, Class II proteins. This means that they show less biochemical specificity in terms of the type of bond they will cleave (Gonzalez and Jordan, 2000). This is opposed to GH76 enzymes which are Class I and so will strictly cleave one type of bond. GH38 enzymes have been shown to possess α-1,2, α-1,3, and α-1,6 enzymatic activity (van der Elsen, Kuntz and Rose, 2001). As with GH76 enzymes, GH38 proteins are retaining enzymes that operate through a classical Koshland double-displacement mechanism. This involves two inversion reactions in order to retain the stereochemistry of the anomeric carbon. This was primarily determined by Howard, He and Withers, (1998), and later confirmed by Numao *et al.,* (2003). Again, GH38 catalytic residues have been shown to be a pair of aspartic acid residues (Howard, He and Withers, 1998; Numao *et al.,* 2003).

GH38 enzymes have primarily been studied using eukaryotic proteins. There is therefore much less known about bacterial GH38 enzymes. According to the CAZy website, there are numerous bacterial species that encode GH38 genes, but only 10 have been characterised to date. Of the three mycobacterial α-mannan degrading enzymes, only the GH38 Rv0648 has been biochemically shown to be active on α-mannan. This work

was done by Rivera-Marrero *et al.,* (2001). In this study, it was first shown that both an attenuated and a virulent strain of *M. tuberculosis* had α-mannanase activity. To do this, cells were lysed and the resulting lysate was used to conduct enzyme assays. These assays were conducted using a fluorescent mannan substrate at varying pH conditions. The result of this was that all lysate extracts were shown to have α-mannanase activity, but only at pH 6.5, and activity increased with concentration of protein. This is shown in Figure 16. Furthermore, the highly virulent strain extracts had a three-fold increase in activity when compared to the attenuated extracts.

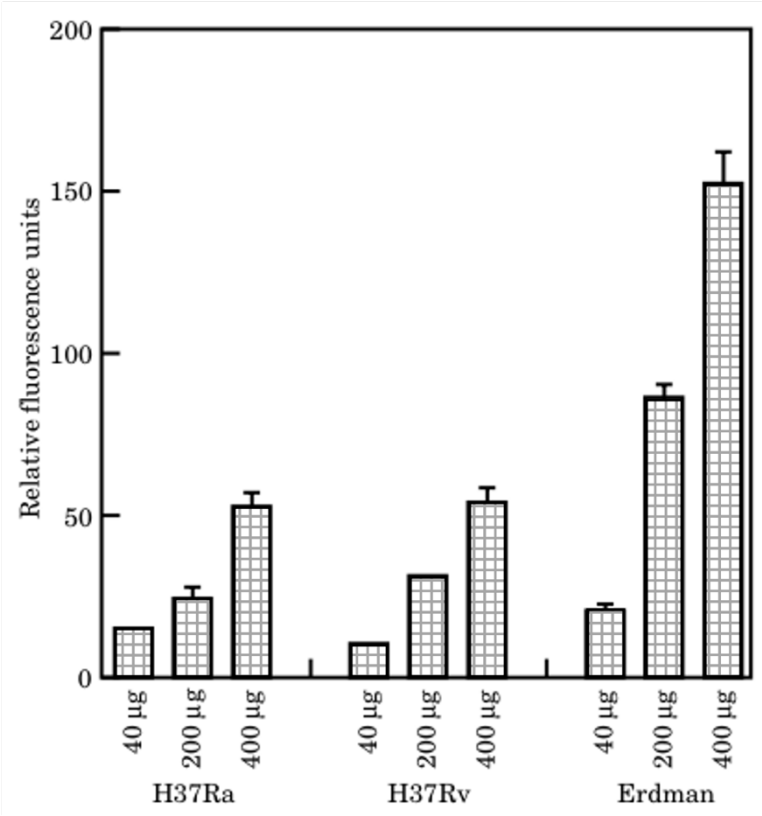

Figure 16: α-mannanase activity of cell lysates on a fluorescent mannan substrate. Cell lysates from the *M. tuberculosis* strains H37Ra (attenuated), H37Rv, and Erdman (highly virulent) were assayed on the fluorescent substrate 4-methylumberlliferyl-α-D-mannopyranoside at protein concentrations of 40, 200, and 400 micrograms. Figure adapted from Rivera-Marrero *et al.,* (2001).

As the gene responsible for this activity was unknown, Rivera-Marrero *et al.,* (2001) conducted a BLAST search of the *Saccharomyces cerevisiae* α-mannosidase gene to look for homologues in the *M. tuberculosis* genome. As a result of this, they identified a coding region of 3.6kb named Rv0648. To confirm this was the enzyme responsible for the α-mannanase activity they detected, the gene was cloned and expressed in *Escherichia coli* and purified. The assays were repeated using the purified protein, and again α-mannanase activity was detected but with an eight-fold increase when compared to the cell lysate assays (Rivera-Marrero *et al.,* 2001).

Rv0648 is a large protein with a molecular mass of 129.9 kDa. It has homologues in *M. bovis, M. marinum,* and *M. smegmatis* (Rivera-Marrero *et al.,* 2001). As with Rv0365c, Rv0648 is a non-essential gene (Griffin *et al.,* 2011) that was identified in the cell membrane fraction of *M. tuberculosis* H37Rv (Mawuenyega *et al.,* 2005). To date, there has been no study on the phenotypic effect on *M. tuberculosis* when Rv0648 activity is lost.

1.8.2 Glycoside hydrolase family 92

Glycoside hydrolase family 92 are exo-acting α-mannanases. As shown in Figure 11, this means they cleave a glycan chain at the end to release one monosaccharide (Davies and Henrissat, 1995). The first GH92 enzyme to be reported was from *Microbacterium* which demonstrated α-1,2 mannanase activity (Maruyama, Nakajima and Ichishima, 1994). Following this, 22 GH92 enzymes were identified in *B. thetaiotaomicron* that demonstrated α-1,2, α-1,3, α-1,4, and α-1,6 biochemical activity (Zhu *et al.,* 2010).

Through Nuclear Magnetic Resonance studies, it has been demonstrated that three different GH92 enzymes all produced β-mannose. This suggests that these enzymes are inverting enzymes and so catalyse the glycosidic bond hydrolysis using a single displacement mechanism. This results in inversion of the anomeric carbon to produce β-mannose (Zhu *et al.,* 2010). GH92 enzymatic activity is usually dependent upon calcium ions (Ca^{2+}). This dependence has, so far, only been found in two other GH families, GH38 and GH47 (Zhu *et al.,* 2010). Interestingly, these three GH families are all exo-acting α-mannanases. This suggests that the interaction with calcium ions is required to provide enough binding energy in the catalytic site to allow hydrolysis to occur (Zhu *et al.,* 2010).

Glycoside hydrolase 92 enzymes have a two-domain structure. There is a small N-terminal domain which is a β-sandwich, and then a large C-terminal domain which adopts the alpha/alpha 6 helix fold. This is shown in Figure 17. The active site is made up of amino acids from both the N-terminal and C-terminal domains (Zhu *et al.,* 2010).

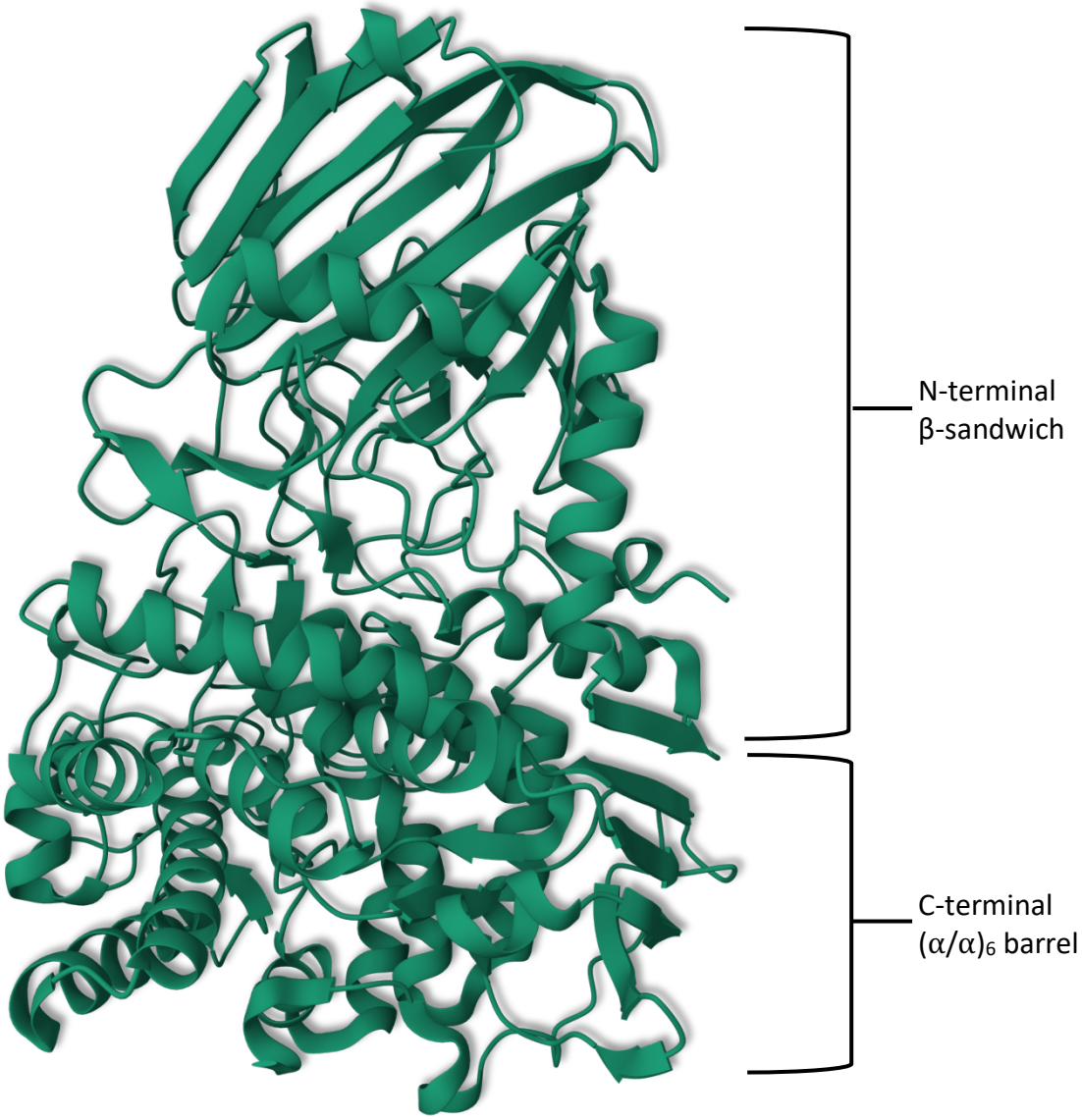

Figure 17: Crystal structure of the GH92 Bt3990. Structure was determined by X-ray diffraction to a resolution of 1.9 angstroms (Zhu *et al.,* 2010).

Rv0584, the predicted GH38 encoded by *M. tuberculosis,* is currently an uncharacterised enzyme which has yet to be studied. It is encoded by a 2634 bp gene which produces a protein product of 92.9 kDa. Interestingly, Rv0584 has homologues in both *M. bovis* and *M. marinum* but does not have a homologue in *M. smegmatis*. This lack of a homologue in *M. smegmatis* may infer a potential role for Rv0584. Previous studies involving Rv0584 have demonstrated that it is a non-essential gene in *M. tuberculosis* (DeJesus *et al.,* 2017; Minato *et al.,* 2019). However, there has been no further study to examine the phenotypic effect that loss of Rv0584 has on *M. tuberculosis*.

1.9 Model Organisms

Due to *M. tuberculosis* being a category three human pathogen, use of this organism in the laboratory requires a dedicated biosafety level three lab as well as substantial training for all staff using the facility. The study of *M. tuberculosis* therefore employs the model organisms *M. bovis* BCG, *M. smegmatis,* and *M. marinum. M. bovis* BCG is a member of the tuberculosis complex but has been attenuated making it safe for use in biosafety level two laboratories. Like *M. tuberculosis*, BCG has a slow growth rate with a doubling time of around every 22 hours and has 99.95% genetic homology to *M. tuberculosis* making it an ideal model organism. However, the slow growth rate of BCG can limit research projects, and so fast-growing species can also be used. *M. smegmatis* is a non-virulent soil dwelling mycobacterial species with a doubling time of 12 hours. It is also more easily genetically manipulated than BCG. *M. smegmatis* does display differences in glycolipid structure however. As described previously, there are differences seen in the capping motifs of *M. smegmatis* LAM compared to *M.*

tuberculosis LAM. *M. marinum* can be a human pathogen but primarily causes a tuberculosis-like infection in ectotherms. It has a doubling rate of 12 hours and is similar to *M. smegmatis* in that it is easily genetically manipulated. These faster-growing mycobacteria are useful as model organisms when time is limited, but due to the high genetic homology of BCG to *M. tuberculosis*, this makes it the ideal model organism (Shiloh and Champion, 2010).

1.10 Aims and Objectives

The current literature regarding the biosynthesis of mycobacterial glycolipids is well-established. Yet, there is extremely limited understanding in regard to how these molecules are broken down and transported to the capsule of the cell. In addition, the role of the three predicted α-mannan degrading enzymes has, to date, yet to be characterised. Considering the previous research conducted by Miller and Shinnick, (2001), where they show the expression of Rv0365c was able to increase the survival rate of *M. smegmatis* cells in macrophages; and the current understanding of the substrate specificities for glycoside hydrolase family 76 enzymes. It is our hypothesis that Rv0365c is the enzyme responsible for hydrolysing the α-1,6 linked mannan backbone of lipoarabinomannan and lipomannan to release arabinomannan and mannan so that they can be trafficked to the capsule. The main objective of this project was therefore to biochemically and phenotypically characterise the α-mannan degrading enzyme, Rv0365c, of *M. tuberculosis*. This was split into two aims:

1. **Biochemically characterise Rv0365c**

This aim involved the expression and purification of Rv0365c, followed by enzymatic assays with different substrates to demonstrate the protein has α-mannanase activity and that it was active on lipoarabinomannan and lipomannan. This aim is explored in Chapter 3.

2. **Phenotypic characterisation of loss of Rv0365c activity**

This aim was centred around a transposon insertion mutant in BCG Danish where the glycoside hydrolase 76 gene was inactivated. This involved analysing the effect on growth, polar lipid composition, glycolipid composition, and capsular polysaccharide content. This aim is investigated in Chapters 4, 5, and 6.

Chapter 2

General Materials and Methods

2. General Materials and Methods

2.1 Culture media

2.1.1 Luria-Bertani Broth

12.5 g of Luria-Bertani (LB) powder (Sigma-Aldrich, L3522) was dissolved into 500 mL of distilled water (dH_2O) and then sterilised by autoclaving at 121 ℃ for 15 mins. LB broth was then stored at room temperature.

2.1.2 Luria-Bertani Agar

18.5 g of LB agar (Sigma-Aldrich, L3147) was dissolved into 500 mL of dH_2O and sterilised by autoclaving at 121 ℃ for 15 mins. Once cooled to 50 ℃, the appropriate antibiotic was added and then 25 mL was dispensed into a Petri dish and allowed to set. LB agar plates were stored at 4 ℃ in a fridge.

2.1.3 Middlebrook 7H9 Media

4.7 g of Middlebrook 7H9 broth base (Sigma-Aldrich, M0178) was dissolved in 900 mL of dH_2O containing 2 mL of glycerol. Once fully dissolved, the media was filter sterilised and then stored at 4 ℃ in a fridge.

2.1.4 Middlebrook 7H10 Agar

9.5 g of Middlebrook 7H10 agar base (Sigma-Aldrich, M0303) was dissolved into 450 mL of dH_2O containing 5 mL of glycerol and then sterilised by autoclaving at 121 ℃ for 15 mins. Once cooled to 50 ℃ 50 mL OADC (oleic acid, albumin, dextrose, catalase) was

added, and then 25 mL was dispensed into a Petri dish and allowed to set. 7H10 agar plates were stored at 4 ℃.

2.1.5 Terrific Broth

47.5 g of terrific broth powder (Sigma-Aldrich, T0918) was dissolved into 1 L of dH_2O containing 5 mL of glycerol and then sterilised by autoclaving at 121 ℃ for 25 mins.

2.2 Bacterial Cultures and Transformations

2.2.1 Bacterial Cultures

Bacteria used for the production of protein and for DNA extraction, *Escherichia coli* strains T7 Shuffle and 10β respectively, were grown in culture tubes in LB media with relevant selection antibiotics at 37 ℃ with shaking at 180 rpm. *E. coli* T7 Shuffle was grown on a large scale in terrific broth using 2 L culture flasks with baffles to increase aeration. *M. bovis* BCG were grown in 9 mL 7H9 media with the addition of 1 mL ADC (Albumin, Dextrose, Catalase) and 25 µl 20% Tween80. For transposon insertion mutants, kanamycin at a concentration of 25 µl/ mL was added. These cultures were grown at 37 ℃ with 5% CO_2. *M. smegmatis* mc^2155 was grown in LB broth at 37 ℃ with shaking at 180 rpm.

2.2.2 Transformation of Competent *E.coli*

5 µl of plasmid DNA was added to 50 µl of *E.coli* 10β cells and incubated on ice for 15 mins. The cells were then heat shocked at 42 ℃ for 45 seconds and then immediately returned to the ice for 5 mins to allow the cells to recover. One mL of LB broth was

added to the cells and then incubated at 37 ℃ for 1 hour. 100 µl of the mixture was then plated out onto an LB agar plate with the relative selection antibiotic and incubated overnight at 37 ℃.

2.2.3 Electroporation of Mycobacteria

To make mycobacteria electrocompetent, cultures were grown until late log phase and then chilled on ice for 1.5 hours. Cells were then harvested by centrifugation at 4000 x *g* for 10 mins at 4 ℃. The cells were resuspended in 20 mL solution of ice cold 10% glycerol + 0.05% Tween 80. The cells were harvested by centrifugation, and this wash was repeated once more. Finally, the cells were resuspended in 3 mL of the above solution and then divided into 150 µl aliquots.

To electroporate plasmid DNA into the electrocompetent cells, 1 µl of plasmid was added to the cells and incubated on ice for 10 mins. The electroporation cuvette was also pre-chilled in the ice. Following this, the cells are transferred to the 2 mm gap electroporation cuvette. Electroporation was performed at 2.5 kV, 800 Ω, 25 µF. The sample was transferred to a falcon tube, and 5 mL 7H9 media was added to electroporated cells before being left to recover 4 hours at 37 ℃. Cells were harvested by centrifugation at 3000 x *g* for 10 mins, and resuspended in 100 µl of 7H9 media. The sample was spread onto a 7H10 agar plate with suitable selection antibiotic and incubated at 37 ℃ for 4 weeks.

2.3 Molecular Biology

2.3.1 Polymerase Chain Reaction

Polymerase Chain Reaction (PCR) was performed using the Q5 Hot Start High-Fidelity 2x Master Mix (NEB, M0494S). Primers were supplied dry by Sigma-Aldrich, resuspended to 100 µM, and then diluted to 10 µM for use. For a 25 µl reaction, 12.5 µl of Q5 Hot Start High-Fidelity 2x Master Mix was added to 9 µl of dH_2O, followed by 1.25 µl of 10 µM forward primer and 1.25 µl of 10 µM reverse primer, and finally 1 µl of template DNA at a concentration of 1-25 ng / µl. The reaction is conducted in a thermocycler using the conditions outlined in table 3.

Table 3: Thermocycling conditions for routine PCR

Step	Temperature (℃)	Time	Cycles
Initial Denaturation	98	30 seconds	1
Denaturation	98	10 seconds	35
Annealing	50-72	30 seconds	
Elongation	72	30 seconds per kb	
Final Extension	72	2 mins	1

2.3.2 Agarose Gel Electrophoresis

To prepare a 1% w/v agarose gel, 0.9 g of agarose powder is dissolved into 100 mL of TAE buffer (40 mM Tris-acetate, 2 mM Na_2EDTA) by heating in a microwave. Once cooled to 50 ℃, 5 µl of Midori Green is mixed in before the solution is poured into the mould with a well-comb and allowed to set. Once the gel had set, the comb is removed and the gel is placed into the gel tank filled with 1x TAE buffer. The DNA samples are mixed with

6x purple loading dye (NEB, B7024S) and loaded into the wells. An additional well containing a 1 kb DNA ladder (NEB, N3232S) mixed with purple loading dye is also loaded. The samples are separated at 140 V, 400 mA, for 50 mins. The gel is then visualised using a Bio-Rad Gel Dock with a U.V. imager.

2.3.3 DNA Extraction from Gel

DNA bands can be removed from the agarose gel using a scalpel and then placed into a pre-weighed 15 mL falcon tube. The DNA is extracted using a Qiagen QIAquick Gel Extraction Kit per manufacturer's instructions. The DNA is eluted from the column using 30 µl elution buffer (10 mM Tris-HCl pH 8.5).

2.3.4 DNA Ligation

To ligate DNA fragments together T4 DNA ligase (NEB, M0202) was used. For a the reaction, 2 µl of T4 DNA ligase buffer, 1 µl T4 DNA ligase, 0.020 pmol of vector DNA, and 0.060 pmol of insert DNA were made up to 20 µl with dH_2O. The reaction was then incubated at room temperature for 2 hours and then heat inactivated at 65 ℃ for 10 mins. The reaction can then be transformed into competent *E. coli.*

To calculate pmols of DNA:

$$\frac{\textit{DNA weight in ng x 1000}}{\textit{Base pairs x 650}}$$

2.3.5 Plasmid Purification from *E. coli*

Plasmid DNA was extracted from 10 mL overnight cultures of *E. coli* using the GeneJET miniprep kit (ThermoFisher, K0502) as per the manufactures instructions. Plasmid DNA

was eluted from the column using 30 µl elution buffer. DNA concentration was determined using a nanodrop.

2.4 Protein Biochemistry

2.4.1 Expression and Purification of Protein

Protein was expressed in *E. coli* T7 Shuffle and subsequently purified. One litre cultures were grown to mid-log phase (OD_{600} 0.5-0.8) in terrific broth at 37 ℃ with 180 rpm shaking. Once mid-log was reached, the cultures were cooled in an ice bath before isopropyl β-D-1-thiogalactopyranoside (IPTG) was added at a final concentration of 100 µM to induce protein expression. The cultures were incubated for a further 16 hours at 16 ℃ and then harvested by centrifugation at 6000 x *g* for 20 mins. The cell pellets were stored at -20 ℃ until use. Cell pellets were resuspended in 30 mL of lysis buffer with the addition of 10 mg lysozyme (Sigma-Aldrich, 89833) and 10 µg/ mL DNase (Sigma-Aldrich, 11284932001). The resuspended cells were then lysed by 3 passages through a French Pressure Cell press before the lysate was collected by centrifugation at 10,000 x *g* for 45 mins at 4 ℃. The clarified lysate was purified by nickel Sepharose affinity chromatography at a rate of 1 mL /minute. The protein of interest was eluted from the column with stepwise elutions of imidazole (25 mM, 50 mM, 100 mM, 250 mM, and 500 mM). Each fraction was collected separately, and positive fractions were identified by sodium dodecyl sulfate-polyacrylamide gel electrophoresis (SDS-PAGE).

2.4.2 Sodium Dodecyl Sulfate-Polyacrylamide Gel Electrophoresis

SDS-PAGE gels were cast at either 12% or 15% for smaller sized protein analysis. The gels consist of both a running gel and a stacking gel. Each of which is prepared separately. Table 4 describes the materials and quantities required for each gel.

Table 4: Preparation of SDS-PAGE gels

Component	Quantity
12% SDS-PAGE Running Gel	
Water	2.7 mL
1.5 M Tris pH 8.0	2.0 mL
30% Acrylamide	3.2 mL
10% SDS	80 µl
TEMED	8 µl
10% APS	80 µl
15% SDS-PAGE Running Gel	
Water	2.4 mL
1.5 M Tris pH 8.0	2.5 mL
30% Acrylamide	5.0 mL
20% SDS	50 µl
TEMED	10 µl
10% APS	100 µl
Stacking gel (6%)	
Water	3.0 mL

1.0 M Tris pH 6.8	1.25 mL
30% Acrylamide	0.7 mL
10% SDS	50 µl
TEMED	5 µl
10% APS	50 µl

Protein samples were prepared by adding 5 µl 6X loading dye (15 mL Tris-Cl pH 6.8, 6 g SDS, 25 mg Bromophenol blue, 30 mL glycerol, and 2 mL Betamercaptomethanol) to 20 µl sample and boiling for 10 mins. The samples were then loaded into the wells of the gel in a stepwise fashion (pre-induction sample, post-induction sample, clarified lysate, flow through, 25mM elution, 50mM elution, 100mM elution, 250mM elution, and 500mM elution) with a Blue Prestained Protein Standard (NEB, P7718S). The samples were separated at 200 v, 40 mA, for 1 hour.

2.4.3 Imidazole removal using dialysis

The fractions containing the protein of interest were loaded into dialysis tubing, with a molecular weight cut off of at least half the size of the protein of interest, and secured at either end. The tubing was placed into 2 L of pre-cooled, imidazole-free buffer for 2 hours with gentle mixing. The buffer was replaced after 2 hours with another 2 L of buffer and left overnight.

2.4.4 Sample Concentration

After dialysis, the protein was removed from the tubing and placed into a molecular weight cut-off sample concentrator which was at least 15 kDa smaller than the protein of interest. The protein was then concentrated down to a desired concentration and volume by centrifugation at 14,000 x *g* at 4 ℃ in 5 mins intervals to ensure stability of the protein. Once a desired concentration and volume was achieved, the protein was flash frozen and stored in 50 µl aliquots at -80 ℃ until use.

2.4.5 Western Blot

Western blot was performed using an unstained SDS-PAGE gel inside a blotting cassette with a Amersham Protean Premium Nitrocellulose Blotting Membrane (GE Healthcare) and separated by electrophoresis in a transfer buffer (25 mM Tris-HCl, 190 mM glycine, 20% methanol) at 100 v, 40 mA, for 1 hour. The nitrocellulose membrane was then removed and washed with tris buffered saline with tween (TBST) (25 mM Tris-HCl pH 7.5, 150 mM NaCl, 0.1% Tween20) for 5 mins. Following this, the membrane is incubated in blocking buffer (5% skimmed milk powder) overnight. In the morning, the blocking buffer is decanted and the primary antibody (5 µl His Mouse IgG primary antibody (Sigma-Aldrich, 11922416001) in 50 mL TBST) is added for 1 hour. Following this, the primary antibody is removed and the membrane is washed 3x with TBST for a total of 30 mins. The secondary antibody (2 µl anti-mouse IgG-alkaline phosphatase secondary antibody (Sigma-Aldrich, A3562) in 50 mL TBST) is added and the membrane is incubated for 1 hour. The membrane is again washed 3x with TBST for a total of 30 mins. The bands

are then detected by dissolving a SIGMAFAST BCIP/NBT tablet in 10 mL dH_2O and incubating the membrane in the solution until bands were visible.

2.5 Enzyme assays

2.5.1 α-mannan purification from *Saccharomyces cerevisiae*

Purification of α-mannan from *S. cerevisiae* was performed by culturing 8 L of the desired *S. cerevisiae* strain in Yeast Extract-Peptone-Dextrose (YPD) media (10 g yeast extract, 20 g peptone, 20 g dextrose dissolved in 1 L dH_2O with 10% glucose) at 37 ℃ for 24 hours. Pellets were harvested by centrifugation at 6000 x *g* for 20 mins. The pellets were then pooled and stored at -20 ℃ until use. The pooled cell pellets were resuspended in 20 mL 0.02 M citrate buffer pH 7.0 and then autoclaved for 90 mins at 121 ℃. The sample is centrifuged at 6000 x *g* for 10 mins, and the supernatant is collected. The remaining pellet was resuspended in 75 mL of 0.02 M citrate buffer pH 7.0 and autoclaved once more at 121 ℃ for 90 mins. The sample was centrifuged at 6000 x *g* for 10 mins, and the resulting supernatant was pooled with that previously collected. A volume of 2X Fehling's reagent, equal to that of the supernatant, is measured out and heated to 40 ℃. The supernatant was carefully added to the 2X Fehling's reagent (7% $CuSO_4$, 35% potassium sodium tartrate, 5% NaOH) and stirred vigorously at 40 ℃ for 1 hour. Following this, the mixture was centrifuged at 6000 x *g* for 10 mins to harvest the pellet. The pellet was dissolved in 8 mL of 3 M hydrochloric acid before 100 mL of methanol: acetic acid solution (8:1 v/v) is added and stirred for 1 hour at room temperature. The mixture was centrifuged at 12,000 x *g* for 15 mins and the pellet was collected. This was resuspended in 20 mL methanol: acetic acid solution

(8:1 v/v) and centrifuged again. This process was repeated until the pellet was colourless. The pellet was the left to dry at room temperature overnight. In the morning, the dry pellet was resuspended in 20 mL dH_2O and then dialysed against 4L of dH_2O for 24 hours. The following day, the dH_2O is replaced for fresh dH_2O and dialysed for a further 2 hours. Finally, the mixture is lyophilised to complete dryness in a pre-weighed falcon tube.

2.5.2 Lipoarabinomannan and Lipomannan Purification from Mycobacteria

Mycobacterial cultures were grown to either mid-log phase or stationary phase before being harvested by centrifugation at 6000 x *g* for 10 mins. The cell mass is measured and recorded. The cells were resuspended in 10 mL PBS, and then centrifuged again. The pellet was resuspended in PBS for a final time before being lysed with a Bead Beater set at 6.0 m/sec for 45 seconds per cycle. The lysate was then transferred to a glass tube, and an equal volume of phenol is added. The mixture was incubated at 85 ℃ for 2 hours, and vortexed at 30 minute intervals. Following this, the aqueous phase was separated from the phenol phase by centrifugation at 4000 x *g* for 10 mins. The aqueous phase is transferred to a clean glass tube. An equal volume of water is added to the remaining phenol phase, and incubated again at 85 ℃ for 2 hours with regular mixing. The aqueous phase is harvested by centrifugation and pooled with the previously collected aqueous phase. The solution is then dialysed against 4L of flowing tap water, overnight, to remove any residual phenol. In the morning, the mixture is further dialysed against 2.5 L dH_2O for 3 hours at room temperature. Finally, the sample is lyophilised to complete dryness. For analysis, glycolipid extracts were resuspended in ddH_2O to a concentration

of 5 mg / mL based on the original cell mass used for extraction. This ensured that an equal volume of cells was being analysed.

2.5.3 General Assay Procedure

For the enzymatic assays conducted, in general, 1 µM of protein was incubated with 0.5 mg / mL substrate with equal volumes of a desired buffer and dH_2O in a total reaction volume of 100 µl. The assay was incubated at 37 ℃ overnight, and then heat inactivated by boiling for 10 mins. Enzyme activity was detected by thin layer chromatography (TLC).

2.5.4 Thin Layer Chromatography

TLC was carried out using silica gel bonded to aluminium sheets (Merck, TLC Silica Gel 60 F_{254}). The TLC sheet was cut to the required size, and then samples were spotted 1 cm from the base of the TLC. The plate is then placed into a TLC tank with a desired solvent system, and run until the solvent front reaches 5 mm from the top of the sheet. The TLC is allowed to dry and then is either stained and heated to reveal products, or exposed to an X-ray film if the samples are radioactive.

2.6 Lipid Extraction and Analysis

2.6.1 Polar Lipid Extraction

Mycobacteria cultures were grown to mid-log phase (OD_{600} 0.6-0.8) and harvested by centrifugation at 6000 x *g* for 10 mins. For radiolabelled cultures, the desired isotope was added once the culture had reached an OD_{600} of 0.1-0.2. The pellets were resuspended in PBS, transferred to glass tubes, and re-pelleted. Following this, 2 mL of

methanol: 0.3% NaCl (100: 10 w/v) and 2 mL petroleum ether (60-80) is added to the pellet. This is mixed on a rotator for 24 hours. The samples were centrifuged at 4000 rpm for 10 mins to form a bilayer, with the top layer being transferred to a fresh tube. An additional 2 mL of petroleum ether is added to the lower layer and mixed on a rotator for a further 1 hour. Again, the samples were centrifuged, and the top layer is pooled with the previous harvest. These are non-polar lipids and were dried down in a pre-weighed tube. To extract the polar lipids, 750 µl of chloroform: methanol: 0.3% NaCl (9: 10: 3 v/v/v) is added to the remaining mixture. This is mixed on a rotator for 2 hours, and then centrifuged at 4,300 rpm for 10 mins. The supernatant is collected and transferred to a fresh tube. Following this, 950 µl chloroform: methanol: 0.3% NaCl (5: 10: 4 v/v/v) is added to the pellet, and mixed for an additional 30 mins. The sample is then centrifuged at 3,500 rpm for 5 mins and the supernatant is pooled. Finally, the polar lipids are harvested by adding 1 mL chloroform and 1 mL 0.3% NaCl to the pooled supernatants and mixing for 10 mins. A bilayer formed and the lower, polar lipid containing, layer was collected and dried down in a pre-weighed tube. The lipid samples were resuspended in chloroform: methanol (2:1 v/v) and analysed on a TLC. For radioactive samples, a 5 µl sample was taken from the resuspended lipids and used to determine the counts per minute of the sample.

2.6.2 Glycolipid Analysis

Analysis of lipomannan and lipoarabinomannan was performed using the Pro-Q Emerald 300 Glycoprotein Stain (ThermoFisher, P21857) and a Bio-Rad Precast Protein Gel 4-20% (Bio-Rad, 4561094). 20 µl of glycolipid sample was mixed with 5 µl 6x loading dye and

then loaded into the wells of the gel. The samples were separated at 200 v, 40 mA, for 1 hour. Following this, the glycolipids were stained and visualised as per the manufacturer's instructions.

2.7 Cell Strains

The strains used in this thesis were: *Escherichia coli* T7 Shuffle (New England Biolabs) which was used to express Rv0365c, catalytic null Rv0365c, and BT3792; *Saccharomyces cerevisiae* Mnn1, Mnn2, and Mnn5; *Mycobacterium bovis* BCG Danish 1331 WT and *Mycobacterium bovis* BCG Δ0378; *Mycobacterium smegmatis* mc^2 155 WT and *Mycobacterium smegmatis* mc^2 155_ Δ0740.

Chapter 3

Biochemical Characterisation of Rv0365c

3. Biochemical Characterisation of Rv0365c

3.1 Introduction

M. tuberculosis encodes just one predicted glycoside hydrolase family 76 enzyme, as shown in Table 1, and this was the primary focus of this chapter. As previously reported by Nakajima, Maitra and Ballou, (1976), GH76 enzymes will specifically recognise and cleave α-1,6 linked mannan. This chapter describes the purification of recombinant Rv0365c expressed in *E. coli* T7 Shuffle and the use of this purified protein to confirm the enzyme possesses GH76 activity. To do this, mannans purified from mutant strains of *Saccharomyces cerevisiae* were used as substrate. Following confirmation that Rv0365c has α-mannanase activity, purified lipomannan and lipoarabinomannan from *M. bovis* BCG were used as enzymatic substrates as this was the basis of the thesis hypothesis. As enzymatic activity was again detected on the hypothesised natural substrates, this chapter next set out to identify the reaction product by employing the use of mass spectrometry. In addition, this chapter will utilise the services of AlphaFold to explore how the predicted structure of Rv0365c compares to that of experimentally determined GH76 structures. Finally, we confirm the catalytic residues in the active site by generating and validating a catalytic null mutant.

3.2 Materials and Methods

3.2.1 Expression and Purification of Rv0365c

The *Rv0365c* gene was purchased as a codon-optimised construct from Twist Biosciences in a pET28a vector including residues 2-376 with an N-terminal hexa-histidine tag (all numbering relative to the genomic annotation). This was transformed into a T7 Shuffle expression strain of *E. coli* and grown in terrific broth at 37 ℃ with 180 rpm shaking until an OD_{600} of 0.6 was reached. At this point, expression of Rv0365c was induced with the addition of 0.1 mM IPTG and the cells were incubated for a further 16 hours at 16 ℃ with 180 rpm shaking. Cell pellets were resuspended in 30 mL of a 100 mM HEPES (N-2-hydroxyethylpiperazine-N'-2-ethanesulfonic acid) pH 8.0, 300 mM NaCl, 5 mM imidazole pH 8.0 buffer with the addition of 5% glycerol and 1% Tween20. Cell lysis and protein purification was as described in Chapter 2.4. Positive fractions, which contained the protein of interest, were identified by SDS-PAGE gel electrophoresis and dialysed into 100 mM HEPES pH 8.0, 150 mM NaCl dialysis buffer for 16 hours at 4 ℃. Protein samples were concentrated to a final volume of 100 µl and a concentration of 5.3 mg / ml. Subsequently, the protein solution was aliquoted and flash frozen until use.

3.2.2 Expression and Purification of BT3792

The *bt3792* gene in a pET28a expression vector was provided to us from our collaborator Dr Elisabeth Lowe based in Newcastle University. The plasmid was transformed into *E. coli* T7 Shuffle and grown in terrific broth at 37 ℃ with 180 rpm shaking until an OD_{600} of 0.6 was reached. Following this, IPTG at a final concentration of 0.2 mM was added

to induce protein expression, and the cultures were incubated for a further 16 hours at 16 ℃ with 180 rpm shaking. Cell pellets were resuspended in 30 mL of a buffer consisting of 150 mM Tris pH 8.0, 300 mM NaCl, 20 mM imidazole pH 8.0. Cell lysis and protein purification was as described in Chapter 2.4. Positive elutions were identified by SDS-PAGE gel electrophoresis and dialysed against 150 mM Tris pH 8.0, 300 mM NaCl dialysis buffer for 16 hours at 4 ℃. Protein was at a suitable concentration for use without the requirement for further concentration.

3.3 Results

3.3.1 Purification of Rv0365c

To begin biochemical characterisation of Rv0365c, the enzyme first needed to be purified. *E. coli* T7 Shuffle was employed to express the recombinant protein upon induction with IPTG. Immobilised metal-ion affinity chromatography and SDS-PAGE gel electrophoresis were utilised to purify the protein from the lysate and identify protein containing fractions. This is shown in Figure 18. Purification of Rv0365c took around 9 months to fully optimise. The presence of disulphide bonds and being a predicted membrane localised protein meant that the protein was largely insoluble. Therefore, a range of detergents and additives were used until the protocol was optimised. The T7 Shuffle strain was used to express the protein because of its ability to correctly fold disulphide bonded proteins. The presence of detergents helps to solubilise membrane associated proteins as well as releasing them from the cell membrane during lysis.

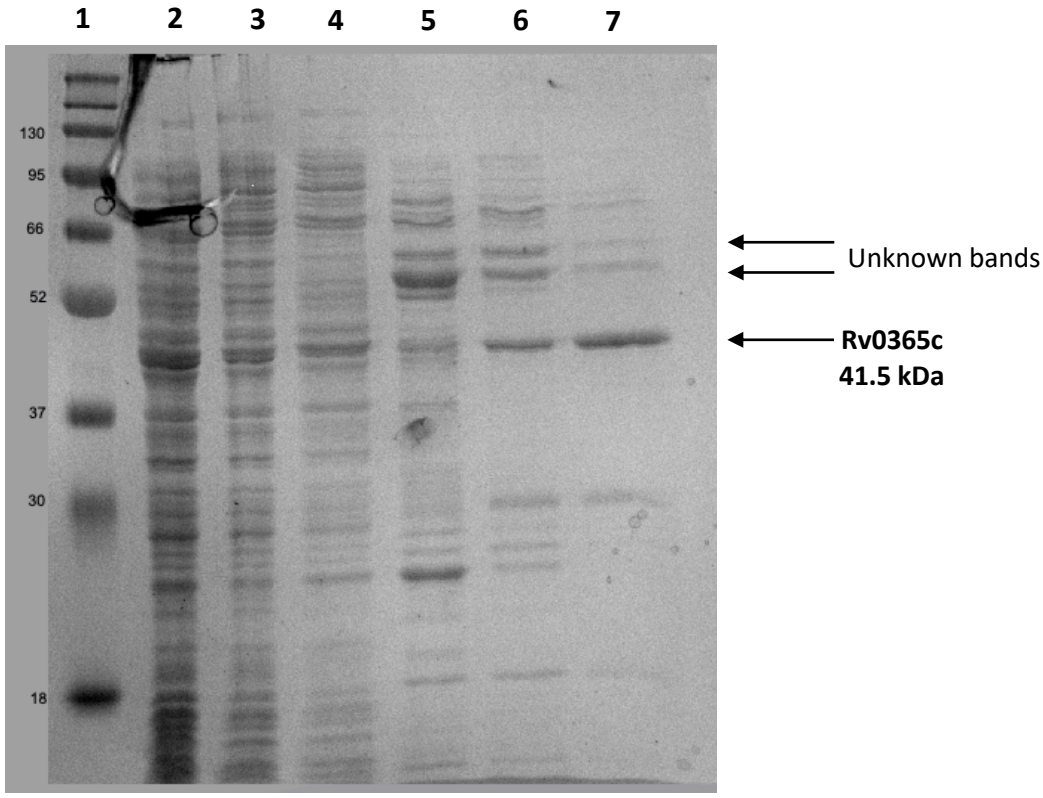

Figure 18: Purification of Rv0365c on an SDS-PAGE gel. Lanes: (1) Pre-stained protein ladder (kDa), (2) cell lysate, (3) flow through, (4) 5 mM imidazole wash, (5) 50 mM imidazole elution, (6) 100 mM imidazole elution, and (7) 500 mM imidazole elution. Protein of interest was present in the 500 mM fraction – indicated by arrow.

3.3.2 Western Blot Analysis

As shown in Figure 18, Rv0365c (41.5 kDa) eluted from the column in the 500 mM imidazole fraction. This was therefore dialysed overnight and subsequently concentrated to 5.3 mg / mL in a 100 µl solution. The protein was then aliquoted into 50 µl samples, flash frozen, and stored at -80 ℃ until use. However, the presence of the two large protein bands in the 50 mM elution and 100 mM elution were a concern. To check if these species were related to the protein of interest, a western blot was performed to identify His-tagged proteins. This is shown in Figure 19.

The western blot revealed that the two larger protein species observed in the 50 mM and 100 mM imidazole fractions were not His-tagged and were therefore not likely related to Rv0365c. Furthermore, the western blot confirmed the presence of His-tagged protein at 41 kDa, consistent with the size of Rv0365c. We were therefore confident that the protein we purified was Rv0365c.

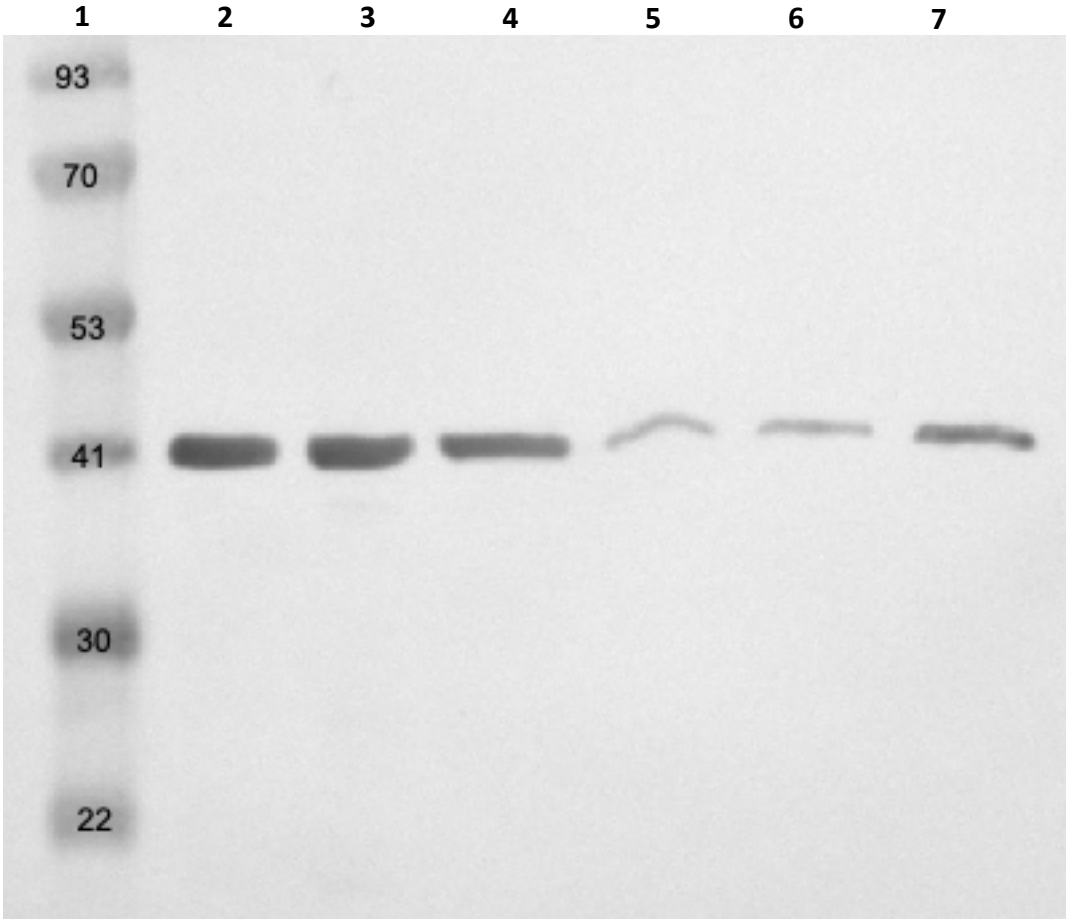

Figure 19: Western blot of Rv0365c. Lanes: (1) Pre-stained protein ladder (kDa), (2) cell lysate, (3) flow through, (4) 5 mM imidazole wash, (5) 50 mM imidazole elution, (6) 100 mM imidazole elution, and (7) 500 mM imidazole elution. Methodology described in Chapter 2.4.5. Results indicated that the only his-tag containing proteins were at the size of the protein of interest.

3.3.3 The structure of Rv0365c is consistent with previously characterised GH76s

We were unable to experimentally determine a structure for this protein, despite repeated attempts to crystalise it. However, during this project AlphaFold 2.0 became available, providing access to a high-confidence predicted structure for this protein. The predicted structure, shown in Figure 20, suggests the overall fold is consistent with previously characterised GH76 enzyme structures. This includes the presence of an alpha/alpha 6 helix fold to create a barrel.

To confirm the structure of Rv0365c was consistent with previously characterised GH76 proteins, a pairwise sequence alignment was performed. This is shown in Figure 21. The alignment was performed using Aman6 (PDB: 4BOK) with the AlphaFold 2.0 predicted structure of Rv0365c (Uniprot: O06315) using the protein data bank pairwise structure alignment tool (https://www.rcsb.org/alignment). The results revealed that the core structure of the protein is consistent with Aman6. The active site of Rv0365c is highly conserved with that of Aman6. However, Rv0365c possesses a unique beta-hairpin cap which covers the predicted active site that is not found in experimentally determined GH76 structures. This can be observed in both Figure 20 and 21. As shown in Figure 21B, the beta-hairpin cap is predicted to cover the active site of the enzyme. Therefore, complex substrates would be unable to enter the active site such as mannan backbones decorated with α-1,2 mannose. This beta-hairpin cap would likely clash with the decorated substrate and result in no cleavage taking place.

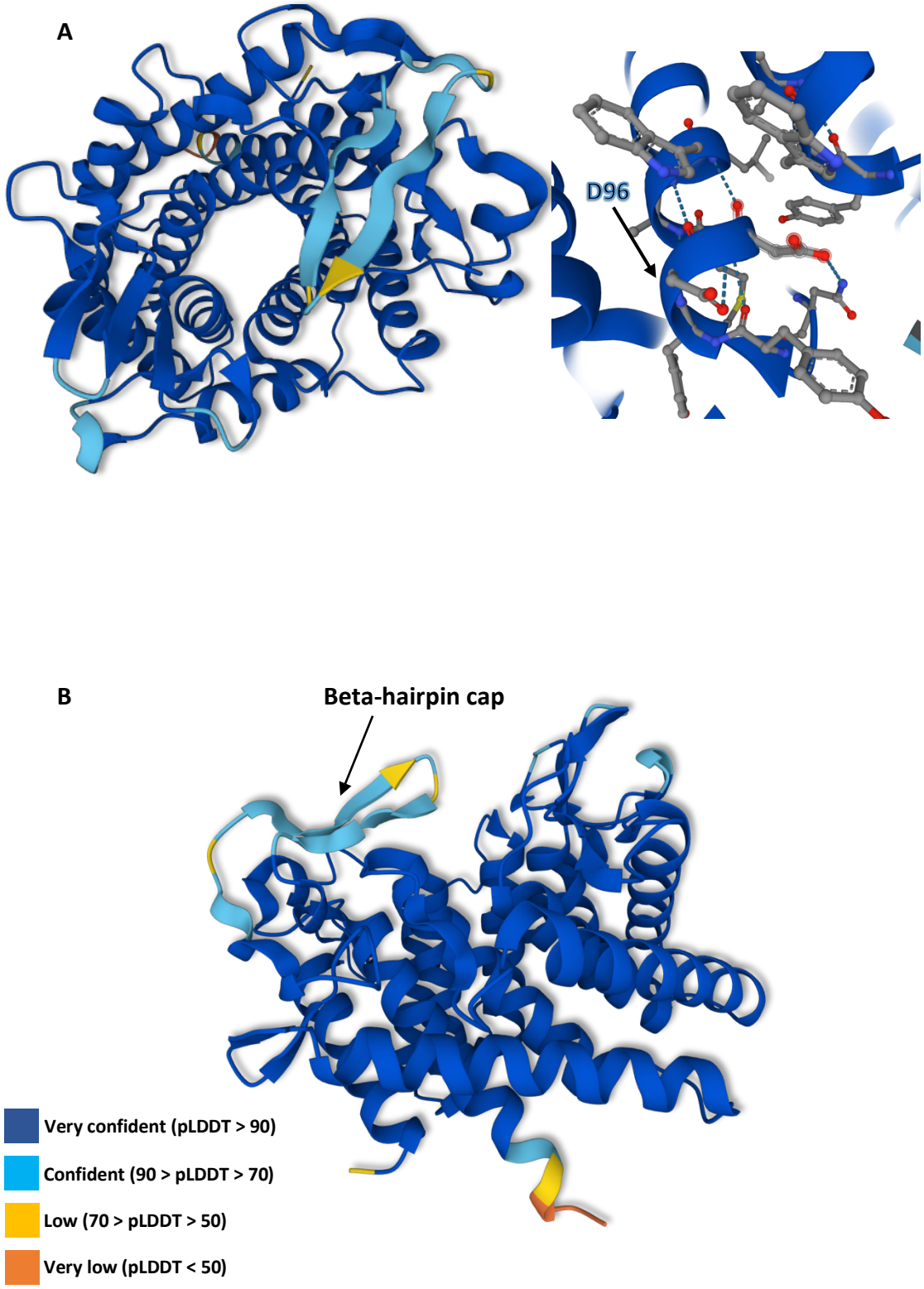

Figure 20: AlphaFold predicted structure of Rv0365c. A) Structure viewed from barrel axis. Predicted catalytic site indicated by arrow **B)** Structure viewed from axis parallel with barrel. Model confidence is indicated by colour shown in key. AlphaFold produces a per-residue confidence score (pLDDT).

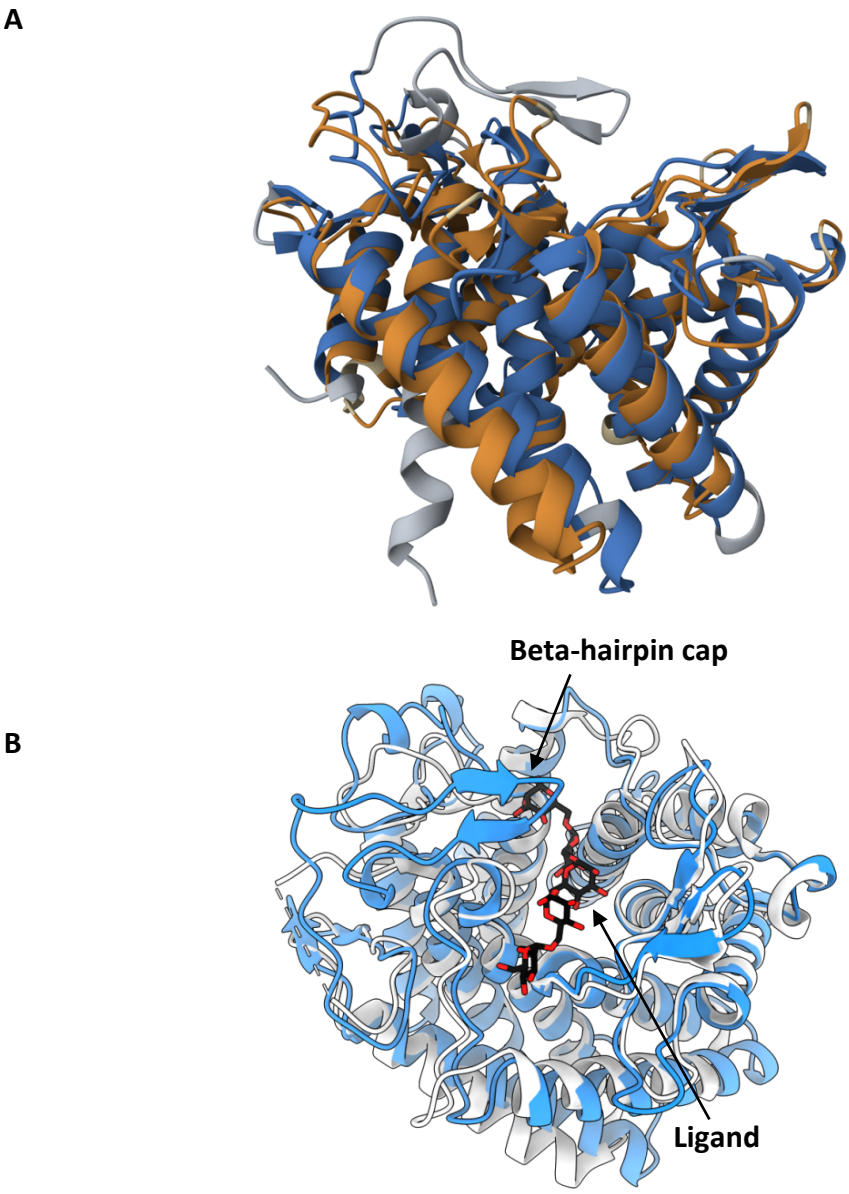

Figure 21: Pairwise structural alignment of Rv0365c (blue) and Aman6 (orange). A) Alignment revealed there are 322 equivalent residues with a root mean square deviation of 2.2 Å. Rv0365c is predicted to possess a beta-hairpin cap which is a structural motif unique to the mycobacterial protein. It is not seen here in Aman6. **B)** Ribbon diagram of Rv0365c aligned with Aman6 in complex with mannotetraose.

3.3.4 Rv0365c has α-mannanase activity

Rv0365c is predicted to be a glycoside hydrolase family 76 enzyme and would therefore likely recognise and cleave α-1,6 linked mannan. Once we had purified the protein, we set out to confirm that Rv0365c was active against α-1,6 linked mannan. To do this, we were provided with three mutant strains of *Saccharomyces cerevisiae* from our collaborator Dr Elisabeth Lowe from Newcastle University (Cuskin & Lowe *et al.,* 2015). These three mutants; Mnn1, Mnn2, and Mnn5, produced mannan with different levels of backbone decoration (Cuskin & Lowe *et al.,* 2015). This is shown in Figure 22. Following the methodology detailed in Chapter 2.5.1, we were able to purify these mutant mannans from the *S. cerevisiae* strains and use them as a substrate for testing for GH76 enzymatic activity.

The three mutant mannans, shown in Figure 22, were purified so that they could be used as a substrate for Rv0365c. These mannans have differing structures ranging from Mnn2 which was the simplest substrate as it consisted of just the core α-1,6 linked mannan backbone with no decorations, to Mnn1 which was the most complex mannan with α-1,2 linked mannose side chains covering the whole of the backbone. To determine if Rv0365c was enzymatically active on any of these substrates, 1 mg / mL of substrate was incubated with 1 µM protein for 16 hours at 37 ℃. A 20 µl sample was then spotted onto a TLC plate and separated in a solvent system consisting of n-butanol: acetic acid: water (2:1:1 v/v/v). To visualise the TLC, it was then stained with orcinol and heated. This is shown in Figure 23.

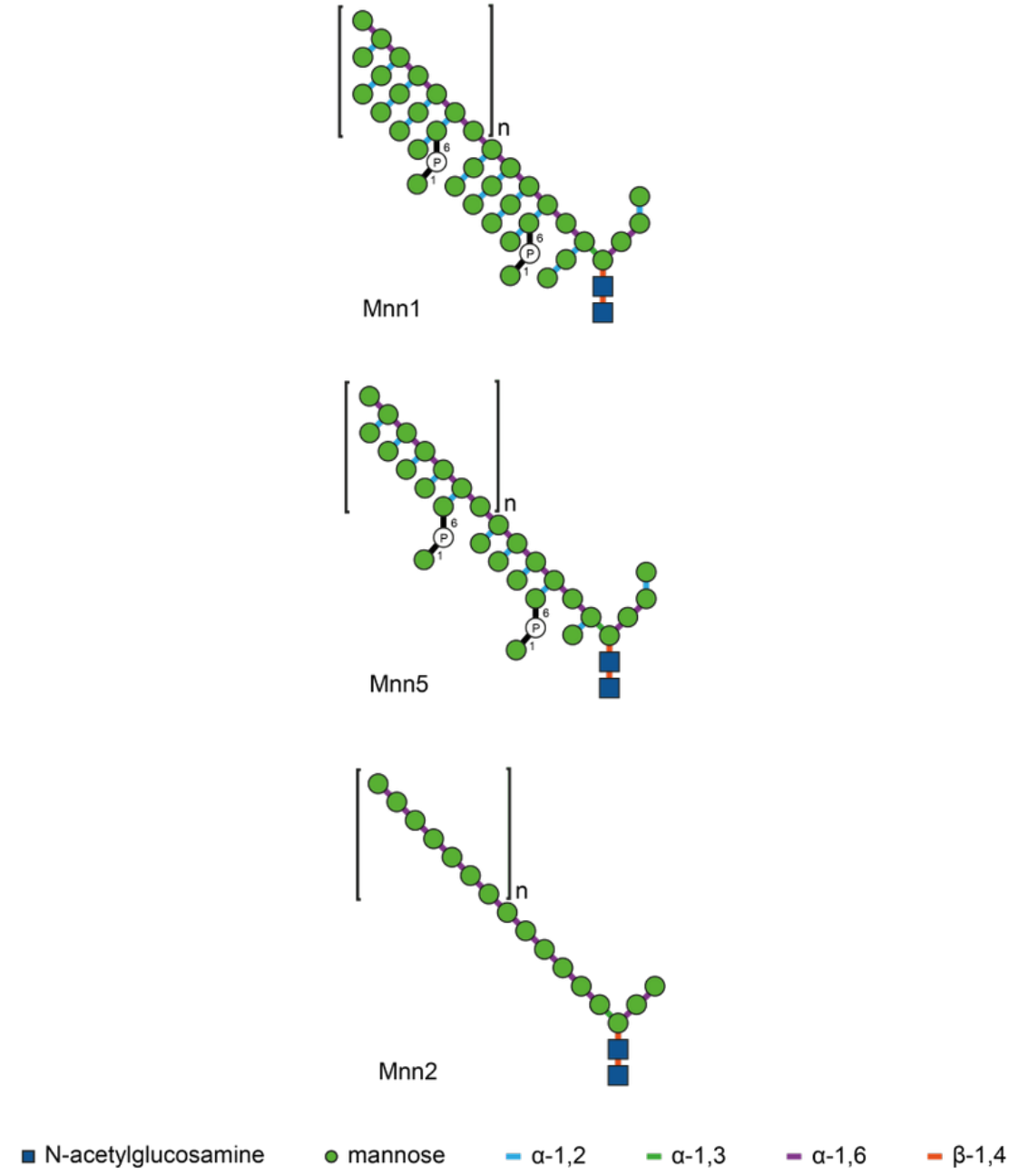

Figure 22: Structure of the mannans purified from the *S. cerevisiae* mutants Mnn1, Mnn2, and Mnn5. Structures vary in their complexity of backbone decoration as a result of loss of glycosyl transferases required for α-1,2 decorations. Key bonds are indicated by colours shown in key.

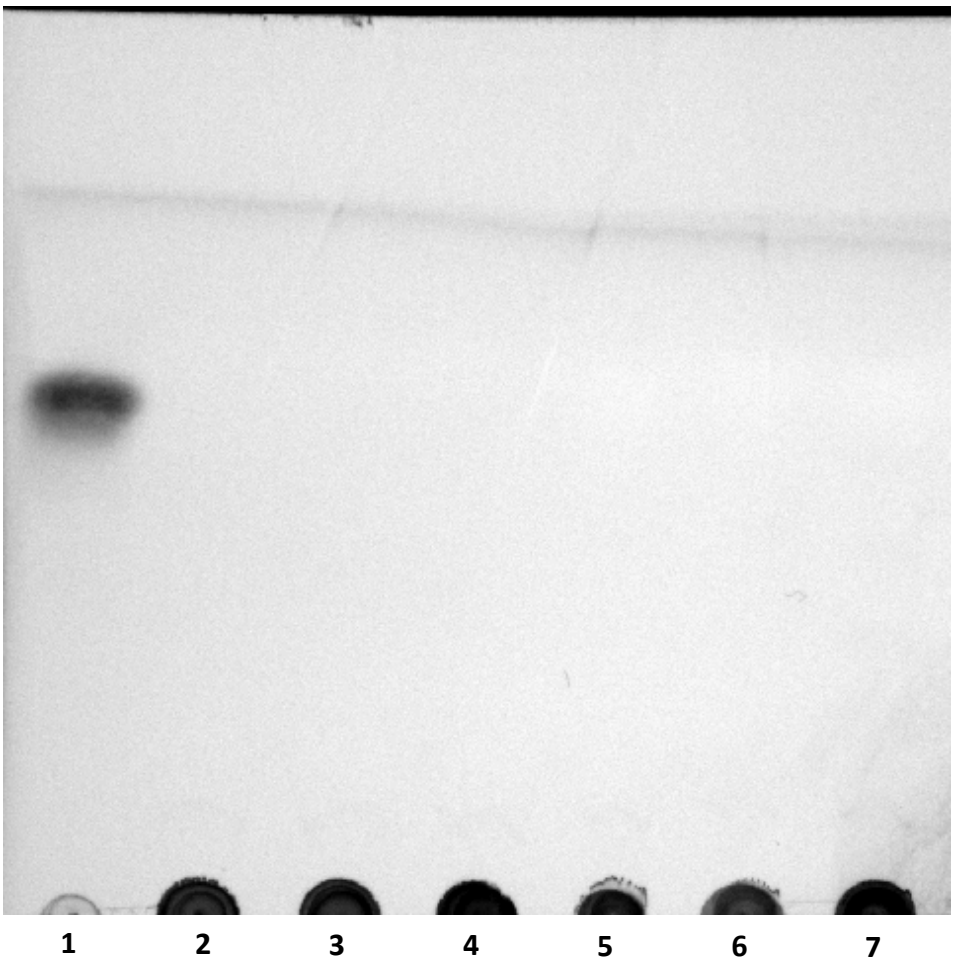

Figure 23: TLC analysis of Rv0365c assay on mannan substrates. (1) Mannose standard (2) Mnn1 enzyme-free control (3) Mnn5 enzyme-free control (4) Mnn2 enzyme-free control (5) Mnn1 with Rv0365c (6) Mnn5 with Rv0365c (7) Mnn2 with Rv0365c. No activity was observed for any of the reactions. TLC was stained with orcinol and then charred to reveal products.

These results showed that Rv0365c was not able to cleave any of these mannan substrates. We hypothesised that these substrates were too large for Rv0365c, and so the next approach was to take a previously characterised glycoside hydrolase 76 enzyme and digest the mannans to produce smaller oligosaccharides. To do this, Dr Elisabeth Lowe provided us with a plasmid containing the gene for expression of BT3792. This is an endo-acting glycoside hydrolase 76 from *Bacteroides thetaiotaomicron* that has formerly been shown to be active on these substrates (Cuskin & Lowe *et al.,* 2015). This plasmid was transformed into a T7 Shuffle expression strain and the protein was expressed and purified as described in Chapter 2.4.

As shown in Figure 24, the 50 mM, 100 mM, and 250 mM imidazole elutions all contained the protein of interest. These were therefore pooled and dialysed for 16 hours. Protein concentration was checked after dialysis and recorded at 3.7 mg / mL. The protein concentration was sufficient for use without the need for further concentration. To produce the shorter mannan oligos, 5 µM of protein was added to 1 mg / mL of substrate and incubated at 37 ℃ for 2 hours. The mixture was then heated at 100 ℃ for 10 mins to denature the enzyme. Figure 25 shows the bonds cleaved by BT3792 and an example of the resulting products produced.

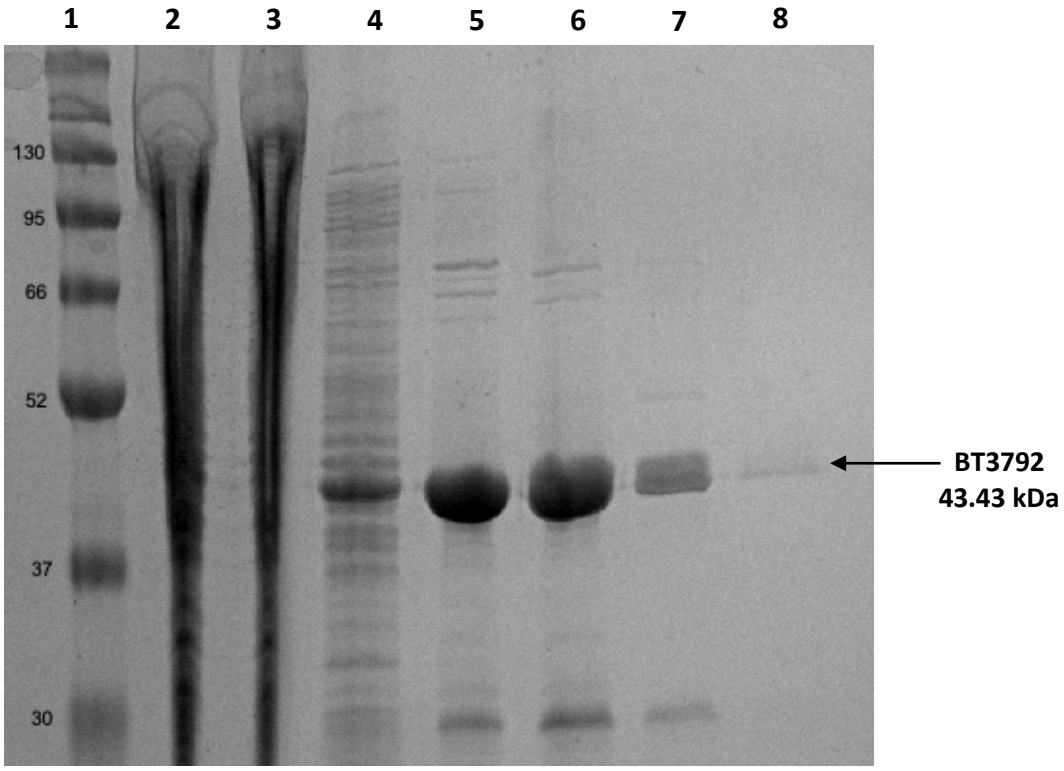

Figure 24: SDS-PAGE gel of BT3792 purification. Lanes: (1) Prestained protein ladder, (2) cell lysate, (3) flow through, (4) 25 mM imidazole wash, (5) 50 mM imidazole elution, (6) 100 mM imidazole elution, (7) 250 mM imidazole elution, and (8) 500 mM imidazole elution. Protein of interest, indicated by the arrow, was well expressed and was present in the 50, 100, and 250 mM fractions.

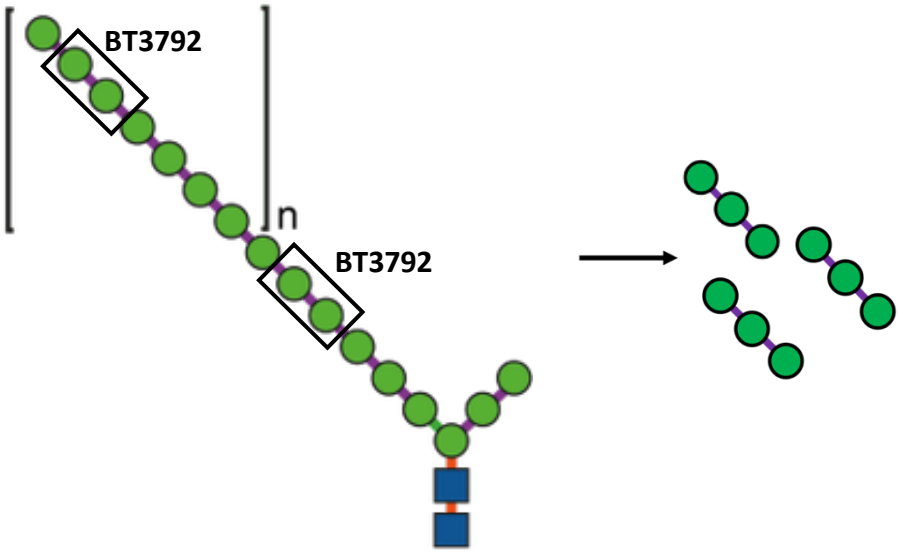

Figure 25: Model of Mnn2 mannan digestion by BT3792. Boxes indicate examples of bonds BT3792 will cleave. BT3792 was digest the α-1,6 glycosidic bonds between the mannose residues in the mannan backbone. This results in the production of shorter α-1,6 linked mannan oligosaccharides including trimannose.

To investigate if Rv0365c was enzymatically active on these shorter substrates, 1 µM of Rv0365c was added to 1 mg / mL of the substrate with 150 mM HEPES buffer at pH 7.5 and incubated for 16 hours at 37 ℃. Subsequently, 20 µl of sample was spotted onto a TLC plate, and separated in a n-butanol: acetic acid: water (2:1:1 v/v/v) solvent system. This is shown in Figure 26.

These results demonstrated that enzymatic activity could be detected when Rv0365c is incubated with the short, undecorated α-1,6 linked mannan oligos. This confirmed that Rv0365c was capable of α-mannanase activity and was therefore a confirmed member of the glycoside hydrolase 76 family. Furthermore, it showed that Rv0365c has a preference for short length oligos of mannan as enzymatic activity was not detected when assayed on the full-length substrate. Following this, a time-course assay was set up. This is shown in Figure 27.

To conduct the time-course assay, a 1 mL reaction was set up consisting of 1 mg / mL substrate and Rv0365c at a concentration of 1 µM. The reaction was incubated at 37 ℃ and a 20 µl sample was taken at the described time points and heated at 100 ℃ for 10 mins to denature the enzyme and stop the reaction. As shown in Figure 27, enzymatic activity could be detected after around 1 hour of incubation.

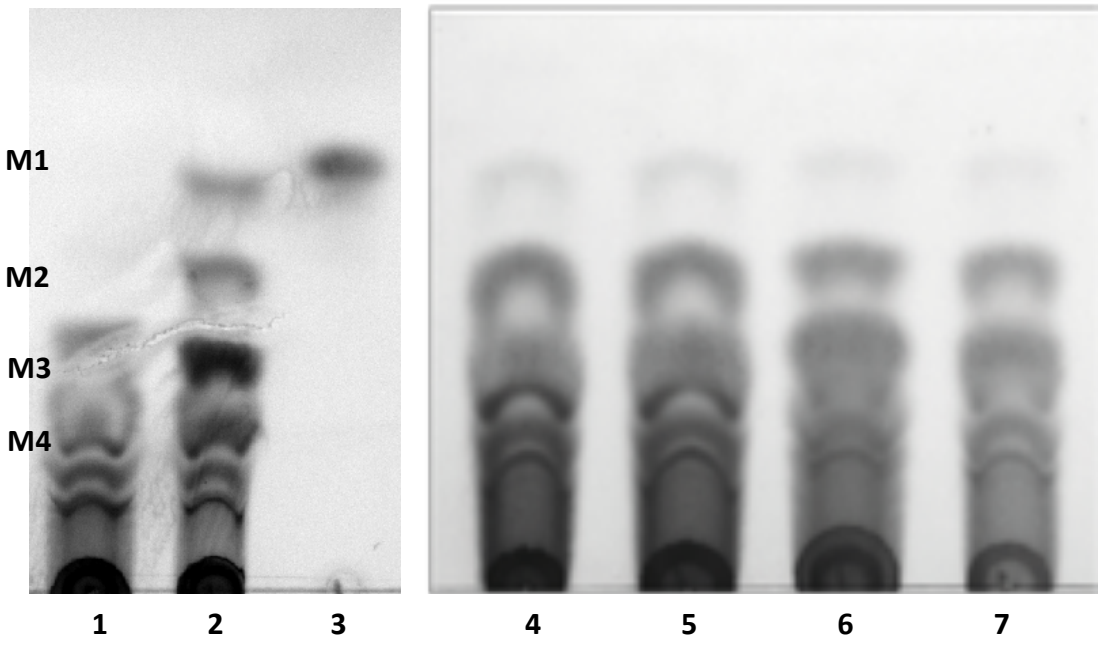

Figure 26: TLC analysis of Rv0365c assay on short mannan oligos. (1) digested Mnn2 enzyme-free control (2) digested Mnn2 with Rv0365c (3) mannose standard (4) digested Mnn1 enzyme-free control (5) digested Mnn1 with Rv0365c (6) digested Mnn5 enzyme-free control (7) digested Mnn5 with Rv0365c. TLC was stained with orcinol and charred to reveal products. Enzymatic activity was detected when Rv0365c was assayed on the shorter Mnn2 oligos.

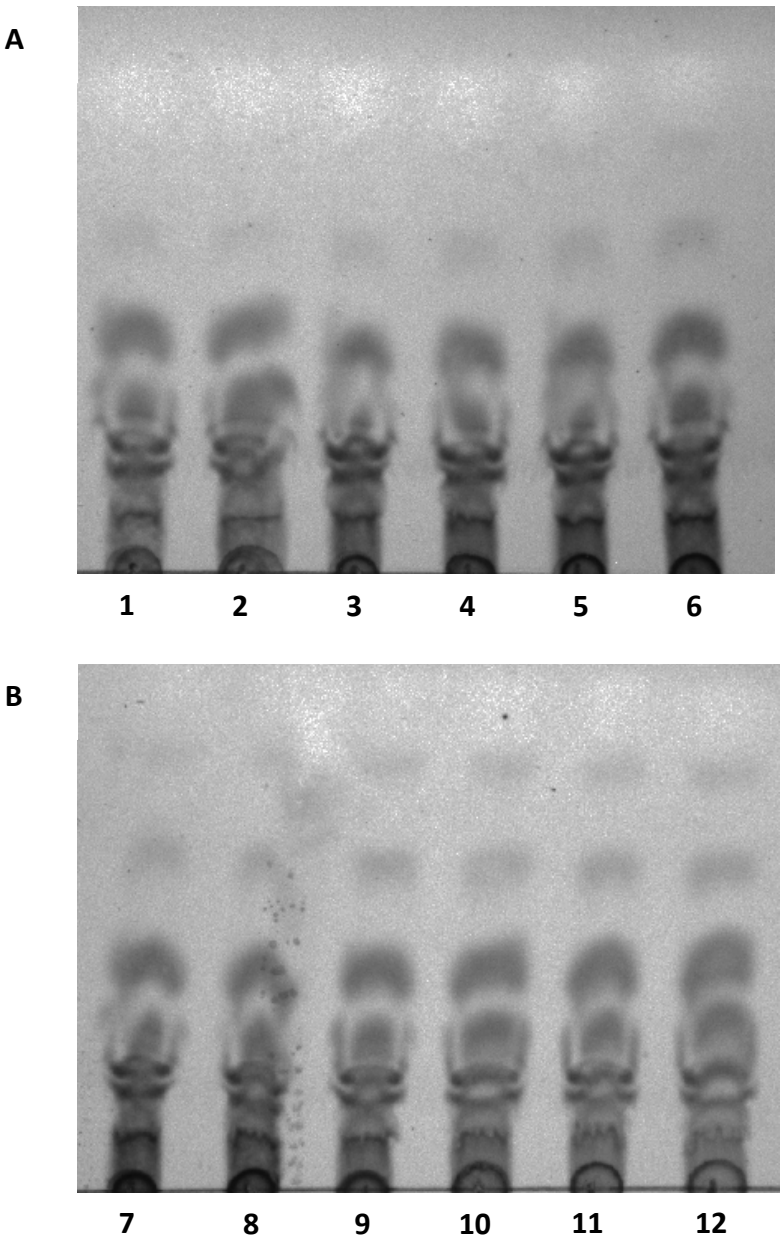

Figure 27: TLC analysis of time-course assay of Rv0365c on short α-1,6 linked mannan oligos. A) (1) 5 minutes (2) 10 minutes (3) 30 minutes (4) 1 hour (5) 1.5 hours (6) 2 hours **B)** (7) 2.5 hours (8) 3 hours (9) 3.5 hours (10) 4 hours (11) 4.5 hours (12) 24 hours. Reactions were separated in n-butanol: acetic acid: water (2:1:1 v/v/v), stained with orcinol, and charred to reveal products. Enzymatic activity could be detected after 1 hour of incubation time.

3.3.5 Rv0365c is active on lipomannan and lipoarabinomannan

Following confirmation that Rv0365c was capable of cleaving α-1,6 linked mannan, we next set out to determine the true substrate of the enzyme in the mycobacterial cell wall. Our hypothesis was that lipoarabinomannan and lipomannan were these substrates, as it contains undecorated α-1,6 linked mannan within the mannan backbone, as shown in Figure 8. Lipoarabinomannan and lipomannan were purified from *M. bovis* BCG Danish as described in Chapter 2.5.2. A 100 mL culture was grown to an OD_{600} of 0.8, and then a phenol extraction was performed. This produced a glycolipid yield of 15 mg dry weight. The lyophilised material was then resuspended in water to a concentration of 5 mg / mL. To test if Rv0365c was active on this LAM/LM mixture, 1 µM of protein was incubated with 1 mg / mL of substrate and incubated for 16 hours at 37 ℃. Following this, the reaction was stopped by heat inactivation at 100 ℃ for 10 mins. A 15 µl sample was spotted onto a TLC plate (Merck, TLC Silica Gel 60 F_{254}) and separated in a chloroform:methanol:water (65:25:4 v/v/v) solvent system. This is shown in Figure 28.

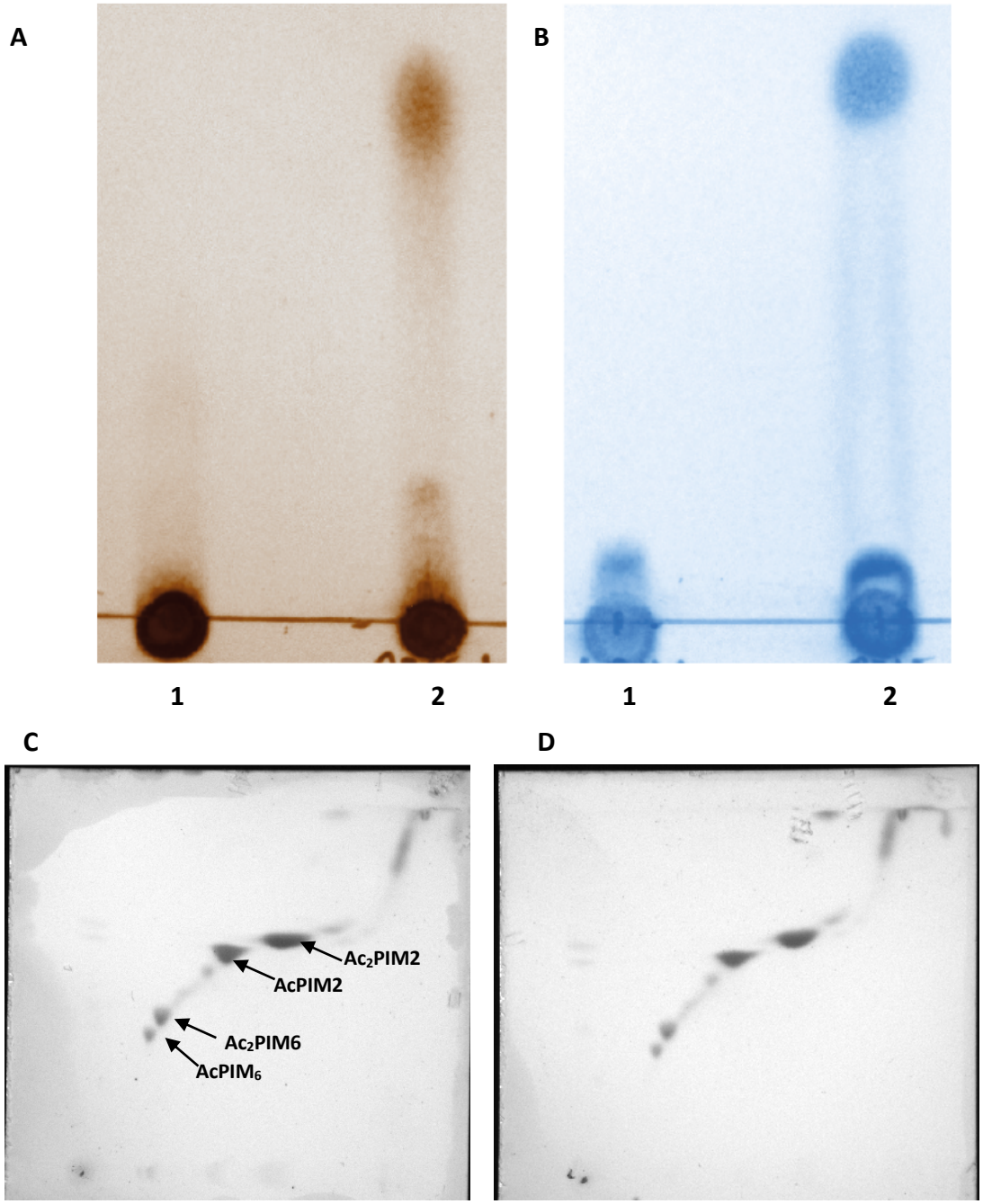

Figure 28: TLC analysis of Rv0365c assay on lipoarabinomannan, lipomannan, and PIMs purified from *M. bovis* BCG Danish. A) Rv0365c assay on LAM/LM. TLC is stained with orcinol and heated to reveal carbohydrate products. **B)** Rv0365c assay on LAM/LM. TLC is stained with phosphomolybdic acid (MPA) and heated to reveal lipid products. Lane 1 represents an enzyme-free control assay. Lane 2 represents the assay containing Rv0365c. Enzymatic activity was detected in protein containing reactions. **C)** Wild-type PIMs extracted from BCG. **D)** Rv0365c assayed with wild-type PIMs. Samples were separated first in chloroform:methanol:water (60:30:6 v/v/v), and in second direction in chloroform:acetic acid:methanol:water (40:25:3:6 v/v/v/v). TLC was stained with orcinol and heated to reveal products.

As shown in Figure 28 enzymatic activity can be detected when Rv0365c is assayed with lipoarabinomannan and lipomannan. There is a small reaction product produced that stains positive for both carbohydrate and lipid, as shown in Figure 28a and 28b respectively. In addition, we also tested the activity on a PIMs extract. PIMs are the precursor molecules of LM and LAM, and so also contain α-1,6 linked mannan. The extracted PIMs were resuspended to a concentration of 10 mg / ml. Subsequently, 1 µM of protein was incubated with 1 mg / mL of PIMs. However, as can be seen in Figure 28d no activity could be detected on the PIMs. This suggests that Rv0365c is specifically active on LM and LAM. Following confirmation that Rv0365c was active on LAM, a time-course assay was performed to monitor the rate of the reaction. As before, 1 µM of protein was incubated with 1 mg / mL of substrate and incubated at 37 ℃. A 20 µl sample was taken at the described time points, and heat inactivated at 100 ℃ for 10 mins. This is shown in Figure 29.

As shown in Figure 29, enzymatic activity could be detected after 30 minutes of incubation. Therefore, a shorter time-course assay was performed where samples were taken and heat inactivated over the course of 1 hour. This is shown in Figure 30.

The short time-course revealed that enzymatic activity could be detected after around 15 minutes of incubation. However, incubation for at least 1 hour was required to achieve a similar intensity to those seen previously.

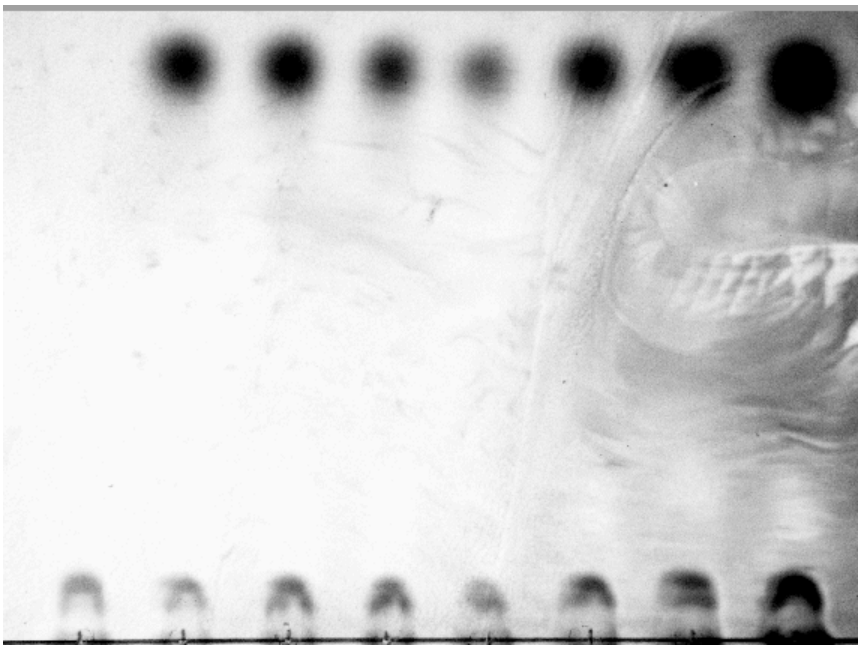

Figure 29: TLC analysis of time-course assay of Rv0365c on LAM and LM. (1) Enzyme-free control (2) 30 minutes (3) 1 hour (4) 1.5 hours (5) 2 hours (6) 2.5 hours (7) 3 hours (8) 16 hours. Reactions were separated in chloroform: methanol: water (65: 25: 4 v/v/v), stained with MPA, and charred to reveal products. Enzymatic activity was seen after 30 minutes of incubation time.

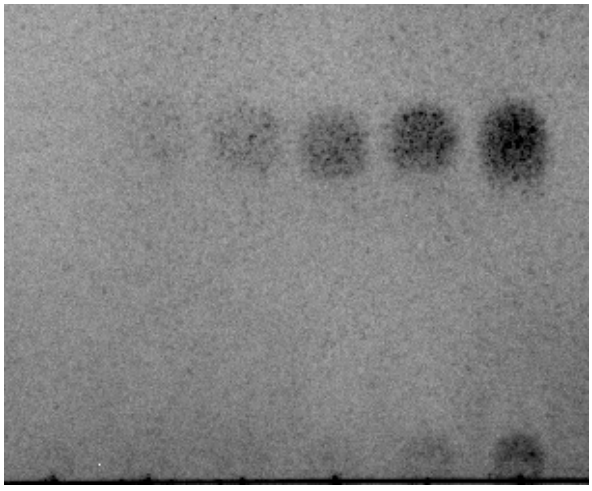

Figure 30: Short time-course assay of Rv0365c on LAM and LM. (1) 1 minute (2) 5 minutes (3) 10 minutes (4) 15 minutes (5) 30 minutes (6) 1 hour. Reactions were separated in chloroform: methanol: water (65: 25: 4 v/v/v), stained with MPA, and charred to reveal products. Activity could be seen after 15 minutes of incubation time.

3.3.6 Digestion of LM/LAM produces AcPIM$_2$ lipid carrier product

After confirmation that Rv0365c was active on LAM and LM, the next aim for this chapter was to identify the small glycolipid reaction product. To isolate the product, 1 mL of chloroform and 1 mL methanol were mixed with a 300 µl reaction to produce a 10:10:3 mixture. This was mixed on a rotator for 1 hour. Subsequently, 1.75 mL chloroform and 750 µl water were added to form a bilayer. The organic phase (lower phase), which contained the lipid product, was transferred to a fresh tube and further purified using a Octadecyl C18 column (Amprep, RPN 110). The sample was eluted from the column with chloroform, and dried under a stream of nitrogen. The dried product could then be resuspended in a mixture of methanol and water (1:1) and submitted for mass spectrometry analysis by Dr Todd Mize at the University of Birmingham. The result of this was a peak of interest at m/z 1413.9. This was further fractionated in MS/MS. The result of this is shown in Figure 31.

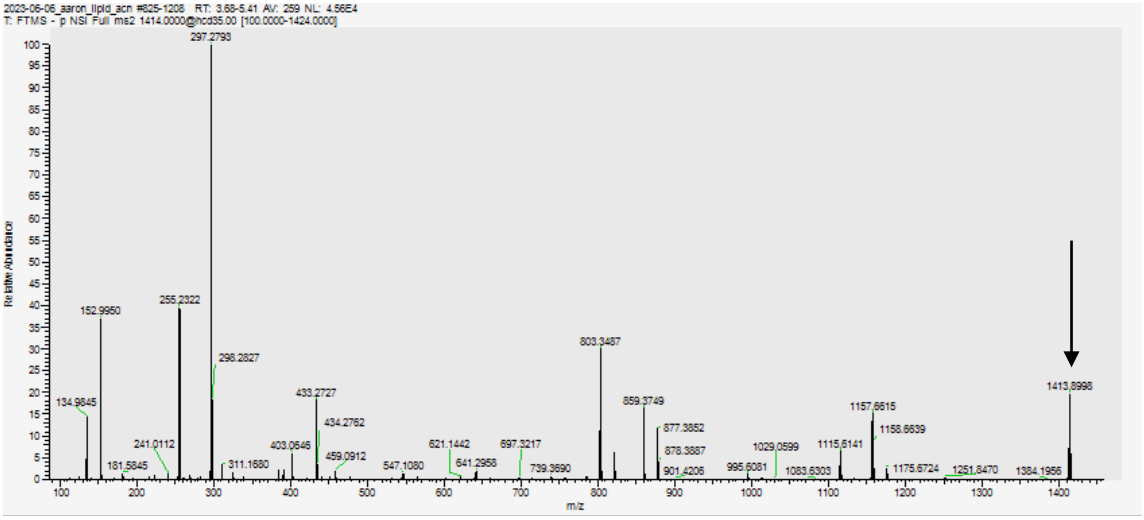

Figure 31: Negative electrospray ionisation process (ESI) mass spectra of reaction product. Reaction product was directly injected and analysed in negative ion mode. Peak indicated by arrow is of interest as it is m/z consistent with $AcPIM_2$ structure. This peak was further fractionated in MS/MS.

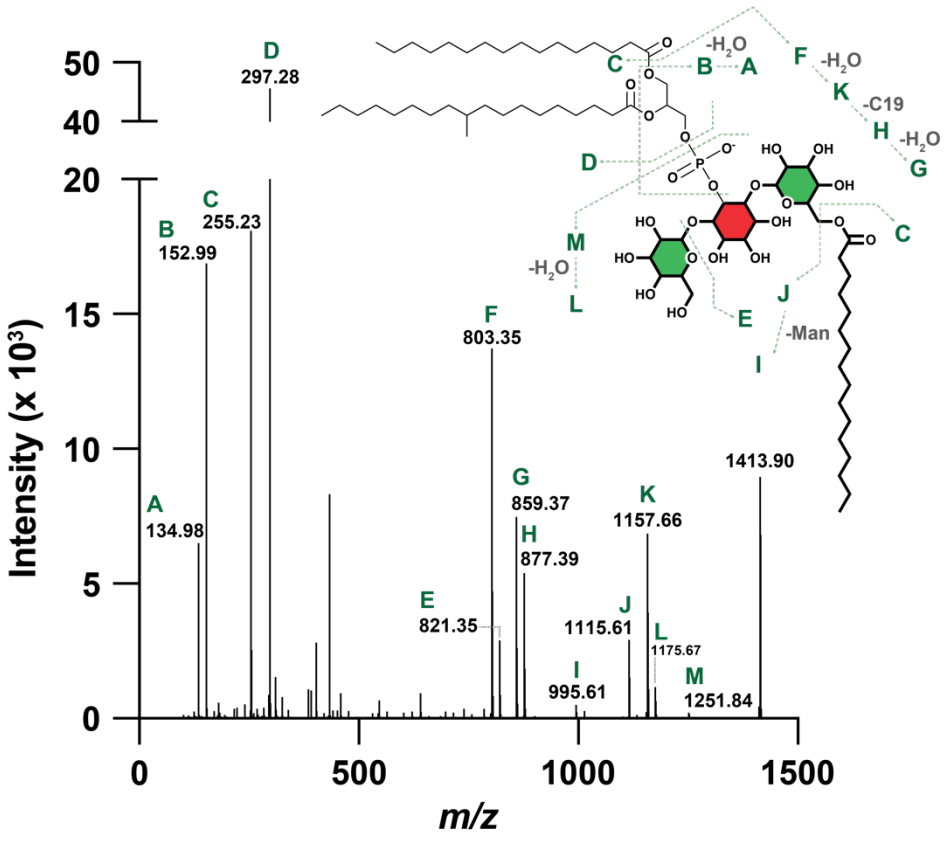

Figure 32: MS/MS profile of isolated reaction product. The peak of interest at m/z 1413.90 was fractionated by ms/ms. The fragmentation pattern is consistent with an $AcPIM_2$ species. This suggests that out isolated reaction product is this species. Also shown is the structure of $AcPIM_2$ and its fragmentation patterns with associated peaks indicated by letters A-M.

The initial direct injection analysis of the purified reaction product revealed a peak at m/z 1413.9. This peak of interest was then fractionated in MS/MS. This data was replotted in Figure 32 to show the fractionation of the product.

There were several possible sites that Rv0365c could be cleaving in the LAM / LM structure. The results shown in Figure 32 demonstrate that the small reaction product we purified had a structure consistent with that of $AcPIM_2$. Therefore, we concluded that Rv0365c is acting on LAM and LM to cleave this small lipid carrier from the molecule.

3.3.7 Catalytic residues are consistent with previously characterised GH76 enzymes

Previously characterised GH76 catalytic residues have been reported to be a pair of consecutive aspartic acids (Cuskin & Lowe *et al.,* 2015; Thompson *et al.,* 2015). To confirm that this was consistent in Rv0365c, the equivalent pair of consecutive aspartic acids were located by comparing the AlphaFold prediction to Aman6 (PDB: 4BOK). The resulting sequence analysis revealed an overall sequence homology of 24.78%. However, the catalytic residues of Aman6 were perfectly aligned with a homologous pair of aspartic acids in Rv0365c. The first of these residues, Asp96 (numbering relative to genomic annotation), was substituted for an alanine using the NEB Q5 mutagenesis protocol. The primers used for this are listed in Table 5. PCR was performed as described in Chapter 2.3.1. The annealing temperature was 58 ℃, and the Kinase, Ligase, DpnI (KLD) treatment was performed as per manufacturer's instructions (https://nebasechangerv1.neb.com).

Table 5: Primers used for Site-Directed Mutagenesis

Name	Sequence	Length	Tm (℃)
CatNull_Fwd	TCCTACTATGgcgACATGGCTTGG	24	58
CatNull_Rvs	GTTGAGCCAGCTAAAG	16	57

The KLD mixture was transformed into competent *E. coli* top 10 cells as per Chapter 2.2.2. Successful transformation was confirmed by sequencing, and the plasmid was transformed into the T7 Shuffle expression strain of *E. coli*. As described in Chapter 2.4, the catalytic null version of Rv0365c was expressed and purified. This is shown in Figure 33.

As shown in Figure 33, the catalytic null version of Rv0365c was present in the 500 mM elution. This was therefore dialysed overnight against 100 mM HEPES pH 8.0, 150 mM NaCl. Following this, the protein solution was concentrated to 3.1 mg / mL and flash frozen in liquid nitrogen.

Following purification of the catalytic null variant of Rv0365c, an assay was prepared using the Mnn2 substrate that had been pre-digested with BT3792 in which Rv0365c enzymatic activity was previously detected. 1 µM of catalytic null Rv0365c was added to 1 mg / mL of pre-digested Mnn2 and incubated for 16 hours at 37 ℃. Following this, 20 µl of sample was spotted onto a TLC plate, and separated in a n-butanol: acetic acid: water (2:1:1 v/v/v) solvent system. This is shown in Figure 34.

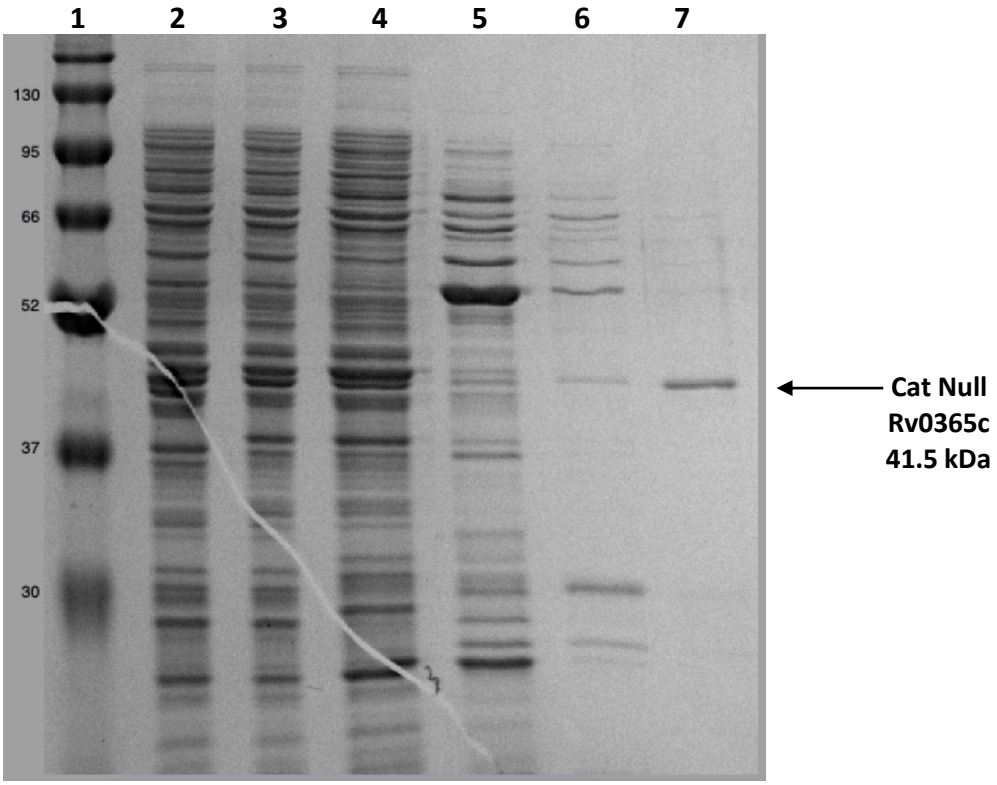

Figure 33: Purification of Catalytic Null Rv0365c on an SDS-PAGE gel. Lanes: (1) Pre-stained protein ladder (kDa), (2) cell lysate, (3) flow through, (4) 5 mM imidazole wash, (5) 50 mM imidazole elution, (6) 100 mM imidazole elution, and (7) 500 mM imidazole elution. Protein of interest, indicated by arrow, was present in the 500 mM fraction.

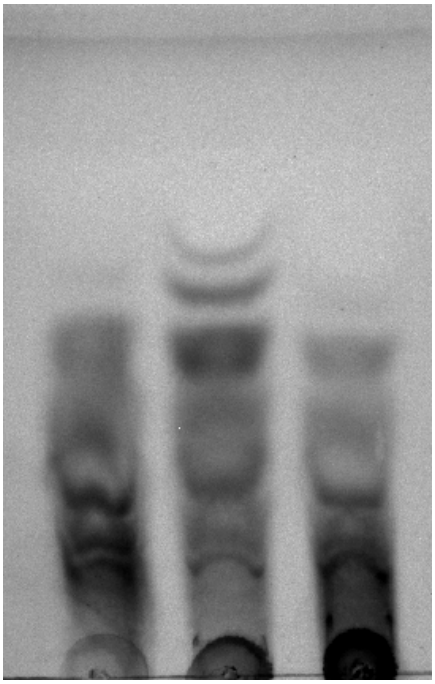

Figure 34: TLC analysis of catalytic null Rv0365c assay on Mnn2. (1) enzyme-free control, (2) Rv0365c assayed with digested Mnn2, (3) catalytic null Rv0365c assayed with digested Mnn2. TLC was stained with orcinol and charred to reveal products. Enzymatic activity was only detected with the wild-type variant of the protein. Catalytic null variant was unable to hydrolyse the substrates.

Figure 34 confirms that when the first catalytic residue, Asp96, is mutated to an alanine there is a complete loss of enzymatic activity. However, enzymatic activity is still detectable in the wild-type version of the protein. This confirmed that the catalytic residues were consistent with previously characterised GH76 proteins. Following this, an assay with the LM/LAM substrate was set up to confirm that enzymatic activity was also lost on the natural substrate for the enzyme. As before, 1 µM of catalytic null Rv0365c was added to 1 mg / mL of LM/LAM and incubated for 16 hours at 37 ℃. Following this, 20 µl of sample was spotted onto a TLC plate, and separated in a chloroform:methanol:water (65:25:4 v/v/v) solvent system. The TLC was stained with MPA and products were revealed with heating. This is shown in Figure 35.

As shown by Figure 35, no enzymatic activity can be detected when the cat null variant of Rv0365c is assayed with the LM/LAM substrate. However, enzymatic activity is detected when the wild-type version of the protein is assayed with LM/LAM. This provided further support that the catalytic residues of Rv0365c are consistent with that of previously characterised GH76's.

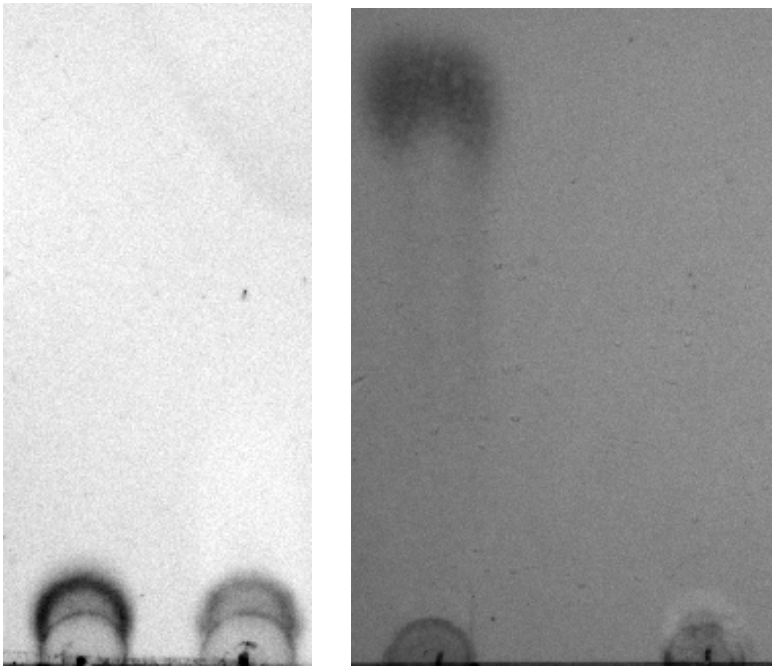

Figure 35: TLC analysis of catalytic null Rv0365c assay on LM/LAM. (1) Enzyme-free control LM/LAM, (2) catalytic null Rv0365c assay on LM/LAM, (3) Rv0365c assay on LM/LAM, (4) Enzyme-free control LM/LAM. TLC was stained with MPA and charred to reveal products. Catalytic null variant of the protein was unable to digest LM/LAM. Enzymatic activity was still seen when substrate was incubated with the wild type protein.

3.3.8 Rv0365c is active on both LAM and LM

The final aim for this chapter was to determine if Rv0365c was active on both lipomannan and lipoarabinomannan. The evidence shown previously in this chapter only confirms that the enzyme is active on the mixture of substrates. Therefore, to determine if the enzyme was active on both LM and LAM, the assays were conducted and separated via SDS-PAGE. Following this, a ProQ Emerald glycolipid gel stain was employed to visualise the separated glycans. As before, 1 µM of enzyme was incubated with 1 mg / mL of the LM/LAM substrate mixture for 4 hours at 37 ℃. 20 µl of reaction was then mixed with 5 µl of 6x loading dye, and the samples were separated on a 4-20% precast gel. The glycolipid stain was performed, as per Chapter 2.6.2, and the results are shown in Figure 36. Three technical replicates are shown whereby the assay was repeated three times using the same protein and substrate stocks.

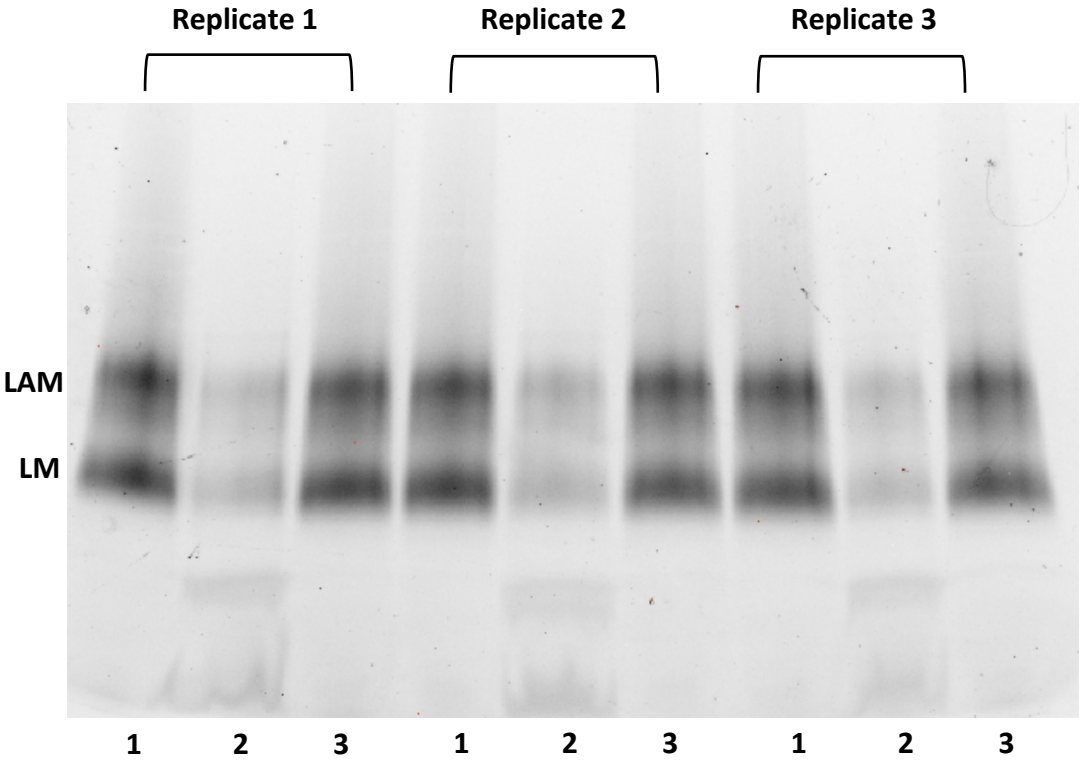

Figure 36: ProQ Emerald 300 Glycoprotein stained gel. Samples were separated at 200 v, 50 mA, for 45 minutes. Bands were visualised with ProQ Emerald staining. (1) Enzyme-free control, (2) Rv0365c assay on LM/LAM, (3) catalytic-null Rv0365c assay on LM/LAM. Wild-type Rv0365c assay resulted in visible reduction of LM/LAM band intensity in each replicate. Catalytic null reaction had no effect on LM or LAM band intensity.

The results shown in Figure 36 show that levels of LAM and LM appear to be reduced when Rv0365c is present. To confirm this, ImageLab software was used to determine the intensity of each of the bands. This is shown in Table 6. The intensity readings were then plotted, and this is shown in Figure 37. The levels of LAM and LM are significantly reduced after enzymatic digestion with Rv0365c. Furthermore, the catalytic null variant of Rv0365c had no significant effect on the level of LAM and LM. This confirmed that Rv0365c was active on both LAM and LM.

Table 6: Fluorescence intensity of bands in Figure 36

Lane	LAM Intensity	LM Intensity
1	2086	2368
2	978	1068
3	2000	2356
4	2068	2322
5	1032	1070
6	2020	2172
7	2094	2273
8	862	923
9	1906	2147

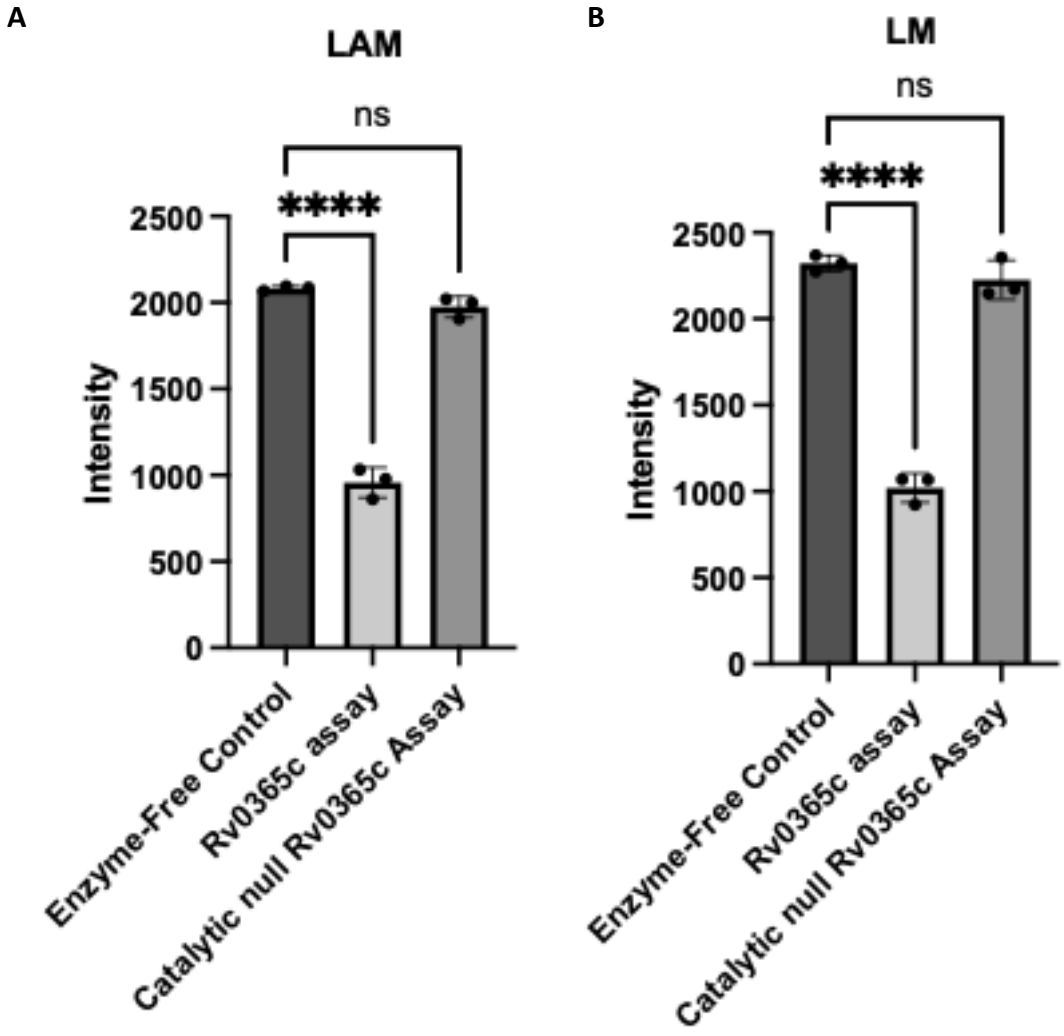

Figure 37: Fluorescence intensity of LM/LAM bands from Table 6. A) LAM and **B)** LM. Intensity of bands was determined using ImageLab software, and then plotted in GraphPad Prism v10.0.2. For each assay n=3, significance determined by one-way ANOVA test where ****p<0001. Values shown are mean with error bars showing standard deviation. Rv0365c incubation resulted in significant reduction in LM/LAM intensity. Catalytic null incubation had no significant effect on levels of LM or LAM.

To further explore the reaction rate of Rv0365c and LM/LAM. A time-course assay was conducted, and samples were taken at various time points. This was repeated for a total of 3 replicates. These samples were analysed via SDS-PAGE with ProQ staining. The results of this are shown in Figure 38.

The results in Figure 38 show that LM and LAM levels reduce over the 4 h incubation time. To quantify this, ImageLab was again used to determine the intensity of each band for each replicate, shown in Table 7. These values were then plotted using GraphPad Prism v10.0.2 and expressed as a percentage of the relevant control, shown in Figure 39.

The results shown in Figure 39 suggest that the rate of reaction is not different between LAM and LM as both substrates decrease at the same rate. For LAM degradation the rate of the liner portion of the curve was 0.82 % / min and for LM degradation the rate was 0.67 % / min. These values were found to be not significantly different by t-test. Therefore, it is not likely that Rv0365c prefers one substrate over the other.

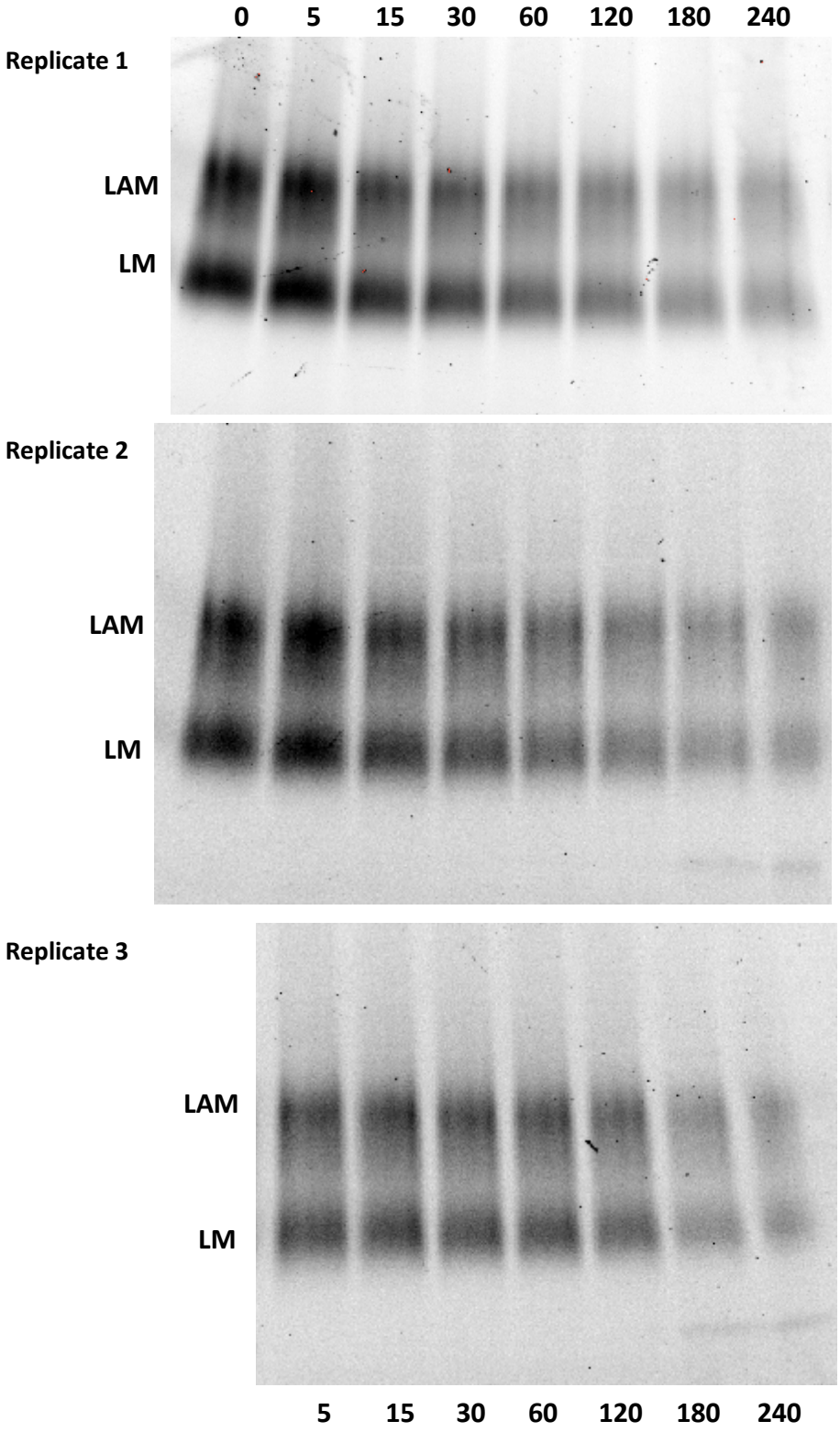

Figure 38: Time course assay of Rv0365c on LM/LAM. Samples separated at 200 v, 50 mA, for 45 minutes. (1) Enzyme-free control (2) 5 minutes (3) 15 minutes (4) 30 minutes (5) 1 hour (6) 2 hours (7) 3 hours (8) 4 hours. Three replicates are shown. Replicate 3 does not have an enzyme-free control. Visible reduction in intensity of both LM and LAM bands can be seen over the 4 hour incubation period.

Table 7: Fluorescence intensity of bands in Figure 38

Lane	LAM Intensity	LM Intensity
Replicate 1		
1	2467	2530
2	2471	2710
3	2073	2272
4	1891	2048
5	1577	1738
6	1426	1578
7	1220	1327
8	1122	1164
Replicate 2		
1	405	443
2	403	436
3	353	371
4	323	334
5	282	291
6	245	251
7	213	206
8	180	179
Replicate 3		
1	405	443

2	331	335
3	323	334
4	298	315
5	287	305
6	241	270
7	179	205
8	151	177

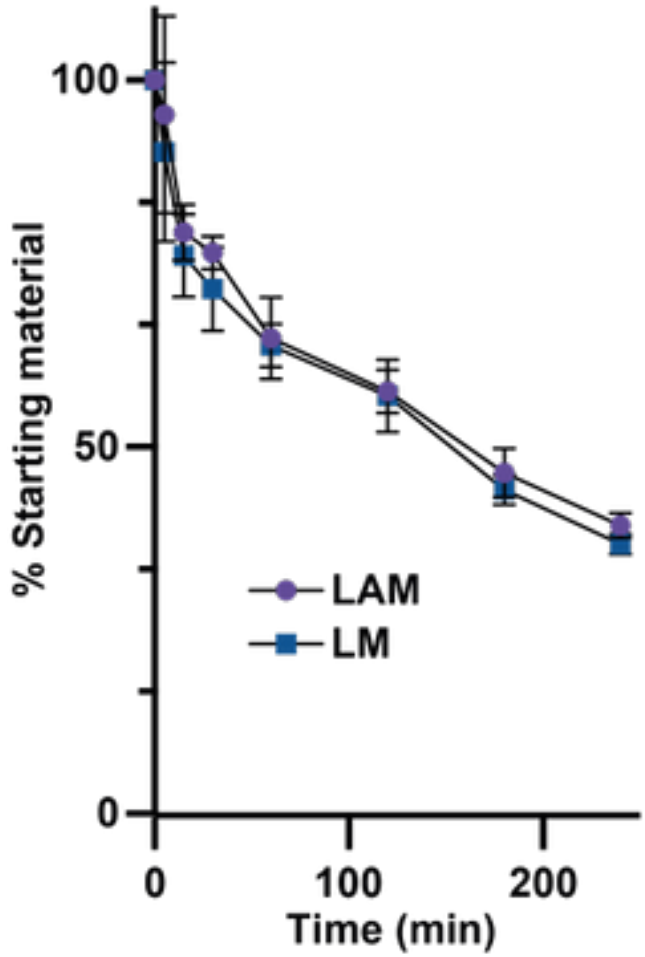

Figure 39: Relative intensity of LAM / LM levels during incubation with Rv0365c. Fluorescence determined using ImageLab and expressed as a percentage of the starting material in GraphPad Prism v10.0.2. Values shown are the mean with error bars showing standard deviation.

3.4 Discussion

The aim of this chapter was to biochemically characterise Rv0365c and confirm that it is a legitimate member of the glycoside hydrolase 76 family. This primarily meant the enzyme needed to be purified, and this presented the first challenge faced in this thesis. Despite good expression of the protein, purification was exceedingly difficult. The majority of our attempts to purify this enzyme resulted in low yields, and precipitated protein. Following a 9-month period, where reduced lab hours and socially distanced training had to take place, the purification protocol was optimised to a point where we could confidently purify the protein and begin biochemical characterisation. The optimised protocol included the addition of 5% glycerol and 1% Tween20 to the lysis buffer. This improved stability of the protein during purification. Furthermore, pre-chilling of the dialysis buffer was essential. The buffer was made at least one-day before use and kept at a constant 4 ℃. Unfortunately, we have not yet been able to purify Rv0365c to a high enough concentration to obtain an experimentally determined crystal structure. We therefore had to rely on the services of AlphaFold to predict the structure and compare this to pre-existing experimentally determined GH76 structures (Jumper *et al.,* 2021; Varadi *et al.,* 2022). In Figure 21 the predicted structure of Rv0365c was compared to the experimentally determined Aman6 (PDB: 4BOK). The structural alignment indicated that the two enzymes are similar (R.M.S.D = 2.2 Å), but that Rv0365c possesses an additional beta-hairpin cap that covers the predicted active site of the enzyme. This appears to be a structural motif which is unique to the mycobacterial protein as it can be seen in the AlphaFold predicted models for MMAR_0667 and

MSMEG_0740. These are the homologues of Rv0365c from *M. marinum* and *M. smegmatis*.

As previously reported, GH76 proteins will specifically recognise and cleave α-1,6 linked mannan (Cuskin & Lowe *et al.,* 2015; Maruyama and Nakajima, 2000; Nakajima, Maitra and Ballou, 1976). Within the mycobacterial cell wall, there is currently only one known, described site of α-1,6 mannan. This is in the mannan backbone of the glycolipids lipoarabinomannan and lipomannan as well as in PIMs which act as precursor molecules. This became the basis of our hypothesis as we predicted that Rv0365c would be active against these substrates. However, first we needed to show that the enzyme was specifically active against α-1,6 mannan. LAM and LM have complex structures, as shown in Figures 7 and 8. This meant they were unsuitable to use as substrates to determine specific linkage activity of this enzyme. We therefore employed three mutant strains of *S. cerevisiae* which lacked glycosyltransferases required to synthesise mannan, and so produced mannans of varying complexity. These mannans, shown in Figure 22, were purified and used for our first assays with Rv0365c. Our initial attempts to demonstrate GH76 activity were unsuccessful. As shown by Figure 23, there were no observable reaction products following the assay indicating that Rv0365c was unable to digest the substrates. The mannan backbone of LAM and LM contains a short stretch of undecorated α-1,6 mannan followed by a longer stretch of α-1,6 mannan decorated with α-1,2 Man*p* side chains. We therefore hypothesised that Rv0365c was specific for the shorter, undecorated α-1,6 mannan. To test this, we used a previously characterised GH76 family protein, BT3792, which has been shown to be active on these substrates to

produce shorter mannan oligos (Cuskin & Lowe *et al.,* 2015). Using these shorter mannan oligos, we were able to confirm GH76 activity as observable reaction products were produced when the enzyme was assayed on the shorter Mnn2 substrate. This is shown in Figure 26. Furthermore, these data also confirmed that the enzyme is unable to act on the backbone when the α-1,2 side chains are present. Taken together, this data suggested that Rv0365c is a genuine member of the GH76 family, and it prefers short, undecorated α-1,6 linked mannan. Additionally, this data supported our theory that Rv0365c was acting on the short, undecorated stretch of α-1,6 mannan at the start of the mannan backbone in the LM/LAM structure.

Following confirmation that Rv0365c was a GH76 family member, we next turned our attention to identifying the true substrate for Rv0365c in the mycobacterial cell wall. To do this, LAM and LM were purified from *M. bovis* BCG Danish and incubated with Rv0365c. To analyse this reaction, a TLC solvent system was utilised that would see the carbohydrate domain retained at the origin but separate any glycolipids. Using this system, we were able to show that when Rv0365c is assayed on LM and LAM it will release a small glycolipid product which stains positive for both carbohydrate and lipid (Figure 28). This small product was isolated from the reaction mixture, further purified using a C18 column, and then analysed by mass spectrometry. The result of this analysis was that we could identify a fragmentation pattern which was consistent with an $AcPIM_2$ structure. This demonstrated that the small product being released from the reaction was $AcPIM_2$. This is a molecule used in the biosynthesis of LM and LAM (Figure 6). This finding led to the hypothesis that this reaction product could be recycled by

mycobacteria, and used to synthesise new PIMs, LM, or LAM. This is a hypothesis which we will test in Chapter 4. As α-1,6 mannan is also present in PIMs, we speculated whether Rv0365c would be active on the higher-order PIMs ($AcPIM_6$ species) and if it would release the same product. To test this, we extracted PIMs from *M. bovis* BCG and assayed Rv0365c on them. To analyse the reactions, we employed the use of two-dimensional thin-layer chromatography. This allows for samples to be separated in two different directions and allows for better separation of the different PIM species. However, the result of this was that we did not detect any visible changes in the PIM profile when incubated with Rv0365c. This suggested that the enzyme was not able to digest the high-order PIMs. Earlier in the chapter, we demonstrated that Rv0365c was only active on undecorated α-1,6 mannan. However, the structure of the $AcPIM_6$ species contains α-1,2 linked Man*p* residues. We therefore speculated that these α-1,2 decorations were inhibiting the activity of the enzyme somehow.

To continue the biochemical characterisation of Rv0365c, we next sought to identify the catalytic residues in this enzyme. Previously characterised GH76 proteins have had catalytic residues which consist of a pair of consecutive aspartic acids (Cuskin & Lowe *et al.,* 2015; Thompson *et al.,* 2015). To confirm that Rv0365c was consistent with the family members, the equivalent pair of aspartic acids were identified as D96 and D97. We then generated a D96A mutant version of the protein and could no longer detect activity when this mutation was present (Figure 35). These findings provided further evidence that Rv0365c was a true GH76 family member.

The final objective for this chapter was to verify that Rv0365c was active against both LM and LAM rather than preferring one substrate over the other. Our data so far had provided evidence that the enzyme was active against a mixture of LM/LAM. To do this, we needed a way to visualise both LM and LAM, and quantify their relative abundance. We therefore separated the reaction products by SDS-PAGE gel electrophoresis and used a ProQ Emerald stain, which generates a fluorescent signal when it reacts with periodic acid-oxidised carbohydrate groups, to visualise the relative levels of LM and LAM (Figure 36). This allowed us to confirm that Rv0365c was active on both LM and LAM, and demonstrate that the catalytic null enzyme had no enzymatic activity. The fluorescence was visualised by U.V. exposure using a GelDoc and quantified using ImageLab. This allowed us to show that the levels of both LM and LAM are significantly reduced when Rv0365c is present. As shown in Figure 38, there is a small band beneath the LM in the Rv0365c reaction which is not present in the control or catalytic null assay. We therefore speculated that this was one of the reaction products. This is supported by Kaur *et al.,* (2008), as they separated LAM, LM, and PIMs by SDS-PAGE gel electrophoresis and identified a band, similar to ours, as PIMs. However, so far, we are yet to confirm that the band seen in Figure 36 is PIMs. Following the success of the ProQ Emerald staining, we utilised the stain to perform a time-course assay in which we could track the abundance of LM and LAM over a period of time. This allowed us to demonstrate that Rv0365c hydrolyses both substrates at a comparable rate, and so does not likely have preference for one structure over the other. This is important as it demonstrates that the enzyme is not affected by the presence of the arabinan domain in LAM. Rv0365c is specific for the glycosidic bond between the second and third α-1,6

man*p* units in the mannan backbone of LM/LAM. The biochemical data we presented on the yeast mannans helps to explain this specificity. The enzyme was only able to digest the short, undecorated α-1,6 mannan substrates. The presence of α-1,2 mannan, even on the pre-digested substrates, inhibited the enzyme to the extent that we could not detect activity. This data clearly shows that Rv0365c is specific for short, undecorated α-1,6 mannan which is only described at the site specified above.

Recent work by Al-Jourani & Benedict *et al.,* (2023), which I was a contributing author on, has identified another mycobacterial GH enzyme that is active on LAM. In this work, the GH183 family enzymes Rv1754c and Rv3707c (named AraH1 and AraH2) are shown to be active on LAM. The study demonstrates that the first of these GH183 enzymes, AraH1 is specific for LAM and is not active on arabinogalactan. The second of these enzymes, AraH2, is active on both LAM and arabinogalactan. It is suggested that these enzymes may have overlapping substrate specificities and that they may compensate for each other if one enzyme's activity is lost. Identification of D-arabinanases when combined with the work described here, demonstrates that following synthesis, LAM is not a static product. Whether these enzymes act synergistically, however, remains to be determined. Taking into account the findings presented in this chapter, it highlights how LAM is a dynamic molecule that can be digested and potentially recycled. Furthermore, there are now two families of enzymes that are known to be active on LAM when prior to these studies there were zero.

As discussed in Chapter 1.7, GH76 enzymes are also capable of glycoside transferase activity. In contrast to GH activity, this is where a mannose unit is transferred from a donor molecule to an acceptor molecule in a condensation reaction as opposed to the hydrolysis reaction observed in the breaking of glycosidic bonds (Davies and Henrissat, 1995). For example, Pan *et al.,* (2021) describe a GH76 gene in *Pyricularia oryzae* which acts as a glycosyl transferase. In this thesis, we have not ruled out the possibility that Rv0365c could also have glycosyl transferase activity. However, based on the biochemical data we have presented we are confident that its primary role is the cleavage of LM and LAM.

In conclusion, the data presented in this chapter provide strong evidence that Rv0365c is an authentic glycoside hydrolase family 76 member with the ability to hydrolyse LM and LAM purified from BCG. We can therefore hypothesise that the role of this enzyme in the mycobacterial cell wall involves the degradation of LM and LAM to release the larger carbohydrate domain from the small $AcPIM_2$ lipid carrier. The fate of these two products is explored in later chapters. We also show that mutation of the predicted catalytic residues results in loss of enzymatic activity, and that the enzyme will digest both LM and LAM at an equal rate with no preference for one substrate over the other. The results discussed in this chapter next led us to speculate how the levels of LM and LAM, in mycobacteria, would be affected when GH76 activity was lost. It has previously been shown that Rv0365c is a non-essential gene (Griffin *et al.,* 2011), and so this meant we could examine how the loss of this enzyme's activity would impact the abundance of its newly identified substrates. This is explored in the following chapter.

M. tuberculosis is predicted to encode three alpha-mannan degrading enzymes. This chapter set out to biochemically characterise the predicted GH76 enzyme, and so to continue the work started here the next aim for this study would be to purify and characterise the other two predicted alpha-mannanases. As shown in Table 1, these are Rv0648 which is predicted to be a GH38 and Rv0584 which is a predicted GH92 family member. Additionally, one of the biggest drawbacks of this chapter is that we were unable to obtain any structural data for Rv0365c. Therefore, given more time, future work would focus on further optimising the purification of Rv0365c so that structural data could be collected. An experimentally determined structure could provide us with an insight into how the D96A mutation effects the structure of the protein, and why the catalytic activity is lost. Finally, AlphaFold cannot teach us about the working mechanisms of Rv0365c or any interactions it may have with other proteins. This is something an experimentally determined structure could help to answer. AlphaFold only predicts one structural conformation of a protein with no corresponding information as to what state it is in. However, proteins will adopt different conformations that can impact the biological role the protein plays. For example, Munoz-Munoz *et al.,* (2017) describe a glycoside hydrolase family 145 enzyme which has an active site located on the posterior surface of the protein. This was something never seen before in other experimentally determined structures of GH145 enzymes. Additionally, it is shown that this enzyme's catalytic apparatus utilises a single histidine residue instead of a canonical pair of carboxylate residues seen in the majority of glycoside hydrolases (Munoz-Munoz *et al.,* 2017).

Chapter 4

Phenotypic Characterisation of Glycolipid Abundance when Glycoside Hydrolase 76 Activity is Lost

4. Phenotypic characterisation of glycolipid abundance when glycoside hydrolase 76 activity is lost

4.1 Introduction

Following the results discussed in Chapter 3, this chapter set out to investigate how a transposon insertion mutant in *M. bovis* BCG Danish in the glycoside hydrolase 76 gene, BCGDan_0378, would affect the abundance of lipoarabinomannan and lipomannan in the cell. BCGDan_0378 is a homolog of Rv0365c with 100% sequence identity. The results discussed in Chapter 3 demonstrated that the protein, Rv0365c, was active on both lipomannan and lipoarabinomannan. Therefore, we were interested to see how loss of the activity of this enzyme would affect the abundance of these glycolipids in the cell. In this chapter, the abundance of LAM and LM are compared between the transposon insertion mutant and the wild type strain of *M. bovis* BCG Danish. Furthermore, the abundance of these glycolipids is compared between exponential growth and stationary phase as previous reports have demonstrated that LAM and LM synthesis is upregulated during stationary phase (Dulberger, Rubin and Boutte, 2020). The findings reported in this chapter reveal that loss of GH76 activity leads to an accumulation of LAM and LM in the cell. Furthermore, to investigate if this phenotype could be complemented, a complementation plasmid was produced with the wild type gene, as well as a complementation plasmid with the catalytic null variant of the gene. The wild type GH76 gene is shown to fully restore the wild-type phenotype, whilst complementation with the catalytic null protein has no effect on the levels of glycolipid. Finally, capsular polysaccharide extracts from these strains show that no capsular

arabinomannan is observed when GH76 activity is lost in BCG. However, arabinomannan can be detected in wild type cells. These findings support the hypothesis that Rv0365c is the enzyme responsible for cleaving LAM to release arabinomannan to the capsule.

4.2 Materials and Methods

4.2.1 Capsular Polysaccharide Extraction

M. bovis BCG cultures were grown on 7H10 agar plates for 4 weeks. Subsequently, cells were scraped from the plates and a cell mess was measured. The cells were then resuspended in ddH_2O and gently vortexed for 1 minute to shed capsular material. Cells were harvested by centrifugation at 2000 x *g* for 10 minutes. The capsule-containing supernatant was collected and filtered using a 0.45 µM Millipore filter to ensure no bacterial debris remained. The capsular extract was frozen and lyophilised to complete dryness. Dry capsular polysaccharides were then resuspended in ddH_2O to a concentration of 10 mg / mL. This was based on the original cell mass used which was harvested and used for capsular polysaccharide extraction. This was to ensure all samples were normalised based on cell mass.

4.2.2 Fluorescent Labelling of Capsule Extracts

Fluorescent labelling of the capsular polysaccharide extracts was carried out following the methods of Ruhaak *et al.,* (2010). In brief, 50 µl of capsular material was mixed with 25 µl of freshly prepared label (48 mg / mL 2-AB in DMSO/acetic acid (85:15 v/v)). Additionally, 25 µl of 1 M 1-picolane-borane in DMSO was added to achieve a final

volume of 100 µl. Subsequently, the mixture was incubated at 65 ℃ for 2 hours. The samples were then allowed to cool to room temperature before being analysed.

4.2.3 High Performance Liquid Chromatography Analysis of Fluorescently Labelled Capsular Polysaccharides

Analysis of the fluorescently labelled capsular extracts was performed using a Phenomenex BioZen 1.8 µM Size Exclusion Chromatography-2 column (BioZen, 00H-4769-E0) at room temperature. Mobile phase was 0.1 M phosphate buffer pH 6.8 with 0.025% sodium azide, flow rate = 0.400 mL / min. Glycans detected with fluorescence detection (Ex = 320 nm Em = 420 nm), sample volume injected = 2.5 µL.

4.3 Results

4.3.1 Loss of GH76 Activity Results in Increased Abundance of LM/LAM

The first aim of this chapter was to determine how the loss of GH76 activity in *M. bovis* BCG Danish would impact the abundance of lipoarabinomannan and lipomannan. Therefore, wild type BCG Danish and BCGDan_Δ0378 were grown in 7H9 media until an OD_{600} of 0.8 was reached. At this point, the cells were harvested at the glycolipids were extracted as per Chapter 2.5.2. The lyophilised extracts were then resuspended in a volume of ddH_2O so that equal concentrations of cells could be analysed. A 10 µl sample of each extract was taken and mixed with 10 µl of ddH_2O and 5 µl of 6X loading dye. The samples were separated via SDS-PAGE using a 4-20% gradient gel, as described in Chapter 2.5.2. The gel was then stained with the ProQ Emerald glycoprotein gel stain and imaged using ImageLab. This is shown in Figure 40.

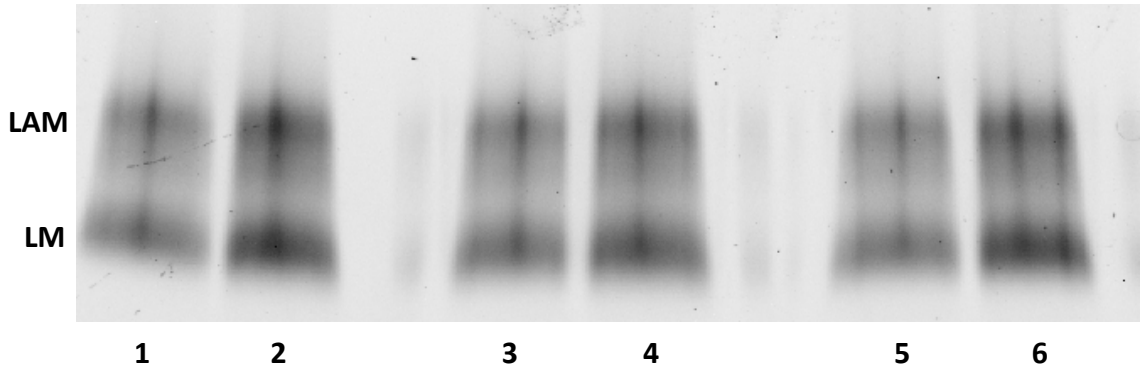

Figure 40: LAM and LM extractions from WT BCG Danish and BCGDanΔ0378 separated via SDS-PAGE and stained with ProQ Emerald glycoprotein stain. Samples separated at 200 v, 50 mA, for 45 minutes. (1) WT BCG replicate 1, (2) BCGDan_Δ0378 replicate 1, (3) WT BCG replicate 2, (4) BCG_DanΔ0378 replicate 2, (5) WT BCG replicate 3, (6) BCGDan_Δ0378 replicate 3. LM/LAM band intensity of BCGDan_Δ0378 appears darker than that of the wild type cells.

Using the ImageLab software, the intensity of each band was determined. This is shown in Table 8. The intensity was then plotted using GraphPad Prism v10.0.2 and a t-test was used to determine significance. This is shown in Figure 41.

Table 8: Fluorescence intensity of bands from Figure 40

Lane	LAM Intensity	LM Intensity
1	1785	1967
2	2322	2583
3	1737	2019
4	2343	2627
5	1715	1990
6	2231	2578

The results from Figure 41 show that when GH76 activity is lost, there is a significant increase in both lipoarabinomannan and lipomannan abundance in *M. bovis* BCG Danish cells. On average, this was an increase of 1.31x more glycolipid in the GH76 knockout cells compared to the wild type cells.

To investigate if this increase in glycolipid abundance was also seen during stationary phase, the experiment was repeated using cells harvested at OD_{600} of 1.10. As before, the samples were separated via SDS-PAGE, stained with ProQ Emerald glycoprotein stain, and then ImageLab was used to visualise the gel (Figure 42), and determine band intensity (Table 9). The intensities were then plotted using GraphPad Prism v10.0.2 (Figure 43).

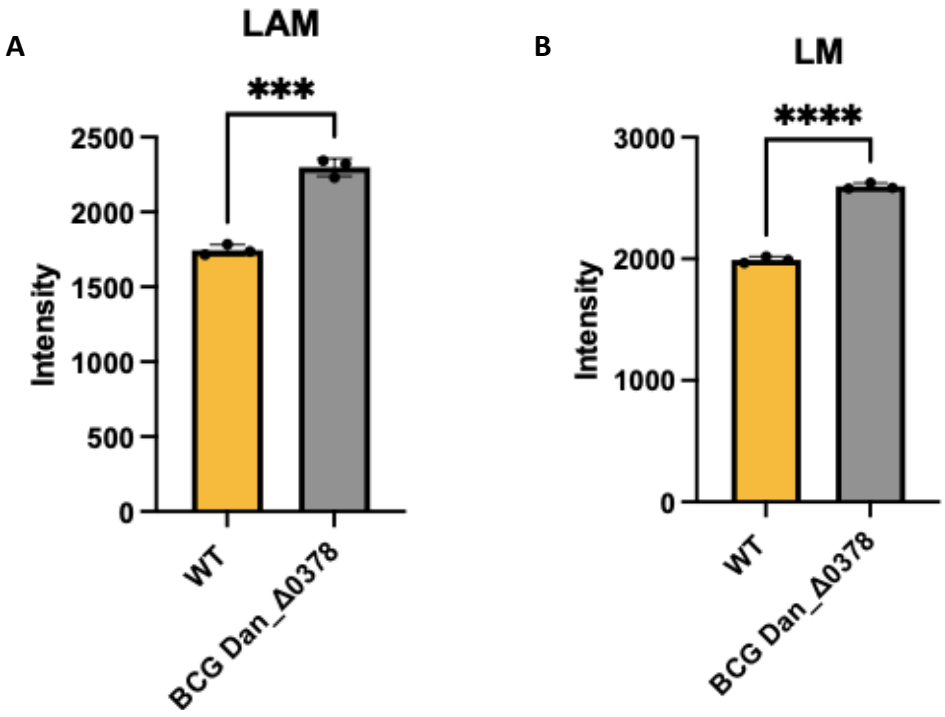

Figure 41: Fluorescence intensity of LM and LAM bands from Figure 40. (A) LAM extracts **(B)** LM extracts. Intensity of bands determined using ImageLab software, and plotted in GraphPad Prism v10.0.2. For each assay n=3, significance determined by t-test where ***p<0.001 and ****p<0001. Values shown are mean with error bars showing standard deviation. Loss of GH76 activity results in significantly increased intensity of LM/LAM bands

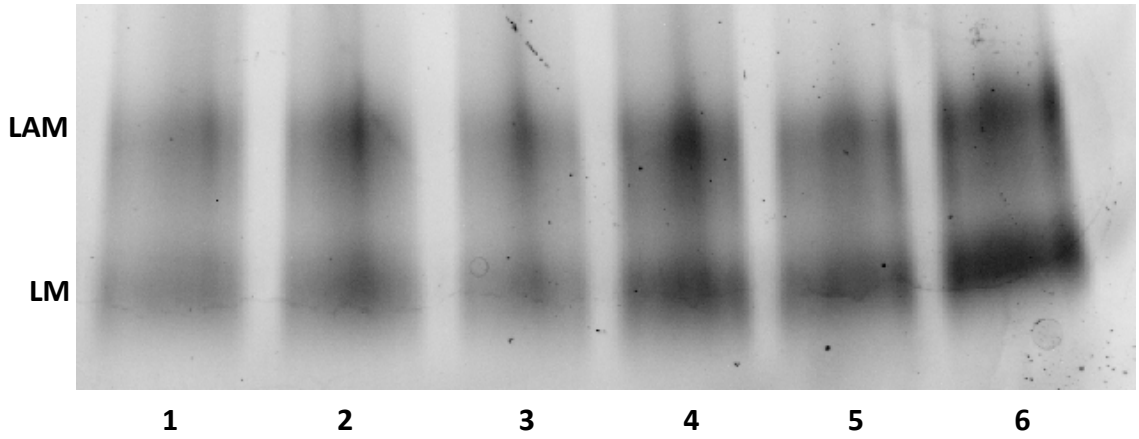

Figure 42: LAM and LM extractions from stationary phase WT BCG Danish and BCGDanΔ0378 separated via SDS-PAGE and stained with ProQ Emerald glycoprotein stain. Samples separated at 200 v, 50 mA, for 45 minutes. (1) WT BCG replicate 1, (2) BCGDan_Δ0378 replicate 1, (3) WT BCG replicate 2, (4) BCGDan_Δ0378 replicate 2, (5) WT BCG replicate 3, (6) BCGDan_Δ0378 replicate 3. Band intensity was measured and plotted in GraphPad Prism v10.0.2.

Table 9: Fluorescence Intensity of bands from Figure 42

Lane	LAM Intensity	LM Intensity
1	1620	1697
2	1950	1975
3	1723	1773
4	2225	2453
5	2058	2363
6	2427	2902

The results displayed in Figure 42 and 43 show that, despite a consistent increase in both lipoarabinomannan and lipomannan abundance during stationary phase, the differences seen are not significant between the wild type and GH76 knock out cells.

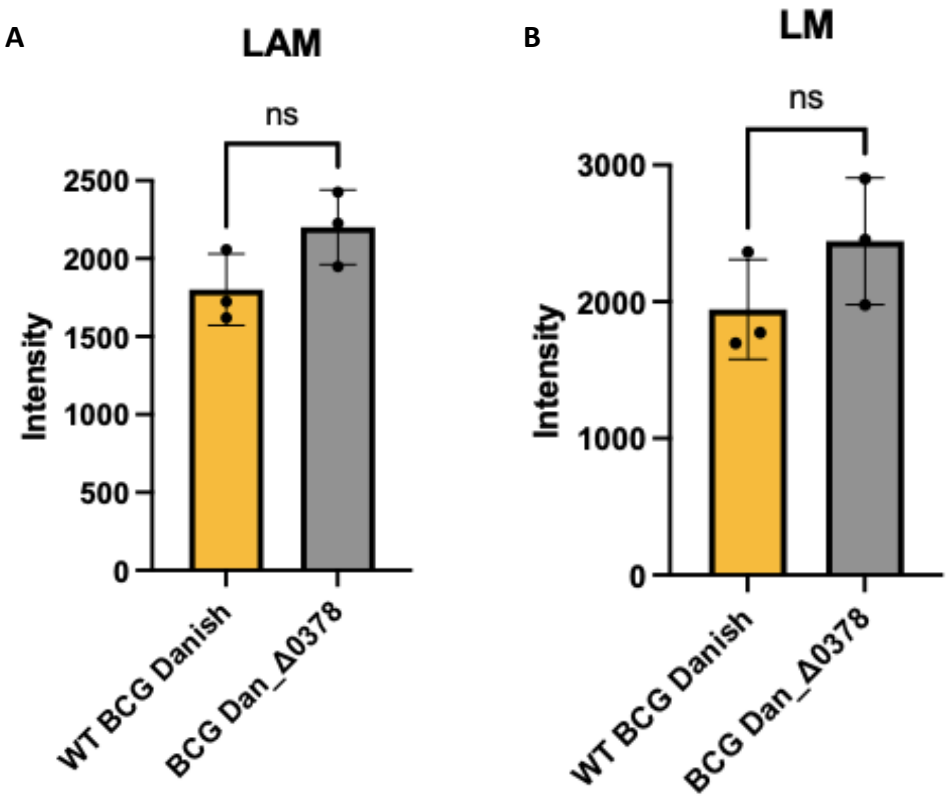

Figure 43: Fluorescence intensity of LM and LAM extracts from stationary phase. (A) LAM extracts **(B)** LM extracts. Intensity of bands determined using ImageLab software, and plotted in GraphPad Prism v10.0.2. For each assay n=3, significance determined by t-test. Values shown are mean with error bars showing standard deviation. There was no significant change in the intensity of LM/LAM bands.

4.3.2 Complementation Returns LM/LAM Levels to Wild Type Phenotype

To investigate if the increased abundance of glycolipids during exponential growth was a true effect of the loss of GH76 function, or if it was a polar effect of the transposon insertion, a complementation plasmid was ordered from GENEWIZ (www.genewiz.com). The wild type *M. bovis* BCG Danish_0378 gene was synthesised into the plasmid backbone pmv306. This included the 250 base pair upstream region of the gene and the presumed native promoter as well as a hygromycin resistance cassette for selection. Furthermore, using the primers from Table 5, a catalytic null variant of the complementation plasmid was produced to use as an additional control. In this variant the mutation D96A was present (where numbering is relative to the *M. tuberculosis* genome). The complementation plasmids were electroporated into electrocompetent BCG Dan_Δ0378 cells, as per Chapter 2.2.3, to produce the strains BCG Dan_Δ0378::0378 and BCG Dan_Δ0378::CatNull0378. Following this, the complemented strains, were cultured to an OD_{600} of 0.8, harvested, and the glycolipids were extracted as per Chapter 2.5.2. As before, the lyophilised extracts were resuspended in ddH_2O based on the wet cell mass to ensure the extracts were normalised. A 10 µl sample of each extract was taken and mixed with 10 µl of ddH_2O and 5 µl of 6X loading dye. The samples were then separated via SDS-PAGE together with the wild type and Δ0378 samples. The gel was stained with ProQ Emerald glycoprotein gel stain and imaged using ImageLab. The result of this is shown in Figure 44. The intensity of each band was determined using ImageLab, as shown in Table 10. These were then plotted using GraphPad Prism v10.0.2 and significance was determined by one-way ANOVA. This is shown in Figure 45.

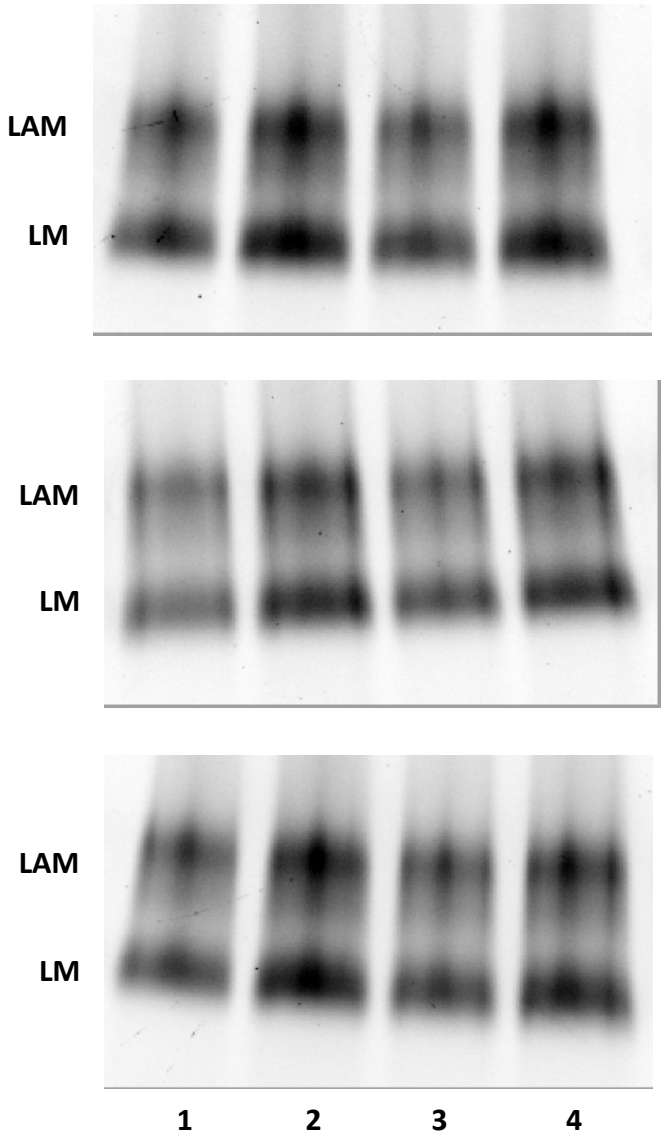

Figure 44: LAM and LM extractions from complement strains. Samples separated at 200 v, 50 mA, for 45 minutes. 1) WT BCG, 2) BCGDan_Δ0378, 3) BCGDan_Δ0378::0378, 4) BCGDan_Δ0378::CatNull0378. Three biological repeats are shown. LM/LAM band intensity was measured using ImageLab software, and plotted using GraphPad Prism v10.0.2.

Table 10: Fluorescence intensity of bands from Figure 44

Lane	LAM Intensity	LM Intensity
Replicate 1		
1	1846	1872
2	2567	2339
3	1901	1808
4	2534	2169
Replicate 2		
1	1656	1848
2	2311	2276
3	1820	1785
4	2203	2145
Replicate 3		
1	1882	1856
2	2628	2347
3	1921	1798
4	2431	2256

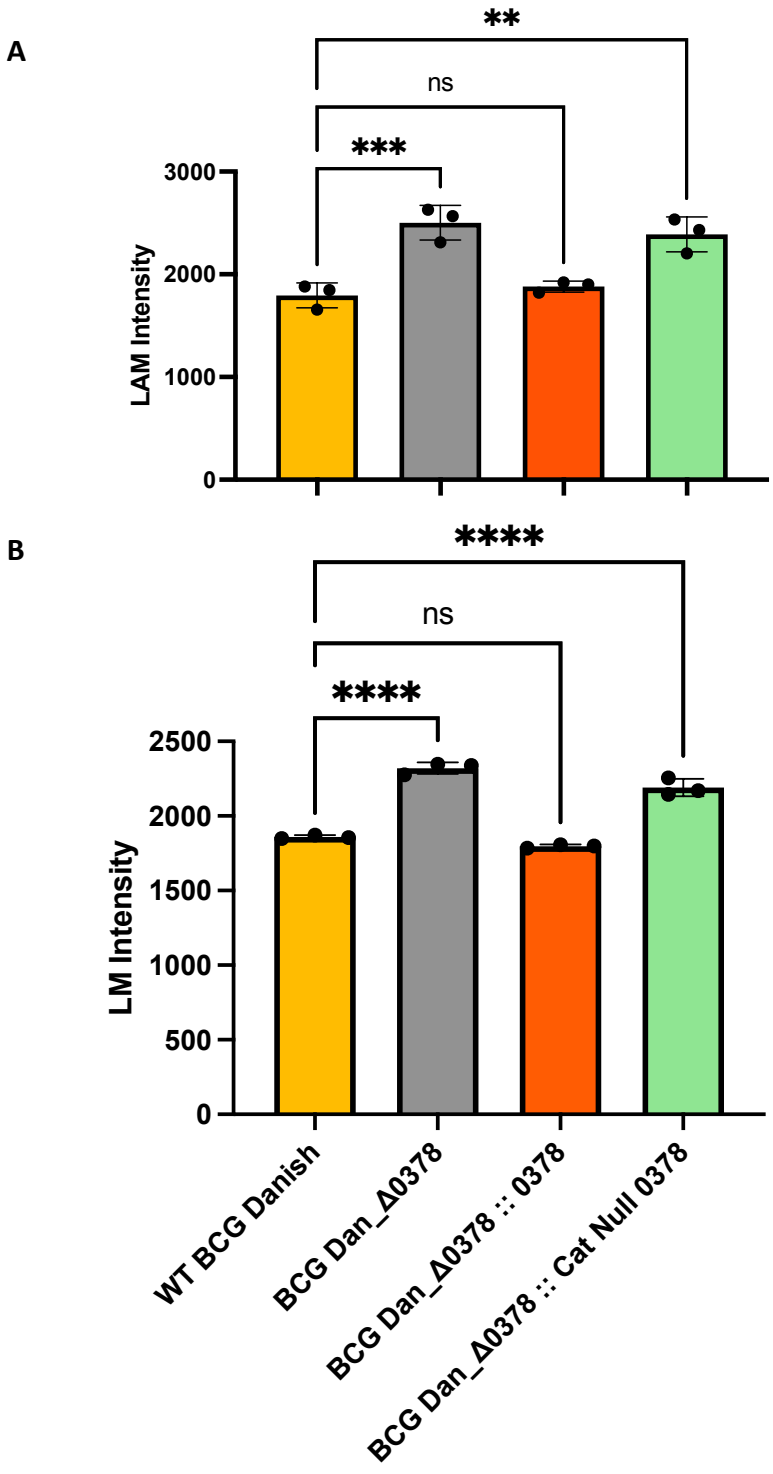

Figure 45: Fluorescence intensity of LM and LAM bands from Figure 44. (A) LAM extracts **(B)** LM extracts. Intensity of bands determined using ImageLab software, and plotted in GraphPad Prism v10.0.2. For each assay n=3, significance determined by one-way ANOVA test where **p<0.01, ***p<0.001, and ****p<0001. Values shown are mean with error bars showing standard deviation. Complementation with wild type gene restores the phenotype, but catalytic null complementation has no effect.

The results shown in Figures 44 and 45 confirm that the increased abundance of glycolipid shown in Figures 40 and 41 is a direct result of loss of GH76 activity. Complementation with the wild type GH76 gene restored the glycolipid abundance to wild-type levels. Furthermore, the abundances for both LAM and LM were not significantly different between the wild type and the complemented cells. However, when the GH76 mutant was complemented with the catalytic null GH76 gene, the glycolipid abundance was unchanged and still significantly higher than the wild type. This provides strong evidence that the phenotype shown is a direct result of loss of GH76 activity, and it is not a polar effect from the transposon insertion.

4.3.3 Loss of GH76 Activity Effect is seen cross species in *M. smegmatis*

To determine if the increase in glycolipid as a result of loss of GH76 activity is an effect seen in other species, the fast-growing *M. smegmatis* mc^2155 and *M. smegmatis* Δ0740 were cultured until an OD_{600} of 0.8 was reached. The *M. smegmatis* mutant was generated by a colleague in the lab, Rudi Sullivan, via ORBIT-mediated mutagenesis (Murphy *et al.,* 2018). The cells were harvested, and the glycolipids were extracted as before. Once again, the extracted glycolipids were separated via SDS-PAGE, and then stained with ProQ Emerald stain. This is shown in Figure 46.

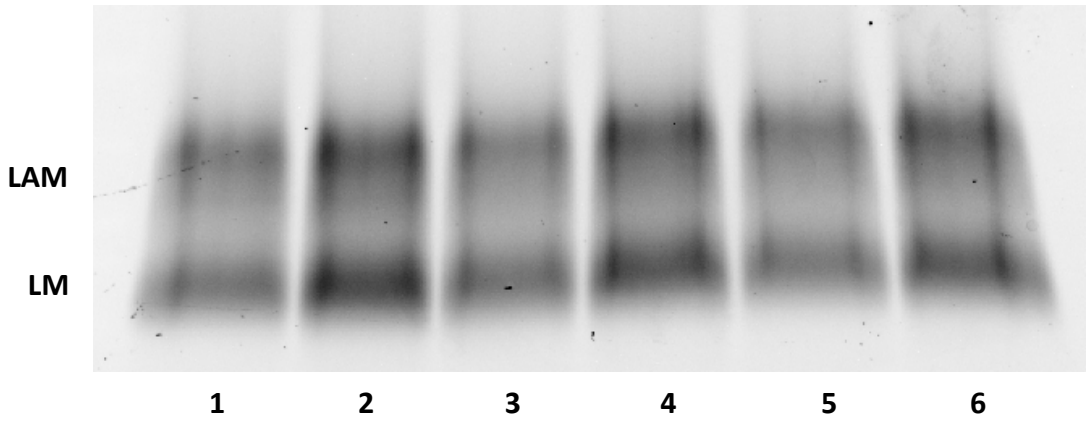

Figure 46: LAM and LM extractions from WT smegmatis and M. smeg_Δ0740 separated via SDS-PAGE and stained with ProQ Emerald glycoprotein stain. Samples separated at 200 v, 50 mA, for 45 minutes. (1) WT smegmatis replicate 1, (2) M. smeg_Δ0740 replicate 1, (3) WT smegmatis replicate 2, (4) M. smeg_Δ0740 replicate 2, (5) WT smegmatis replicate 3, (6) M. smeg_Δ0740 replicate 3. Visible increase in band intensity can be seen in mutant samples.

The bands shown in Figure 46 were quantified by determining their intensity in ImageLab. These values are shown in Table 11. These values were then plotted using GraphPad Prism v10.0.2, and significance was determined using an unpaired t test. This is shown in Figure 47.

Table 11: Fluorescence intensity of bands from Figure 46

Lane	LAM Intensity	LM Intensity
1	1903	2141
2	2537	2938
3	2111	2300
4	2562	2764
5	2086	2170
6	2426	2625

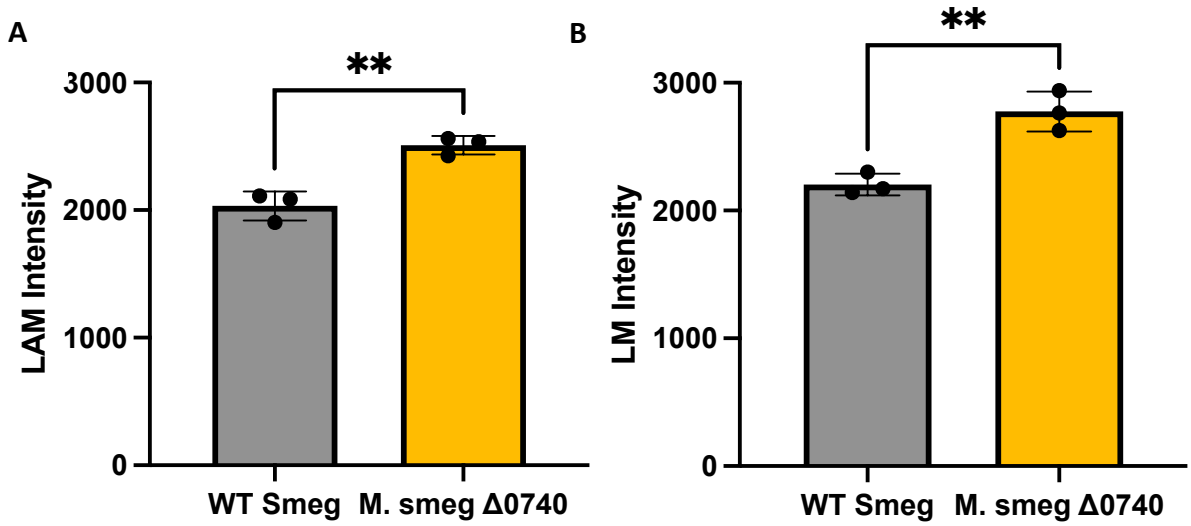

Figure 47: Fluorescence intensity of LM and LAM bands from Figure 46. (A) LAM extracts **(B)** LM extracts. Intensity of bands determined using ImageLab software, and plotted in GraphPad Prism v10.0.2. For each assay n=3, significance determined by t-test where ***p*<0.01. Values shown are mean with error bars showing standard deviation.

The results shown in Figures 46 and 47 confirm that the increase in glycolipid abundance as a result of loss of GH76 function is observed cross-species. Figure 47 shows that both LAM and LM were significantly higher in the GH76 deficient cells compared to wild type *M. smegmatis*.

4.3.4 Loss of capsular AM is observed when GH76 activity is lost

The next aim for this chapter was to determine how the capsular polysaccharide content compared when GH76 activity was lost. As reported by Ortalo-Magne *et al.,* (1996), the capsule of slow-growing mycobacteria consists primarily of polysaccharide. Kalscheuer *et al.,* (2019), identified that these glycan rich capsules consist of around 70% α-D-glucan; 20% D-arabino-D-mannan (AM); and 5% D-mannan as well as small quantities of other glycans such as xylose. We hypothesised that loss of GH76 activity could lead to a reduction in AM and mannan in the capsule. To test this, wild type BCG and BCG Dan-_Δ0378 were cultured on 7H10 agar and allowed to grow for around 4 weeks. Following this, the capsule was extracted as per Chapter 4.2.1. To analyse the capsular material we separated the polysaccharides via size exclusion chromatography. This was possible due to significant size differences in the three main capsular polysaccharides. α-D-glucan is approximately 100 kDa, AM is 14 kDa, and mannan is 4 kDa (Kalscheuer *et al.,* 2019). To detect the sugars, 2-aminobenzamide, which is fluorescent, was added to the reducing terminus of the glycan, as per Chapter 4.2.2. As observed in Figure 48, we were able to detect α-D-glucan and AM in the wild type samples.

This was consistent with the findings reported by Kalscheuer *et al.,* (2019), as the predominant polysaccharide was the α-D-glucan and there was only a smaller abundance of AM present. However, analysis of the BCG Dan_Δ0378 capsule extracts revealed no detectable AM, as shown in Figure 49.

The data presented in Figure 49 confirmed our hypothesis showing that no AM was detectable in the capsular extracts of BCG Dan_Δ0378 cells. There was however, an α-D-glucan peak suggesting that this glycan is unaffected by the loss of GH76 activity. To confirm that the peaks we observed were in fact the glycans we believed them to be, an amylase, arabinanase, and mannanase were used to digest the peaks to confirm their identity. To do this, wild type extract was incubated with each of the three enzymes separately. To digest the α-D-glucan peak, an α-amylase from *Aspergillus oryzae* (Sigma-Aldrich, 10065) was incubated with 5 mM calcium chloride and the wild type capsule extract for 3 hours at 37 ℃. Subsequently, the reaction was heat inactivated at 100 ℃, and the labelling process was repeated (Chapter 4.2.2). To digest the AM peak, the wild type sample was incubated with an endo-D-arabinanase, Rv3707 (Al-Jourani & Benedict *et al.,* 2023), and a GH76 mannanase, BT3792 (Cuskin & Lowe *et al.,* 2015), separately and as a co-digestion. The reactions were inactivated as before and labelled once again. The samples were then analysed via HPLC size exclusion. The result of this, as shown in Figure 50, confirmed the identity of the peaks as α-D-glucan and arabinomannan.

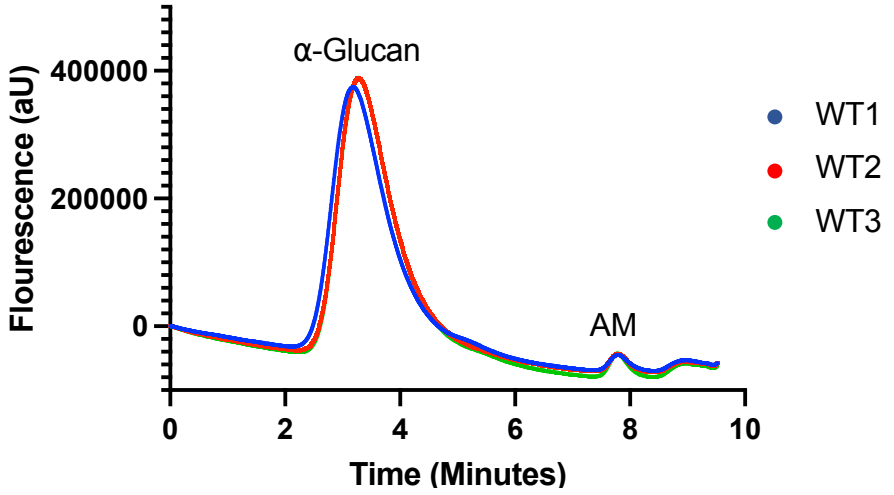

Figure 48: Size exclusion chromatogram of wild type capsular polysaccharides. Capsular material was harvested, fluorescently labelled, and separated. Three biological replicates were analysed and the glycans α-D-glucan (retention time between 2 and 5 minutes) and AM (retention time between 7 and 8 minutes) were detected.

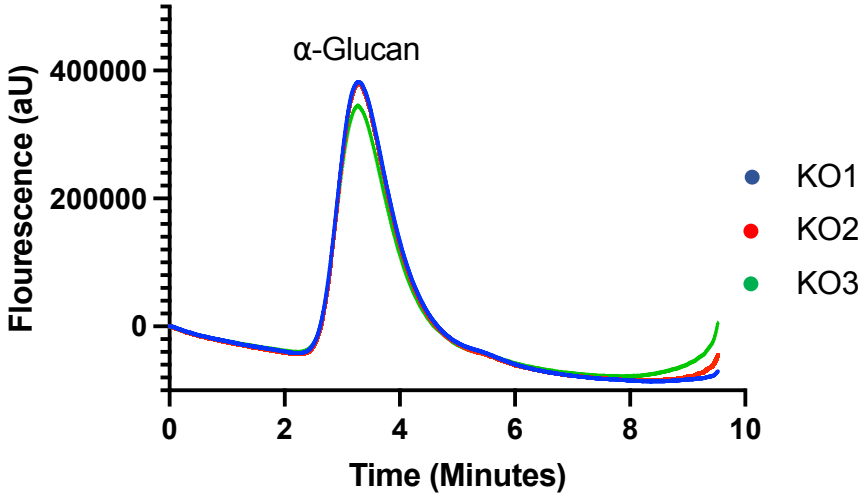

Figure 49: Size exclusion chromatogram of GH76 knock-out capsular polysaccharides. Capsular material was harvested, fluorescently labelled, and separated. Three biological replicates were analysed and only α-D-glucan (retention time between 2 and 6 minutes) was detected.

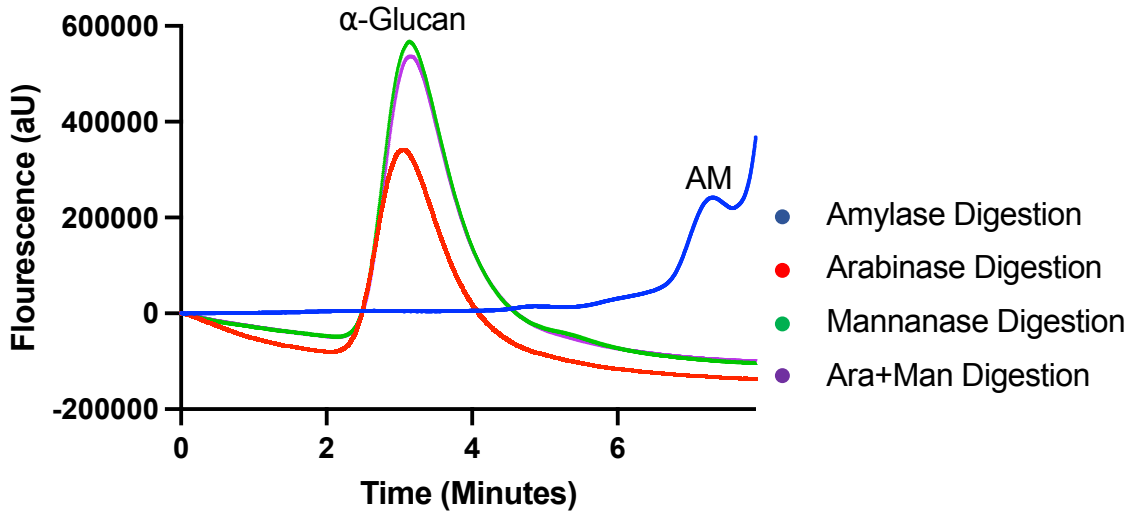

Figure 50: Size exclusion chromatogram of enzymatically-digested capsular polysaccharides. Wild-type capsular polysaccharides were digested with specified enzymes, fluorescently labelled, and separated to confirm identity of each peak. Each assay was conducted one time, and so only one replicate is shown for each assay.

As shown in Figure 50, when the capsular polysaccharides are digested with the amylase, there is a complete loss of detectable α-D-glucan, but the AM peak remains. In this case, the AM peak has started to merge with a neighbouring peak which we hypothesise to be the products of the amylase digestion. When incubated with the endo-D-arabinase and the mannanase, as well as the co-incubation, there is complete loss of the AM peak. We were therefore confident that the peaks we had previously assigned as α-D-glucan and AM were in fact these glycans.

We previously demonstrated that complementation with the wild type GH76 gene restored LM and LAM levels to that of the wild-type phenotype. To investigate if the complement could also restore the capsular AM phenotype, the capsular polysaccharide extraction was repeated with the strains BCG Dan_Δ0378::0378 and BCG Dan_Δ0378::CatNull0378. The extracts were labelled with 2-AB, and separated as before. As shown in Figure 51, complementation with the wild type GH76 gene restored the capsular AM phenotype.

To confirm that the restoration of the wild-type phenotype was due to catalytic activity of the GH76 in the complement, the catalytic null complement capsular polysaccharides were analysed. As shown in Figure 52, complementation with the catalytic null variant of the GH76 resulted in no capsular AM being detected, suggesting that the catalytic activity of the enzyme is required for the presence of AM in the capsule.

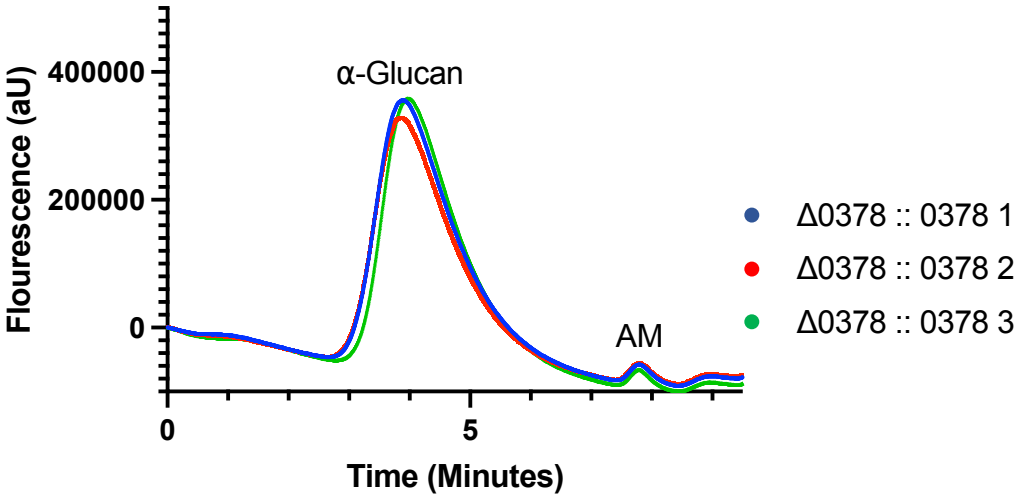

Figure 51: Size exclusion chromatogram of BCG Dan_Δ0378::0378 capsular polysaccharides. Capsule material was harvested, fluorescently labelled, and separated. Three biological replicates were analysed, and both α-D-glucan (retention time 3-6 minutes) and arabinomannan (retention time 7.5 – 8.5 minutes) could be identified.

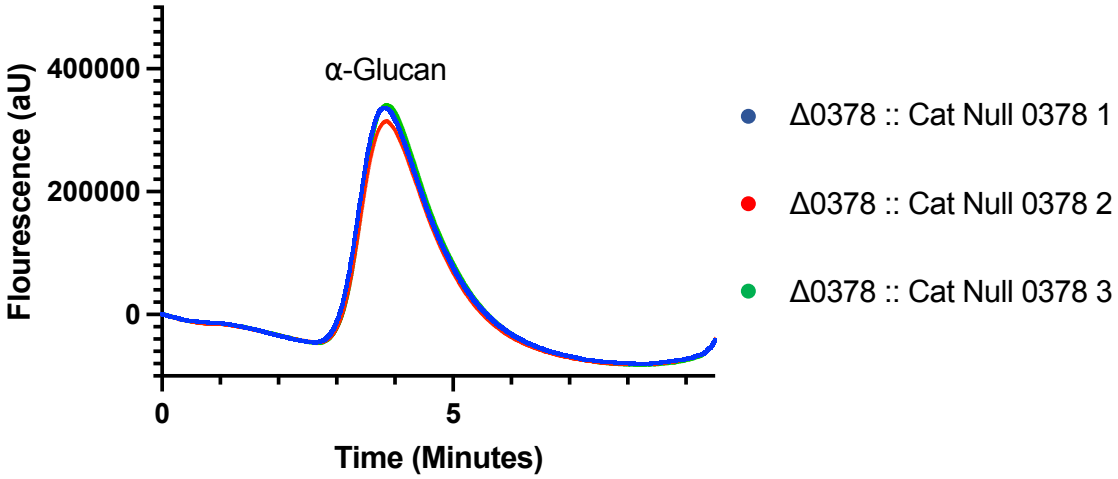

Figure 52: Size exclusion chromatogram of BCG Dan_Δ0378::CatNull0378 capsular polysaccharides. Capsular material was harvested, fluorescently labelled, and separated. Three biological replicates were analysed, and only α-$_D$-glucan (retention time 3-6 minutes) could be identified.

To further investigate to what extent the complementation restored the wild-type phenotype, the α-D-glucan and arabinomannan peaks were quantified, and then the AM was plotted as a percentage of the total capsular polysaccharide abundance. This is shown in Figure 53. The results of which show that only partial complementation of the capsular arabinomannan phenotype had occurred.

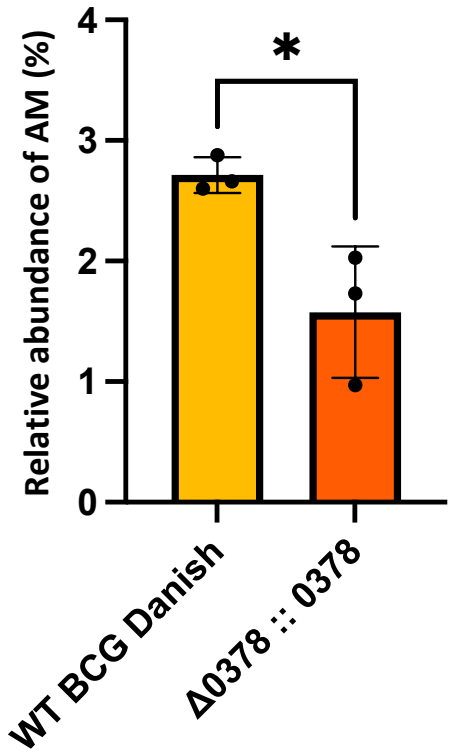

Figure 53: Relative quantity of arabinomannan in wild-type BCG and BCG Dan_Δ0378::0378. For each sample n=3, significance determined by t-test where *p<0.05. Values shown are mean with error bars showing standard deviation. Complemented cells are producing significantly lower amount of AM.

4.3.5 Loss of GH76 activity results in accumulation of Ac_2PIM_2

The penultimate aim for this chapter was to investigate how the abundance of PIMs differed between our GH76 knock-out strain and wild type BCG. As PIMs, LM, and LAM share a common biosynthetic pathway, we were interested to see how the accumulation of LM and LAM may alter the PIM profile of the GH76 knock-out strain. To do this, wild type BCG and BCG Dan_Δ0378 were grown until an OD_{600} of 0.2 was reached. At this point, the cultures were labelled with 10 µl of [^{14}C] acetic acid (10,545,000 cpm, Perkin Elmer) and incubated for a further 72 hours. Following this, the cultures were pelleted by centrifugation and then the polar lipids were extracted as described in Chapter 2.6.1. To visualise the PIM profiles, the polar lipid extracts were analysed via two-dimensional TLC. Equal counts were loaded onto the lower left corner of a 6 x 6 cm TLC plate. The samples were separated in the first direction in a chloroform:methanol:water (60:30:6 v/v/v) solvent system, and then in a chloroform:acetic acid:methanol:water (40:25:3:6 v/v/v/v) solvent system in the second direction. Following this, the PIMs were visualised by exposure to x-ray film by autoradiography for 48 hours (Kodak Biomax MR film). The result of this is shown in Figure 54.

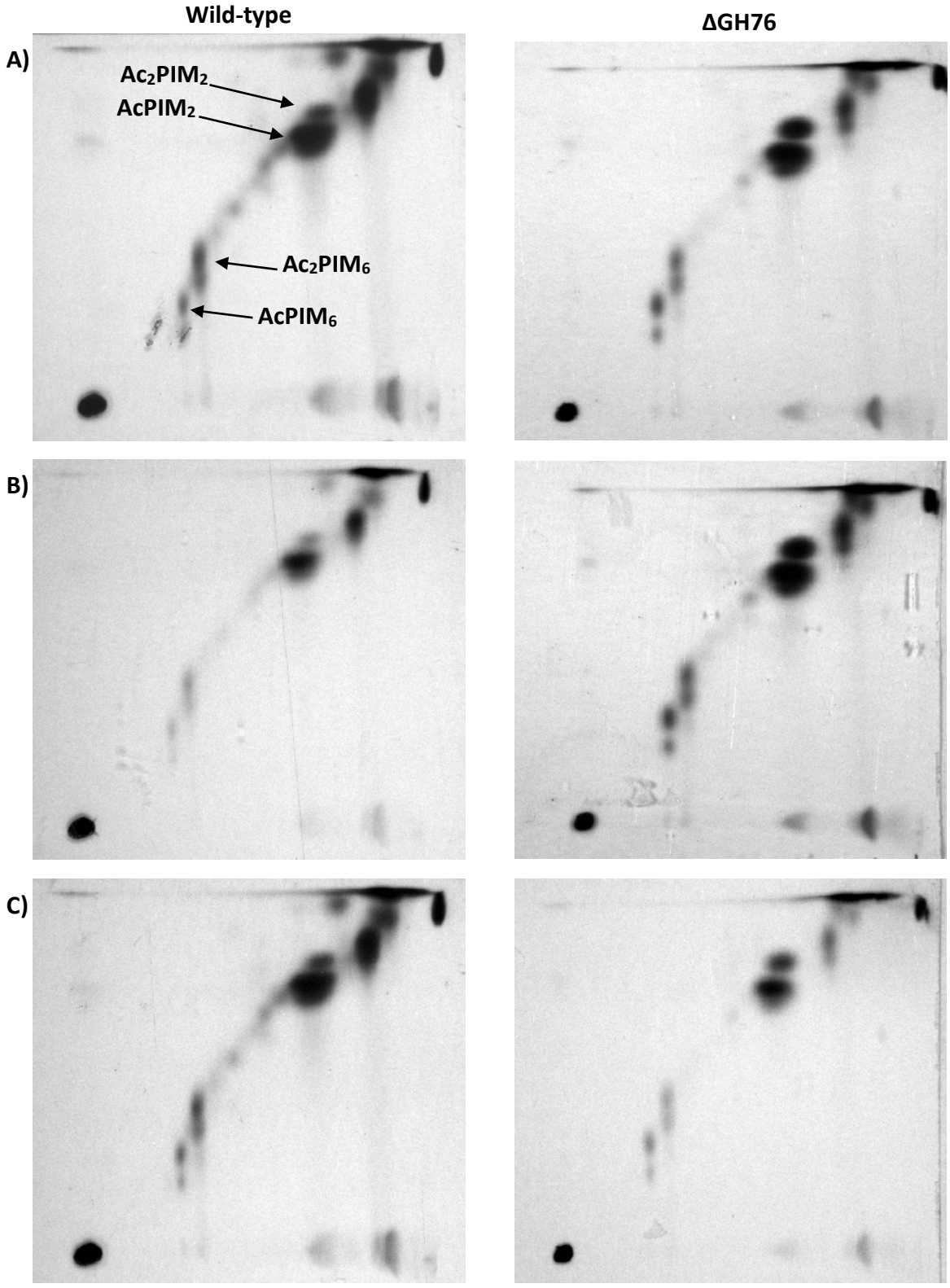

Figure 54: 2D TLC profile of [^{14}C] labelled polar lipids from wild type and BCG Dan_Δ0378. A) replicate 1 **B)** replicate 2 **C)** replicate 3. Radiolabelled polar lipids were extracted, separated by two-dimensional TLC, and visualised by autoradiography. TLC annotated as per Driessen *et al.,* (2009).

The polar lipid profiles shown in Figure 54 were annotated to identify the PIM species. The intensity of each spot was then quantified using ImageLab and plotted as a percentage of pixel density of the total pixel density on the TLC. These values are shown in Table 12. The relative abundance of each PIM species could then be compared between the two strains. This is shown in Figure 55.

Table 12: Relative intensity of PIM species

Ac_2PIM_2		$AcPIM_2$		AC_2PIM_6		$AcPIM_6$	
WT	**ΔGH76**	**WT**	**ΔGH76**	**WT**	**ΔGH76**	**WT**	**ΔGH76**
0.39	1.04	1.9	1.5	0.21	0.42	0.21	0.29
0.39	0.96	1.69	1.49	0.37	0.42	0.12	0.33
0.32	0.83	1.47	1.14	0.16	0.31	0.16	0.19

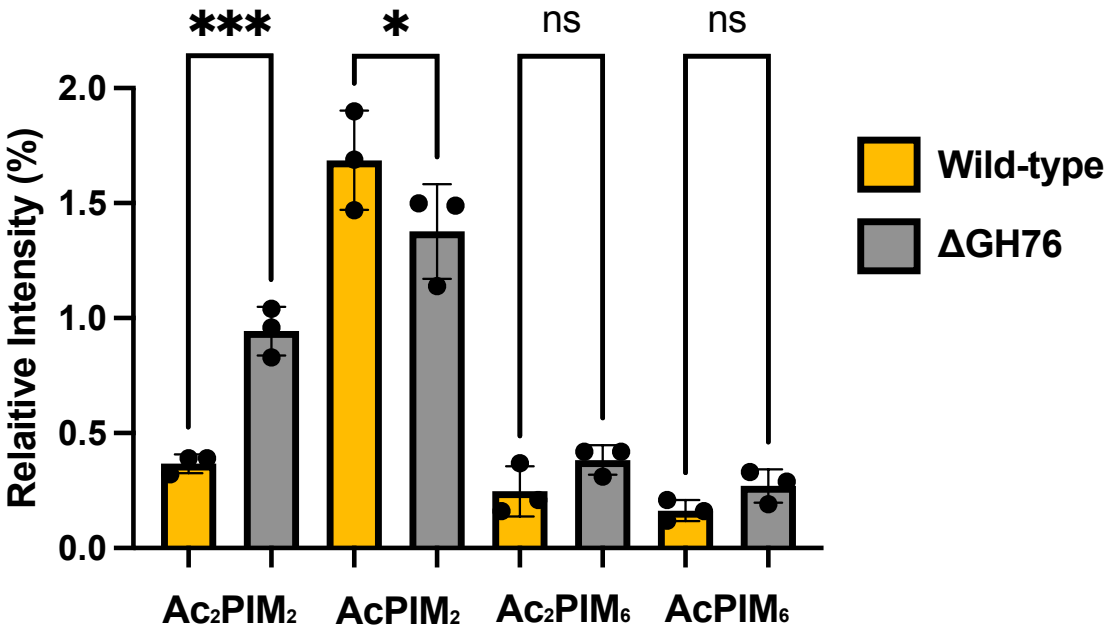

Figure 55: Relative intensity of PIM species in wild-type and BCG Dan_Δ0378 cells. Intensity determined using ImageLab For each sample n=3, significance determined by one-way ANOVA test where *p<0.05 and ***p<0.001. Values shown are mean with error bars showing standard deviation. Loss of GH76 activity results in significant accumulation of Ac_2PIM_2 and $AcPIM_2$.

As shown by Figure 55, the loss of GH76 activity results in a significant increase in Ac_2PIM_2 species, but a significant decrease in $AcPIM_2$ species. There was no significant change in the higher-order PIM_6 species.

4.3.6 PIM recycling pathway

LM and LAM are often considered dead-end products (Kaur *et al.,* 2008). As the results from Chapter 3 demonstrated that the lipid carrier of LM/LAM could be released from the carbohydrate domain and as this is the same structure as the LM/LAM precursor $AcPIM_2$, we speculated that this lipid carrier could be recycled by the bacteria to synthesise new LM/LAM or higher-order PIMs. To test this, radiolabelled LM and LAM were extracted from *M. smegmatis* and digested with Rv0365c. We then extracted the radiolabelled $AcPIM_2$ product. This was then fed to fresh cultures and the LM/LAM extraction was repeated. This protocol is summarised in Figure 56.

The results of this experiment did not show any recycling activity. When the LM/LAM extraction was carried out on the cultures, 5% of the sample was used to determine the CPM. The CPM of the LM/LAM extraction was 12, indicating that the sample did not contain any radioactive material. For a radioactive sample, a CPM value would be around 30,000. We therefore decided not to analyse the samples via SDS-PAGE and x-ray autoradiography.

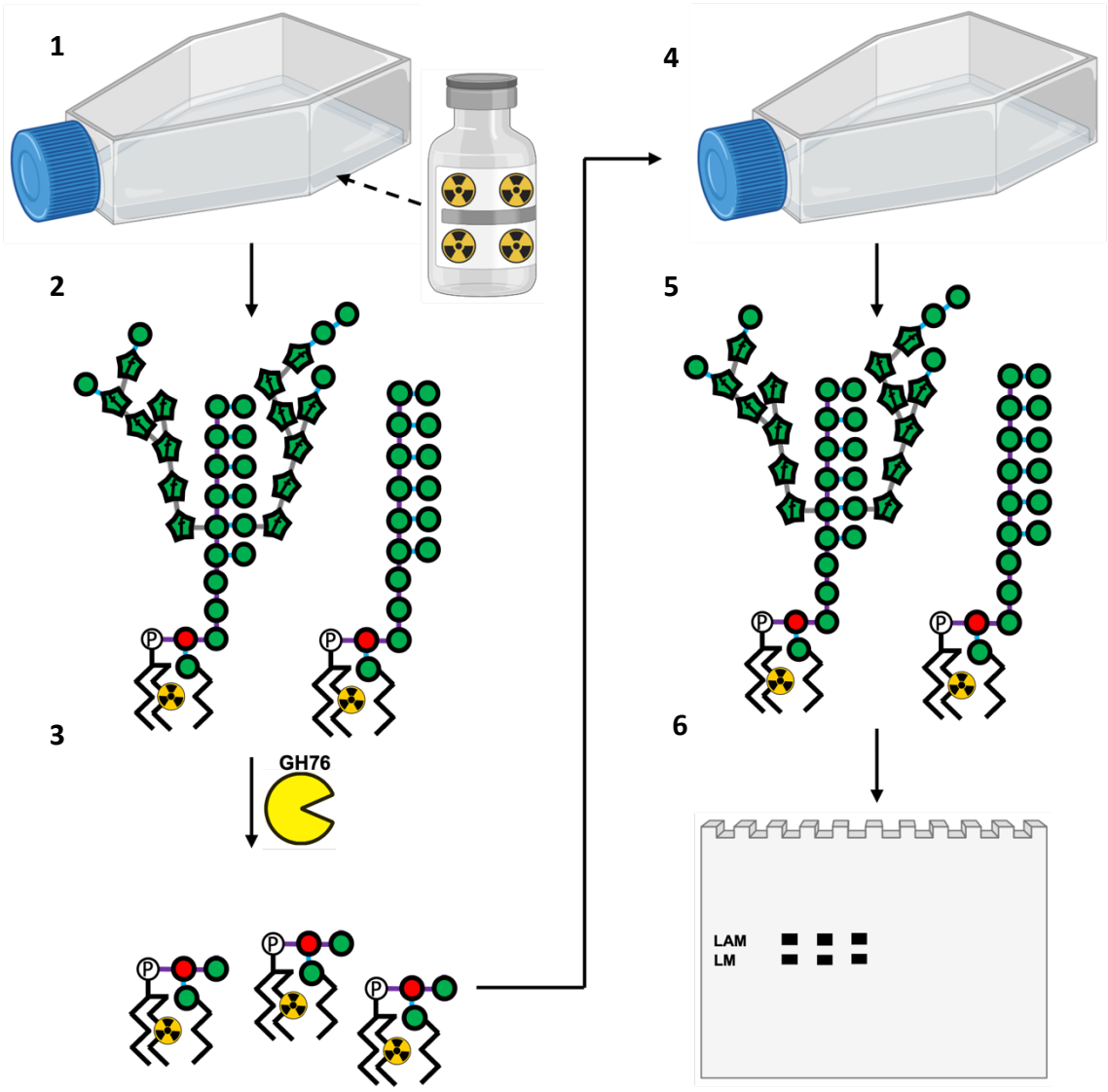

Figure 56: Summary of recycling assay. (1) A 100 ml culture of wild-type *M. smegmatis* was grown to an OD_{600} of 0.2 and labelled with 100 µl of [^{14}C] acetic acid (10,545,000 cpm, Perkin Elmer). The culture was then further incubated for 24 hours. (2) The cells were harvested by centrifugation, and as described in Chapter 2.5.2, the radiolabelled glycolipids were extracted from the cells. (3) The glycolipids are digested with Rv0365c, and the $AcPIM_2$ lipid carrier is isolated using a 10:10:3 separation. (4) The radiolabelled lipid carrier is added to a fresh culture of *M. smegmatis* and allowed to grow for 4 generations. (5) The LM/LAM extraction is repeated. (6) The extracted LM/LAM is separated by SDS-PAGE, the gel is dried, and then visualised by exposure to x-ray film by autoradiography for 48 hours (Kodak Biomax MR film).

4.4 Discussion

In Chapter 3, we provided evidence that Rv0365c was digesting the substrates lipomannan and lipoarabinomannan to release the lipid carrier, $AcPIM_2$, from the carbohydrate domain. The aim of this chapter therefore, was to investigate how the loss of Rv0365c activity would affect the abundance of these substrates in the model organism *M. bovis* BCG Danish. BCG is an excellent model organism for studying cell envelope biogenesis in *M. tuberculosis* as the species is 99% identical to that of *M. tuberculosis*. Fortunately, we had access to an ordered gene deletion library of this organism where each non-essential gene is knocked-out by transposon insertion. As our previous results had shown that this GH76 was responsible for degrading the LM and LAM, we hypothesised that loss of activity would result in an increase in abundance of these glycolipids. To test this, wild-type and our knock-out strain were grown to mid-log phase, and the glycolipids were harvested. By normalising our analysis based on the initial cell mass, we could then load an equal volume of cellular glycolipid on the gel. This meant that any difference we observed on the gel would be as a result of the knock-out, and not a difference based on unequal loading. Furthermore, we employed the use of the ProQ Emerald glycolipid stain, used in Chapter 3, so that we could quantify the differences we observed. The result of this was that the loss of GH76 activity resulted in significant accumulation of both LM and LAM in the cell. In each case, we observed an approximately 30% increase in glycolipid when GH76 activity was lost (mean = 1.31x increase in LAM and 1.30x increase in LM in mutant). As has been reported previously, expression of LM and LAM is increased during stationary phase (Dulberger, Rubin and Boutte, 2020). We therefore repeated the analysis, but used cells harvested from

stationary phase cells. In this case, we did not see a significant increase in levels of LM or LAM. It is possible that rather than the cells actively upregulating the biosynthesis of LAM during stationary phase, they are instead down-regulating the expression of *rv0365c*. Therefore, during stationary phase in wild-type cells LM and LAM levels will naturally increase as less GH76 is available to digest them. This may explain why we did not see a significant increase in levels of LM/LAM in our mutant cells during stationary phase. To confirm that the effect seen during exponential growth was seen in other mycobacterial species, the experiment was again repeated using *M. smegmatis* and the knock-out of the GH76 gene, msmeg_0740. As before, when the glycolipids were extracted and analysed, we found that there was significantly higher levels of LM and LAM in the GH76 knock-out cells when compared to the wild-type. The effect was not as pronounced however, with around a 20% increase observed in this fast-growing species.

To confirm that the effects we were observing were a direct result of the loss of GH76 activity, and not a polar effect from the transposon insertion, we synthesised a complementation plasmid and a catalytic null complementation plasmid. Production of this plasmid however, presented the second major issue faced in this thesis. We initially attempted to use Gibson Assembly to produce the plasmid. However, despite numerous attempts we were unsuccessful in obtaining the plasmid. Following this, we tried restriction free cloning. Again, we were unsuccessful in doing this as obtaining colonies after transformation was proving elusive. Eventually, in the interest of saving time, we decided to have the plasmid synthesised by GeneWiz. Upon delivery of the plasmid

however, we realised that we had included the wrong resistance cassette. Our complementation plasmid contained the kanamycin resistance gene which was also present in our *M. bovis* BCG mutant. We would therefore be unable to select for successfully transformed cells after electroporation. Fortunately, we were able to easily clone out and swap for an alternative resistance gene, and obtain our complementation plasmid. To do this, we cloned out the kanamycin resistance gene and then inserted a hygromycin resistance gene. The complementation plasmid consisted of the wild type gene, and the 250 base pair upstream region of the gene as this would likely contain the native promoter of the gene. Mycobacterial promoter regions are unlike traditional bacterial promoter elements. There have been no recognisable -10 or -35 elements described to date, and so we were unable to confidently identify the promoter. The complementation plasmids were electroporated into our BCG mutant, and the glycolipid analysis was repeated. The results of this demonstrated that the differences we had previously observed were a direct result of the loss of enzyme activity, as complementation with the wild-type gene fully restored the phenotype. However, complementation with the catalytic null gene provided no difference to the glycolipid levels. We were therefore confident that the increase in LM and LAM abundance in our mutant was a direct result of loss of GH76 activity.

Increased levels of LM and LAM have previously been reported by McCarthy *et al.,* (2005). In this work, they demonstrate that the overexpression of *Rv3257c*, the gene encoding the ManB enzyme, in *M. smegmatis* resulted in increased abundance of PIMs, LM, and LAM when compared to a wild-type control culture. The ManB enzyme is

involved in the conversion of mannose-6-phosphate to mannose-1-phosphate to produce GDP-mannose (McCarthy *et al.,* 2005). GDP-mannose is the primary mannose-donor used by mycobacteria during the biosynthesis of PIMs. This work suggests that the increased abundance of GDP-mannose led to increased production of PIMs and therefore LM and LAM. The study conducted by McCarthy *et al.,* (2005), suggests that biosynthesis of PIMs, LM, and LAM is a tightly regulated process, and the increased abundance of GDP-mannose can cause an increase in abundance of these glycolipids. The authors also demonstrate that an increase in LM and LAM is associated with greater association with human macrophages. The findings we presented in Chapter 3 may help to explain this. The increased abundance of LM and LAM in the periplasm may be acted upon by the GH76. This could result in an increased abundance of capsular AM and may therefore lead to greater recognition of host cell receptors compared to the wild-type cells, where LM/LAM levels are lower and so less capsular AM is being produced by the GH76.

As reported by Kalscheuer *et al.,* (2019), the capsule of slow-growing mycobacteria consists primarily of α-D-glucan; with smaller levels of D-arabino-D-mannan; and D-mannan. It is not thought that LAM extends to the capsule, illustrated by Alsteens *et al.,* (2008), where they show that LAM can only be detected on the surface of mycobacteria when the cells are first treated with the anti-mycobacterial drugs isoniazid and ethambutol. Our overall hypothesis for this thesis was that Rv0365c is responsible for cleaving LAM to release the AM so that it can be trafficked to the capsule. The results so far had supported this theory, and so our next step was to investigate how the loss of

GH76 activity would affect the capsular polysaccharides of BCG. Based on our hypothesis, we predicted that loss of GH76 activity would result in a decrease in capsular AM. To test this, we purified the capsular material from wild-type and GH76 knock-out BCG, labelled it with a fluorescent tag, and analysed it via size-exclusion. The result of this was that, consistent with previous reports, α-D-glucan was the predominant polysaccharide in the capsule with much smaller amounts of AM present. However, when GH76 activity was lost, we were unable to detect any capsular AM. We confirmed the peaks identity by enzymatic digestion and were therefore confident in our results. This data demonstrated that loss of GH76 activity results in a loss of AM in the capsule. This supported our hypothesis, and provided strong evidence that Rv0365c is degrading LAM to release AM to the capsule.

As we had previously demonstrated that complementation with the wild type GH76 gene fully restored the levels of LM and LAM, we were interested to see if this complementation would extend to the capsular AM. Analysis of the capsular polysaccharides extracted from the complement strains revealed that AM could be detected when the wild type gene was present. However, when the catalytic null variant was complemented, there was no AM present in the capsule extracts. This indicates that catalytic activity of the GH76 is required for the release of AM to the capsule. To investigate to what extent the complementation restored the wild type phenotype, the relative abundance of AM was quantified in the wild type and complement strains. This showed that there was a significant difference in the relative abundance of AM in the capsules, and suggested that there was only partial complementation taking place.

The importance of the mycobacterial capsule has been highlighted by Prados-Rosales *et al.,* (2016). In this study, the authors demonstrate that *M. bovis* BCG, when grown in the presence of detergents, did not produce a capsule. This resulted in a much reduced immune response in mice compared to BCG that were fully encapsulated (Prados-Rosales *et al.,* 2016). These findings detail the importance of the capsule to mycobacteria and its ability to interact with the host immune system. Taking into account the findings we have presented in this chapter, where loss of GH76 activity results in loss of capsular AM, it suggests that the activity of Rv0365c is required for effective interaction with the host immune system during infection. Loss of capsular material has been shown to be connected to a reduced host immune response (Prados-Rosales *et al.,* 2016), and so loss of GH76 activity and subsequent loss of capsular AM would also likely result in a reduced host immune response during infection.

The next aim for this chapter was to investigate the PIM profiles of wild-type and GH76 knock-out BCG. We were interested to see how the PIM profile of the mutant strain would compare to wild-type, as PIMs act as precursor molecules to LM and LAM. The results of this showed that when GH76 activity is lost, there is a significant increase in Ac_2PIM_2, as well as a reduction in $AcPIM_2$. There were no significant differences observed in the other PIM species. As reported by Nguyen *et al.,* (2022), inositol acylation is a membrane stress response. We therefore hypothesised that the increase in Ac_2PIM_2 we were observing was a stress response to the other phenotypes we had previously observed. It is possible that the increased levels of glycolipid in the cell combined with the loss of capsular AM was affecting the integrity of the membrane. To

compensate for this, the cells were upregulating synthesis of Ac_2PIM_2 as a way of responding to the stress. Interestingly, $AcPIM_2$, the small reaction product produced from Rv0365c digestion of LM/LAM, was significantly reduced in the mutant. This could be because this species is being acylated to produce Ac_2PIM_2, as previously discussed. Alternatively, perhaps the reduction we are seeing is due to the loss of GH76 activity meaning that the reaction product is not being produced. Therefore, the levels of $AcPIM_2$ are lower than that seen in the wild-type cells.

The final aim for this chapter was to investigate the possibility that PIMs, LM, and LAM are involved in a previously undescribed recycling pathway. The glycolipids, LM and LAM, have previously been described as dead-end products (Kaur *et al.,* 2008). However, we wanted to explore the possibility that the lipid carrier, that is cleaved off by Rv0365c, could be recycled by the bacteria and used to synthesise new LM or LAM. The reaction product produced, $AcPIM_2$, is one of the earliest PIMs in the biosynthesis pathway of LM/LAM production. However, it is not clear if $AcPIM_2$ is used on the inner or the outer leaflet of the cytoplasmic membrane. If it is used on the outer face, then the product could be recycled without the need for translocation across the membrane. However, transport across the membrane would be necessary if the product is used on the inner face of the membrane. This could be a problem, as such a transporter has yet to be described. If the product is recycled, and used to make LM/LAM, then this would be a novel pathway for mycobacteria, as no such mechanism has been described previously. To test this, we planned to digest radiolabelled LM/LAM with Rv0365c, isolate the reaction product, and feed it back into new cultures. We could then extract the LM/LAM

and check if it was ^{14}C labelled. Our initial attempt at this suggested that the product was not being recycled by the bacteria under the conditions we have tested. We hypothesised that the complexity of the mycobacterial cell wall was preventing the lipid carrier from reaching the cytoplasmic membrane where PIM/LM/LAM biosynthesis takes place. Therefore, to continue the work started in this chapter, the next aim would be to increase the likelihood that the labelled lipid carrier can reach the cytoplasm. One possible mechanism to do this would be to form mycobacterial spheroplasts and then repeat the recycling assay. A spheroplast is a microbial cell which has lost its cell wall/envelope and is bound by just the plasma membrane. The cells therefore appear spherical as the shape-defining cell wall is lost. (Jurkowitz *et al.,* 2022). To form the spheroplasts, the cells are grown in the presence of 20% glycine. Following this, the cells are harvested, washed in a sucrose, magnesium chloride, maleate solution, and then re-cultured in this solution with the addition of lysozyme. Our hypothesis here would be that the lack of cell wall would allow the radiolabelled lipid carrier to be localised to the cytoplasmic membrane and be incorporated into the predicted novel recycling pathway. Once the recycling assay was performed, the cells would be allowed to grow in 7H9 media and reform the cell wall structures. The glycolipids would then be harvested, and checked to see if they are radiolabelled.

In conclusion, the data presented in this chapter demonstrates that the loss of GH76 activity results in an increased abundance of LM and LAM within the cell. These findings support our hypothesis that Rv0365c is the enzyme responsible for degrading LM and LAM to release the carbohydrate domains to the capsule. Furthermore, we show that

loss of GH76 activity results in a loss of capsular AM. This is summarised in Figure 57. This provides further support to our hypothesis. The data presented in this chapter comply with the findings reported in Chapter 3 where we identified that Rv0365c was active on LM and LAM. Therefore, it is logical that loss of enzymatic activity would lead to an increased abundance of these substrates.

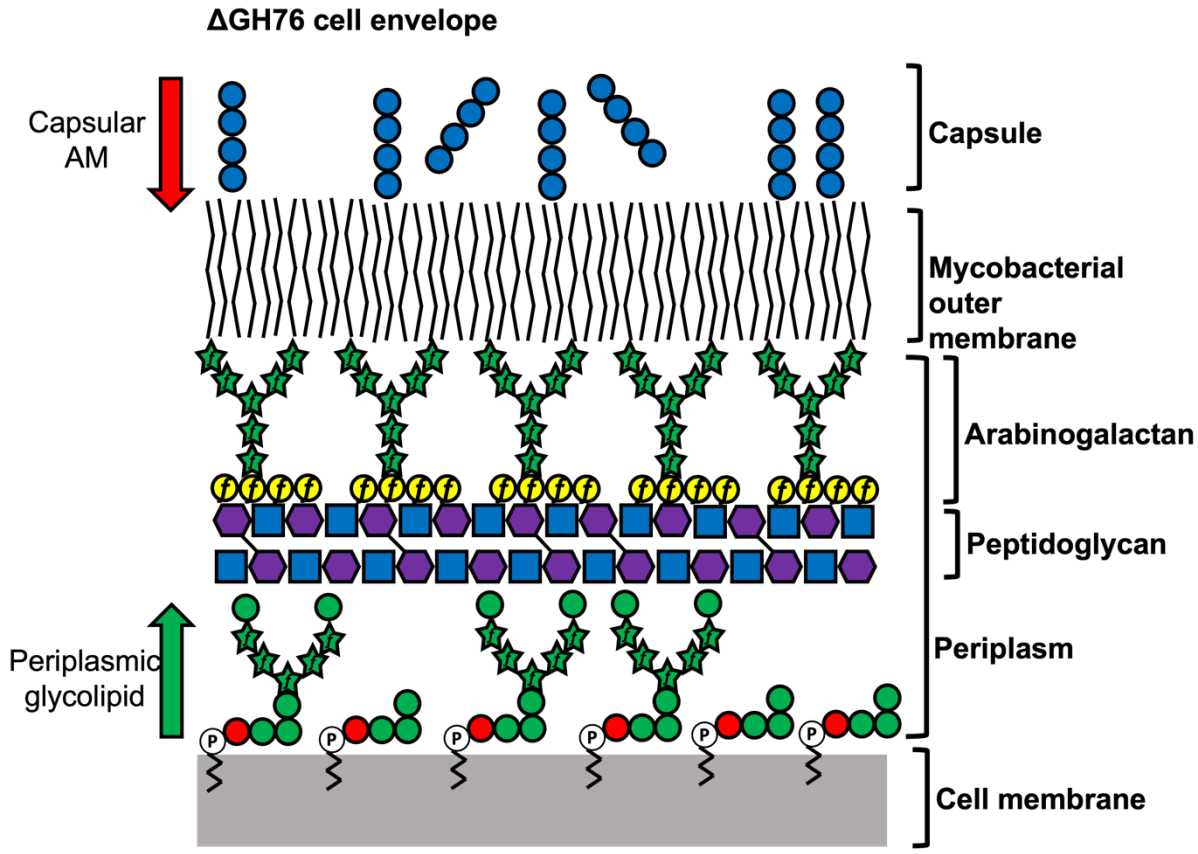

Figure 57: Hypothesised BCG Dan_Δ0378 cell wall. Green arrow indicated increased levels of periplasmic lipomannan and lipoarabinomannan. Red arrow indicates loss of capsular arabinomannan.

Chapter 5

Proteomic analysis of BCG Dan_Δ0378

5. Proteomic analysis of BCG Dan_Δ0378

5.1 Introduction

The results discussed in Chapter 4 demonstrated that the loss of GH76 activity results in an accumulation of LM and LAM in mycobacteria. However, we were surprised that this was not a greater effect than the 30% increase we observed. The aim of this chapter was therefore to investigate why the levels of LM and LAM were not more pronounced in the knock-out strain. To do this, we conducted a whole-cell proteomics study of cells harvested at mid-log phase. With the help of Dr Nichollas Scott, from the University of Melbourne, we show that our knock-out cells respond to the increased abundance of LM and LAM by downregulating several proteins involved in their biosynthesis pathway. This therefore allows for the cells to reduce the production of LM and LAM. Furthermore, this provides evidence that the synthesis and the levels of LM and LAM in mycobacteria is a tightly controlled process, as the bacteria actively respond to increased glycolipid by downregulating its production.

5.2 Materials and Methods

5.2.1 Preparation of proteomics samples

Wild-type and BCG Dan_Δ0378 cultures were grown in 7H9 minimal media (0.6% glucose replaces ADC) until mid-log phase (OD_{600} = 0.8) was reached. The cells were harvested by centrifugation, washed with PBS to remove media proteins, and then boiled in 4% SDS, 100 mM Tris-HCL pH 8.5 for 20 minutes. The sample was pelleted, and the protein containing supernatant was acetone precipitated. To acetone precipitate

the supernatant was incubated with 1 M NaCl and ice cold acetone overnight at -20 ℃. The following day, the sample was centrifuged at 4000 x *g* for 10 minutes and the supernatant was discarded. The protein pellet was then resuspended in ddH_2O and further incubated with ice cold acetone at -20 ℃ for 4 hours. Finally, the sample was centrifuged at 6000 x *g* for 15 minutes, and the resulting pellet was allowed to air dry overnight. The samples were then sent for analysis with Dr Nichollas Scott at the University of Melbourne.

5.3 Results

5.3.1 BCG Dan_Δ0378 downregulates proteins involved in LM/LAM biosynthesis

The aim of this chapter was to investigate how the proteome of our BCG Dan_Δ0378 strain compared to wild-type BCG. Protein samples were prepared from cells harvested at mid-exponential phase, and sent for proteomic analysis. The results of this are shown in Figure 57. The analysis demonstrates that the cells are responding to the increased abundance of glycolipid by downregulating the synthesis of enzymes involved in the production of LM and LAM. As shown in Figure 58, there are 8 key LM/LAM biosynthesis proteins that are all downregulated in the GH76 knock-out strain: AftB, PimB', AftD, AftC, MptA, EmbC, PimA, and PatA. However, whilst PimA and PatA are downregulated, they are not significantly downregulated. A summary of the LM/LAM biosynthesis pathway and the involvement of these proteins is shown in Figure 59.

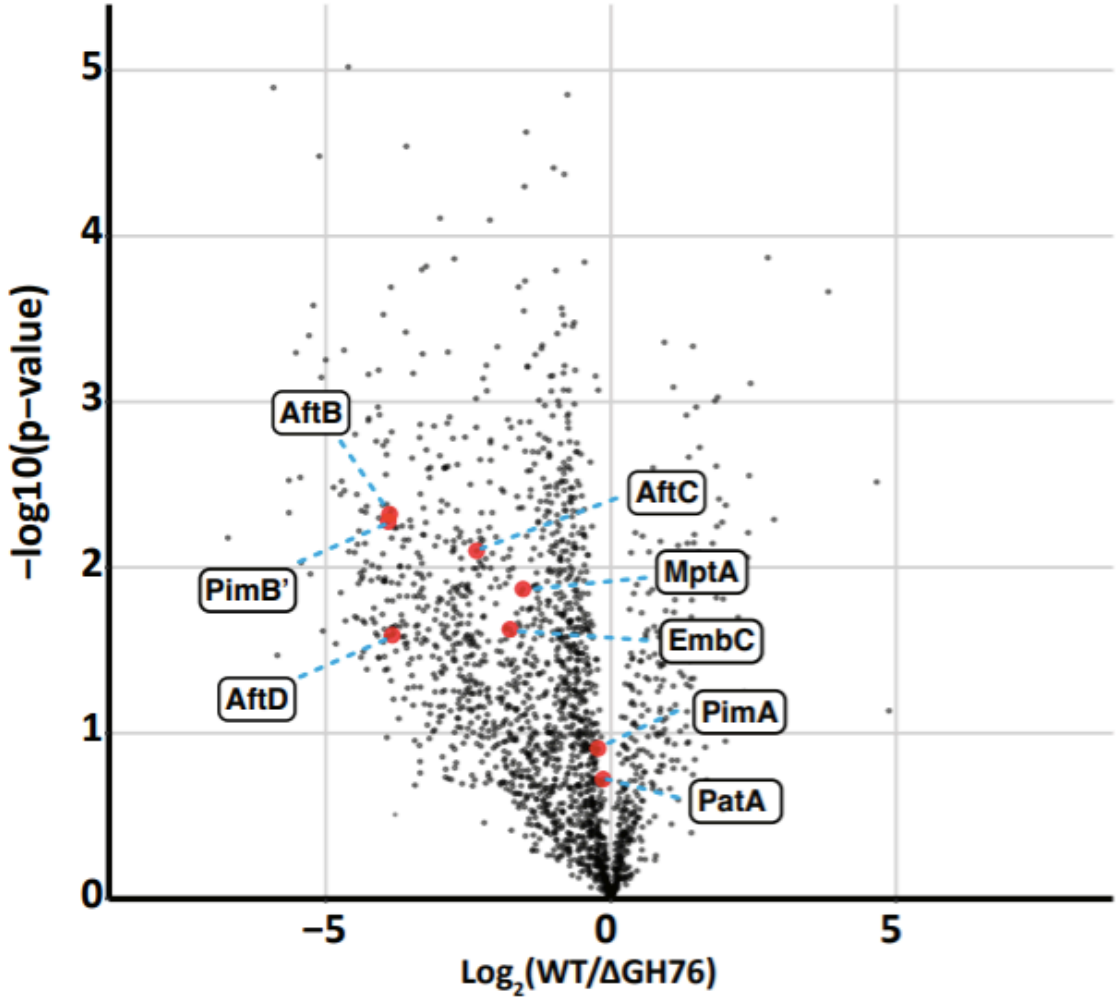

Figure 58: Proteome analysis of WT BCG Danish and BCG Dan_Δ0378. Protein samples were extracted from cultures harvested at mid-log phase. Three biological replicates were analysed for each strain. Volcano plot showing proteome variations between WT and ΔGH76 BCG. Proteins of interest involved in the LM/LAM biosynthesis pathway are shown as red dots with accompanying labels. Analysis carried out by Dr Nick Scott at the University of Melbourne. Proteins identified by mass spectrometry and comparison to existing BCG protein database.

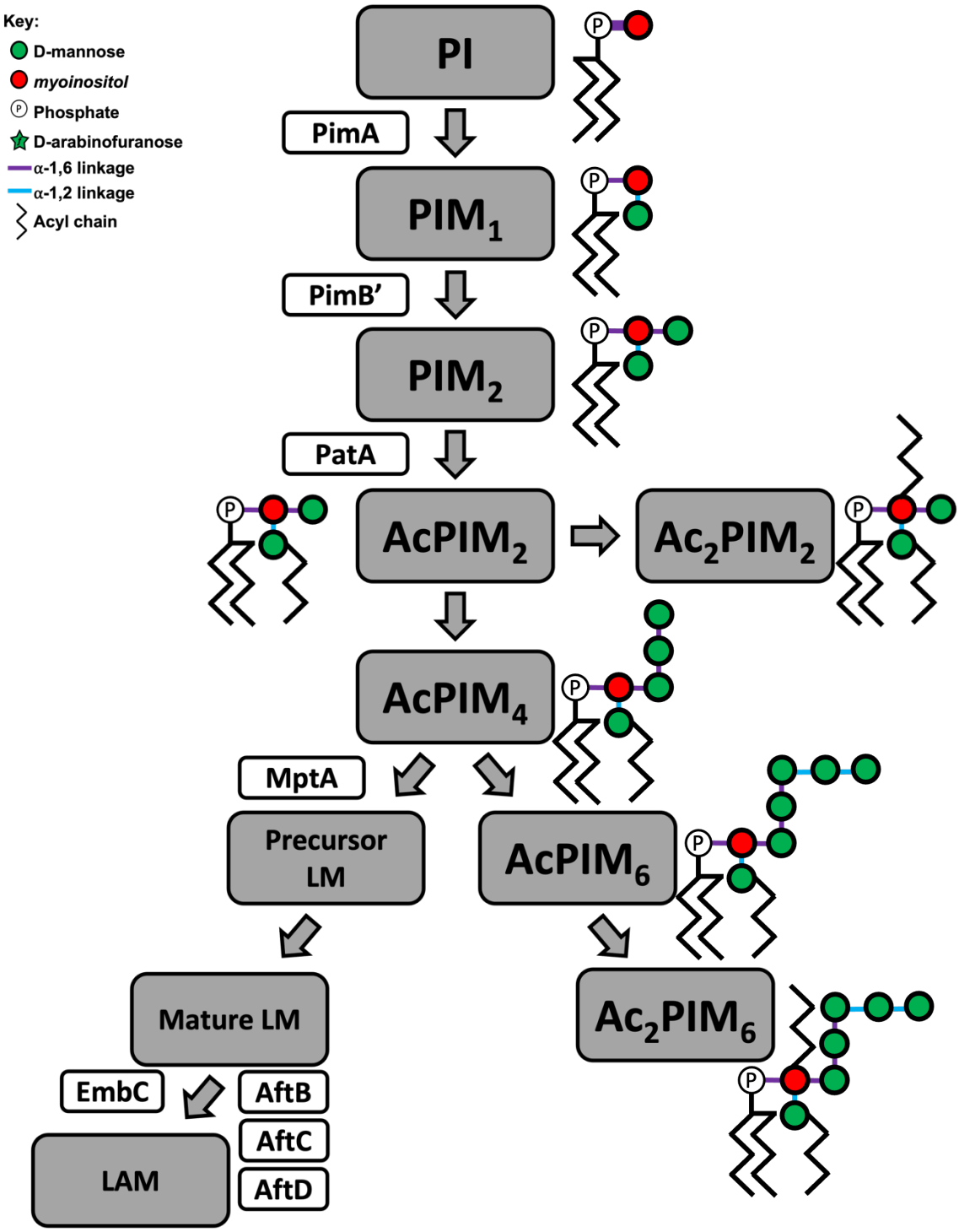

Figure 59: Summary of LM/LAM biosynthesis pathway. Enzymes identified as being downregulated when GH76 activity is lost are shown in white boxes next to the process for which they are involved in. Enzymes identified as being downregulated were predominantly involved in the conversion of mature LM to LAM (Korduláková *et al.,* 2002; Boldrin *et al.,* 2021; Guerin *et al.,* 2009; Mishra *et al.,* 2008; Shi *et al.,* 2006; Birch *et al.,* 2008; Jankute *et al.,* 2017; Seidel *et al.,* 2007).

As shown in Figure 59, most of the LM / LAM biosynthesis pathway proteins identified as being downregulated are involved in the conversion of mature LM to LAM. These are the enzymes responsible for the addition of the arabinan domain to LM (Shi *et al.,* 2006; Birch *et al.,* 2008; Jankute *et al.,* 2017; Seidel *et al.,* 2007). Additionally, the first mannosyltransferase, MptA, responsible for hyper-extending the mannan backbone to produce precursor LM (Mishra *et al.,* 2008), is also downregulated. Finally, the two mannosyltransferases, PimA, PimB', and the acyltransferase PatA which are involved in the biosynthesis of lower-order PIMs (Korduláková *et al.,* 2002; Guerin *et al.,* 2009; Boldrin *et al.,* 2021), are also downregulated.

5.3.2 Loss of GH76 activity results in upregulation and downregulation of non-LM/LAM biosynthesis proteins

In addition to those proteins involved in the biosynthesis of LM and LAM, there were also proteins not involved in this pathway which were either upregulated or downregulated. Table 13 details the five of the most upregulated proteins when GH76 activity is lost as well as five of the most downregulated proteins.

Table 13: The five most upregulated and downregulated proteins in BCG Dan_Δ0378

Protein	Proposed Function
5 most upregulated proteins	
FCU26_1041	Hypothetical protein, involved in translation
FCU26_1812	L-gulono-1,4-lactone dehydrogenase
FCU26_2650	Hypothetical protein, unknown function

FCU26_1533	Putative transcriptional regulatory protein
FCU26_0935	Hypothetical protein, unknown function
5 most downregulated proteins	
FCU26_1842	PPE family protein
FCU26_4023	Conserved component of ESX-1 type VII secretion system
FCU26_1526	Putative acyl-CoA dehydrogenase
FCU26_2330	Putative cutinase
FCU26_1841	PPE family protein

As displayed in Table 13, the five most upregulated proteins when GH76 activity is lost have unknown functions or functions not involved in the biosynthesis of glycolipids. FCU26_1812 is predicted to be involved in the production of vitamin C. Vitamin C has been shown to act as an inhibitor of (p)ppGpp synthesis (Syal, Bhardwaj & Chatterji, 2017). (p)ppGpp is the master regulator of the stringent response in bacteria. This is a response to stress, such as membrane stress, which will divert resources in the cell away from growth and division to prioritise amino acid production (Syal, Bhardwaj & Chatterji, 2017). Interestingly, vitamin C has been shown to inhibit (p)ppGpp synthesis to reduce the impact of the stress response (Syal, Bhardwaj & Chatterji, 2017). Our mutant is actively upregulating production of FCU26_1812 to increase production of vitamin C. This suggests the cell is trying to inhibit the stringent response.

The most downregulated gene in our mutant was FCU26_1842. This is a PPE family protein. The PPE proteins are only found in pathogenic, slow growing mycobacteria and

their main function is involvement in host-pathogen interactions (Qian *et al.,* 2020). However, the function of most of the PPE family proteins remains unknown. As we have previously demonstrated, the loss of GH76 activity results in loss of capsular arabinomannan. This would likely reduce the pathogenicity of the cells as arabinomannan is required to interact with host cell receptors. Interestingly, our mutant is responding to the loss of GH76 activity by downregulating a protein that could be involved in host-pathogen interactions. Perhaps this is because the cell is diverting resources from pathogenicity towards cell survival. Additionally, the protein FCU26_4023 was shown to be downregulated. This protein is involved in the ESX-1 type VII secretion system where in interacts with four other membrane proteins to form the ESX-1 complex. This is a specialised type VII secretion system that is essential for virulence of mycobacteria (Soler-Arnedo *et al.,* 2019). As before, it would appear that our mutant is responding to the loss of GH76 activity by downregulating proteins involved in virulence. This provides further evidence that the cells are diverting resources away from host-pathogen interactions and towards cell survival.

5.4 Discussion

We demonstrated previously that the loss of GH76 activity in mycobacteria results in the increased abundance of LM and LAM in the cell. For each of these glycolipids, there was a relative increase of approximately 30% when GH76 activity was lost. Despite this, we were interested to understand why the increase was not more pronounced. We therefore conducted a whole-cell proteomics study – a technique which would allow us to compare the proteome of our GH76 mutant cells to wild-type BCG, and the relative

abundancies of each protein. The results of this study highlighted a huge number of proteins that were either up, or down regulated in our mutant cells, including several enzymes involved in the biosynthesis of LM and LAM which were downregulated in the mutant.

The enzymes EmbC, AftB, AftC, and AftD were all identified as being downregulated in the GH76 mutant. EmbC is an arabinosyltransferase responsible for synthesising the linear α-1,5 linked arabinofuranose residues in the arabinan domain of LAM (Shi *et al.,* 2006; Goude *et al.,* 2008; Korkegian *et al.,* 2014). AftC and AftD are also arabinosyltransferases, and these enzymes are responsible for integrating α-1,3 linkages into the α-1,5 linked linear chains (Birch *et al.,* 2008; Skovierová *et al.,* 2009; Birch *et al.,* 2010; Madduri *et al.,* 2022;). AftB will terminate the arabinan domain with β-1,2 linked arabinofuranose residues (Jankute *et al.,* 2017; Seidel *et al.,* 2007). The downregulation of these enzymes will therefore result in a decrease in the biosynthesis of LAM from LM. This provides evidence as to why the loss of GH76 activity did not have a more profound effect on the levels of LAM.

MptA was also identified as being downregulated in the GH76 knock-out. MptA is the first mannosyltransferase that commits the branch point PIM ($AcPIM_4$) to become LM (Mishra *et al.,* 2007; Mishra *et al.,* 2008; Rahlwes, Osman & Morita, 2020; Sparks *et al.,* 2023). It is responsible for hyper-mannosylation of the α-1,6 mannan backbone of LM. Therefore, downregulation of MptA would result in a reduced relative abundance of LM.

This provides evidence as to why the GH76 knock-out cells did not have massive amounts of LM within them.

Taken together, the downregulation of these enzymes involved in the biosynthesis of LM and LAM suggest that mycobacteria respond to increased levels of LM and LAM by downregulating the biosynthesis of these glycolipids. It implies that this is a tightly controlled process, and that LM and LAM levels may be actively sensed by the cell so that they can adjust synthesis accordingly.

In addition to the enzymes discussed above, also identified as being downregulated was the enzyme PimB', and also PimA and PatA though not to the same significance. These enzymes are all involved in the biosynthesis of PIMs up to the branch point. PimA is responsible for the addition of the first mannopyranose to the phosphatidyl inositol anchor to produce PIM_1 (Crellin *et al.,* 2008; Boldrin *et al.,* 2014). PimB' will add the second mannopyranose to produce PIM_2 (Schaeffer *et al.,* 1999; Guerin *et al.,* 2009; Fukuda *et al.,* 2013), and then PatA will add the first acyl chain to produce $AcPIM_2$ (Boldrin *et al.,* 2021; Albesa-Jové *et al.,* 2016). The downregulation of these enzymes will therefore result in less branch point PIM being made, and so less substrate available for synthesis of more LM and LAM. This provides yet more evidence that mycobacteria are actively downregulating the synthesis of LM and LAM as a response to the increased levels during loss of GH76 activity.

As discussed in Chapter 4, the loss of GH76 activity is resulting in an altered cell envelope morphology. This proteomics study highlights that the cells are actively responding to this altered cell envelope by changing the expression of a range of proteins. The increased abundance of periplasmic LM and LAM combined with the loss of capsular arabinomannan may be causing stress to the cell. Along with the proteins already discussed which are involved in the biosynthesis of these glycolipids, we identified a number of other proteins which were significantly up- or down-regulated in our mutant. An important protein we identified as being upregulated in our mutant was FCU26_1812. This is an enzyme believed to be involved in the production of vitamin C in mycobacteria. Vitamin C is an inhibitor of (p)ppGpp synthesis which acts as the master regulator for the stringent response (Syal, Bhardwaj & Chatterji, 2017). This suggests that our mutant is actively trying to reduce the effect of the stringent response. The stringent response will divert resources in the cell towards cell survival when a stress is applied. However, our mutant is reducing the effect of this response.

In mycobacteria, there are two other predicted α-mannanases, a GH38 and GH92. In our proteomics study we did not see a significant change in expression of either of these two proteins. This suggests that the expression of these two proteins is not directly affected by the activity of the GH76 enzyme. However, our hypothesis is that these other two α-mannanases are also acting on LM and LAM, although we are yet to confirm this. Therefore I would have expected that an increase in substrate for these enzymes may have led to an increase in their expression. Whilst our dataset does not support our

theory, it does not rule it out either. The activity of the GH38 and GH92 still remain of interest and will be a follow up study to this thesis.

In Chapter 4, we demonstrated that during stationary phase there was no significant increase in LM or LAM levels in our mutant. Therefore, if we were to repeat this proteomics study using cells harvested during stationary phase, we might expect to see less significant downregulation of the genes involved in the production of LM and LAM. Additionally, the results of this proteomics study may also help to explain what happens in wild-type mycobacteria during stationary phase. As reported by (Dulberger, Rubin and Boutte, 2020), LM and LAM levels are upregulated during stationary phase. Therefore, as the levels of LM and LAM are increased, the wild-type mycobacteria will actively downregulate production of enzymes involved in their biosynthesis to ensure that the levels of glycolipid do not increase too much. This would be similar to what we observe in our mutant where expression of these enzymes is downregulated to account for the high levels of LM and LAM.

In conclusion, this chapter highlights that PIM/LM/LAM biosynthesis is a tightly controlled process and that mycobacteria actively respond to increased levels of LM and LAM by downregulating production of these glycolipids. Additionally, the activity of Rv0365c is necessary to maintain LM/LAM homeostasis.

Chapter 6

Phenotypic Characterisation of Growth when Glycoside Hydrolase 76 Activity is Lost

6. Phenotypic characterisation of growth when glycoside hydrolase 76 activity is lost

6.1 Introduction

Whilst conducting the experiments discussed in previous chapters, it quickly became apparent that the GH76 knock-out cells had a slower growth rate compared to the wild type cells. *M. bovis* is already a slow-growing species of mycobacteria, but the GH76 mutant was taking a significantly longer time to reach desired growth points. In this chapter we therefore set out to quantify this phenotype. We identify that the loss of GH76 activity results in an increased lag phase, and slower exponential growth. In addition to this, we confirm that the slow growth phenotype observed is a result of loss of GH76 activity as complementation with the wild type GH76 gene provides partial restoration of the growth phenotype. However, complementation with the catalytic null GH76 has no effect on the growth of the mutant. Finally, to further investigate the slow growth phenotype, we investigate if the loss of AM in the capsule is responsible. We show that adding enzymatically derived AM to BCG Dan_Δ0378 cultures can increase the growth rate and reduce the lag phase that was observed. Additionally, we show that this is a dose response, as higher concentrations are required to reduce the lag phase.

6.2 Materials and Methods

6.2.1 Growth Point Determination

Bacterial growth was recorded by taking OD_{600} readings daily, using a portable spectrophotometer until stationary phase was reached. Cultures were grown static, in triplicate, in 7H9 media at 37 ℃ with 5% CO_2 using Corning culture flasks (Sigma-Aldrich, CLS431082). Starter cultures were grown until mid-log phase (OD_{600} = 0.6) was reached. Equal volumes were then used to inoculate 10 mL 7H9 media, and growth was recorded every 24 hours.

6.3 Results

6.3.1 Loss of GH76 activity results in an increased lag phase

The first aim for this chapter was to record the growth of wild type BCG Danish and BCG Dan_Δ0378 in order to compare them. OD_{600} reading were taken each day over the course of a 20-day period. The data was then plotted using GraphPad Prism v10.0.2. As shown in Figure 60 the loss of GH76 activity resulted in an increased lag phase when compared to the wild type.

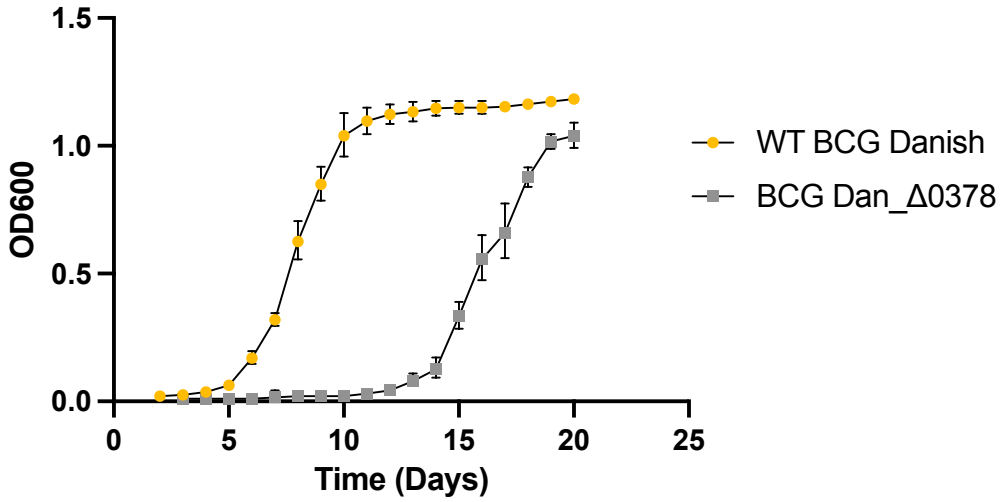

Figure 60: Growth curve of wild type BCG Danish and BCG Dan_Δ0378. OD_{600} readings were taken every day for 21 days, and then plotted using GraphPad Prism v10.0.2. Values shown are mean with error bars indicating standard deviation. Three biological replicates were plotted. Mutant cells exhibit lag-phase growth defect.

The data presented in Figure 60 demonstrated that loss of GH76 activity results in an increase in lag phase, from a period of 4 to 5 days seen in the wild type cultures, to a period of around 13 days in the mutant. To investigate if the growth rate was consistent during exponential growth, the data points for these periods were taken and simple linear regression was performed. This was then plotted in GraphPad Prism v10.0.2. As can be seen in Figure 61, the growth rate during exponential growth was significantly lower in the BCG Dan_Δ0378 cells compared to wild type BCG.

Following this, we wanted to determine if the differences observed in growth were a direct result of loss of GH76 activity, or if it was a polar effect from the transposon insertion. Therefore, the BCG Dan_Δ0378 strain was complemented with both the wild type BCG Dan_0378 gene as well as a catalytic null version of the gene. The growth analysis was then repeated. As shown in Figure 61, complementation with the wild type GH76 gene provided partial restoration on the growth phenotype.

Complementation with the wild type gene, as shown in Figure 62, did not fully restore the growth phenotype. However, it did reduce the lag phase to around 9 days. Following this, we repeated the analysis of the exponential growth period to assess if complementation had restored the phenotype (Figure 63).

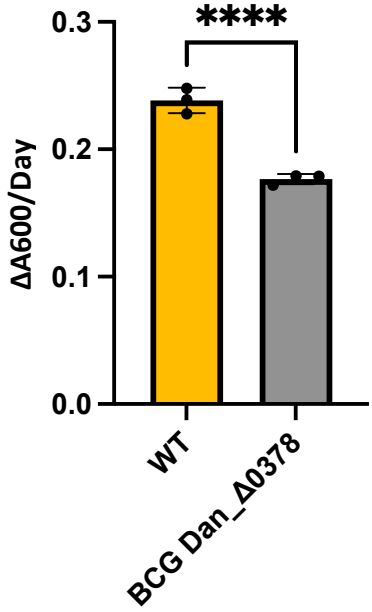

Figure 61: Growth rate during exponential phase. Data points for exponential growth period were analysed with simple linear regression. For each sample n=3, significance determined by T- test where ****p<0001. Values shown are mean with error bars showing standard deviation. Mutant cells have significantly slower exponential growth rate.

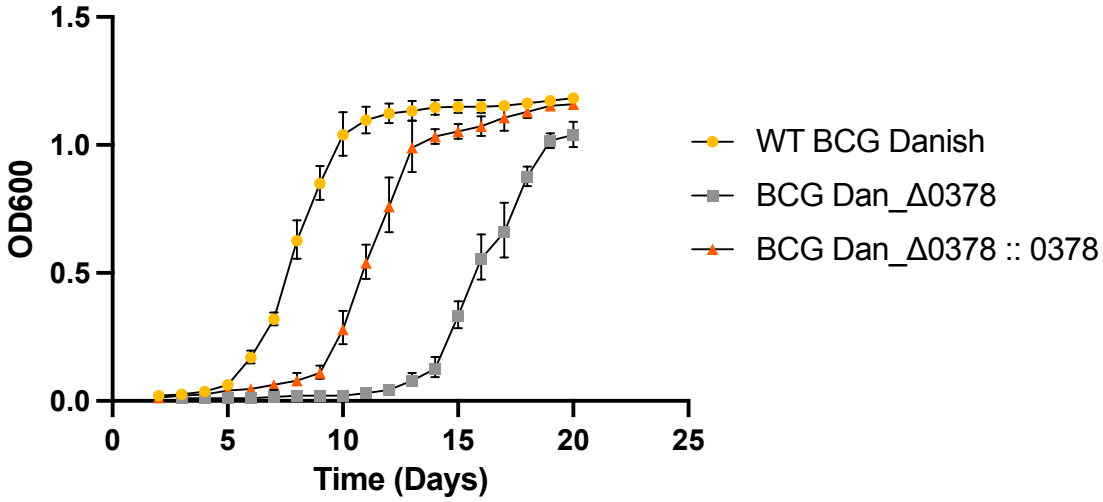

Figure 62: Growth curve of wild type BCG Danish, BCG Dan_Δ0378, and BCG Dan_Δ0378::0378. OD_{600} readings were taken every day for 21 days, and then plotted using GraphPad Prism v10.0.2. Values shown are mean with error bars indicating standard deviation. Three biological replicates were plotted. Complemented cells have reduced lag-phase growth defect.

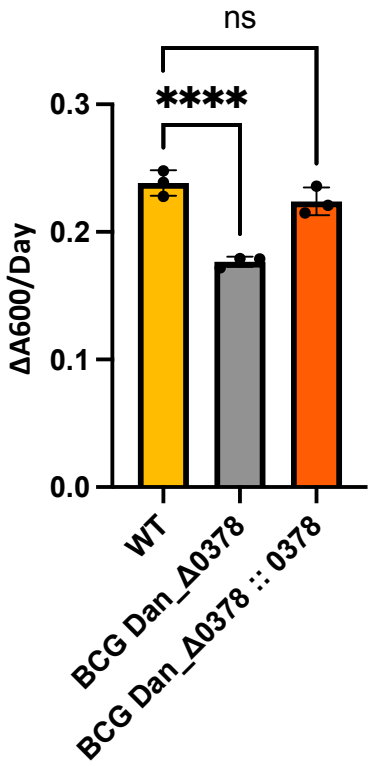

Figure 63: Growth rate during exponential phase with complemented strain. Data points for exponential growth period were analysed with simple linear regression. For each sample n=3, significance determined by one-way ANOVA test where ****p<0001. Values shown are mean with error bars showing standard deviation. Complemented cells restore the exponential phase growth rate to wild type levels.

Figure 63 reveals that complementation with the wild type GH76 gene restored growth during exponential phase to that of the wild type as there is no significant difference between the two. To confirm that this was a direct effect of complementation with the wild type gene, we then repeated the growth analysis again with a BCG Dan_Δ0378 strain complemented with a catalytic null version of the GH76 gene. The result of this is shown in Figure 64.

As shown in Figure 64, complementation with the catalytic null version of the GH76 gene had no effect on the growth rate of the cells. Furthermore, the growth rate during exponential phase was also unchanged from that of the knock out strain, as shown by Figure 65.

These results indicated that the catalytic null variant of the GH76 had no effect on either reducing the lag phase, or returning the exponential growth rate back to that of wild type BCG. We were therefore confident that the phenotype observed when BCG Dan-_Δ0378 was complemented with the wild type gene was a direct result of the GH76 activity in the cell.

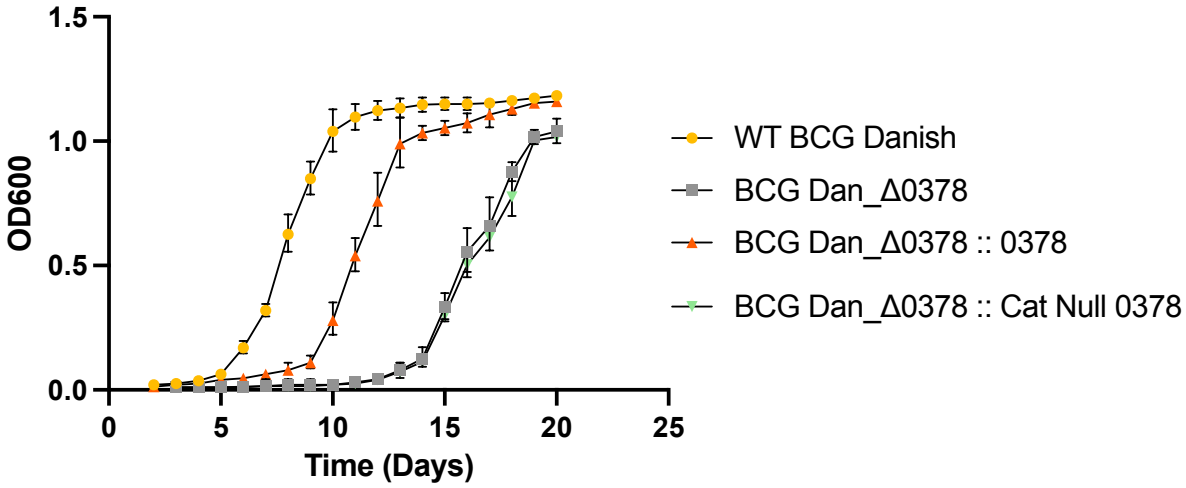

Figure 64: Growth curve of wild type BCG Danish, BCG Dan_Δ0378, BCG Dan_Δ0378::0378, and BCG Dan_Δ0378::CatNull0378. OD_{600} readings were taken every day for 21 days, and then plotted using GraphPad Prism v10.0.2. Values shown are mean with error bars indicating standard deviation. Three biological replicates were plotted. Catalytic null complement had no effect on the lag-phase defect.

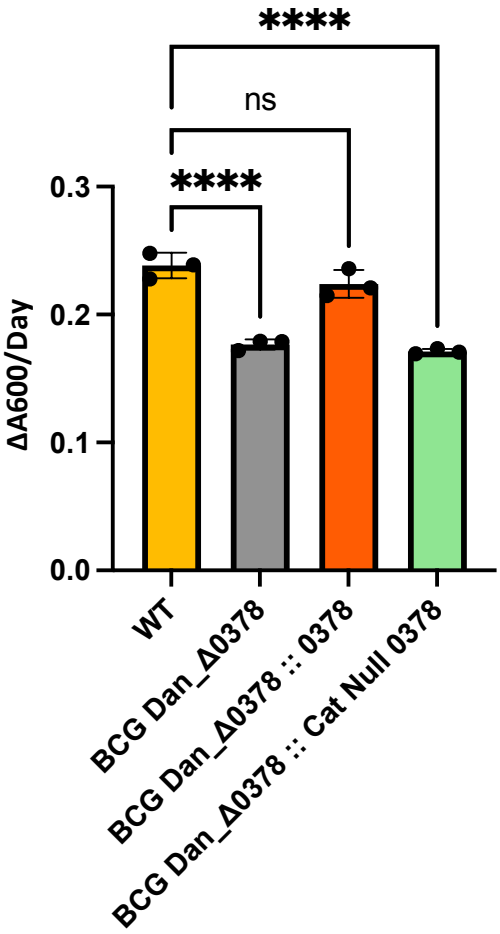

Figure 65: Growth rate during exponential phase with complemented strains. Data points for exponential growth period were analysed with simple linear regression. For each sample n=3, significance determined by one-way ANOVA test where ****p<0001. Values shown are mean with error bars showing standard deviation. Catalytic null complementation had no effect on the exponential growth rate.

6.3.2 Growing BCG Dan_Δ0378 in spent media had very little effect on growth

Following the reduced growth phenotype we observed, it was hypothesised that the lack of AM in the capsule of BCG Dan_Δ0378 cells, shown previously in Chapter 3.3.4, was playing a role in triggering the switch from lag phase to exponential growth. Alternatively, the capsular AM could have a role in quorum sensing, and so the loss of capsular AM in the BCG Dan_Δ0378 cells was delaying the initiation of exponential growth phase. To test this, we first explored the idea that wild-type BCG may release capsular AM into the media, and this could be used to trigger growth in BCG Dan_Δ0378 cells. Therefore, wild type BCG was grown in 100 mL 7H9 media until mid-log phase was reached (OD_{600} = 0.8). At this point, the cells were harvested and the media was filter sterilised to remove any remaining wild type cells. The media was not autoclaved, as we expected that this may have an adverse effect. Subsequently, BCG Dan_Δ0378 was cultured in the spent media alongside BCG Dan_Δ0378 cultured in fresh media. As before, OD_{600} readings were taken on a daily basis until stationary phase was reached. The data was then plotted using GraphPad Prism v10.0.2, as shown in Figure 66.

Figure 65 revealed that the spent media had very little effect on the growth of BCG Dan-_Δ0378 in terms of reducing the lag phase, as the cells grown in spent media appeared to enter exponential growth just one day earlier than those cells grown in fresh media. However, when the exponential growth rates were compared we found that the cells grown in spent media had a significantly higher growth rate compared to the cells grown in fresh media. This is shown in Figure 67.

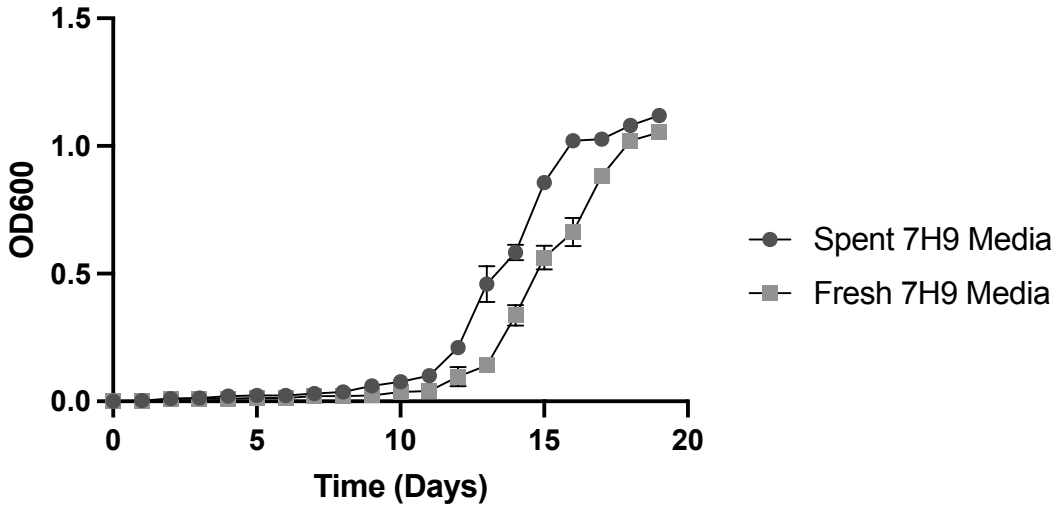

Figure 66: Growth curve of BCG Dan_Δ0378 grown in fresh and spent 7H9 media. OD_{600} readings were taken every day for 21 days, and then plotted using GraphPad Prism v10.0.2. Values shown are mean with error bars indicating standard deviation. Three biological replicates were plotted. Cultures grown in the spent media exhibited transition into log-phase one day earlier than those grown in fresh media.

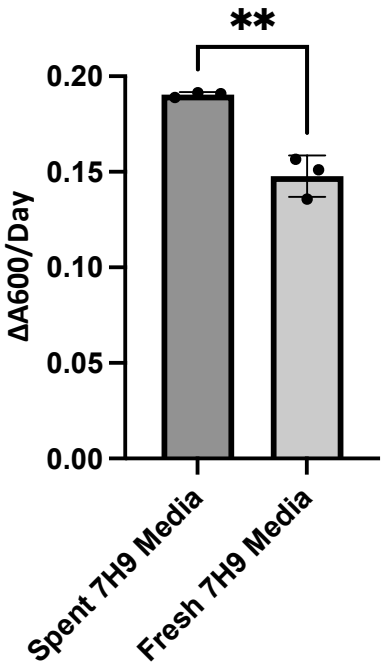

Figure 67: Growth rate during exponential phase of BCG Dan_Δ0378 grown in fresh and spent media. Data points for exponential growth period were analysed with simple linear regression. For each sample n=3, significance determined by t-test where ***p*<0.01. Values shown are mean with error bars showing standard deviation. Log-phase growth was significantly reduced in the cultures grown in fresh media.

The data presented in Figure 67 suggests that the spent media is playing some sort of role in increasing the growth rate of exponentially growing BCG Dan_Δ0378 cells. However, the spent media only had a small impact on triggering the switch from logarithmic growth to exponential growth in BCG Dan_Δ0378 cells.

6.3.3 Feeding AM to BCG Dan_Δ0378 cultures reduced lag phase

As the spent media had little impact on the growth rate of BCG Dan_Δ0378, we next investigated whether the addition of enzymatically derived AM to naïve media would affect the growth rate. To do this, LAM and LM were incubated with Rv0365c for 4 hours, and then a 10:10:3 separation was performed to isolate the resulting carbohydrates. Following this, the derived AM was added to 7H9 media at a final concentration of 0.05 mg / mL. Growth was measured every 24 hours, and compared to a control culture. This is shown in Figure 68.

As shown in Figure 68, the addition of 0.05 mg / mL AM had no effect on the growth of BCG Dan_Δ0378. We therefore speculated that the dosage was not high enough for an effect to be seen, and so we repeated the experiment with an increased concentration of AM. In this case, AM was added to the media at a final concentration of 0.5 mg / mL. The results of this are shown in Figure 69.

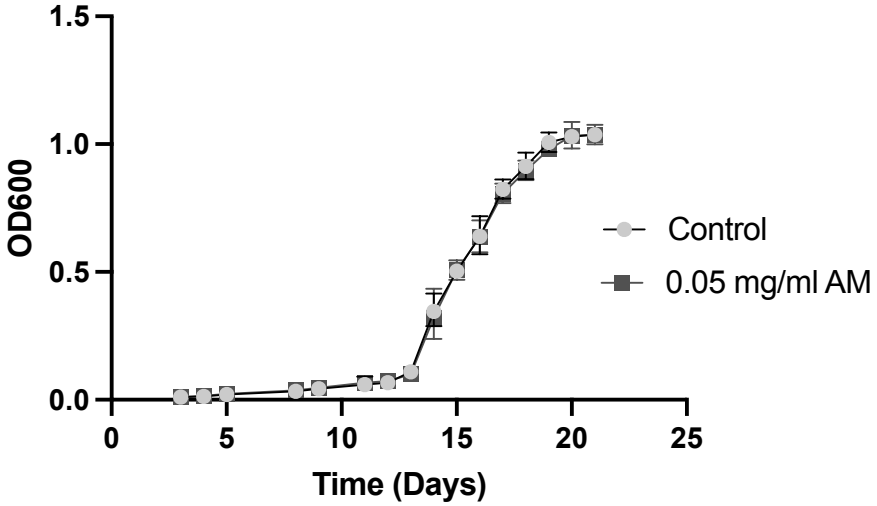

Figure 68: Growth curve of BCG Dan_Δ0378 grown in 7H9 media supplemented with purified AM. OD_{600} readings were taken every day for 21 days, and then plotted using GraphPad Prism v10.0.2. Values shown are mean with error bars indicating standard deviation. Three biological replicates were plotted. Addition of the AM supplement had no effect on the growth rate.

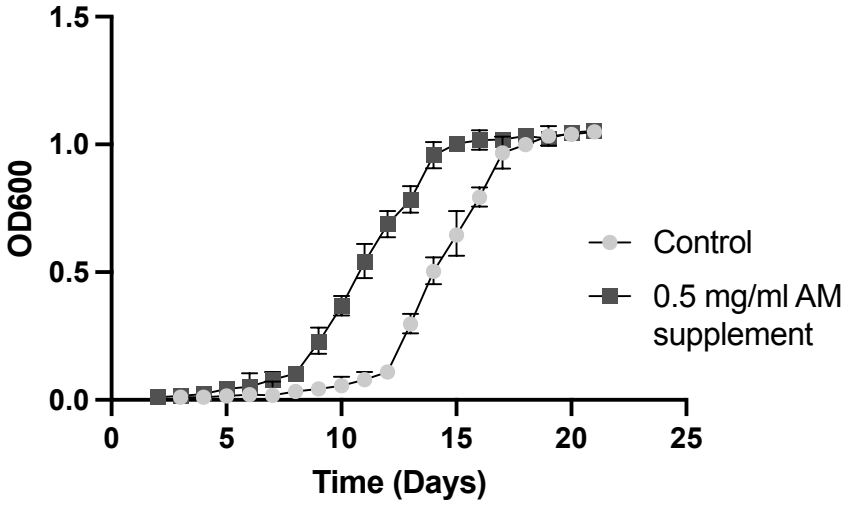

Figure 69: Growth curve of BCG Dan_Δ0378 grown in 7H9 media with increased concentration of purified AM. OD_{600} readings were taken every day for 21 days, and then plotted using GraphPad Prism v10.0.2. Values shown are mean with error bars indicating standard deviation. Three biological replicates were plotted. Higher concentration of AM supplement had reduced the lag-phase defect.

As shown in Figure 69, when the increased concentration of purified AM was added to 7H9 media, it resulted in an improved growth rate of BCG Dan_Δ0378. The cells entered exponential growth around 4 days earlier than the control cultures demonstrating that the increased lag phase could be rescued by addition of AM to the media. To further investigate if the addition of 0.5 mg / mL AM improved the growth rate of the cultures, the growth during exponential phase was compared to both the wild type BCG as well as BCG Dan_Δ0378 :: 0378. This is shown in Figure 70.

Analysis of the exponential growth rate of the AM supplemented cells revealed that growth during this period was significantly different to that of the wild-type or the complemented strains. This suggests that the addition of AM alone is not enough to restore the exponential growth to the wild-type phenotype, and there must be alternative pathways involved for processing the AM.

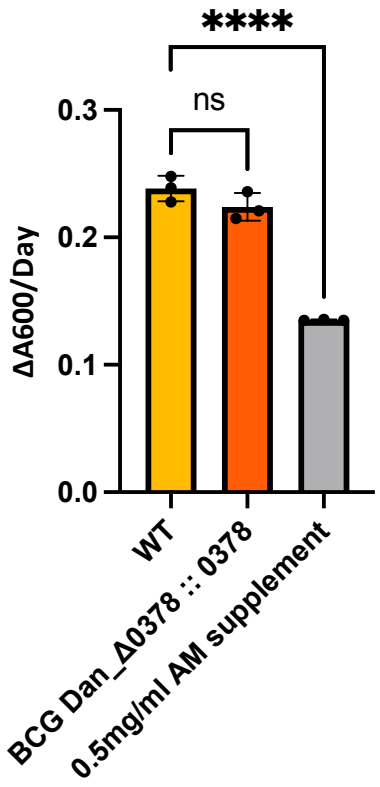

Figure 70: Growth rate during exponential phase of wild-type BCG, BCG Dan_Δ0378:: 0378, and BCG Dan_Δ0378 supplemented with 0.5 mg / ml arabinomannan. Data points for exponential growth period were analysed with simple linear regression. For each sample n=3, significance determined by one-way ANOVA test where ****p<0001. Values shown are mean with error bars showing standard deviation. The exponential growth rate of AM supplemented cells is significantly lower than the wild-type phenotype.

6.4 Discussion

Whilst conducting the experiments detailed in earlier chapters with the BCG Dan_Δ0378 strain, it became evident that this mutant had a growth defect when compared to wild-type BCG Danish. The aim of this chapter, therefore, was to investigate this growth phenotype and explore what was causing it. The first objective was to record the growth of the knock-out strain and generate a growth curve. As the generation time of slow-growing mycobacteria is around 20 hours, I decided to take one OD_{600} reading per day. This continued until the cultures reached stationary phase. The growth curves were repeated in triplicate, and the data was plotted using GraphPad Prism v10.0.2. From this, we were able to demonstrate that the loss of GH76 activity in BCG Danish causes an increase in lag phase. The wild type cultures spent around 5 days in lag phase before entering exponential growth. In contrast, the knock-out cultures spent around 14 days in lag phase before entering exponential growth. In addition to this, we were able to show that during exponential phase the growth rate of the knock-out cells is slower than that of the wild type cultures.

To prove that this growth defect phenotype was a result of the loss of GH76 activity, and not a polar effect from the transposon insertion, the complemented strains growth was also quantified. Complementation with the wild-type gene provided partial restoration of the growth phenotype, and fully restored the growth rate during exponential growth. However, complementation with the catalytic null variant had no effect on the growth defect, as well as not effecting the growth during exponential phase. We were therefore

confident that the growth phenotype we were observing was a direct result of the loss of GH76 activity, and not due to any polar effects from the transposon insertion.

Recent work published by Sparks *et al.,* (2023), indicated that LAM plays an important role in septation of mycobacteria. They show that *M. smegmatis* cells deficient in LAM but not LM are unable to maintain cell wall integrity in certain media, as well as having deformed envelopes. Additionally, they have a blebbing morphology. Furthermore, these cells with deformed LAM exhibited an increase in peptidoglycan. In addition, they highlight that mutants producing abnormally large LAM formed multi-septations and new poles. Taken together, these results highlight that LAM plays an important role in the growth and division of mycobacteria. This is comparable to the role lipoteichoic acids play in Gram-positive bacteria. As discussed by Cleveland *et al.,* (1975) loss of lipoteichoic acids will result in poor septation and cell division. These studies demonstrate how glycoconjugates are important molecules for growth.

Based on our growth results where the loss of GH76 activity results in an increased lag phase, we hypothesised that the resulting products of the enzymatic breakdown of LM and LAM may be acting as signals to enter exponential growth. Our first attempt at testing this was to grow BCG Dan_Δ0378 in spent media which had been used to culture wild type BCG. The inclusion of tween-80 in the media would cause the capsular material to be shed. Therefore, after pelleting the cells, the resulting spent media would contain the capsular material from the wild-type cells. Our theory was that the spent media would be able to rescue the lag phase defect as the presence of the left over AM would

act as a growth signal, and trigger exponential growth. When growth was quantified, we were able to demonstrate that the spent media was able to partially rescue the lag phase phenotype. Furthermore, the spent media provided an increase in exponential growth in the spent media cultures.

To further investigate this, we followed this up by adding enzymatically derived AM to naïve media and quantifying the growth of BCG Dan_Δ0378. Initially, we added purified AM at a final concentration of 0.05 mg / mL to the media. This had no effect on growth as the final growth curves were almost identical. Therefore, we increased the concentration of AM to 0.5 mg / mL. This had a profound effect, and the lag phase phenotype was restored to the same extent that complementation with the wild-type gene achieved. This demonstrated a dosage response of AM addition, as a higher concentration was required to trigger the transition from lag phase to exponential growth. However, the addition of AM alone was not enough to restore the exponential growth phase. Comparison of logarithmic growth between wild-type and the AM supplemented cells revealed that the growth was significantly slower in the AM supplemented cells compared to the wild-type strains. This suggested that there must be further processing of capsular AM required to fully restore the log-phase. This may involve removal of the arabinan domain and/or removal of the mannose caps from AM.

Taking these findings together, we deduce that capsular arabinomannan plays a role in triggering exponential growth in lag phase cultures. In wild-type cells, the gradual accumulation of AM in the media eventually causes the culture to exit lag phase.

However, in our BCG Dan_Δ0378 cells, where we have previously shown that AM is lacking in the capsule, it takes a lot longer for the transition to exponential growth to occur. Capsular AM therefore acts as a molecular signal for exponential growth in mycobacteria.

The partial restoration of the growth phenotype by the complement strain may be, in part, explained by the results discussed in Chapter 4. In this chapter, we demonstrated that the complement strain does not fully restore the capsular AM phenotype observed in the wild type cells. Therefore, during lag phase there will be less capsular AM present in the complement cells compared to the wild type cells. Taking into account the results discussed above, this may explain why the complement strain did not fully restore the lag phase phenotype.

As discussed by Li *et al.,* (2016), lag phase is the delay during growth as bacteria adapt to a new environment/media. The authors report that bacteria can increase their lag period as a mechanism for dealing with antibiotic stress. The increased lag time allows for the cells to increase their tolerance to the stress before entering exponential growth. This was termed 'tolerance by lag' by Fridman *et al.,* (2014), and is a way for bacteria to tolerate environmental stresses and build resistance. The findings by Li *et al.,* (2016), discuss how this tolerance by lag is a mechanism for surviving antibiotic stresses, and how increased concentrations of antibiotic result in increased lag phases in *E. coli* and *Pseudomonas aeruginosa*. They also report that increased lag phases can be associated with injured or stressed cells. These studies highlight the importance of lag phase to

bacteria and suggests that the lag phase defect we have detailed in this chapter may be a mechanism for our mutant to deal with stress. We have previously demonstrated that the GH76 knock-out mutant has an altered cell envelope physiology with increased abundance of LM/LAM, altered PIM profiles, and loss of capsular AM. These changes may be causing membrane stresses that the cells are responding to by increasing their lag phase. The addition of AM to the media may help relieve this stress and signal transition to exponential growth. The low abundance of cells during lag phase, combined with the slow generation time of mycobacteria, makes it a challenging growth period to study.

Extended lag phases in mycobacteria have only been described previously by Liu *et al.,* (2017). In this study, they demonstrated that overexpression of the *Rv2629* gene leads to delayed entry into exponential growth in *M. smegmatis*. Additionally, they show that this increased lag phase also increases the pathogenicity of *M. smegmatis* when infecting mice. *Rv2629* is a member of the dosR dormancy regulon (Liu *et al.,* 2017). This is a region of the mycobacterial genome which is expressed at low level during lag phase and is completely repressed during logarithmic growth. The genes in this regulon have been shown to be upregulated in response to low oxygen levels (Liu *et al.,* 2017). Additionally, it has been suggested that expression of *Rv2629* correlates with higher survival rates of drug-resistant strains of *M. tuberculosis*. The study by Liu *et al.,* (2017), speculates that the overexpression of *Rv2629* delays entry into exponential growth by inhibiting protein biosynthesis. This delay in growth is advantageous to the bacteria as it increases their chance of survival in the host. In this work, the authors demonstrate

that the strains overexpressing *Rv2629* have increased survival rates in the mouse model compared to wild type *M. smegmatis* strains. These finding further demonstrate that the increased lag phase is a survival mechanism in bacteria, and that it can allow for bacteria to adapt to stresses before entering exponential growth.

When considering the biological context of mycobacteria and the life cycle of TB during the infection process, the transition from lag phase to exponential growth could be an important switch to control for the bacteria. As discussed in Chapter 1, the majority of TB infections result in a latent infection where the bacteria are contained by the immune system but not cleared. The bacteria remain dormant in a lag phase period where they are not actively growing but waiting for the immune system to weaken. Therefore, once the cells can sense the weakening of the host immune system, they will need a signal to trigger exponential growth. This signal could therefore be capsular AM. Upon recognition that the host immune system is compromised, the enzymatic cleavage of LAM to release AM to the capsule may act to trigger exponential growth of dormant TB and lead to active TB disease. This suggests that this enzyme could be an important drug target for reducing reactivation of latent TB infections.

In conclusion, the findings in this chapter demonstrate that capsular AM is required to trigger exponential growth in mycobacteria. However, the results discussed here have not differentiated between the different glycan products produced by the digestion of LM and LAM. In our sample, we are adding both arabinomannan and mannan to the samples. It is therefore not clear which of these glycans, if not both, is responsible for

acting as the molecular signal. To test this, we would need to separate LAM from LM, repeat the enzymatic digestion, and then test the separate glycans. It is my hypothesis that the glycan responsible for triggering outgrowth is AM. This is because, it is found in much larger abundance in the capsule than mannan is and would therefore be more likely to act as a signalling molecule. The next aim for this chapter would therefore be to investigate how the different derived glycans would impact the growth of our knock-out mutant.

Chapter 7

Conclusions

7. Conclusion

The hypothesis for this thesis was that Rv0365c was the missing enzyme responsible for the cleavage of lipomannan and lipoarabinomannan to release the carbohydrate domains so that they can be trafficked to the capsule of the cell. To investigate this, the thesis was split into two aims. First, to biochemically characterise Rv0365c to show that the enzyme possessed α-mannanase activity, and more specifically GH76 activity, and that the enzyme was active on both LM and LAM. The second aim of this thesis was to investigate the phenotypic effects of loss of Rv0365c activity, including the glycolipid composition, capsular polysaccharide content, polar lipid composition, protein expression, and growth.

In Chapter 3, Rv0365c was purified and GH76 activity was confirmed by assaying the enzyme on a mannan substrate consisting of only an α-1,6 linked backbone. In addition to this, the enzyme was shown to be active on both LM and LAM purified from *M. bovis* BCG. This reaction produced a small glycolipid product which was isolated and analysed by mass spectrometry. It was identified that this small product had a structure consistent with that of $AcPIM_2$, demonstrating that Rv0365c was cleaving this small lipid carrier off of LM and LAM to release the carbohydrate domains. Following this, in Chapter 4, the abundance of LM and LAM when Rv0365c activity was lost was analysed. In this chapter, it was shown that loss of Rv0365c activity results in a significant accumulation of LM and LAM in the cells. Furthermore, it was shown that the loss of Rv0365c activity results in no detectable arabinomannan in capsular polysaccharide extracts. These results provide evidence to support our theory that Rv0365c is the

missing enzyme responsible for releasing the carbohydrate domains from LM and LAM so that they can be trafficked to the capsule. Additionally, this thesis describes the first extended lag phase in mycobacteria as a result of an altered LM/LAM phenotype.

The results presented in this thesis will serve as a basis for further studies into a currently under-developed area of research – the breakdown and recycling of mycobacterial glycolipids. The current literature is well established regarding the synthesis of LM and LAM, but the degradation of these molecules is an area of research that has so far been overlooked. There is also a plethora of research regarding the role LM and LAM play in pathogenesis. However, there must be an additional function of LM and LAM beyond virulence. All mycobacteria produce LM and LAM in some form, but not all mycobacteria are pathogenic. This suggests that LM and LAM must play additional roles in the cell. In this thesis, we have provided evidence of this as the lipid-free derivatives of these glycolipids can be used as growth signals.

Arabinomannan is an important polysaccharide found in the capsule of pathogenic mycobacteria. Although the specific function of AM has yet to be clearly defined, it has been shown by Chen *et al.,* (2020), that AM is important for binding of tuberculosis bacilli to the human macrophage antibody IgG, as when antibodies specific for AM are depleted binding is significantly reduced. This implies that AM plays a role in binding to host cell receptors in order adhere to macrophages. In addition, Ishida *et al.,* (2021), demonstrated that human antibodies can recognise a range of AM oligosaccharide motifs and are specific for AM over LAM. These studies have highlighted the importance

of capsular AM to mycobacteria in regards to host-pathogen interactions. It implies that capsular AM may play an important role in the infection process, and therefore loss of capsular AM could be associated with a reduction in virulence. Studies conducted by Miller and Shinnick (2001), showed that the expression of Rv0365c in *M. smegmatis* increased the survival rate of the non-pathogenic bacteria inside macrophages. The results discussed in this thesis could help to provide some explanation as to why this might be. In fast-growing mycobacteria, the capsules are predominantly protein based (Ortalo-Magne *et al.,* 1995; Ortalo-Magne, Andersen and Daffe, 1996). Therefore, the expression of Rv0365c may have increased the amount of AM present in the *M. smegmatis* capsule. This could have resulted in increased virulence of the bacteria as the cells are better equipped to interact with the host cell. This, in turn, could have resulted in the increased survival rates of the Rv0365c expressing *M. smegmatis* cells.

The work presented in this thesis provides the evidence to justify the hypothesis that Rv0365c cleaves LM and LAM to release AM and mannan from the lipid carrier. However, the work carried out in this thesis does not provide an explanation for how AM and mannan are trafficked from the periplasm to the capsule. This would become the basis of future work that we would carry out following this thesis. To do this, we would first need to identify proteins that associate with AM. We could identify these proteins by digesting LAM with Rv0365c, isolating the AM product, and using it to generate an AM-based affinity chromatography resin. This could be done by forming *C*-glycoside ketones, a technique where the glycan is modified with a ketone at the reducing end to facilitate attachment to a resin. Following this, whole-cell mycobacterial

lysates would be passed over the column. The only proteins that will bind to the resin will be those associated with AM. We could identify these proteins, with the help of Dr Nichollas Scott, by proteomics. Any identified proteins would therefore be the basis of our future studies. This future work would help to uncover more of the mystery of LM/LAM digestion and help to explain how the carbohydrate motifs are trafficked from the periplasm to the capsule.

Additionally, future work following on from this thesis would look to characterise the other two mannanases present in mycobacteria. These proteins belong to the families GH92 and GH38 and will therefore cleave α-1,2 linked mannan. Within the LM/LAM structure there are α-1,2 mannan linkages protruding from the mannan backbone. Furthermore, in mannose-capped LAM there are α-1,2 linkages present in the capping motifs. Previous work by Rivera-Marrero *et al.,* (2001), has demonstrated that the GH38 family protein Rv0648 has α-mannanase activity. The specific linkage being cleaved has not been determined, however. To date, the GH92 family protein Rv0584 has not been biochemically characterised. Therefore, future work would seek to purify both proteins and assay them on the range of substrates we have purified already. We hypothesise that both mannanases may be involved in the degradation of LM and LAM. Rv0584 has homologues in *M. bovis* and *M. marinum*, but does not have a homologue in *M. smegmatis*. *M. smegmatis* is a fast-growing *Mycobacterium* and does not produce ManLAM. Therefore, it is possible that Rv0584 is targeting the α-1,2 linkages present in the capping motifs of ManLAM in slow-growing, predominantly pathogenic mycobacteria. Rv0648 however, has homologues in *M. bovis, M. marinum,* and *M.*

smegmatis. Therefore, this enzyme must be targeting α-1,2 linkages which are present in all these species. It is possible that Rv0648 is the enzyme acting on the α-1,2 linkages which decorate the mannan backbone of LM and LAM. Alternatively, it is possible that either of these α-1,2 mannanases could be acting on mannoproteins in mycobacteria, and play no role in the digestion of LM and LAM.

One potential avenue that we did not explore in this thesis was how overexpression of *Rv0365c* would impact the phenotypes we observed. Overexpression of the GH76 gene would result in a higher concentration of the protein in the cell. Whilst we cannot tell how this may affect the bacteria, we can speculate that higher concentrations of Rv0365c may lead to an increase in LM and LAM hydrolysis. Therefore, we would likely see a reduction in LM/LAM in the cell compared to wild-type as well as an increase in capsular AM. Additionally, the increased cleavage of LM may increase the amount of mannan in the capsule to a level where we can detect in during size exclusion. If capsular AM was increased, this has the potential to increase the growth rate of the bacteria and trigger an earlier entry into exponential growth.

The biochemical activity of Rv0365c we have described in this thesis has implications as a potential molecular tool for characterising lipid carriers from LM and LAM in other mycobacterial species and clinical isolates of *M. tuberculosis*. We have demonstrated that Rv0365c will cleave the lipid carrier, $AcPIM_2$, off of LM/LAM extracted from *M. bovis* BCG. However, future studies could employ the catalytic ability of Rv0365c to study the lipid carriers in other mycobacterial LM and LAMs. The purification of the isolated lipid

carrier and analysis through mass spectrometry could provide an insight into if all mycobacterial LM and LAM is assembled using the same lipid carrier. As previously discussed, there are differences in the capping of LAM observed in different species of mycobacteria (Brown and Taffet, 1995; Dinadayala *et al.,* 2006; Kaur *et al.,* 2008). Therefore, it is not impossible that there could be structural differences observed in the lipid anchor in which these molecules are built upon.

Finally, the presence of LAM in urine has been used to diagnose active tuberculosis in HIV positive individuals (Bulterys *et al.,* 2019). However, it has remained unclear as to how LAM is shed from the bacteria to end up in the urine. The biochemical activity of Rv0365c presented in this thesis could provide some insight as to how LAM (or AM) is released from *M. tuberculosis* during active infection, and why it is subsequently detected in urine samples. As a molecular tool, Rv0365c could allow for digestion of LM/LAM from clinical isolates so that the carbohydrate domain can be better characterised and understood.

To conclude, this thesis has provided evidence that Rv0365c is an authentic member of the GH76 family. The catalytic activity of this enzyme is required for the digestion of LM and LAM to release AM to the capsule. Capsular AM is an important signalling molecule required to trigger exponential growth phase from stationary phase and can be used to recover a lag phase defect in GH76 knock-out cells. However, further investigation is required into whether the arabinan or the mannan is the signalling molecule, and if further processing of the AM is required to rescue the log phase defect observed.

References

References

1. Abrahams, K. A. and Besra, G. S. (2018) 'Mycobacterial cell wall biosynthesis: a multifaceted antibiotic target', *Parasitology,* 145(2), pp. 116-133.
2. Adam, A., Petit, J. F., Wietzerbin-Falszpan, J., Sinay, P., Thomas, D. W. and Lederer, E. (1969) 'L'acide N-glycolyl-muramique, constituant des parois de Mycobacterium smegmatis: Identification par spectrometrie de masse', *FEBS Lett,* 4(2), pp. 87-92.
3. Afonso-Barroso, A., Clark, S. O., Williams, A., Rosa, G. T., Nóbrega, C., Silva-Gomes, S., Vale-Costa, S., Ummels, R., Stoker, N., Movahedzadeh, F., van der Ley, P., Sloots, A., Cot, M., Appelmelk, B. J., Puzo, G., Nigou, J., Geurtsen, J. and Appelberg, R. (2013) 'Lipoarabinomannan mannose caps do not affect mycobacterial virulence or the induction of protective immunity in experimental animal models of infection and have minimal impact on in vitro inflammatory responses', *Cell Microbiol,* 15(4), pp. 660-74.
4. Al-Jourani, O., Benedict, S. T., Ross, J., Layton, A. J., van der Peet, P., Marando, V. M., Bailey, N. P., Heunis, T., Manion, J., Mensitieri, F., Franklin, A., Abellon-Ruiz, J., Oram, S. L., Parsons, L., Cartmell, A., Wright, G. S. A., Baslé, A., Trost, M., Henrissat, B., Munoz-Munoz, J., Hirt, R. P., Kiessling, L. L., Lovering, A. L., Williams, S. J., Lowe, E. C. and Moynihan, P. J. (2023) 'Identification of D-arabinan-degrading enzymes in mycobacteria', *Nat Commun,* 14(1), pp. 2233.
5. Albesa-Jové, D., Svetlíková, Z., Tersa, M., Sancho-Vaello, E., Carreras-González, A., Bonnet, P., Arrasate, P., Eguskiza, A., Angala, S. K., Cifuente, J. O.,

Korduláková, J., Jackson, M., Mikušová, K. and Guerin, M. E. (2016) 'Structural basis for selective recognition of acyl chains by the membrane-associated acyltransferase PatA', *Nat Commun,* 7, pp. 10906.

6. Alsteens, D., Verbelen, C., Dague, E., Raze, D., Baulard, A. R. and Dufrêne, Y. F. (2008) 'Organization of the mycobacterial cell wall: a nanoscale view', *Pflugers Arch,*456(1), pp. 117-25.
7. Amin, K., Tranchimand, S., Benvegnu, T., Abdel-Razzak, Z. and Chamieh, H. (2021) 'Glycoside Hydrolases and Glycosyltransferases from Hyperthermophilic Archaea: Insights on Their Characteristics and Applications in Biotechnology', *Biomolecules,* 11(11).
8. Angala, S. K., Belardinelli, J. M., Huc-Claustre, E., Wheat, W. H. and Jackson, M. (2014) 'The cell envelope glycoconjugates of Mycobacterium tuberculosis', *Crit Rev Biochem Mol Biol,* 49(5), pp. 361-99.
9. Ardèvol, A. and Rovira, C. (2015) 'Reaction Mechanisms in Carbohydrate-Active Enzymes: Glycoside Hydrolases and Glycosyltransferases. Insights from ab Initio Quantum Mechanics/Molecular Mechanics Dynamic Simulations', *J Am Chem Soc,* 137(24), pp. 7528-47.
10. ASSELINEAU, J. and LEDERER, E. (1950) 'Structure of the mycolic acids of Mycobacteria', *Nature,* 166(4227), pp. 782-3.
11. Bacon, J., Alderwick, L. J., Allnutt, J. A., Gabasova, E., Watson, R., Hatch, K. A., Clark, S. O., Jeeves, R. E., Marriott, A., Rayner, E., Tolley, H., Pearson, G., Hall, G., Besra, G. S., Wernisch, L., Williams, A. and Marsh, P. D. (2014) 'Non-replicating Mycobacterium tuberculosis elicits a reduced infectivity profile with

corresponding modifications to the cell wall and extracellular matrix', *PLoS One,* 9(2), pp. e87329.

12. BALLOU, C. E., VILKAS, E. and LEDERER, E. (1963) 'Structural studies on the myo-inositol phospholipids of Mycobacterium tuberculosis (var. bovis, strain BCG)', *J Biol Chem,* 238, pp. 69-76.
13. Bansal, R., Sharma, D. and Singh, R. (2018) 'Tuberculosis and its Treatment: An Overview', *Mini Rev Med Chem,* 18(1), pp. 58-71.
14. Bansal-Mutalik, R. and Nikaido, H. (2014) 'Mycobacterial outer membrane is a lipid bilayer and the inner membrane is unusually rich in diacyl phosphatidylinositol dimannosides', *Proc Natl Acad Sci U S A,* 111(13), pp. 4958-63.
15. Barberis, I., Bragazzi, N. L., Galluzzo, L. and Martini, M. (2017) 'The history of tuberculosis: from the first historical records to the isolation of Koch's bacillus', *J Prev Med Hyg,* 58(1), pp. E9-E12.
16. Barksdale, L. and Kim, K. S. (1977) 'Mycobacterium', *Bacteriol Rev,* 41(1), pp. 217-372.
17. Basso, L. A., da Silva, L. H., Fett-Neto, A. G., de Azevedo, W. F., Moreira, I. e. S., Palma, M. S., Calixto, J. B., Astolfi Filho, S., dos Santos, R. R., Soares, M. B. and Santos, D. S. (2005) 'The use of biodiversity as source of new chemical entities against defined molecular targets for treatment of malaria, tuberculosis, and T-cell mediated diseases--a review', *Mem Inst Oswaldo Cruz,* 100(6), pp. 475-506.
18. Bayot, M. L., Mirza, T. M. and Sharma, S. (2022) 'StatPearls'.

19. Bellinzoni, M., Haouz, A., Miras, I., Magnet, S., André-Leroux, G., Mukherjee, R., Shepard, W., Cole, S. T. and Alzari, P. M. (2014) 'Structural studies suggest a peptidoglycan hydrolase function for the Mycobacterium tuberculosis Tat-secreted protein Rv2525c', *J Struct Biol,* 188(2), pp. 156-64.
20. Berg, S., Kaur, D., Jackson, M. and Brennan, P. J. (2007) 'The glycosyltransferases of Mycobacterium tuberculosis - roles in the synthesis of arabinogalactan, lipoarabinomannan, and other glycoconjugates', *Glycobiology,* 17(6), pp. 35-56R.
21. Besra, G. S., Khoo, K. H., McNeil, M. R., Dell, A., Morris, H. R. and Brennan, P. J. (1995) 'A new interpretation of the structure of the mycolyl-arabinogalactan complex of Mycobacterium tuberculosis as revealed through characterization of oligoglycosylalditol fragments by fast-atom bombardment mass spectrometry and 1H nuclear magnetic resonance spectroscopy', *Biochemistry,* 34(13), pp. 4257-66.
22. Betts, J. C., Lukey, P. T., Robb, L. C., McAdam, R. A. and Duncan, K. (2002) 'Evaluation of a nutrient starvation model of Mycobacterium tuberculosis persistence by gene and protein expression profiling', *Mol Microbiol,* 43(3), pp. 717-31.
23. Birch, H. L., Alderwick, L. J., Appelmelk, B. J., Maaskant, J., Bhatt, A., Singh, A., Nigou, J., Eggeling, L., Geurtsen, J. and Besra, G. S. (2010) 'A truncated lipoglycan from mycobacteria with altered immunological properties', *Proc Natl Acad Sci U S A,* 107(6), pp. 2634-9.

24. Birch, H. L., Alderwick, L. J., Bhatt, A., Rittmann, D., Krumbach, K., Singh, A., Bai, Y., Lowary, T. L., Eggeling, L. and Besra, G. S. (2008) 'Biosynthesis of mycobacterial arabinogalactan: identification of a novel alpha(1-->3) arabinofuranosyltransferase', *Mol Microbiol,* 69(5), pp. 1191-206.
25. Boldrin, F., Anso, I., Alebouyeh, S., Sevilla, I. A., Geijo, M., Garrido, J. M., Marina, A., Cioetto Mazzabò, L., Segafreddo, G., Guerin, M. E., Manganelli, R. and Prados-Rosales, R. (2021) 'The Phosphatidyl- *myo*-Inositol Dimannoside Acyltransferase PatA Is Essential for Mycobacterium tuberculosis Growth *In Vitro* and *In Vivo*', *J Bacteriol,* 203(7).
26. Boldrin, F., Ventura, M., Degiacomi, G., Ravishankar, S., Sala, C., Svetlikova, Z., Ambady, A., Dhar, N., Kordulakova, J., Zhang, M., Serafini, A., Vishwas, K. G., Kolly, G. S., Kumar, N., Palù, G., Guerin, M. E., Mikusova, K., Cole, S. T. and Manganelli, R. (2014) 'The phosphatidyl-myo-inositol mannosyltransferase PimA is essential for Mycobacterium tuberculosis growth in vitro and in vivo', *J Bacteriol,* 196(19), pp. 3441-51.
27. Brown, M. C. and Taffet, S. M. (1995) 'Lipoarabinomannans derived from different strains of Mycobacterium tuberculosis differentially stimulate the activation of NF-kappa B and KBF1 in murine macrophages', *Infect Immun,* 63(5), pp. 1960-8.
28. Bulterys, M. A., Wagner, B., Redard-Jacot, M., Suresh, A., Pollock, N. R., Moreau, E., Denkinger, C. M., Drain, P. K. and Broger, T. (2019) 'Point-Of-Care Urine LAM Tests for Tuberculosis Diagnosis: A Status Update', *J Clin Med,* 9(1).

29. Cambier, C. J., Falkow, S. and Ramakrishnan, L. (2014) 'Host evasion and exploitation schemes of Mycobacterium tuberculosis', *Cell,* 159(7), pp. 1497-509.
30. CDC (2016) *History of World TB Day*. Available at: https://www.cdc.gov/tb/worldtbday/history.htm.
31. Chen, T., Blanc, C., Liu, Y., Ishida, E., Singer, S., Xu, J., Joe, M., Jenny-Avital, E. R., Chan, J., Lowary, T. L. and Achkar, J. M. (2020) 'Capsular glycan recognition provides antibody-mediated immunity against tuberculosis', *J Clin Invest,* 130(4), pp. 1808-1822.
32. Churchyard, G., Kim, P., Shah, N. S., Rustomjee, R., Gandhi, N., Mathema, B., Dowdy, D., Kasmar, A. and Cardenas, V. (2017) 'What We Know About Tuberculosis Transmission: An Overview', *J Infect Dis,* 216(suppl_6), pp. S629-S635.
33. Cleveland, R. F., Holtje, J. V., Wicken, A. J., Tomasz, A., Daneo-Moore, L. and Shockman, G. D. (1975) 'Inhibition of bacterial wall lysins by lipoteichoic acids and related compounds', *Biochem Biophys Res Commun,* 67(3), pp. 1128-35.
34. Cohen-Gonsaud, M., Keep, N. H., Davies, A. P., Ward, J., Henderson, B. and Labesse, G. (2004) 'Resuscitation-promoting factors possess a lysozyme-like domain', *Trends Biochem Sci,* 29(1), pp. 7-10.
35. Cook, G. M., Berney, M., Gebhard, S., Heinemann, M., Cox, R. A., Danilchanka, O. and Niederweis, M. (2009) 'Physiology of mycobacteria', *Adv Microb Physiol,* 55, pp. 81-182, 318-9.

36. Correia-Neves, M., Sundling, C., Cooper, A. and Källenius, G. (2019) 'Lipoarabinomannan in Active and Passive Protection Against Tuberculosis', *Front Immunol,* 10, pp. 1968.
37. Court, N., Rose, S., Bourigault, M. L., Front, S., Martin, O. R., Dowling, J. K., Kenny, E. F., O'Neill, L., Erard, F. and Quesniaux, V. F. (2011) 'Mycobacterial PIMs inhibit host inflammatory responses through CD14-dependent and CD14-independent mechanisms', *PLoS One,* 6(9), pp. e24631.
38. Crellin, P. K., Kovacevic, S., Martin, K. L., Brammananth, R., Morita, Y. S., Billman-Jacobe, H., McConville, M. J. and Coppel, R. L. (2008) 'Mutations in pimE restore lipoarabinomannan synthesis and growth in a Mycobacterium smegmatis lpqW mutant', *J Bacteriol,* 190(10), pp. 3690-9.
39. Cuskin, F., Lowe, E. C., Temple, M. J., Zhu, Y., Cameron, E., Pudlo, N. A., Porter, N. T., Urs, K., Thompson, A. J., Cartmell, A., Rogowski, A., Hamilton, B. S., Chen, R., Tolbert, T. J., Piens, K., Bracke, D., Vervecken, W., Hakki, Z., Speciale, G., Munōz-Munōz, J. L., Day, A., Peña, M. J., McLean, R., Suits, M. D., Boraston, A. B., Atherly, T., Ziemer, C. J., Williams, S. J., Davies, G. J., Abbott, D. W., Martens, E. C. and Gilbert, H. J. (2015) 'Human gut Bacteroidetes can utilize yeast mannan through a selfish mechanism', *Nature,* 517(7533), pp. 165-169.
40. Daffé, M. and Etienne, G. (1999) 'The capsule of Mycobacterium tuberculosis and its implications for pathogenicity', *Tuber Lung Dis,* 79(3), pp. 153-69.
41. Daniel, T. M. (2006) 'The history of tuberculosis', *Respir Med,* 100(11), pp. 1862-70.

42. Daniel, V. S. and Daniel, T. M. (1999) 'Old Testament biblical references to tuberculosis', *Clin Infect Dis,* 29(6), pp. 1557-8.

43. Dao, D. N., Kremer, L., Guérardel, Y., Molano, A., Jacobs, W. R., Porcelli, S. A. and Briken, V. (2004) 'Mycobacterium tuberculosis lipomannan induces apoptosis and interleukin-12 production in macrophages', *Infect Immun,* 72(4), pp. 2067-74.

44. Davies, G. and Henrissat, B. (1995) 'Structures and mechanisms of glycosyl hydrolases', *Structure,* 3(9), pp. 853-9.

45. Davies, G. J., Gloster, T. M. and Henrissat, B. (2005) 'Recent structural insights into the expanding world of carbohydrate-active enzymes', *Curr Opin Struct Biol,* 15(6), pp. 637-45.

46. de Souza, G. A., Leversen, N. A., Målen, H. and Wiker, H. G. (2011) 'Bacterial proteins with cleaved or uncleaved signal peptides of the general secretory pathway', *J Proteomics,* 75(2), pp. 502-10.

47. Decout, A., Silva-Gomes, S., Drocourt, D., Blattes, E., Rivière, M., Prandi, J., Larrouy-Maumus, G., Caminade, A. M., Hamasur, B., Källenius, G., Kaur, D., Dobos, K. M., Lucas, M., Sutcliffe, I. C., Besra, G. S., Appelmelk, B. J., Gilleron, M., Jackson, M., Vercellone, A., Tiraby, G. and Nigou, J. (2018) 'Deciphering the molecular basis of mycobacteria and lipoglycan recognition by the C-type lectin Dectin-2', *Sci Rep,* 8(1), pp. 16840.

48. DeJesus, M. A., Gerrick, E. R., Xu, W., Park, S. W., Long, J. E., Boutte, C. C., Rubin, E. J., Schnappinger, D., Ehrt, S., Fortune, S. M., Sassetti, C. M. and Ioerger, T. R.

(2017) 'Comprehensive Essentiality Analysis of the Mycobacterium tuberculosis Genome via Saturating Transposon Mutagenesis', *mBio,* 8(1).

49. Delogu, G., Sali, M. and Fadda, G. (2013) 'The biology of mycobacterium tuberculosis infection', *Mediterr J Hematol Infect Dis,* 5(1), pp. e2013070.
50. Dinadayala, P., Kaur, D., Berg, S., Amin, A. G., Vissa, V. D., Chatterjee, D., Brennan, P. J. and Crick, D. C. (2006) 'Genetic basis for the synthesis of the immunomodulatory mannose caps of lipoarabinomannan in Mycobacterium tuberculosis', *J Biol Chem,* 281(29), pp. 20027-35.
51. Driessen, N. N., Ummels, R., Maaskant, J. J., Gurcha, S. S., Besra, G. S., Ainge, G. D., Larsen, D. S., Painter, G. F., Vandenbroucke-Grauls, C. M., Geurtsen, J. and Appelmelk, B. J. (2009) 'Role of phosphatidylinositol mannosides in the interaction between mycobacteria and DC-SIGN', *Infect Immun,* 77(10), pp. 4538-47.
52. Dulberger, C. L., Rubin, E. J. and Boutte, C. C. (2020) 'The mycobacterial cell envelope - a moving target', *Nat Rev Microbiol,* 18(1), pp. 47-59.
53. Eagen, W. J., Baumoel, L. R., Osman, S. H., Rahlwes, K. C. and Morita, Y. S. (2018) 'Deletion of PimE mannosyltransferase results in increased copper sensitivity in Mycobacterium smegmatis', *FEMS Microbiol Lett,* 365(6).
54. Fachri, M., Hatta, M., Abadi, S., Santoso, S. S., Wikanningtyas, T. A., Syarifuddin, A., Dwiyanti, R. and Noviyanthi, R. A. (2018) 'Comparison of acid fast bacilli (AFB) smear for', *Respir Med Case Rep,* 23, pp. 158-162.
55. Fedrizzi, T., Meehan, C. J., Grottola, A., Giacobazzi, E., Fregni Serpini, G., Tagliazucchi, S., Fabio, A., Bettua, C., Bertorelli, R., De Sanctis, V., Rumpianesi,

F., Pecorari, M., Jousson, O., Tortoli, E. and Segata, N. (2017) 'Genomic characterization of Nontuberculous Mycobacteria', *Sci Rep,* 7, pp. 45258.

56. Flores, J., Cancino, J. C. and Chavez-Galan, L. (2021) 'Lipoarabinomannan as a Point-of-Care Assay for Diagnosis of Tuberculosis: How Far Are We to Use It?', *Front Microbiol,* 12, pp. 638047.
57. Fratti, R. A., Chua, J., Vergne, I. and Deretic, V. (2003) 'Mycobacterium tuberculosis glycosylated phosphatidylinositol causes phagosome maturation arrest', *Proc Natl Acad Sci U S A,* 100(9), pp. 5437-42.
58. Fridman, O., Goldberg, A., Ronin, I., Shoresh, N. and Balaban, N. Q. (2014) 'Optimization of lag time underlies antibiotic tolerance in evolved bacterial populations', *Nature,* 513(7518), pp. 418-21.
59. Fukuda, T., Matsumura, T., Ato, M., Hamasaki, M., Nishiuchi, Y., Murakami, Y., Maeda, Y., Yoshimori, T., Matsumoto, S., Kobayashi, K., Kinoshita, T. and Morita, Y. S. (2013) 'Critical roles for lipomannan and lipoarabinomannan in cell wall integrity of mycobacteria and pathogenesis of tuberculosis', *mBio,* 4(1), pp. e00472-12.
60. Gaur, R. L., Ren, K., Blumenthal, A., Bhamidi, S., González-Nilo, F. D., Jackson, M., Zare, R. N., Ehrt, S., Ernst, J. D. and Banaei, N. (2014) 'LprG-mediated surface expression of lipoarabinomannan is essential for virulence of Mycobacterium tuberculosis', *PLoS Pathog,* 10(9), pp. e1004376.
61. Ghosh, S. and Chaudhuri, S. (2015) 'Chronicles of Gerhard-Henrik Armauer Hansen's Life and Work', *Indian J Dermatol,* 60(3), pp. 219-21.

62. Githinji, L. N., Gray, D. M. and Zar, H. J. (2018) 'Lung function in HIV-infected children and adolescents', *Pneumonia (Nathan),* 10, pp. 6.

63. Glass, L. N., Swapna, G., Chavadi, S. S., Tufariello, J. M., Mi, K., Drumm, J. E., Lam, T. T., Zhu, G., Zhan, C., Vilchéze, C., Arcos, J., Chen, Y., Bi, L., Mehta, S., Porcelli, S. A., Almo, S. C., Yeh, S. R., Jacobs, W. R., Torrelles, J. B. and Chan, J. (2017) 'Mycobacterium tuberculosis universal stress protein Rv2623 interacts with the putative ATP binding cassette (ABC) transporter Rv1747 to regulate mycobacterial growth', *PLoS Pathog,* 13(7), pp. e1006515.

64. Glatman-Freedman, A., Casadevall, A., Dai, Z., Jacobs, W. R., Li, A., Morris, S. L., Navoa, J. A., Piperdi, S., Robbins, J. B., Schneerson, R., Schwebach, J. R. and Shapiro, M. (2004) 'Antigenic evidence of prevalence and diversity of Mycobacterium tuberculosis arabinomannan', *J Clin Microbiol,* 42(7), pp. 3225-31.

65. Gonzalez, D. S. and Jordan, I. K. (2000) 'The alpha-mannosidases: phylogeny and adaptive diversification', *Mol Biol Evol,* 17(2), pp. 292-300.

66. Goude, R., Amin, A. G., Chatterjee, D. and Parish, T. (2008) 'The critical role of embC in Mycobacterium tuberculosis', *J Bacteriol,* 190(12), pp. 4335-41.

67. Gov.UK (2022) *National quarterly report of tuberculosis in England: Quarter 3, 2022 provisional data*. Available at: https://www.gov.uk/government/statistics/tuberculosis-in-england-national-quarterly-reports/national-quarterly-report-of-tuberculosis-in-england-quarter-3-2022-provisional-data.

68. Gradmann, C. (2001) 'Robert Koch and the pressures of scientific research: tuberculosis and tuberculin', *Med Hist,* 45(1), pp. 1-32.

69. Griffin, J. E., Gawronski, J. D., Dejesus, M. A., Ioerger, T. R., Akerley, B. J. and Sassetti, C. M. (2011) 'High-resolution phenotypic profiling defines genes essential for mycobacterial growth and cholesterol catabolism', *PLoS Pathog,* 7(9), pp. e1002251.

70. Guerardel, Y., Maes, E., Elass, E., Leroy, Y., Timmerman, P., Besra, G. S., Locht, C., Strecker, G. and Kremer, L. (2002) 'Structural study of lipomannan and lipoarabinomannan from Mycobacterium chelonae. Presence of unusual components with alpha 1,3-mannopyranose side chains', *J Biol Chem,* 277(34), pp. 30635-48.

71. Guerin, M. E., Kaur, D., Somashekar, B. S., Gibbs, S., Gest, P., Chatterjee, D., Brennan, P. J. and Jackson, M. (2009) 'New insights into the early steps of phosphatidylinositol mannoside biosynthesis in mycobacteria: PimB' is an essential enzyme of Mycobacterium smegmatis', *J Biol Chem,* 284(38), pp. 25687-96.

72. Gupta, R. S., Lo, B. and Son, J. (2018) 'Phylogenomics and Comparative Genomic Studies Robustly Support Division of the Genus', *Front Microbiol,* 9, pp. 67.

73. Gutierrez, M. C., Brisse, S., Brosch, R., Fabre, M., Omaïs, B., Marmiesse, M., Supply, P. and Vincent, V. (2005) 'Ancient origin and gene mosaicism of the progenitor of Mycobacterium tuberculosis', *PLoS Pathog,* 1(1), pp. e5.

74. Haddad, M. B., Raz, K. M., Lash, T. L., Hill, A. N., Kammerer, J. S., Winston, C. A., Castro, K. G., Gandhi, N. R. and Navin, T. R. (2018) 'Simple Estimates for Local

Prevalence of Latent Tuberculosis Infection, United States, 2011-2015', *Emerg Infect Dis,* 24(10), pp. 1930-1933.

75. Hayman, J. (1984) 'Mycobacterium ulcerans: an infection from Jurassic time?', *Lancet,* 2(8410), pp. 1015-6.
76. Henrissat, B. and Romeu, A. (1995) 'Families, superfamilies and subfamilies of glycosyl hydrolases', *Biochem J,* 311 (Pt 1)(Pt 1), pp. 350-1.
77. Hoffmann, C., Leis, A., Niederweis, M., Plitzko, J. M. and Engelhardt, H. (2008) 'Disclosure of the mycobacterial outer membrane: cryo-electron tomography and vitreous sections reveal the lipid bilayer structure', *Proc Natl Acad Sci U S A,* 105(10), pp. 3963-7.
78. Howard, S., He, S. and Withers, S. G. (1998) 'Identification of the active site nucleophile in jack bean alpha-mannosidase using 5-fluoro-beta-L-gulosyl fluoride', *J Biol Chem,* 273(4), pp. 2067-72.
79. Innes, S., Schaaf, H. S. and Cotton, M. F. (2009) 'CAVITATION OF THE GHON FOCUS IN AN HIV-INFECTED INFANT WHO ACQUIRED TUBERCULOSIS AFTER THE INITIATION OF HAART', *South Afr J HIV Med,* 10(1), pp. 44-48.
80. Ishida, E., Corrigan, D. T., Malonis, R. J., Hofmann, D., Chen, T., Amin, A. G., Chatterjee, D., Joe, M., Lowary, T. L., Lai, J. R. and Achkar, J. M. (2021) 'Monoclonal antibodies from humans with Mycobacterium tuberculosis exposure or latent infection recognize distinct arabinomannan epitopes', *Commun Biol,* 4(1), pp. 1181.
81. Jankute, M., Alderwick, L. J., Noack, S., Veerapen, N., Nigou, J. and Besra, G. S. (2017) 'Disruption of Mycobacterial AftB Results in Complete Loss of Terminal

β(1 → 2) Arabinofuranose Residues of Lipoarabinomannan', *ACS Chem Biol,*12(1), pp. 183-190.

82. Jarlier, V. and Nikaido, H. (1994) 'Mycobacterial cell wall: structure and role in natural resistance to antibiotics', *FEMS Microbiol Lett,* 123(1-2), pp. 11-8.
83. Jumper, J., Evans, R., Pritzel, A., Green, T., Figurnov, M., Ronneberger, O., Tunyasuvunakool, K., Bates, R., Žídek, A., Potapenko, A., Bridgland, A., Meyer, C., Kohl, S. A. A., Ballard, A. J., Cowie, A., Romera-Paredes, B., Nikolov, S., Jain, R., Adler, J., Back, T., Petersen, S., Reiman, D., Clancy, E., Zielinski, M., Steinegger, M., Pacholska, M., Berghammer, T., Bodenstein, S., Silver, D., Vinyals, O., Senior, A. W., Kavukcuoglu, K., Kohli, P. and Hassabis, D. (2021) 'Highly accurate protein structure prediction with AlphaFold', *Nature,* 596(7873), pp. 583-589.
84. Jurkowitz, M. S., Azad, A. K., Monsma, P. C., Keiser, T. L., Kanyo, J., Lam, T. T., Bell, C. E. and Schlesinger, L. S. (2022) 'Mycobacterium tuberculosis encodes a YhhN family membrane protein with lysoplasmalogenase activity that protects against toxic host lysolipids', *J Biol Chem,* 298(5), pp. 101849.
85. Kalscheuer, R., Palacios, A., Anso, I., Cifuente, J., Anguita, J., Jacobs, W. R., Guerin, M. E. and Prados-Rosales, R. (2019) 'The *Mycobacterium tuberculosis* capsule: a cell structure with key implications in pathogenesis', *Biochem J,*476(14), pp. 1995-2016.
86. Kaur, D., Obregón-Henao, A., Pham, H., Chatterjee, D., Brennan, P. J. and Jackson, M. (2008) 'Lipoarabinomannan of Mycobacterium: mannose capping

by a multifunctional terminal mannosyltransferase', *Proc Natl Acad Sci U S A,*105(46), pp. 17973-7.

87. KB., L. and R., N. (1896) 'Atlas und Grundriss der Bakeriologie und Lehrbuch der speziellen bakteriologischen Diagnositk', (First edition).
88. Kitagaki, H., Wu, H., Shimoi, H. and Ito, K. (2002) 'Two homologous genes, DCW1 (YKL046c) and DFG5, are essential for cell growth and encode glycosylphosphatidylinositol (GPI)-anchored membrane proteins required for cell wall biogenesis in Saccharomyces cerevisiae', *Mol Microbiol,* 46(4), pp. 1011-22.
89. Kobro, I. (1925) 'Gerhard Henrik Armauer Hansen (1841-1912)', *Ann Med Hist,* 7(2), pp. 127-132.
90. Koeck, D. E., Pechtl, A., Zverlov, V. V. and Schwarz, W. H. (2014) 'Genomics of cellulolytic bacteria', *Curr Opin Biotechnol,* 29, pp. 171-83.
91. Korduláková, J., Gilleron, M., Mikusova, K., Puzo, G., Brennan, P. J., Gicquel, B. and Jackson, M. (2002) 'Definition of the first mannosylation step in phosphatidylinositol mannoside synthesis. PimA is essential for growth of mycobacteria', *J Biol Chem,* 277(35), pp. 31335-44.
92. Korkegian, A., Roberts, D. M., Blair, R. and Parish, T. (2014) 'Mutations in the essential arabinosyltransferase EmbC lead to alterations in Mycobacterium tuberculosis lipoarabinomannan', *J Biol Chem,* 289(51), pp. 35172-81.
93. Kremer, L., Gurcha, S. S., Bifani, P., Hitchen, P. G., Baulard, A., Morris, H. R., Dell, A., Brennan, P. J. and Besra, G. S. (2002) 'Characterization of a putative alpha-

mannosyltransferase involved in phosphatidylinositol trimannoside biosynthesis in Mycobacterium tuberculosis', *Biochem J,* 363(Pt 3), pp. 437-47.

94. Larrouy-Maumus, G., Marino, L. B., Madduri, A. V., Ragan, T. J., Hunt, D. M., Bassano, L., Gutierrez, M. G., Moody, D. B., Pavan, F. R. and de Carvalho, L. P. (2016) 'Cell-Envelope Remodeling as a Determinant of Phenotypic Antibacterial Tolerance in', *ACS Infect Dis,* 2(5), pp. 352-360.
95. Lederer, E., Adam, A., Ciorbaru, R., Petit, J. F. and Wietzerbin, J. (1975) 'Cell walls of Mycobacteria and related organisms; chemistry and immunostimulant properties', *Mol Cell Biochem,* 7(2), pp. 87-104.
96. Li, B., Qiu, Y., Shi, H. and Yin, H. (2016) 'The importance of lag time extension in determining bacterial resistance to antibiotics', *Analyst,* 141(10), pp. 3059-67.
97. Liu, D., Hao, K., Wang, W., Peng, C., Dai, Y., Jin, R., Xu, W., He, L., Wang, H., Zhang, L. and Wang, Q. (2017) '*Rv2629* Overexpression Delays *Mycobacterium smegmatis* and *Mycobacteria tuberculosis* Entry into Log-Phase and Increases Pathogenicity *of Mycobacterium smegmatis* in Mice', *Front Microbiol,* 8, pp. 2231.
98. Liu, J., Barry, C. E., Besra, G. S. and Nikaido, H. (1996) 'Mycolic acid structure determines the fluidity of the mycobacterial cell wall', *J Biol Chem,* 271(47), pp. 29545-51.
99. Lowary, T. L. and Achkar, J. M. (2022) 'Tailor made: New insights into lipoarabinomannan structure may improve TB diagnosis', *J Biol Chem,* 298(3), pp. 101678.

100. Lu, Y. J., Barreira-Silva, P., Boyce, S., Powers, J., Cavallo, K. and Behar, S. M. (2021) 'CD4 T cell help prevents CD8 T cell exhaustion and promotes control of Mycobacterium tuberculosis infection', *Cell Rep,* 36(11), pp. 109696.

101. MacPherson, P., Lebina, L., Motsomi, K., Bosch, Z., Milovanovic, M., Ratsela, A., Lala, S., Variava, E., Golub, J. E., Webb, E. L. and Martinson, N. A. (2020) 'Prevalence and risk factors for latent tuberculosis infection among household contacts of index cases in two South African provinces: Analysis of baseline data from a cluster-randomised trial', *PLoS One,* 15(3), pp. e0230376.

102. Madduri, B. T. S. A., Allen, L., Taylor, S. C., Besra, G. S. and Alderwick, L. J. (2022) 'Enhanced immunogenicity of *Mycobacterium bovis*BCG through CRISPRi mediated depletion of AftC', *Cell Surf,* 8, pp. 100088.

103. Maeda, N., Nigou, J., Herrmann, J. L., Jackson, M., Amara, A., Lagrange, P. H., Puzo, G., Gicquel, B. and Neyrolles, O. (2003) 'The cell surface receptor DC-SIGN discriminates between Mycobacterium species through selective recognition of the mannose caps on lipoarabinomannan', *J Biol Chem,* 278(8), pp. 5513-6.

104. Maruyama, Y. and Nakajima, T. (2000) 'The aman6 gene encoding a yeast mannan backbone degrading 1,6-alpha-D-mannanase in Bacillus circulans: cloning, sequence analysis, and expression', *Biosci Biotechnol Biochem,* 64(9), pp. 2018-20.

105. Maruyama, Y., Nakajima, T. and Ichishima, E. (1994) 'A 1,2-alpha-D-mannosidase from a Bacillus sp.: purification, characterization, and mode of action', *Carbohydr Res,* 251, pp. 89-98.

106. Mawuenyega, K. G., Forst, C. V., Dobos, K. M., Belisle, J. T., Chen, J., Bradbury, E. M., Bradbury, A. R. and Chen, X. (2005) 'Mycobacterium tuberculosis functional network analysis by global subcellular protein profiling', *Mol Biol Cell,*16(1), pp. 396-404.

107. Mba Medie, F., Vincentelli, R., Drancourt, M. and Henrissat, B. (2011) 'Mycobacterium tuberculosis Rv1090 and Rv1987 encode functional β-glucan-targeting proteins', *Protein Expr Purif,* 75(2), pp. 172-6.

108. McCarter, J. D. and Withers, S. G. (1994) 'Mechanisms of enzymatic glycoside hydrolysis', *Curr Opin Struct Biol,* 4(6), pp. 885-92.

109. McCarthy, T. R., Torrelles, J. B., MacFarlane, A. S., Katawczik, M., Kutzbach, B., Desjardin, L. E., Clegg, S., Goldberg, J. B. and Schlesinger, L. S. (2005) 'Overexpression of Mycobacterium tuberculosis manB, a phosphomannomutase that increases phosphatidylinositol mannoside biosynthesis in Mycobacterium smegmatis and mycobacterial association with human macrophages', *Mol Microbiol,* 58(3), pp. 774-90.

110. McNeil, M., Wallner, S. J., Hunter, S. W. and Brennan, P. J. (1987) 'Demonstration that the galactosyl and arabinosyl residues in the cell-wall arabinogalactan of Mycobacterium leprae and Mycobacterium tuberculosis are furanoid', *Carbohydr Res,* 166(2), pp. 299-308.

111. Meehan, C. J., Barco, R. A., Loh, Y. E., Cogneau, S. and Rigouts, L. (2021) 'Reconstituting the genus', *Int J Syst Evol Microbiol,* 71(9).

112. Miller, B. H. and Shinnick, T. M. (2001) 'Identification of two Mycobacterium tuberculosis H37Rv ORFs involved in resistance to killing by human macrophages', *BMC Microbiol,* 1, pp. 26.

113. Minato, Y., Gohl, D. M., Thiede, J. M., Chacón, J. M., Harcombe, W. R., Maruyama, F. and Baughn, A. D. (2019) 'Genomewide Assessment of Mycobacterium tuberculosis Conditionally Essential Metabolic Pathways', *mSystems,* 4(4).

114. Mishra, A. K., Alderwick, L. J., Rittmann, D., Tatituri, R. V., Nigou, J., Gilleron, M., Eggeling, L. and Besra, G. S. (2007) 'Identification of an alpha(1-->6) mannopyranosyltransferase (MptA), involved in Corynebacterium glutamicum lipomanann biosynthesis, and identification of its orthologue in Mycobacterium tuberculosis', *Mol Microbiol,* 65(6), pp. 1503-17.

115. Mishra, A. K., Alderwick, L. J., Rittmann, D., Wang, C., Bhatt, A., Jacobs, W. R., Takayama, K., Eggeling, L. and Besra, G. S. (2008) 'Identification of a novel alpha(1-->6) mannopyranosyltransferase MptB from Corynebacterium glutamicum by deletion of a conserved gene, NCgl1505, affords a lipomannan- and lipoarabinomannan-deficient mutant', *Mol Microbiol,* 68(6), pp. 1595-613.

116. Mishra, A. K., Krumbach, K., Rittmann, D., Appelmelk, B., Pathak, V., Pathak, A. K., Nigou, J., Geurtsen, J., Eggeling, L. and Besra, G. S. (2011) 'Lipoarabinomannan biosynthesis in Corynebacterineae: the interplay of two α(1→2)-mannopyranosyltransferases MptC and MptD in mannan branching', *Mol Microbiol,* 80(5), pp. 1241-59.

117. Morita, Y. S., Patterson, J. H., Billman-Jacobe, H. and McConville, M. J. (2004) 'Biosynthesis of mycobacterial phosphatidylinositol mannosides', *Biochem J,* 378(Pt 2), pp. 589-97.

118. Morita, Y. S., Sena, C. B., Waller, R. F., Kurokawa, K., Sernee, M. F., Nakatani, F., Haites, R. E., Billman-Jacobe, H., McConville, M. J., Maeda, Y. and Kinoshita, T. (2006) 'PimE is a polyprenol-phosphate-mannose-dependent mannosyltransferase that transfers the fifth mannose of phosphatidylinositol mannoside in mycobacteria', *J Biol Chem,* 281(35), pp. 25143-55.

119. MORSE, D., BROTHWELL, D. R. and UCKO, P. J. (1964) 'TUBERCULOSIS IN ANCIENT EGYPT', *Am Rev Respir Dis,* 90, pp. 524-41.

120. Munoz-Munoz, J., Cartmell, A., Terrapon, N., Henrissat, B. and Gilbert, H. J. (2017) 'Unusual active site location and catalytic apparatus in a glycoside hydrolase family', *Proc Natl Acad Sci U S A,* 114(19), pp. 4936-4941.

121. Murphy, K. C., Nelson, S. J., Nambi, S., Papavinasasundaram, K., Baer, C. E. and Sassetti, C. M. (2018) 'ORBIT: a New Paradigm for Genetic Engineering of Mycobacterial Chromosomes', *mBio,* 9(6).

122. Nakajima, T., Maitra, S. K. and Ballou, C. E. (1976) 'An endo-alpha1 leads to 6-D-mannanase from a soil bacterium. Purification, properties, and mode of action', *J Biol Chem,* 251(1), pp. 174-81.

123. Nataraj, V., Varela, C., Javid, A., Singh, A., Besra, G. S. and Bhatt, A. (2015a) 'Mycolic acids: deciphering and targeting the Achilles' heel of the tubercle bacillus', *Mol Microbiol,* 98(1), pp. 7-16.

124. Nataraj, V., Varela, C., Javid, A., Singh, A., Besra, G. S. and Bhatt, A. (2015b) 'Mycolic acids: deciphering and targeting the Achilles' heel of the tubercle bacillus', *Mol Microbiol,* 98(1), pp. 7-16.

125. Naumoff, D. G. (2011) 'Hierarchical classification of glycoside hydrolases', *Biochemistry (Mosc),* 76(6), pp. 622-35.

126. Nayak, S. and Acharjya, B. (2012) 'Mantoux test and its interpretation', *Indian Dermatol Online J,* 3(1), pp. 2-6.

127. Nguyen, P. P., Kado, T., Prithviraj, M., Siegrist, M. S. and Morita, Y. S. (2022) 'Inositol acylation of phosphatidylinositol mannosides: a rapid mass response to membrane fluidization in mycobacteria', *J Lipid Res,* 63(9), pp. 100262.

128. Numao, S., Kuntz, D. A., Withers, S. G. and Rose, D. R. (2003) 'Insights into the mechanism of Drosophila melanogaster Golgi alpha-mannosidase II through the structural analysis of covalent reaction intermediates', *J Biol Chem,*278(48), pp. 48074-83.

129. Organisation, W. H. (2021) *Global Tuberculosis Report 2021*. Available at: https://www.who.int/publications/i/item/9789240037021.

130. Organisation, W. H. (2022) *Tuberculosis*. Available at: https://www.who.int/news-room/fact-sheets/detail/tuberculosis (Accessed: 20th December 2022.

131. Ortalo-Magné, A., Andersen, Å. and Daffé, M. (1996) 'The outermost capsular arabinomannans and other mannoconjugates of virulent and avirulent tubercle bacilli', *Microbiology (Reading),* 142 (Pt 4), pp. 927-935.

132. Ortalo-Magné, A., Dupont, M. A., Lemassu, A., Andersen, A. B., Gounon, P. and Daffé, M. (1995) 'Molecular composition of the outermost capsular material of the tubercle bacillus', *Microbiology (Reading),* 141 (Pt 7), pp. 1609-20.

133. Ortalo-Magné, A., Lemassu, A., Lanéelle, M. A., Bardou, F., Silve, G., Gounon, P., Marchal, G. and Daffé, M. (1996) 'Identification of the surface-exposed lipids on the cell envelopes of Mycobacterium tuberculosis and other mycobacterial species', *J Bacteriol,* 178(2), pp. 456-61.

134. Pai, M., Denkinger, C. M., Kik, S. V., Rangaka, M. X., Zwerling, A., Oxlade, O., Metcalfe, J. Z., Cattamanchi, A., Dowdy, D. W., Dheda, K. and Banaei, N. (2014) 'Gamma interferon release assays for detection of Mycobacterium tuberculosis infection', *Clin Microbiol Rev,* 27(1), pp. 3-20.

135. Pan, S., Tang, L., Pan, X., Qi, L. and Yang, J. (2021) 'A member of the glycoside hydrolase family 76 is involved in growth, conidiation, and virulence in rice blast fungus', *Physiological and Molecular Plant Pathology,* 113(101587).

136. Pang, X., Vu, P., Byrd, T. F., Ghanny, S., Soteropoulos, P., Mukamolova, G. V., Wu, S., Samten, B. and Howard, S. T. (2007) 'Evidence for complex interactions of stress-associated regulons in an mprAB deletion mutant of Mycobacterium tuberculosis', *Microbiology (Reading),* 153(Pt 4), pp. 1229-1242.

137. Patterson, J. H., Waller, R. F., Jeevarajah, D., Billman-Jacobe, H. and McConville, M. J. (2003) 'Mannose metabolism is required for mycobacterial growth', *Biochem J,* 372(Pt 1), pp. 77-86.

138. Peloquin, C. A. and Davies, G. R. (2021) 'The Treatment of Tuberculosis', *Clin Pharmacol Ther,* 110(6), pp. 1455-1466.

139. Peterson, E. J., Bailo, R., Rothchild, A. C., Arrieta-Ortiz, M. L., Kaur, A., Pan, M., Mai, D., Abidi, A. A., Cooper, C., Aderem, A., Bhatt, A. and Baliga, N. S. (2019) 'Path-seq identifies an essential mycolate remodeling program for mycobacterial host adaptation', *Mol Syst Biol,* 15(3), pp. e8584.

140. Petit, J. F., Adam, A., Wietzerbin-Falszpan, J., Lederer, E. and Ghuysen, J. M. (1969) 'Chemical structure of the cell wall of Mycobacterium smegmatis. I. Isolation and partial characterization of the peptidoglycan', *Biochem Biophys Res Commun,* 35(4), pp. 478-85.

141. Pfyffer, G. E. and Wittwer, F. (2012) 'Incubation time of mycobacterial cultures: how long is long enough to issue a final negative report to the clinician?', *J Clin Microbiol,* 50(12), pp. 4188-9.

142. Pitarque, S., Larrouy-Maumus, G., Payré, B., Jackson, M., Puzo, G. and Nigou, J. (2008) 'The immunomodulatory lipoglycans, lipoarabinomannan and lipomannan, are exposed at the mycobacterial cell surface', *Tuberculosis (Edinb),*88(6), pp. 560-5.

143. Prados-Rosales, R., Carreño, L. J., Weinrick, B., Batista-Gonzalez, A., Glatman-Freedman, A., Xu, J., Chan, J., Jacobs, W. R., Porcelli, S. A. and Casadevall, A. (2016) 'The Type of Growth Medium Affects the Presence of a Mycobacterial Capsule and Is Associated With Differences in Protective Efficacy of BCG Vaccination Against Mycobacterium tuberculosis', *J Infect Dis,* 214(3), pp. 426-37.

144. Qian, J., Chen, R., Wang, H. and Zhang, X. (2020) 'Role of the PE/PPE Family in Host-Pathogen Interactions and Prospects for Anti-Tuberculosis Vaccine and Diagnostic Tool Design', *Front Cell Infect Microbiol,* 10, pp. 594288.

145. Rahlwes, K. C., Osman, S. H. and Morita, Y. S. (2020) 'Role of LmeA, a Mycobacterial Periplasmic Protein, in Maintaining the Mannosyltransferase MptA and Its Product Lipomannan under Stress', *mSphere,* 5(6).

146. Rashid, A. M., Batey, S. F., Syson, K., Koliwer-Brandl, H., Miah, F., Barclay, J. E., Findlay, K. C., Nartowski, K. P., Khimyak, Y. Z., Kalscheuer, R. and Bornemann, S. (2016) 'Assembly of α-Glucan by GlgE and GlgB in Mycobacteria and Streptomycetes', *Biochemistry,* 55(23), pp. 3270-84.

147. Rivera-Marrero, C. A., Ritzenthaler, J. D., Roman, J. and Moremen, K. W. (2001a) 'Molecular cloning and expression of an alpha-mannosidase gene in Mycobacterium tuberculosis', *Microb Pathog,* 30(1), pp. 9-18.

148. Rivera-Marrero, C. A., Ritzenthaler, J. D., Roman, J. and Moremen, K. W. (2001b) 'Molecular cloning and expression of an alpha-mannosidase gene in Mycobacterium tuberculosis', *Microb Pathog,* 30(1), pp. 9-18.

149. Roy Chowdhury, R., Vallania, F., Yang, Q., Lopez Angel, C. J., Darboe, F., Penn-Nicholson, A., Rozot, V., Nemes, E., Malherbe, S. T., Ronacher, K., Walzl, G., Hanekom, W., Davis, M. M., Winter, J., Chen, X., Scriba, T. J., Khatri, P. and Chien, Y. H. (2018) 'A multi-cohort study of the immune factors associated with M. tuberculosis infection outcomes', *Nature,* 560(7720), pp. 644-648.

150. Ruhaak, L. R., Steenvoorden, E., Koeleman, C. A., Deelder, A. M. and Wuhrer, M. (2010) '2-picoline-borane: a non-toxic reducing agent for

oligosaccharide labeling by reductive amination', *Proteomics,* 10(12), pp. 2330-6.

151. Rustad, T. R., Harrell, M. I., Liao, R. and Sherman, D. R. (2008) 'The enduring hypoxic response of Mycobacterium tuberculosis', *PLoS One,* 3(1), pp. e1502.

152. Saint-Joanis, B., Demangel, C., Jackson, M., Brodin, P., Marsollier, L., Boshoff, H. and Cole, S. T. (2006) 'Inactivation of Rv2525c, a substrate of the twin arginine translocation (Tat) system of Mycobacterium tuberculosis, increases beta-lactam susceptibility and virulence', *J Bacteriol,* 188(18), pp. 6669-79.

153. Sassetti, C. M., Boyd, D. H. and Rubin, E. J. (2003) 'Genes required for mycobacterial growth defined by high density mutagenesis', *Mol Microbiol,* 48(1), pp. 77-84.

154. Schaeffer, M. L., Khoo, K. H., Besra, G. S., Chatterjee, D., Brennan, P. J., Belisle, J. T. and Inamine, J. M. (1999) 'The pimB gene of Mycobacterium tuberculosis encodes a mannosyltransferase involved in lipoarabinomannan biosynthesis', *J Biol Chem,* 274(44), pp. 31625-31.

155. Schnaar, R. L. (2015) 'Glycans and glycan-binding proteins in immune regulation: A concise introduction to glycobiology for the allergist', *J Allergy Clin Immunol,* 135(3), pp. 609-15.

156. Seidel, M., Alderwick, L. J., Birch, H. L., Sahm, H., Eggeling, L. and Besra, G. S. (2007) 'Identification of a novel arabinofuranosyltransferase AftB involved in a terminal step of cell wall arabinan biosynthesis in Corynebacterianeae, such

as Corynebacterium glutamicum and Mycobacterium tuberculosis', *J Biol Chem,* 282(20), pp. 14729-40.

157. Seung, K. J., Keshavjee, S. and Rich, M. L. (2015) 'Multidrug-Resistant Tuberculosis and Extensively Drug-Resistant Tuberculosis', *Cold Spring Harb Perspect Med,* 5(9), pp. a017863.

158. Shetty, A. and Dick, T. (2018) 'Mycobacterial Cell Wall Synthesis Inhibitors Cause Lethal ATP Burst', *Front Microbiol,* 9, pp. 1898.

159. Shi, L., Berg, S., Lee, A., Spencer, J. S., Zhang, J., Vissa, V., McNeil, M. R., Khoo, K. H. and Chatterjee, D. (2006) 'The carboxy terminus of EmbC from Mycobacterium smegmatis mediates chain length extension of the arabinan in lipoarabinomannan', *J Biol Chem,* 281(28), pp. 19512-26.

160. Shiloh, M. U. and Champion, P. A. (2010) 'To catch a killer. What can mycobacterial models teach us about Mycobacterium tuberculosis pathogenesis?', *Curr Opin Microbiol,* 13(1), pp. 86-92.

161. Shukla, S., Richardson, E. T., Athman, J. J., Shi, L., Wearsch, P. A., McDonald, D., Banaei, N., Boom, W. H., Jackson, M. and Harding, C. V. (2014) 'Mycobacterium tuberculosis lipoprotein LprG binds lipoarabinomannan and determines its cell envelope localization to control phagolysosomal fusion', *PLoS Pathog,* 10(10), pp. e1004471.

162. Sigal, G. B., Pinter, A., Lowary, T. L., Kawasaki, M., Li, A., Mathew, A., Tsionsky, M., Zheng, R. B., Plisova, T., Shen, K., Katsuragi, K., Choudhary, A., Honnen, W. J., Nahid, P., Denkinger, C. M. and Broger, T. (2018) 'A Novel Sensitive Immunoassay Targeting the 5-Methylthio-d-Xylofuranose-

Lipoarabinomannan Epitope Meets the WHO's Performance Target for Tuberculosis Diagnosis', *J Clin Microbiol,* 56(12).

163. Skovierová, H., Larrouy-Maumus, G., Zhang, J., Kaur, D., Barilone, N., Korduláková, J., Gilleron, M., Guadagnini, S., Belanová, M., Prevost, M. C., Gicquel, B., Puzo, G., Chatterjee, D., Brennan, P. J., Nigou, J. and Jackson, M. (2009) 'AftD, a novel essential arabinofuranosyltransferase from mycobacteria', *Glycobiology,* 19(11), pp. 1235-47.

164. Solanki, V., Krüger, K., Crawford, C. J., Pardo-Vargas, A., Danglad-Flores, J., Hoang, K. L. M., Klassen, L., Abbott, D. W., Seeberger, P. H., Amann, R. I., Teeling, H. and Hehemann, J. H. (2022) 'Glycoside hydrolase from the GH76 family indicates that marine Salegentibacter sp. Hel_I_6 consumes alpha-mannan from fungi', *ISME J,* 16(7), pp. 1818-1830.

165. Soler-Arnedo, P., Sala, C., Zhang, M., Cole, S. T. and Piton, J. (2020) 'Polarly Localized EccE 1 Is Required for ESX-1 Function and Stabilization of ESX-1 Membrane Proteins in *Mycobacterium tuberculosis*', *J Bacteriol,* 202(5).

166. Sparks, I. L., Nijjer, J., Yan, J. and Morita, Y. S. (2023) 'Lipoarabinomannan regulates septation in Mycobacterium smegmatis', *bioRxiv*.

167. Stam, M. R., Danchin, E. G., Rancurel, C., Coutinho, P. M. and Henrissat, B. (2006) 'Dividing the large glycoside hydrolase family 13 into subfamilies: towards improved functional annotations of alpha-amylase-related proteins', *Protein Eng Des Sel,* 19(12), pp. 555-62.

168. Stoop, E. J., Mishra, A. K., Driessen, N. N., van Stempvoort, G., Bouchier, P., Verboom, T., van Leeuwen, L. M., Sparrius, M., Raadsen, S. A., van Zon, M.,

van der Wel, N. N., Besra, G. S., Geurtsen, J., Bitter, W., Appelmelk, B. J. and van der Sar, A. M. (2013) 'Mannan core branching of lipo(arabino)mannan is required for mycobacterial virulence in the context of innate immunity', *Cell Microbiol,* 15(12), pp. 2093-108.

169. Striebeck, A., Robinson, D. A., Schüttelkopf, A. W. and van Aalten, D. M. (2013) 'Yeast Mnn9 is both a priming glycosyltransferase and an allosteric activator of mannan biosynthesis', *Open Biol,* 3(9), pp. 130022.

170. Sweet, L., Singh, P. P., Azad, A. K., Rajaram, M. V., Schlesinger, L. S. and Schorey, J. S. (2010) 'Mannose receptor-dependent delay in phagosome maturation by Mycobacterium avium glycopeptidolipids', *Infect Immun,* 78(1), pp. 518-26.

171. Syal, K., Bhardwaj, N. and Chatterji, D. (2017) 'Vitamin C targets (p)ppGpp synthesis leading to stalling of long-term survival and biofilm formation in Mycobacterium smegmatis', *FEMS Microbiol Lett,* 364(1).

172. Thompson, A. J., Speciale, G., Iglesias-Fernández, J., Hakki, Z., Belz, T., Cartmell, A., Spears, R. J., Chandler, E., Temple, M. J., Stepper, J., Gilbert, H. J., Rovira, C., Williams, S. J. and Davies, G. J. (2015) 'Evidence for a boat conformation at the transition state of GH76 α-1,6-mannanases--key enzymes in bacterial and fungal mannoprotein metabolism', *Angew Chem Int Ed Engl,* 54(18), pp. 5378-82.

173. Torrelles, J. B. and Schlesinger, L. S. (2010) 'Diversity in Mycobacterium tuberculosis mannosylated cell wall determinants impacts adaptation to the host', *Tuberculosis (Edinb),* 90(2), pp. 84-93.

174. Trivedi, A., Mavi, P. S., Bhatt, D. and Kumar, A. (2016) 'Thiol reductive stress induces cellulose-anchored biofilm formation in Mycobacterium tuberculosis', *Nat Commun,* 7, pp. 11392.

175. Tsukamura, M. (1967) 'Identification of mycobacteria', *Tubercle,* 48(4), pp. 311-38.

176. Urdahl, K. B., Shafiani, S. and Ernst, J. D. (2011) 'Initiation and regulation of T-cell responses in tuberculosis', *Mucosal Immunol,* 4(3), pp. 288-93.

177. van den Elsen, J. M., Kuntz, D. A. and Rose, D. R. (2001) 'Structure of Golgi alpha-mannosidase II: a target for inhibition of growth and metastasis of cancer cells', *EMBO J,* 20(12), pp. 3008-17.

178. van Wyk, N., Drancourt, M., Henrissat, B. and Kremer, L. (2017) 'Current perspectives on the families of glycoside hydrolases of Mycobacterium tuberculosis: their importance and prospects for assigning function to unknowns', *Glycobiology,* 27(2), pp. 112-122.

179. Varadi, M., Anyango, S., Deshpande, M., Nair, S., Natassia, C., Yordanova, G., Yuan, D., Stroe, O., Wood, G., Laydon, A., Žídek, A., Green, T., Tunyasuvunakool, K., Petersen, S., Jumper, J., Clancy, E., Green, R., Vora, A., Lutfi, M., Figurnov, M., Cowie, A., Hobbs, N., Kohli, P., Kleywegt, G., Birney, E., Hassabis, D. and Velankar, S. (2022b) 'AlphaFold Protein Structure Database: massively expanding the structural coverage of protein-sequence space with high-accuracy models', *Nucleic Acids Res,*50(D1), pp. D439-D444.

180. Varrot, A., Leydier, S., Pell, G., Macdonald, J. M., Stick, R. V., Henrissat, B., Gilbert, H. J. and Davies, G. J. (2005) 'Mycobacterium tuberculosis strains possess functional cellulases', *J Biol Chem,* 280(21), pp. 20181-4.

181. Vogt, M. S., Schmitz, G. F., Varón Silva, D., Mösch, H. U. and Essen, L. O. (2020) 'Structural base for the transfer of GPI-anchored glycoproteins into fungal cell walls', *Proc Natl Acad Sci U S A,* 117(36), pp. 22061-22067.

182. Vollmer, W., Blanot, D. and de Pedro, M. A. (2008) 'Peptidoglycan structure and architecture', *FEMS Microbiol Rev,* 32(2), pp. 149-67.

183. Vollmer, W., Joris, B., Charlier, P. and Foster, S. (2008) 'Bacterial peptidoglycan (murein) hydrolases', *FEMS Microbiol Rev,* 32(2), pp. 259-86.

184. Vuong, T. V. and Wilson, D. B. (2010) 'Glycoside hydrolases: catalytic base/nucleophile diversity', *Biotechnol Bioeng,* 107(2), pp. 195-205.

185. Wietzerbin-Falszpan, J., Das, B. C., Azuma, I., Adam, A., Petit, J. F. and Lederer, E. (1970) 'Isolation and mass spectrometric identification of the peptide subunits of mycobacterial cell walls', *Biochem Biophys Res Commun,* 40(1), pp. 57-63.

186. Williams, S. T., Locci, R., Beswick, A., Kurtböke, D. I., Kuznetsov, V. D., Le Monnier, F. J., Long, P. F., Maycroft, K. A., Palma, R. A. and Petrolini, B. (1993) 'Detection and identification of novel actinomycetes', *Res Microbiol,* 144(8), pp. 653-6.

187. Wright, A. J. (1999) 'The penicillins', *Mayo Clin Proc,* 74(3), pp. 290-307.

188. Xiong, Y., Chalmers, M. J., Gao, F. P., Cross, T. A. and Marshall, A. G. (2005) 'Identification of Mycobacterium tuberculosis H37Rv integral membrane

proteins by one-dimensional gel electrophoresis and liquid chromatography electrospray ionization tandem mass spectrometry', *J Proteome Res,* 4(3), pp. 855-61.

189. Xue, Y., Zhou, J., Wang, P., Lan, J. H., Lian, W. Q., Fan, Y. Y., Xu, B. N., Yin, J. P., Feng, Z. H. and Jia, C. Y. (2022) 'Burden of tuberculosis and its association with socio-economic development status in 204 countries and territories, 1990-2019', *Front Med (Lausanne),* 9, pp. 905245.

190. Yonekawa, A., Saijo, S., Hoshino, Y., Miyake, Y., Ishikawa, E., Suzukawa, M., Inoue, H., Tanaka, M., Yoneyama, M., Oh-Hora, M., Akashi, K. and Yamasaki, S. (2014) 'Dectin-2 is a direct receptor for mannose-capped lipoarabinomannan of mycobacteria', *Immunity,* 41(3), pp. 402-413.

191. Young, D. B., Gideon, H. P. and Wilkinson, R. J. (2009) 'Eliminating latent tuberculosis', *Trends Microbiol,* 17(5), pp. 183-8.

192. Zaman, K. (2010) 'Tuberculosis: a global health problem', *J Health Popul Nutr,* 28(2), pp. 111-3.

193. Zhang, Y. J., Reddy, M. C., Ioerger, T. R., Rothchild, A. C., Dartois, V., Schuster, B. M., Trauner, A., Wallis, D., Galaviz, S., Huttenhower, C., Sacchettini, J. C., Behar, S. M. and Rubin, E. J. (2013) 'Tryptophan biosynthesis protects mycobacteria from CD4 T-cell-mediated killing', *Cell,* 155(6), pp. 1296-308.

194. Zhu, Y., Suits, M. D., Thompson, A. J., Chavan, S., Dinev, Z., Dumon, C., Smith, N., Moremen, K. W., Xiang, Y., Siriwardena, A., Williams, S. J., Gilbert, H. J. and Davies, G. J. (2010) 'Mechanistic insights into a Ca2+-dependent family of alpha-mannosidases in a human gut symbiont', *Nat Chem Biol,* 6(2), pp. 125-32.